INFRARED INTENSITIES OF ALCOHOLS AND ETHERS

By

JERRY DALE ROGERS

A DISSERTATION PRESENTED TO THE GRADUATE COUNCIL
OF THE UNIVERSITY OF FLORIDA IN
PARTIAL FULFILLMENT OF THE REQUIREMENTS
FOR THE DEGREE OF DOCTOR OF PHILOSOPHY

UNIVERSITY OF FLORIDA
1980

ACKNOWLEDGMENTS

I would especially like to thank Profesor Willis B. Person for his encouragement, guidance, and patience. I wish to thank also Dr. James Newton, Dr. Barbara Zilles, and Mr. Roberto Maia, each of whom has provided years of appreciated friendship. Thanks are due also to Mr. Alan Brower for hours of help with the quantum mechanical calculations. I wish to thank Mr. Beny Rub and Mr. Sandy Goldman for measuring absolute intensities for acetone (and also carbon dioxide).

I am grateful to Dr. Person for doing the *ab initio* calculations for methanol, and we are both grateful to the University of London for providing the necessary computer time.

Partial support from NSF Research Grant No. CHE-78-18940 is gratefully acknowledged as is also a supplemental fellowship from the Graduate School of the University of Florida.

Finally, I wish to thank Ms. Joan Raudenbush for many faithful hours of expert typing.

TABLE OF CONTENTS

	Page
ACKNOWLEDGMENTS	ii
LIST OF TABLES	vi
LIST OF FIGURES	x
ABSTRACT	xiii
CHAPTER	
1. INTRODUCTION	1
Experimental Absolute Intensities	2
Quantum Mechanical Treatment of Infrared Intensities	4
Interpretative Approaches to Intensities	5
2. EXPERIMENTAL INTENSITIES	10
Experimental Outline	13
Spectrometers	13
General Procedure	15
Methanol	18
Survey Spectrum	18
Experimental Conditions	20
Absolute Band Intensities for Methanol	26
Estimation of Absolute Intensities for the Normal Vibrational Modes of Methanol	31
Ethanol	35
Survey Spectrum	35
Experimental Conditions	37
Absolute Band Intensities for Ethanol	39
Dimethyl Ether	53
Survey Spectrum	53
Experimental Conditions	53
Absolute Band Intensities for Diemthyl Ether	55

3. ATOMIC POLAR TENSORS ---------- 59

Normal Coordinate Analysis ---------- 59
Displacement Coordinate Spaces ---------- 59
Evaluation of the Normal Coordinates ---- 63
Intensity Analysis ---------- 66
Atomic Polar Tensors ---------- 66
Effective Charges ---------- 71

4. EXPERIMENTAL ATOMIC POLAR TENSORS FOR METHANOL- 74

The Experimental P_Q Matrix for Methanol ----- 74
Atomic Polar Tensors for Methanol ---------- 76
Effect of the Normal Coordinates on the APT's for Methanol ---------- 89
Choice of APT's for Methanol ---------- 91

5. PREDICTION OF INFRARED INTENSITIES ---------- 106

Transferred APT's and Predicted Intensities - 106
Ab Initio APT's and Predicted Intensities --- 108
Methanol ---------- 112
APT's and Absolute Intensities for Methanol ---------- 112
Discussion of Results for Methanol ------ 120
Predicted absolute intensities ------ 120
Simulated spectra ---------- 124
Comparison of APT's for methanol ---- 129
P_Q matrices for methanol ---------- 136
Ethanol ---------- 139
APT's and Absolute Intensities for Ethanol ---------- 139
Discussion of Results for Ethanol ------- 149
Force fields for ethanol ---------- 149
Predicted absolute intensities ------ 151
Simulated spectra ---------- 154
Comparison of APT's for ethanol ----- 161
Dimethyl Ether ---------- 168
APT's and Absolute Intensities for Dimethyl Ether ---------- 170
Discussion of Results for Dimethyl Ether- 176
Predicted absolute intensities ------ 176
Simulated spectra ---------- 177
Comparison of absolute intensities predicted by transferred APT's and by quantum mechanical calculations-- 180
Formaldehyde ---------- 181
APT's and Absolute Intensities for Formaldehyde ---------- 181

Discussion of Results for Formaldehyde -- 184
Predicted absolute intensities ------ 184
Comparison of APT's for formaldehyde- 187
Acetone ---------- 191
APT's and Absolute Intensities for Acetone ---------- 192
Discussion of Results for Acetone ------- 198
Predicted absolute intensities ------ 198
Simulated spectra ---------- 201
Comparison of APT's for acetone with the APT's for other molecules ------ 205
Summary ---------- 217

APPENDICES

A. NORMAL COORDINATE ANALYSIS ---------- 219
Methanol ---------- 219
Ethanol ---------- 220
Dimethyl Ether ---------- 221
Formaldehyde ---------- 222
Acetone ---------- 222

B. SIMULATED INFRARED SPECTRA ---------- 268

REFERENCES ---------- 276

BIOGRAPHICAL SKETCH ---------- 282

LIST OF TABLES

TABLE		Page
2-1.	EXPERIMENTAL GAS-PHASE ABSOLUTE BAND INTENSITIES FOR METHANOL	29
2-2.	EXPERIMENTAL ABSOLUTE INTENSITIES FOR THE NORMAL MODES OF METHANOL	33
2-3.	ABSOLUTE INTENSITIES FOR ETHANOL	44
2-4.	COMPARISON OF ABSOLUTE INTENSITIES FOR METHANOL AND ETHANOL MEASURED HERE AND MEASURED WITH LIGHT REFRACTION STUDIES	52
2-5.	ABSOLUTE INTENSITIES FOR DIMETHYL ETHER	57
4-1.	EXPERIMENTAL MAGNITUDES FOR THE $\underline{P}_Q$ MATRIX ELEMENTS FOR METHANOL	77
4-2.	QUANTUM MECHANICAL $\underline{P}_Q$ MATRIX FOR METHANOL	78
4-3.	DATA FOR THE ROTATIONAL CORRECTION TENSOR CALCULATIONS FOR METHANOL	80
4-4.	ROTATIONAL CORRECTION TENSORS FOR METHANOL	83
4-5.	THE EXPERIMENTAL $\underline{P}_Q$ MATRIX FOR METHANOL	85
4-6.	ATOMIC POLAR TENSORS FOR METHANOL	86
4-7.	ALTERNATE APT'S FOR METHANOL BASED ON OTHER SIGN CHOICES	87
4-8.	ATOMIC POLAR TENSORS FOR METHANOL BASED ON AN ALTERNATE SET OF NORMAL COORDINATES	92
4-9.	HYDROXYL GROUP APT'S FOR METHANOL	95
4-10.	METHYL GROUP EXPERIMENTAL APT'S FOR METHANOL	98
4-11.	HYDROXYL HYDROGEN APT'S FOR WATER AND METHANOL	100

4-12. METHYL HDYROGEN APT'S FOR VARIOUS MOLECULES ---- 103

5-1. TRANSFERRED AND QUANTUM MECHANICAL APT'S FOR METHANOL ---------- 115

5-2. PREDICTED ABSOLUTE INTENSITIES FOR METHANOL ---- 118

5-3. COMPARISON OF APT'S FOR METHANOL ---------- 130

5-4. APT'S RESULTING FROM TRANSFERRING THE OXYGEN APT FROM WATER ---------- 134

5-5. $\underline{P}_Q$ MATRICES FOR METHANOL ---------- 137

5-6. TRANSFERRED AND QUANTUM MECHANICAL APT'S FOR ETHANOL ---------- 142

5-7. APT'S FOR THE METHYL AND METHYLENE CARBONS IN ETHANOL ---------- 144

5-8. PREDICTED ABSOLUTE INTENSITIES FOR ETHANOL ----- 146

5-9. COMPARISON OF AB INITIO APT'S FOR METHANOL AND ETHANOL ---------- 165

5-10. TRANSFERRED APT'S FOR DIMETHYL ETHER ---------- 172

5-11. PREDICTED ABSOLUTE INTENSITIES FOR DIMETHYL ETHER ---------- 174

5-12. EXPERIMENTAL AND QUANTUM MECHANICAL APT'S FOR FORMALDEHYDE ---------- 183

5-13. QUANTUM MECHANICALLY PREDICTED ABSOLUTE INTENSITIES ---------- 185

5-14. COMPARISON OF EXPERIMENTAL AND QUANTUM MECHANICAL APT'S FOR HYDROGEN IN FORMALDEHYDE ---------- 190

5-15. TRANSFERRED AND QUANTUM MECHANICAL APT'S FOR ACETONE ---------- 194

5-16. PREDICTED ABSOLUTE INTENSITIES FOR ACETONE ----- 196

5-17. COMPARISON OF AB INITIO APT'S FOR FORMALDEHYDE AND ACETONE ---------- 208

5-18. COMPARISON OF QUANTUM MECHANICAL APT'S FOR METHANOL AND ACETONE ---------- 214

A-1. INTERNAL DISPLACEMENT COORDINATES FOR METHANOL -- 225

A-2. UNNORMALIZED SYMMETRY COORDINATES FOR METHANOL -- 226

A-3. THE $\underline{A}$ MATRIX FOR METHANOL BASED ON MALLINSON'S FORCE FIELD ---------- 227

A-4. THE $\underline{L}$ MATRIX FOR METHANOL BASED ON MALLINSON'S FORCE FIELD ---------- 228

A-5. THE $\underline{B}$ MATRIX FOR METHANOL BASED ON MALLINSON'S FORCE FIELD ---------- 229

A-6. THE $\underline{L}^{-1}$ MATRIX FOR METHANOL BASED ON MALLINSON'S FORCE FIELD ---------- 230

A-7. THE $\underline{A}$ MATRIX FOR METHANOL BASED ON BLOM, OTTO, AND ALTONA'S FORCE FIELD ---------- 231

A-8. THE $\underline{L}$ MATRIX FOR METHANOL BASED ON BLOM, OTTO, AND ALTONA'S FORCE FIELD ---------- 232

A-9. THE $\underline{B}$ MATRIX FOR METHANOL BASED ON BLOM, OTTO, AND ALTONA'S FORCE FIELD ---------- 233

A-10. THE $\underline{L}^{-1}$ MATRIX FOR METHANOL BASED ON BLOM, OTTO, AND ALTONA'S FORCE FIELD ---------- 234

A-11. INTERNAL DISPLACEMENT COORDINATES FOR ETHANOL --- 236

A-12. UNNORMALIZED SYMMETRY COORDINATES FOR ETHANOL --- 237

A-13. UPPER TRIANGLE OF THE SYMMETRIZED $\underline{F}$ MATRIX FOR ETHANOL ---------- 238

A-14. CALCULATED FREQUENCIES USING TRANSFERRED FORCE CONSTANTS FOR ETHANOL ---------- 239

A-15. THE $\underline{A}$ MATRIX FOR ETHANOL BASED ON TRANSFERRED FORCE CONSTANTS ---------- 240

A-16. THE SYMMETRIZED $\underline{A}$ MATRIX FOR ETHANOL BASED ON THE FORCE FIELD AND GEOMETRY REPORTED BY ZEMLYANUKHINA AND SVERDLOV ---------- 243

A-17. THE $\underline{L}$ MATRIX FOR ETHANOL BASED ON TRANSFERRED FORCE CONSTANTS ---------- 246

A-18. THE L MATRIX FOR ETHANOL DERIVED FROM THE FORCE FIELD REPORTED BY ZEMLYANUKHINA AND SVERDLOV--- 248

A-19. INTERNAL DISPLACEMENT COORDINATES FOR DIMETHYL ETHER ---------- 251

A-20. UNNORMALIZED SYMMETRY COORDINATES FOR DIMETHYL ETHER ---------- 252

A-21. THE $\underline{A}$ MATRIX FOR DIMETHYL ETHER ---------- 253

A-22. THE L MATRIX FOR DIMETHYL ETHER ---------- 256

A-23. INTERNAL DISPLACEMENT COORDINATES FOR FORMALDEHYDE ---------- 258

A-24. UNNORMALIZED SYMMETRY COORDINATES FOR FORMALDEHYDE ---------- 258

A-25. THE SYMMETRIZED $\underline{A}$ MATRIX FOR FORMALDEHYDE ------ 259

A-26. THE L MATRIX FOR FORMALDEHYDE ---------- 259

A-27. INTERNAL DISPLACEMENT COORDINATES FOR ACETONE -- 261

A-28. UNNORMALIZED SYMMETRY COORDINATES FOR ACETONE -- 262

A-29. THE $\underline{A}$ MATRIX FOR ACETONE ---------- 264

A-30. THE L MATRIX FOR ACETONE ---------- 267

B-1. PARAMETERS FOR SIMULATED SPECTRA OF METHANOL --- 272

B-2. PARAMETERS FOR SIMULATED SPECTRA OF ETHANOL ---- 273

B-3. PARAMETERS FOR SIMULATED SPECTRA OF DIMETHYL ETHER ---------- 274

B-4. PARAMETERS FOR SIMULATED SPECTRA OF ACETONE ---- 275

LIST OF FIGURES

Figure		Page
2-1.	Survey infrared spectrum of methanol vapor ------	19
2-2.	The integrated area of the C-O stretching region of methanol as a function of total pressure ----	22
2-3.	The effect of pressure broadening on the appearance of the C-O stretching region of the infrared spectrum of methanol ----------	24
2-4.	Beer's law plots for the spectral regions of the infrared spectrum of methanol ----------	28
2-5.	Survey infrared spectrum of ethanol vapor -------	36
2-6.	Beer's law plots for the spectral regions of the infrared spectrum of ethanol involving no ambiguity in choice of baseline ----------	41
2-7.	Beer's law plots for the spectral regions of the infrared spectrum of ethanol involving an ambiguity in the choice of baseline ----------	43
2-8.	Beer's law plots for regions of the infrared spectrum of ethanol under different sample conditions ----------	50
2-9.	Survey spectrum of dimethyl ether vapor ---------	54
2-10.	Beer's law plots for the spectral regionsof the infrared spectrum of dimethyl ether ----------	56
4-1.	Location of the principal axes of inertia of methanol ----------	81
4-2.	Space-fixed cartesian coordinate system for methanol ----------	82
4-3.	Bond cartesian coordinate systems for the two atoms of the hydroxyl group of methanol --------	94

4-4. Bond cartesian coordinate systems for the methyl group experimental APT's for methanol ---------- 97

4-5. Bond cartesian coordinate system for the hydroxyl hydrogen ---------- 99

4-6. Bond cartesian coordinate system for the methyl hydrogen ---------- 102

5-1. Comparison of simulated and experimental spectra for methanol ---------- 127

5-2. Cartesian coordinate system for ethanol --------- 141

5-3. Simulated spectra for ethanol showing the effect of L on the predicted intensities ---------- 157

5-4. Simulated spectra for ethanol showing the effect of APT's transferred from different molecules -- 159

5-5. Bond coordinate systems for comparing APT's in methanol and ethanol ---------- 164

5-6. Coordinate system for dimethyl ether ---------- 171

5-7. Comparison of simulated and experimental spectra for dimethyl ether ---------- 179

5-8. Coordinate system for formaldehyde ---------- 182

5-9. Bond coordinate system for hydrogen ---------- 188

5-10. Coordinate system for acetone ---------- 193

5-11. Comparison of simulated and experimental spectra for acetone ---------- 203

5-12. Bond cartesian coordinate system for comparison of the APT's for the carbonyl carbon and oxygen atoms of formaldehyde (R=H) and acetone ($R=CH_3$)- 207

5-13. Coordinate system for comparison of APT's in methanol and in acetone ---------- 213

A-1. Geometry for methanol ---------- 224

A-2. Geometry for ethanol ---------- 235

A-3. Geometry for dimethyl ether ---------- 250

A-4. Geometry for formaldehyde ---------- 257

A-5. Geometry for acetone ---------- 260

Abstract of Dissertation Presented to the Graduate Council
of the University of Florida in Partial Fullfillment of the
Requirements for the Degree of Doctor of Philosophy

INFRARED INTENSITIES OF ALCOHOLS AND ETHERS

By

Jerry Dale Rogers

August, 1980

Chairman: Willis B. Person
Major Department: Chemistry

Infrared intensities of gas-phase methanol have been remeasured experimentally using the technique of Wilson and Wells as modified by Penner and Weber. The values measured are in reasonable agreement with literature values, and best estimates are made for the absolute intensities of the vibrational modes of methanol. These intensities are used together with an ab initio quantum mechanical calculation of the signs of the dipole moment derivatives to derive atomic polar tensors for methanol. The effects both of the normal coordinates and of other sign choices on the atomic polar tensors for methanol are discussed. These polar tensors are used to predict the infrared intensities for ethers and higher alcohols.

The infrared intensities of methanol, ethanol, dimethyl ether, and acetone are predicted using atomic polar tensors transferred from other molecules. The absolute intensities predicted for these molecules are compared with the experimental absolute intensities,

which have been remeasured. The intensities predicted for the alcohols and the ether agree with the experimental intensities to within a factor of two, but serious discrepancies are seen in the intensities predicted for the ketone.

The atomic polar tensors for methanol, ethanol, formaldehyde, and acetone have been calculated by the self-consistent field method using a 4-31G basis set. The absolute intensities predicted by these quantum mechanically calculated polar tensors are in factor-of-two agreement with experiment both for the alcohols and for the ketones.

The comparison of the transferred atomic polar tensors and the quantum mechanically calculated atomic polar tensors is discussed for each molecule. This comparison for acetone indicates that the polar tensors transferred from formaldehyde to acetone do not predict correctly the intensity of the carbonyl stretch because the methyl groups in acetone are donating electrons to the carbonyl group. The comparison of the atomic polar tensors quantum mechanically calculated for the methyl hydrogens in methanol and in acetone indicates that the differences are due to the interactions of the methyl hydrogens in methanol with the trans nonbonding electrons on the oxygen atom.

CHAPTER 1
INTRODUCTION

Infrared intensities have been studied for many years; a major goal has always been to be able to predict accurately the expected infrared absorption intensities for the fundamental modes of vibration of any molecule. This idea of predicting infrared intensities is analogous to predicting the absorption frequencies of the vibrational modes of a molecule. Our ability to predict accurate frequencies for many molecular vibrations is well established, but a method for accurate intensity predictions has proved to be most elusive (1).

One problem with intensity data analyses and intensity predictions arises because the intensity of a particular normal mode of vibration depends upon the exact form of that vibrational mode (2,3). Furthermore, since absorption of infrared radiation by a molecule occurs only if there is a concomitant change in the molecular dipole moment and further that the resultant intensity depends upon the square of this dipole moment change (2), one finds that to analyze intensity data he needs some reliable method for establishing the direction, or the sign, of the dipole moment change. Another problem with intensity studies is that to even measure the absorption intensity of a vibrational mode can be a difficult task because a slightly haphazard experimental procedure can result in a band intensity value in error by integral multiples of the true value.

If the difficulties with infrared intensity analyses could be overcome to the point where accurate intensities were known for molecules, the results would be well worth the effort. Not only could one identify an unknown compound by its infrared absorption frequencies, but he could also check to see that the relative intensity pattern in the infrared spectrum was consistent with a presumed molecular structure. Another use for absolute intensities exists, but first we must consider the experimental definition of the absolute intensity of an infrared absorption band.

Experimental Absolute Intensities

The experimental infrared absolute band intensity may be defined as follows (4):

$$A_i = (1/C\ell) \int_{\text{Band}} \log_e (I_o/I) d\bar{\nu} \qquad (1\text{-}1)$$

Here A_i is the absolute intensity of the ith normal mode of vibration, C is the sample concentration, ℓ is the optical pathlength through the sample, I_o is the intensity of light incident on the detector in the absence of sample, I is the intensity of light incident on the detector in the presence of sample, $\bar{\nu}$ is the wavenumber of the radiation, and finally the integration is performed over the entire absorption band. We shall express the wavenumber $\bar{\nu}$ in units of cm^{-1}, the concentration in moles per cubic decimeter, and the optical pathlength in centimeters. The absolute intensity (A_i) will be reported in units of kilometers per mole. These units require that the right hand side of Eq. (1-1) be divided by 100.

There is an alternate definition for the absolute intensity wherein the integration is carried out with respect to d ($\log_e \bar{\nu}$); the

absolute intensity defined in this manner is given the symbol Γ_i (4):

$$\Gamma_i = (1/C\ell) \int_{\text{Band}} \log_e (I_o/I) d(\log_e \bar{\nu}) \qquad (1\text{-}2)$$

The definition of Γ is more closely related to the quantum mechanical result for the absolute intensity of an infrared transition than is A, but integration with respect to $\bar{\nu}$ has been easier to apply in practice, so A is in wider usage at the present time. Integration with respect to $\bar{\nu}$ has been easier to do mainly because most infrared spectrometers record spectra linear in wavenumber. The distinction between A and Γ is normally not too serious as the two quantities are related (4):

$$A_i \cong \Gamma_i \bar{\nu}_i \qquad (1\text{-}3)$$

where $\bar{\nu}_i$ is the band origin of the ith vibrational mode.

Absolute intensities are measured by making Beer's law plots of $AC\ell$ vs. $C\ell$ and the slope of the least squares fit to the data is taken as the absolute intensity. We shall discuss in Chapter 2 how linear Beer's law plots for infrared absorption bands can be obtained.

Another application of absolute intensities now suggests itself. One can estimate concentrations of substances that are not easily determined by other techniques. One can measure the integrated area of a sample band, and, knowing the absolute intensity, calculate the concentration-pathlength product. If he is clever enough to find a way of estimating the pathlength, he can calculate the concentration. Such a procedure has been used to estimate concentrations in matrix-isolated samples (5).

Quantum Mechanical Treatment of Infrared Intensities

The absolute intensity of an infrared absorption band is equal to (4)

$$A_i = (8\pi^3 N\bar{\nu}_i/3hc)\,|\langle\psi_{v'}|\hat{\vec{p}}|\psi_{v''}\rangle|^2 \qquad (1\text{-}4)$$

where $\psi_{v'}$ is the wavefunction for the vibrationally excited state v' and $\psi_{v''}$ is the wavefunction for the initial state v". The $\hat{\vec{p}}$ is the dipole moment operator, and $\bar{\nu}_i$ is the wavenumberof the ith absorption band. The dipole moment function is usually expanded in a Taylor series in the normal coordinates and only the linear terms are kept. If now harmonic oscillator wavefunctions are substituted into Eq. (1-4), the following expression for A_i is obtained (4):

$$A_i = (N\pi d_i/3c^2)\,|\partial\vec{p}/\partial Q_i|^2 \qquad (1\text{-}5)$$

Here N is Avogadro's number, d_i is the degeneracy of the ith fundamental vibration, and c is the velocity of light. The quantity $\partial\vec{p}/\partial Q_i$ is the dipole moment change that occurs when the ith normal mode (Q_i) is excited. The magnitude of this dipole moment change may be calculated from experimentally measured absolute intensities by combining Eqs. (1-1) and (1-5). The sign of the dipole moment change will remain indeterminant because the dipole moment change is squared in Eq. (1-5). We shall see that determining this sign can be a major problem indeed in the interpretation and prediction of infrared absolute intensities.

Equation (1-5) also implies that the absolute intensity depends upon the form of the normal coordinate Q. These normal coordinates (2) are the vibrational coordinates for which the Schrödinger equation for harmonic oscillator wavefunctions becomes separable (6). Unfortunately, the vibrational motions of the molecules represented by these normal

coordinates are not very useful for interpretative purposes as several or all of the nuclei are in motion at the same time. These normal coordinate vibrations may, however, be expressed as linear combinations of vibrations in internal coordinate space (3) where now the vibrations are combinations of simple bond stretches, angle deformations, or torsions about chemical bonds. The dipole derivatives may also be transformed to this internal coordinate space; such a transformation yields dipole derivatives which have a chemical meaning. The dipole moment change that results when an O-H bond in one alcohol is stretched may be compared with that for another alcohol. Or, the dipole moment change for one molecule may be transferred to another similar molecule to test the transferability of the intensity parameter. In actual practice a rotational correction (7) is required before dipole derivatives in internal coordinate space are compared for different molecules. This point will be discussed in some detail later.

Interpretative Approaches to Intensities

Workers in the field of infrared spectroscopy have tried to use the dipole moment changes with respect to internal coordinates to predict infrared absolute band intensities (8). It was hoped, for example, that an O-H stretch in one alcohol would have the same dipole moment change as another related alcohol, or that a methylene bending vibration would induce the same dipole moment change for related compounds all containing a methylene group.

The use of electro-optical intensity parameters (6,9) has been pioneered by Soviet workers (10). In this intensity model, the total molecular dipole moment is taken as a sum of all the individual bond

dipole moments. This sum is then differentiated with respect to the internal coordinates to obtain the electro-optical parameters. However, such a differentiation leads to cross terms such as the change in the dipole moment of one C-H bond with respect to stretching another C-H bond. Such terms are difficult to put on an intuitive basis for sign prediction, especially when such cross terms may be just as large as those involving the same bond (11). Often, the signs of these electro-optical parameters are chosen purely upon the basis of chemical intuition.

The atomic polar tensor method of analyzing intensity data was introduced in 1961 by Biarge, Herranz, and Morcillo (12) and later reformulated by Person and Newton (13). In the atomic polar tensor (APT) approach, the dipole derivatives are transformed from internal coordinate space to space-fixed cartesian coordinate space. The resulting dipole moment derivatives are now no longer associated with bond or angle changes, but with cartesian displacement coordinates of the atoms of the molecule. The APT dipole derivatives are the changes in the x, y, and z components of the total molecular dipole moment when a particular atom in the molecule is displaced along one of the space-fixed cartesian axes x, y, or z. The APT for an atom is thus a tensor of the second rank, and we define a typical element as $\partial p_i / \partial j_\alpha$ where p_i is the ith component (x, y, or z) of the molecular dipole moment p, and j_α is the displacement direction (x, y, or z) of atom α. One would hope, then, that these APT's would be characteristic of the atom and would be transferable to other like atoms in similar molecules. Such investigations of the transferability of APT's for certain atoms, notably fluorine, have met with reasonable success in the prediction of

infrared intensities (14-17). We hope to demonstrate in this dissertation that APT's are often transferable among organic molecules with similar structural units.

We might briefly contrast the differences in the electro-optical and atomic polar tensor theories for infrared intensities. Let us consider the electro-optical and APT approaches applied to the specific case of ethanol for predicting the absolute intensities of the twenty-one fundamental modes of vibration. In the electro-optical treatment (18), twenty-six intensity parameters were needed for the first-order approximation (6). Six of these parameters were transferred from the electro-optical parameters for methanol (18) and two parameters from propane (19); the other eighteen electro-optical parameters were adjusted until the twenty-six parameters for ethanol reproduced the experimental absolute intensities. In the APT approach used in this dissertation, APT's for the atoms in the CH_2OH group will be transferred to ethanol from methanol, and APT's for the atoms in the CH_3 structural unit of ethanol will be transferred from ethane. Prediction of the absolute intensities for ethanol in the APT approach is thus indeed a prediction - no parameter fitting to the experimental data is made.

We might also mention that these APT's are particularly easy, conceptually at least, to calculate quantum mechanically. The term $\partial p_i/\partial j_\alpha$ is approximated as $\Delta p_i/\Delta j_\alpha$ and from a calculation of the equilibrium dipole moment and a calculation of the dipole moment after displacement of the αth atom of the molecule a small distance along j, $\partial p_i/\partial j_\alpha$ can be calculated. The displacements for the atoms are particularly well-defined and easily applied because the displacements

are along the space-fixed axis system. The disadvantage to such a procedure for calculating the APT's is that in the most general case, the dipole moment calculation must be repeated six times for each atom in the molecule. (Here we assume that both positive and negative displacements along each of the three space-fixed cartesian axes will be averaged to better approximate the anharmonicity of the dipole derivative.) To be sure, molecular symmetry and the null condition governing the APT's (Chapter 3, Eq. (3-25)) reduces the total number of calculations necessary, but the number is still quite large for moderately sized molecules of low symmetry. Recently, Komornicki and McIver (20) have introduced a much more computationally feasible method for calculating dipole moment derivatives. This method involves a calculation of the potential energy gradient in the presence of an applied external electric field. The resulting derivatives are equivalent to the APT elements.

We shall be concerned in this dissertation with the absolute intensities of the absorption bands in the infrared spectra of the organic molecules methanol, ethanol, dimethyl ether, formaldehyde, and acetone. We shall discuss in Chapter 2 the measurements of the absolute intensities for the infrared absorption bands of the first three molecules. The absolute intensities we have measured for methanol, ethanol, and dimethyl ether are in reasonable agreement with previous measurements; our error limits are rather small for the intensity measurements we made with a Nicolet Model 7199 Fourier Transform Infrared Spectrometer (FT-IR), and we expect to see a rapid growth in studies of infrared intensities once computerized spectrometers are routinely available in chemical laboratories.

We have used the absolute intensities measured for the infrared absorption bands of methanol to derive, using the method of analysis outlined in Chapter 3, a set of experimental atomic polar tensors for methanol. This analysis is presented in Chapter 4. We shall be most interested to see how well these APT's transferred to other organic molecules can be used to predict infrared intensities for these other molecules. The intensities predicted for the infrared absorption bands of many of our series of molecules are discussed in Chapter 5.

Chapter 5 also presents a quantum mechanical investigation of the APT's and infrared intensities for our series of molecules. We shall be interested in ascertaining how well an ab initio calculation using a 4-31G basis set predicts infrared intensities for these molecules. The results of the ab initio intensity calculation for methanol will be used in conjunction with the experimental absolute intensities for the vibrational bands of methanol to derive experimental APT's. We shall also present a comparison of the ab initio calculated APT's for the same atoms in different molecules.

CHAPTER 2
EXPERIMENTAL INTENSITIES

Absolute infrared band intensities for gas phase molecules have proved to be rather difficult to measure accurately, and values reported by different workers often disagree by twenty percent or more; even factor-of-two disagreements are not unknown. We have, therefore, remeasured the gas phase absolute band intensities for the fundamental vibrations of methanol with the view toward deriving atomic polar tensors for methanol from the experimental data. We have also remeasured the gas phase absolute band intensities for ethanol and dimethyl ether in order to provide experimental data with which to compare our predicted intensities. This chapter contains a discussion of the experimental procedures.

The absolute intensity of an infrared absorption band was defined in Chapter 1 (Eq. (1-1) and the definition is repeated below:

$$A(\text{km mol}^{-1}) = (1/100C\ell) \int_{\text{Band}} \log_e (I_o/I)\, d\nu \qquad (2\text{-}1)$$

Here the concentration C is expressed in mol dm^{-3}, and the cell pathlength ℓ is expressed in cm. Measurements of an absolute intensity are difficult primarily because I_o and I and hence the integral in Eq. (2-1) are difficult to measure accurately.

One of the difficulties encountered with intensity measurements made with a prism or grating spectrometer arises because a monochromator set at ν_o actually transmits a range of frequencies. This frequency

distribution about ν_o arises both from diffraction effects determined by the dimensions of the dispersing element and from diffraction around the finite slit openings through which the light passes (21). The distribution about ν_o is given by the spectrometer slit function $g(\nu,\nu_o)$ (4). For infinitely narrow slits, the intensity distribution of the frequencies about ν_o is a sinc function; finite slit widths distort this distribution, and the exact functional form of $g(\nu,\nu_o)$ becomes difficult to evaluate. Fortunately, $g(\nu,\nu_o)$ rapidly approaches zero as ν becomes much different from ν_o if the monochromator is reasonably efficient.

The spectrometer slit function must be explicitly considered in the calculation of the intensity I at frequency ν_o. Thus we write (4)

$$T(\nu_o) = \int_0^\infty I(\nu)g(\nu,\nu_o)d\nu \qquad (2\text{-}2)$$

where $I(\nu)$ is the intensity at ν and $T(\nu_o)$ is the apparent intensity at ν_o. The expression for the absolute intensity (Eq. (2-1)) must also be modified because of this finite slit width problem:

$$A_i = (1/C\ell) \int_{Band} \log_e \left\{ \frac{\int_0^\infty I_o(\nu)g(\nu,\nu_o)d\nu}{\int_0^\infty I(\nu)g(\nu,\nu_o)d\nu} \right\} d\nu \qquad (2\text{-}3)$$

Equation (2-3) is a much more formidable expression for the absolute intensity than is Eq. (2-1), and the task becomes one of finding experimental conditions for which Eq. (2-3) reduces to Eq. (2-1).

Wilson and Wells (22) showed that if neither I_o nor I varied rapidly over the spectrometer slit function half-width (See Appendix B

for a discussion of half-widths), Eq. (2-3) reduces to Eq. (2-1) as the concentration-pathlength product approaches zero. Thus, by plotting ACℓ *vs.* Cℓ and calculating the slope of the tangent at the origin, one obtains the true intensity. The experimental conditions necessary to fulfill the assumptions made by Wilson and Wells are not easily met. The intensity I_o fluctuates rapidly in regions of atmospheric water and carbon dioxide absorptions if the spectrometer is not carefully purged with a non-absorbing gas. More difficult to overcome is the condition that I be relatively constant over the spectral slit width. For gaseous molecules at low pressure, the rational fine structure of the vibrational bands has half-widths on the order of thousandths of a wavenumber; grating spectrometers usually have resolutions approaching only half a wavenumber or so under the best of conditions. The condition of a slowly varying I is thus not easily met for gas phase intensity measurements.

Penner and Weber (23) demonstrated that straight line Beer's law plots passing through the origin could be obtained if an inert foreign gas were added to the sample gas to broaden the individual vibration-rotation lines until their half-widths were large compared to the resolution of the spectrometer. The pressure of broadening gas necessary for a straight line Beer's law plot can be experimentally determined from a plot of ACℓ for a particular choice of Cℓ *vs.* broadening gas pressure. The apparent integrated area at first increases and then becomes constant as the pressure is increased. Broadening gas pressures corresponding to the constant portion of the curve are required if accurate absolute intensities are to be

measured. In practice, small, light molecules such as CO or HCl with large rotational line spacings require higher broadening gas pressures than do heavier molecules such as dimethyl ether with small line spacings. For a molecule such as dimethyl ether, the density of vibration-rotation states is very large, and even a moderate total pressure causes the absorption lines to begin to overlap. For a given region of the infrared spectrum of dimethyl ether, there also may be several different overlapping vibrational modes which further increase the density of absorption lines. For HCl the rotational lines lie far apart (about 21 cm^{-1} (24)), so enough pressurizing gas must be added to broaden each line until the half-width is large compared to the resolution of the spectrometer.

Experimental Outline

We have remeasured the gas phase absolute band intensities for the fundamental vibrational bands of methanol, ethanol, and dimethyl ether. The absolute intensities were determined by applying the technique of Wilson and Wells (22) as modified by Penner and Weber (23). Before describing the detailed experimental procedures, we shall briefly describe the different spectrometers used for the intensity measurements.

Spectrometers

A Perkin-Elmer Model E-14 spectrometer and a Perkin-Elmer Model 621 spectrometer were used for the intensity measurements of the vibrational modes of methanol. The Perkin-Elmer Model E-14 spectrometer (described more fully in reference 25) is a single beam instrument utilizing a monochromator with an Ebert mounting.

The spectrometer records spectra linear in wavelength rather than wavenumber; the ordinate scale is linear in transmittance. The whole optical cavity of the spectrometer can be continuously purged with dry nitrogen gas. The Perkin-Elmer Model 621 spectrometer is a double beam instrument and has a modified sample compartment capable of accepting gas cells up to 29 cm in length. The Model 621 records spectra linear in wavenumber, and the ordinate scale can be plotted linear in either absorbance or percent transmittance. Maximum resolution on either instrument is limited to several tenths of a wavenumber.

Some time after the measurements for methanol were completed, the University of Florida received a Nicolet Instrument Corp. Model 7199 Fourier transform infrared spectrometer (FT-IR). The absolute intensity measurements for ethanol and dimethyl ether were made with the Nicolet Model 7199 FT-IR. The heart of this spectrometer system is a Michelson interferometer which gives a guaranteed maximum resolution of 0.06 cm^{-1}; this resolution is at least an order of magnitude better than that provided by either of the two Perkin-Elmer grating spectrometers described above. Like the Perkin-Elmer Model E-14 spectrometer, the Nicolet Model 7199 FT-IR operates in a single beam mode. Any atmospheric water or carbon dioxide present in the optical path can appear in the ratioed spectrum if the amounts differ for the sample scan and the background scan. Although the whole optical bench was continuously purged with dry nitrogen, ratioed spectra almost always still showed positive or negative water and/or carbon dioxide absorption bands.

General Procedure

Curves of I_o as a function of wavenumber were measured by filling an evacuated sample cell with only the pressurizing gas and then scanning the infrared spectrum. To obtain the I curve, the cell was evacuated and then filled to the desired pressure of sample gas. The pressurizing gas was not immediately added to the cell; rather, the entire line up to the cell inlet valve was pressurized up to the pressure used to determine I_o and then pumped back down. This line flushing procedure was repeated three times before the pressurizing gas was actually admitted to the cell. The pressurizing gas was admitted to the cell by opening the cell valve for about three seconds. The spectrum of this mixture was scanned to provide the I curve. Computation of the quantity $\log_e(I_o/I)$ as a function of wavenumber (manually for spectra recorded with the Perkin-Elmer spectrometers or by computer for spectra measured with the FT-IR) gave the spectral band which was to be integrated as suggested by Eq. (2-1).

Spectral regions measured on the Perkin-Elmer Model E-14 spectrometer were numerically integrated as follows. Values of I_o and I as a function of wavelength were read off the spectral recordings; these values were then used to compute $\log_e(I_o/I)$ as a function of wavelength. After conversion of the wavelength values to wavenumber values, the resulting absorption bands were numerically integrated using a programmable calculator according to Simpson's rule. The number of wavenumber points used to numerically compute the quantity $\int \log_e(I_o/I)d\nu$ in each spectral region was chosen by reintegrating the area for a particular sample concentration with

ever smaller wavenumber increments until no significant change in the total area occurred. About a hundred points were usually required. Numerical integrations for spectra recorded with the Perkin-Elmer Model 621 spectrometer were made in exactly the same way as with the data recorded with the Perkin-Elmer Model E-14 except that the abscissa was already linear in wavenumber.

Integrations for spectra recorded with the Nicolet Model 7199 FT-IR were inherently easier. Band integrations were made using the integration routine supplied by Nicolet Instrument Corp. as part of the FT-IR software package (26). This routine numerically computes $\int A d\nu$ between the specified integer wavenumber limits of integration. The absorbance values, though, are computed as $\log_{10}(I_o/I)$ by the Nicolet computer, so the resulting areas must be multiplied by 2.303 to obtain integrated areas relative to absorbances defined as $\log_e(I_o/I)$. We found that the option to have the computer draw a baseline between the limits of integration did not produce accurate numerical integrations if a spectrum was at all noisy. Absorption band integrations were therefore made without a computer-drawn baseline, and then a baseline was manually drawn across a plot of each spectral region. The area contained beneath this manually drawn baseline was subtracted from the total band area calculated by the Nicolet computer.

The sequence to measure I_o and I and to integrate the resulting spectral absorption regions was repeated for several sample pressures. The data were plotted according to Beer's law as $AC\ell$ *vs.* $C\ell$, and the slope of the least squares fit (27) to the data gave the absolute intensity.

The sample cells had to be capable of withstanding large pressures for the intensity measurements done at several atmospheres of total pressure. We have used brass cells of a design described by Levine (25). The cells are fitted with 2.5 cm thick potassium bromide windows, and we have used pressures of over twenty atmospheres in such cells with no accidents. The cell inlet valve (Whitey union bonnet metering valve, 31 series) is mounted such that the gases are admitted tangentially to the cell cavity to promote better gas mixing. All the intensity measurements for methanol and dimethyl ether were made with such cells. The methanol measurements were made with either a 3.28 $\pm$ 0.02 cm brass cell or a 22.7 $\pm$ 0.1 cm brass cell depending upon the intensity of the spectral region. The measurements for dimethyl ether were all made using the 3.28 cm brass cell. Some of the measurements for ethanol were made using the 3.28 cm brass cell; unfortunately, some spectral regions of ethanol were too weak to obtain reliable integrated areas with the 3.28 cm brass cell. Since the 22.7 cm brass cell would not fit inside the sample compartment of the Nicolet Model 7199 FT-IR, glass sample cells had to be used for ethanol for some of the measurements. Of course, only atmospheric pressures of nitrogen could be used in these glass cells.

The sample gas pressures were measured with both an open-ended mercury manometer and an MKS Instruments Baratron Type 221 capacitance manometer with a range of 0 to 100 torr (0Pa to 13.3 kPa). Pressure readings measured with the MKS baratron were calibrated against the pressure readings on a McLeod gauge covering the range of 0.7 Pa to 0.3 kPa (1 kPa = 7.502 torr). Pressure readings of 5 torr on the MKS baratron could be read to 0.01 torr and were reproducible to at

least ± 0.02 torr. A Matheson Type 2 two-stage regulator was used to measure nitrogen pressures greater than 0.1 MPa (0.987 atm); nitrogen pressures of 0.1 MPa (1 atm) were measured with an open-ended manometer.

Sample concentrations were calculated from the measured sample pressures using the ideal gas law (C = P/RT). One might expect methanol, ethanol, and dimethyl ether to be rather non-ideal gases due to intermolecular interactions, so the concentration for the highest sample pressure ever used in these measurements was also calculated for each gas using the van der Waals equation of state. The van der Waals constants for the three gases were taken from reference 28. Comparison of the concentrations calculated from the two equations of state for each gas showed that the nonideality of any of the gases was entirely negligible over the pressure ranges used in this study.

Methanol

Survey Spectrum

Figure 2-1 shows a survey infrared spectrum of methanol vapor measured with the Nicolet Model 7199 FT-IR. We first briefly locate the major absorption regions due to methanol. The O-H stretching mode ν_1 is found at about 3670 cm^{-1}. The absorption feature just below 3000 cm^{-1} is due to the C-H stretching modes ν_2, ν_3 and ν_9. The methyl group bending vibrations (ν_4, ν_5, and ν_{10}) occur around 1450 cm^{-1} and are partially overlapped by the COH bending mode ν_6 at about 1340 cm^{-1}. The other large absorption feature in the spectrum is the C-O stretching mode ν_8 occurring at 1034 cm^{-1}. The two methyl twisting vibrations ν_7 and ν_{11} occur at 1145 cm^{-1} and 1077 cm^{-1}, respectively; ν_{11} is so weak as to be nondiscernible, while ν_7 is overlapped by the R-branch

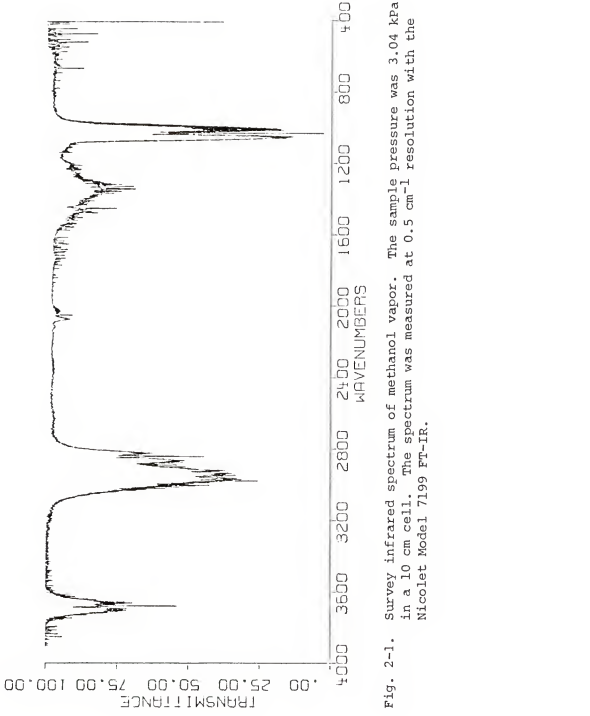

Fig. 2-1. Survey infrared spectrum of methanol vapor. The sample pressure was 3.04 kPa in a 10 cm cell. The spectrum was measured at 0.5 cm-1 resolution with the Nicolet Model 7199 FT-IR.

of the C-O stretching mode. Finally, the O-H torsional mode ν_{12} at 272 cm^{-1} falls below the lower wavenumber limit accessible with potassium bromide windows and is not visible in Fig. 2-1. We might also point out that the feature at 2055 cm^{-1} is the first overtone of the C-O stretch and that water vapor in the optical path is responsible for the line absorptions around 3700 cm^{-1} and 1700 cm^{-1}. The "noise" on many of the absorption bands (e.g. the C-O stretching region) is actually vibration-rotation fine structure; the true noise level can easily be estimated from the baseline absorbance around 2200 cm^{-1}.

Experimental Conditions

No impurities were detected in the infrared spectra of either the prepurified nitrogen (Airco) or the methanol (Mallinckrodt spectrophotometric grade), so they were used without purification, except that the methanol was stored over molecular sieve. Pressures of methanol (vapor pressure at 25°C = 15.3 kPa (28)) ranged from 0.8 kPa up to 6.7 kPa, and were measured with the MKS baratron. For the weak O-H stretching mode, pressures ranged from 3.3 kPa up to 11.3 kPa. (Note that 1 kPa = 7.502 torr.).

Spectra for the intensity measurements were recorded with the Perkin-Elmer Model E-14 spectrometer. The O-H and C-H stretching regions of methanol were recorded at an average spectral slit width of 0.9 cm^{-1} while the C-O stretching region was recorded at an average spectral slit width of 0.6 cm^{-1}. For the intensity measurements on the weakly absorbing CH_3 bending vibrational modes, the 22.7 cm brass cell had to be used instead of the 3.28 cm brass cell used for the regions mentioned above. The 22.7 cm cell, however, would not fit inside the sample compartment of the Perkin-Elmer Model E-14 spectrometer, so

the Perkin-Elmer Model 621 was used. The average spectral slit width on the Model 621 was set at 0.8 cm^{-1}. A measurement of the C-O stretching intensity with both the spectrometers resulted in comparable intensity values.

We have investigated the effect of pressure broadening on the measured intensities. The broadening gas pressure should be sufficiently large to broaden the sample absorption line half-widths to a much larger value than the resolution of the spectrometer. This condition is met when the apparent integrated area of an absorption band becomes constant with respect to increasing broadening gas pressure. A curve of the apparent intensity of the C-O stretching vibration of methanol as a function of broadening gas pressure is shown in Fig. 2-2. The spectra were scanned with the Perkin-Elmer Model E-14 spectrometer; the spectral slit width was set at 0.6 cm^{-1}. While the magnitudes of the data points suggest a slight increase in integrated area as the pressure of nitrogen is increased, the error limits prevent such a definite conclusion. We decided that approximately 1.13 MPa (11.2 atm) total pressure was sufficient at 0.6 cm^{-1} resolution for accurate intensity measurements of the C-O stretching region of methanol.

Ideally, the procedure represented by Fig. 2-2 should be repeated for each absorption region; practically, this is a time-consuming process, and only the C-O and C-H stretching regions of methanol were checked for sufficient pressure broadening. As the C-O stretching region of methanol shows the most resolvable band structure under moderate (0.5 cm^{-1}) and also high (0.06 cm^{-1}) resolution (See Fig. 2-3(a)), the other bands should certainly be sufficiently pressure broadened at the same pressures of nitrogen gas as was used for the C-O stretching region measurements.

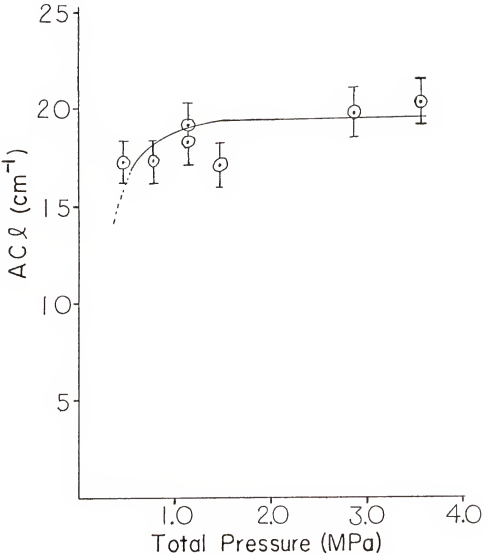

Fig. 2-2. The integrated area of the C-O stretching region of methanol as a function of total pressure. The pressure of methanol was held constant as the pressure of nitrogen was varied. Spectra were measured with the Perkin-Elmer Model 3-14 spectrometer.

Fig. 2-3. The effect of pressure broadening on the appearance of the C-O stretching region of the infrared spectrum of methanol. (a). The C-O stretching region of methanol is shown recorded at 0.5 cm^{-1} resolution with no pressurizing gas added. The spectrum for one of the rotational lines scanned at 0.06 cm^{-1} resolution is also shown. (b). The spectrum of the same region of methanol is shown scanned at 0.06cm^{-1} resolution with 1.13 MPa of nitrogen added. Spectra were recorded with the Nicolet Model 7199 FT-IR.

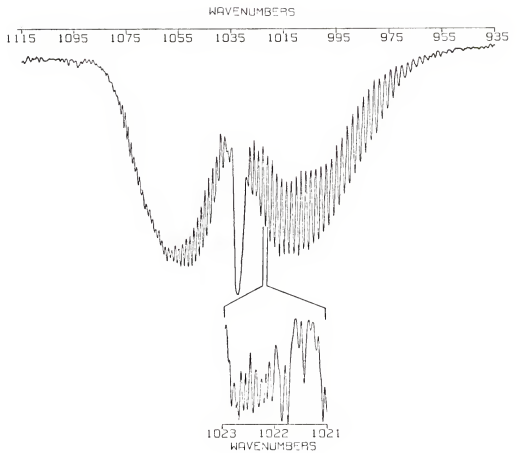
WAVENUMBERS
1115 1095 1075 1055 1035 1015 995 975 955 935
1023 1022 1021
WAVENUMBERS

(a)

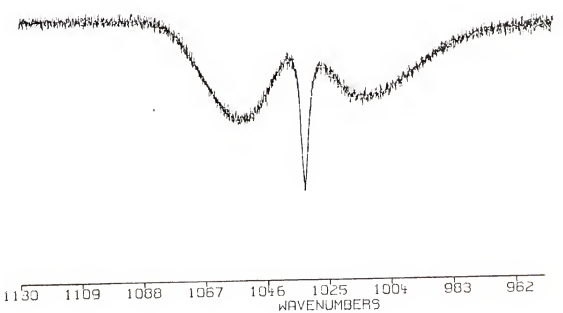
1130 1109 1088 1067 1046 1025 1004 983 962
WAVENUMBERS

(b)

The spectra shown in Fig. 2-3 were all measured with the Nicolet Model 7199 FT-IR, and we present in Fig. 2-3(b) the resulting band shape at 0.06 cm^{-1} resolution when 1.13 MPa of nitrogen is added. Fig. 2-3 dramatically shows the effects of pressure broadening. The total pressure of broadening gas necessary for the measurements of the absolute intensities for all the spectral regions of methanol was chosen to be 1.13 MPa.

Measurements of the integrated band intensities for methanol were made by first determining the I_o curve. The evacuated cell was filled with 1.13 MPa of prepurified nitrogen, and the spectral region of interest was scanned. The cell was next re-evacuated and methanol vapor admitted. The total cell pressure was increased to 1.13 MPa by the addition of nitrogen, and the spectrum was again recorded to provide the I curve. Mixing of the methanol vapor and nitrogen was aided by the fact that the cell inlet valve was mounted tangentially to the cell cavity. Furthermore, spectra were not scanned until thirty minutes had elapsed. Throughout this whole procedure of baseline and sample scanning, the cell was left undisturbed in the sample compartment of the spectrometer; this was made possible by fastening the cell inside the spectrometer and then connecting the cell with copper tubing to both the vacuum and high pressure lines.

We have measured absolute intensities for the O-H stretching region, integrated from 3850 cm^{-1} to 3571 cm^{-1}; the C-H stretching region, integrated from 3175 cm^{-1} to 2650 cm^{-1}; the C-H and O-H bending region, integrated from 1600 cm^{-1} to 1172 cm^{-1}; and the C-O stretching region, integrated from 1130 cm^{-1} to 930 cm^{-1}. The O-H torsional region at 272 cm^{-1} is outside the infrared transparent range of the potassium

bromide windows used for these intensity measurements; consequently, we have not measured the absolute intensity for this region.

Absolute Band Intensities for Methanol

Beer's law plots of the integrated areas for the four spectral regions we measured for methanol are shown in Fig. 2-4. Table 2-1 shows the absolute intensities we calculated from the Beer's law plots for the four absorption regions.

Table 2-1 also presents a comparison of the absolute intensities we determined for the spectral regions of methanol with literature values reported by various workers (18, 29-31). The comparison of our results with those reported by Zemlyanukhina, Sverdlov, and Finkel (18) is fairly good with the possible exceptions of the total intensities for the C-H and C-O stretching regions. The measurements reported by Zemlyanukhina et al. (18) were made using only 0.1 MPa pressure of nitrogen for pressure broadening; we found that under such conditions the rotational structure of the C-O stretching mode is not completely coalesced. This rotational structure is smoothed at the 1.3 MPa pressure used here (Fig. 2-3).

We have obtained "best estimates" of the total band intensities for the spectral regions of the infrared spectrum of methanol as follows. For the O-H stretching region, the value determined here (22 ± 3 km mol^{-1}) is the same as that reported by Zemlyanukhina et al. (18). The value measured here also agrees quite nicely with the value of 21 ± 5 km mol^{-1} reported by Broun (29). The value of 9.8 ± 5 km mol^{-1} reported by Inskeep, Kelliher, McMahon, and Somers (30) for the O-H stretching absolute intensity appears to be incorrect. The probable cause of such a low value for the absolute intensity is the low spectral resolution

Fig. 2-4. Beer's law plots for the spectral regions of the infrared spectrum of methanol.

(a) The O-H stretching region, integrated from 3850 cm^{-1} to 3571 cm^{-1}.
(b) The C-H stretching region, integrated from 3175 cm^{-1} to 2650 cm^{-1}.
(c) The C-H and O-H bending region, integrated from 1600 cm^{-1} to 1172 cm^{-1}.
(d) The C-O stretching region, integrated from 1130 cm^{-1} to 930 cm^{-1}.

The least squares line fit to the data for each of the regions is indicated.

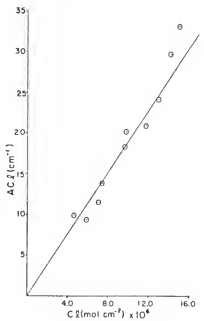
A C ℓ (cm⁻¹)
C ℓ (mol cm⁻²) x 10⁶
4.0
8.0
12.0
16.0
5
10
15
20
25
30
35

(a)

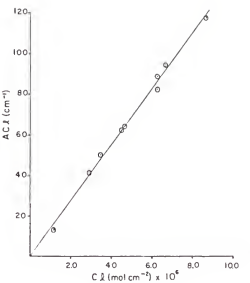
A C ℓ (cm⁻¹)
C ℓ (mol cm⁻²) x 10⁶
2.0
4.0
6.0
8.0
10.0
20
40
60
80
100
120

(b)

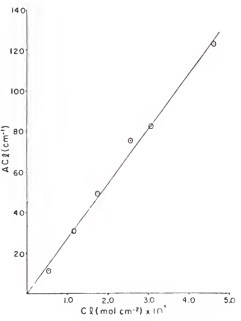
A C ℓ (cm⁻¹)
C ℓ (mol cm⁻²) x 10⁶
1.0
2.0
3.0
4.0
5.0
20
40
60
80
100
120
140

(c)

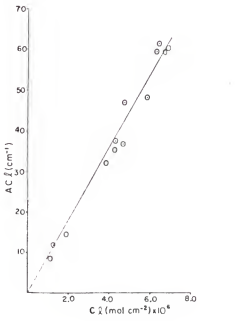
A C ℓ (cm⁻¹)
C ℓ (mol cm⁻²) x 10⁶
2.0
4.0
6.0
8.0
10
20
30
40
50
60
70

(d)

TABLE 2-1
EXPERIMENTAL GAS-PHASE ABSOLUTE BAND INTENSITIES FOR METHANOL
(units are km mol^{-1})

Spectral Region	Zemlyanukhina et al.[a]	Broun[b]	Inskeep et al.[c]	Margottin-Maclou and Henry[d]	This Work	Best Estimate[e]
O-H Stretch	22	21±5	9.8±5		22±3	22±1
C-H Stretch	116	109±15			138±8	127±10
C-H and O-H Bend	31				27.2±1.8	29±2
C-O Stretch	109			125±5	92±5	100±10
O-H Torsion	56				[f]	56±9

[a] Zemlyanukhina, Sverdlov, and Finkel(18). Note that $A(km\ mol^{-1}) = (N/cx10^5)A(cm^2\ molec^{-1}\ sec^{-1})$ $= 2.009x10^8 A(cm^2\ molec^{-1}\ sec^{-1})$

[b] Broun (29)

[c] Inskeep, Kelliher, McMahon, and Somers (30)

[d] Margottin-Maclou and Henry (31)

[e] See text

[f] Not measured in this work

(5 cm^{-1}) used by Inskeep et al. (30). Based on all the values available for the absolute intensity of the O-H stretching region except the value reported by Inskeep et al. (30), we estimate the absolute intensity to be 22 $\pm$ 1 km mol^{-1}.

The absolute intensity of 138 $\pm$ 8 km mol^{-1} for the C-H stretching region is substantially higher than either the value reported by Zemlyanukhina et al. (18) or Broun (29) (116 km mol^{-1} and 109 $\pm$ 15 km mol^{-1}, respectively). We shall disregard the value given by Broun because the intensity was measured in solution and then scaled to produce a gas phase value. (See reference 29 for details.) We have simply averaged the total intensity reported here and the one reported by Zemlyanukhina et al. (18) to obtain a best estimate of 127 $\pm$ 10 km mol^{-1} for the absolute intensity of the C-H stretching region.

Our value of 27.2 $\pm$ 1.8 km mol^{-1} for the absolute intensity of the C-H and O-H bending region is in reasonable agreement with the value (31 km mol^{-1}) reported by Zemlyanukhina et al. (18). We have arrived at a best estimate of 29 $\pm$ 2 km mol^{-1} for this region by averaging the two values.

For the C-O stretching region, our measured value of 92 $\pm$ 5 km mol^{-1} for the absolute intensity is in fair agreement with the value (109 km mol^{-1}) reported by Zemlyanukhina et al. (18), but quite lower than the value of 125 $\pm$ 5 km mol^{-1} reported by Margottin-Maclou and Henry (31). We have assumed our value and the value reported by Zemlyanukhina et al. to be more accurate and have averaged these two values to arrive at a best estimate of 100 $\pm$ 10 km mol^{-1} for the absolute intensity.

Finally, the only available datum for the absolute intensity of the O-H torsional region (about 270 cm^{-1}) is that reported by

Zemlyanukhina et al. (18), so the value of 56 km mol^{-1} they report is assumed to be correct. We were not able to measure the absolute intensity of this region because it lies outside the accessible frequency range of the potassium bromide cell windows.

Estimation of Absolute Intensities for the Normal Vibrational Modes of Methanol

In anticipation of deriving atomic polar tensors for methanol (Chapter 4) from the experimental intensity data, we shall discuss the division of the total intensity for each of the spectral regions among the normal modes. Accomplishing this separation from a purely experimental point of view is virtually impossible due to overlapping normal modes; for example, five normal modes (ν_4, ν_5, ν_6, ν_{10}, and ν_{11}) occur in the C-H and O-H bending region (See Fig. 2-1). We do have available, however, the calculated intensity separation based on electro-optical parameters (18) and also a quantum mechanical intensity separation reported by Serrallach, Meyer, and Günthard (32). The quantum mechanical calculation (33) of the relative absolute intensities for the vibrational bands of methanol was an ab initio self-consistent field calculation near the Hartree-Fock limit (34). We have used the results of these two calculations (18, 32) to aid in the estimation of the absolute intensity for each normal mode of methanol.

Absolute intensities for two of the vibrational modes of methanol can be assigned immediately. Since the O-H stretching region contains only ν_1, the intensity is taken directly from Table 2-1 as 22 $\pm$ 1 km mol^{-1}. Only one normal mode (ν_{12}) occurs below 400 cm^{-1}, so the O-H torsional mode is assumed to have an absolute intensity of 56 $\pm$ 9 km mol^{-1} as listed in Table 2-1. The absolute intensities estimated for ν_1 and ν_{12},

as well as the normal modes discussed below, are collected in Table 2-2. The intensity distributions calculated by Zemlyanukhina et al. (18) and by Serrallach et al. (32) are also indicated in Table 2-2.

Best estimates for the absolute intensities of the three normal modes (ν_2, ν_3, and ν_9) in the C-H stretching region are more difficult to make because the three modes overlap. The absolute intensity for ν_3, which is experimentally fairly well separated except for the R-branch from the other two stretching modes, is taken to be 28 $\pm$ 1 km mol^{-1}. This value was obtained by assuming that the R-branch of the PQR structure of ν_3 was of the same intensity distribution as the P-branch and then numerically integrating the area of the resulting band shape. This procedure was followed for all the measurements made on the C-H stretching region, and from a Beer's law plot of the results, the absolute intensity of ν_3 was calculated to be 28 $\pm$ 1 km mol^{-1}. The estimate for the absolute intensity of ν_2 is the average of the intensities calculated by Zemlyanukhina et al. (18) and Serrallach et al. (32). The absolute intensity for ν_9 is then given by the condition that the total intensity for the C-H stretching region is 127 km mol^{-1}. We chose the averaging procedure for ν_2 rather than for ν_9 because the two sets of calculated values (Table 2-2) are in closer agreement for ν_2 than for ν_9.

The C-H and O-H bending region contains five overlapping modes (ν_4, ν_5, ν_6, ν_{10}, and ν_{11}). The values for the individual absolute intensities of all the normal modes in this region except the O-H bending mode ν_6 are again the average of the values calculated by Zemlyanukhina et al. (18) and by Serrallach et al. (32). The intensity

TABLE 2-2

EXPERIMENTAL ABSOLUTE INTENSITIES FOR THE NORMAL MODES OF METHANOL

(units are km mol^{-1})

Mode[a]		Best Estimate for Region[b]	Calculated Separation of Intensities: Electro-optical Parameters[c]	Calculated Separation of Intensities: ab initio[d]	Best Estimate for Separation[e]
ν(OH)	ν_1(3667)	22±1	22	22[f]	22±1
$\nu(CH)_{a.\ sym.}$	ν_2(3005)	127±10	39	30	35±5
$\nu(CH)_{a.\ sym.}$	ν_9(2962)		46	71	64±13
$\nu(CH)_{sym.}$	ν_3(2848)		29	39	28±1
$\delta(CH)_{a.\ sym.}$	ν_4(1474)	29±2	1.6	0.7	1.2±0.5
$\delta(CH)_{a.\ sym.}$	ν_{10}(1466)		1.7	1.5	1.6±0.1
$\delta(CH)_{sym.}$	ν_5(1451)		7.8	6.4	7.1±0.4
δ(OH)	ν_6(1335)		18.3	13.5	18±3
$\gamma_{\perp}$ (CH)	ν_{11}(1145)		1.5	0.4	1.0±0.6
$\gamma_{\parallel}$ (CH)	ν_7(1077)	100±10	30	2.8	4±0.4
ν(CO)	ν_8(1034)		82	71	96±10
τ(OH)	ν_{12}(272)	56±9	56	[g]	56±9

---

continued

TABLE 2-2-continued

[a]Assignments and frequencies from Mallinson (56). The symbols are defined as: $\nu \equiv$ stretch, $\delta \equiv$ bend, $\gamma \equiv$ twist, $\tau \equiv$ torsion, and a. sym. $\equiv$ antisymmetric

[b]Taken from TABLE 2-1

[c]Zemlyanukhina, Sverdlov, and Finkel (18)

[d]Serrallach, Meyer, and Gunthard (32)

[e]See text

[f]All relative intensities in reference (32) normalized to this experimental absolute intensity

[g]Value not given in reference (32)

for ν_6 is obtained from the condition that the total absolute intensity for the region be 29 km mol^{-1}. The absolute intensity for ν_6 was chosen in this way because the value most differs in the two calculations (Table 2-2).

Two normal modes (ν_7 and ν_8) occur in the C-O stretching region of methanol. The R-branch of the very intense C-O stretching vibration (ν_8) completely overlaps the weak parallel twisting vibration (ν_7) of the methyl group. The assignment of 27% of the total intensity to ν_7 by Zemlyanukhina et al. (18) seems much too high compared to the relative intensities observed in matrix spectra of methanol (32). The 4% contribution by ν_7 to the total intensity as calculated by Serrallach et al. (32) is therefore assumed to be correct. On this basis, ν_7 is estimated to have an absolute intensity of 4 km mol^{-1}, while ν_8 then has an absolute intensity of 96 km mol^{-1}.

Ethanol

Survey Spectrum

A survey infrared spectrum of ethanol vapor is shown in Fig. 2-5. The spectrum was measured with the Nicolet Model 7199 FT-IR. The O-H stretching region containing ν_1 is centered at 3660 cm^{-1}. The two overlapped regions near 3000 cm^{-1} are due to the methyl and methylene hydrogen stretching modes (ν_2, ν_3, ν_4, ν_{14}, and ν_{15}). Several methyl and methylene hydrogen bending modes (ν_5, ν_6, ν_7, ν_8, and ν_{16}) absorb near 1400 cm^{-1}. The COH bending mode ν_9 absorbs at 1241 cm^{-1}; overlapped by ν_9 is a weak methylene twisting mode (ν_{17}). The C-O stretching mode (ν_{10}) absorbs at 1061 cm^{-1}; two twisting motions of C-H (ν_{11} and ν_{18}) also occur in this region and are obscured by the C-O stretching mode. The feature at 883 cm^{-1} is the C-C stretching mode (ν_{12}), while the weak absorption feature at

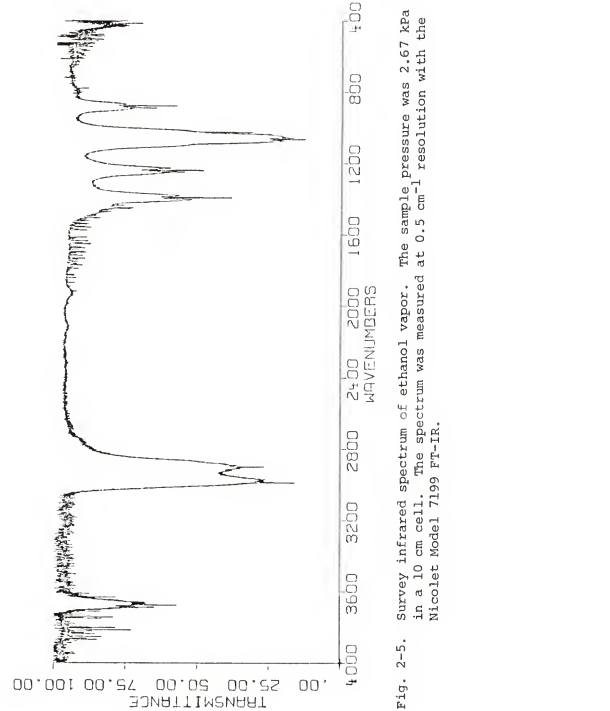

Fig. 2-5. Survey infrared spectrum of ethanol vapor. The sample pressure was 2.67 kPa in a 10 cm cell. The spectrum was measured at 0.5 cm^{-1} resolution with the Nicolet Model 7199 FT-IR.

801 cm^{-1} is another methylene twisting mode (ν_{19}). The absorption band superimposed on the large amplitude noise at 422 cm^{-1} is the CCO bending mode (ν_{13}). Both the methyl and hydroxyl torsional modes (ν_{20} and ν_{21}, respectively) absorb at 224 cm^{-1} and so they lie outside the infrared-transparent region spanned by the potassium bromide cell windows. Finally, excess atmospheric water in the sample scan compared to the empty cell scan gives rise to absorptions by water around 3800 cm^{-1} and 1600 cm^{-1} and also around 400 cm^{-1}.

Experimental Conditions

The absolute intensities of the vibrational modes of ethanol (U. S. Industrial Chemicals, absolute) were measured using both the 3.28 cm brass cell described earlier and glass cells (10 cm and 25 cm) fitted with 5 mm thick potassium bromide windows. Sample pressures of ethanol (vapor pressure at 25°C = 7.29 kPa (28)) ranged from 1.3 kPa up to 4.0 kPa; the pressures were measured with the MKS Baratron. The pressure readings measured with the MKS baratron were always checked against the open-ended mercury manometer to ensure that consistent readings were being measured. Several measurements of the absolute intensities for ethanol were made using 1.13 MPa of prepurified nitrogen (Airco) for pressure broadening, while other data were measured using only 0.1 MPa of nitrogen.

Spectra for samples at 1.13 MPa total pressure in the 3.28 cm brass cell were scanned at 0.5 cm^{-1} resolution. However, the low vapor pressure (7.29 kPa) of ethanol severely curtailed the accessible range of sample pressures. We found it necessary to use longer cells to give more intense absorption bands and still be able to use sample pressures below the vapor pressure of ethanol. The 22.7 cm brass cell would not

fit inside the sample compartment of the Nicolet Model 7199 FT-IR, so we used glass cells of 10 cm and 25 cm pathlength. Samples contained in the glass cells could be pressurized to only 0.1 MPa, so for these samples, the resolution was increased to 0.24 cm^{-1}.

Spectra were recorded on the Nicolet Model 7199 FT-IR. One hundred interferograms were averaged for each I_o and I curve. One level of zero filling (35, 36) was used, and the interferograms were Fourier transformed using a triangular apodization function. Triangular apodization was chosen as it most nearly corresponds to a grating spectrometer slit function (37). After the I_o and I curves had been scanned and the computer had transformed the interferograms, the infrared spectrum, linear in percent transmittance, was calculated by the computer. This spectrum was then converted by the computer to a spectrum linear in absorbance. General considerations for intensity measurements with Fourier Transform spectrometers have been further discussed by Scanlon, Laux, and Overend (37).

One spectrum of ethanol pressurized by nitrogen to 0.1 MPa was scanned at 0.06 cm^{-1} resolution to check that 0.24 cm^{-1} resolution at 0.1 MPa total pressure was sufficient to reproduce accurately the contours of the fundamental absorption bands. Several samples were scanned at 0.5 cm^{-1} resolution and with 1.13 MPa total pressure (brass cell!) to check that 0.1 MPa total pressure was sufficient for accurate band intensity measurements.

Water interferences in the ethanol O-H stretching region and the C-H bending region were removed by computer absorbance subtraction of a water absorbance spectrum from an ethanol absorbance spectrum. This was done by displaying both the water and ethanol absorbance spectra

simultaneously on the display screen of the Nicolet Model 7199 FT-IR. The water absorbance spectrum was then multiplied by various factors until the difference spectrum (ethanol-water) showed no water lines. The difference spectrum was then integrated over the spectral regions of interest. Anderson and Griffiths (38) have suggested that such subtraction procedures may have certain errors associated with them. Consequently, we reintegrated the C-H stretching region after the absorbance subtraction for several samples. The average deviation in the C-H stretching region was found to be less than $\pm$ 1% relative to the results obtained from the spectra still containing water.

Finally, we define the limits of numerical integration we used for the absorption regions of ethanol. The O-H stretching region was integrated between the limits of 3740 cm^{-1} and 3580 cm^{-1}, the C-H stretching region was integrated between 3080 cm^{-1} and 2600 cm^{-1}, the C-H bending region was integrated between 1600 cm^{-1} and 1318 cm^{-1}, the O-H bending region was integrated between 1318 cm^{-1} and 1168 cm^{-1}, the C-O stretching region was integrated between 1168 cm^{-1} and 952 cm^{-1}, and finally the C-C stretching region was integrated between 952 cm^{-1} and 825 cm^{-1}.

Absolute Band Intensities for Ethanol

Beer's law plots for the intensities of the infrared bands of ethanol are shown in Figs. 2-6 and 2-7. The absolute intensities, as well as 2σ error limits of the least squares lines through the data, are presented in Table 2-3. As we pointed out in the discussion of the survey infrared spectrum of ethanol, the normal modes ν_{13}, ν_{20}, and ν_{21} fall outside the range of the potassium bromide windows and hence were not measured here.

Fig. 2-6. Beer's law plots for the spectral regions of the infrared spectrum of ethanol involving no ambiguity in choice of baseline.

(a) The O-H stretching region, integrated from 3740 cm^{-1} to 3580 cm^{-1}.
(b) The C-H stretching region, integrated from 3080 cm^{-1} to 2600 cm^{-1}.
(c) The C-H bending region, integrated from 1600 cm^{-1} to 1318 cm^{-1}.

The least squares line fit to the data for each of the regions is indicated.

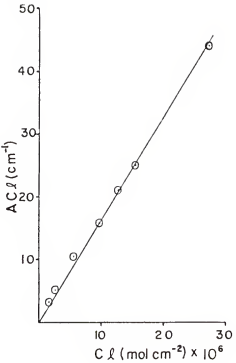
50
40
30
20
10
A C ℓ (cm⁻¹)
10
20
30
C ℓ (mol cm⁻²) x 10⁶

(a)

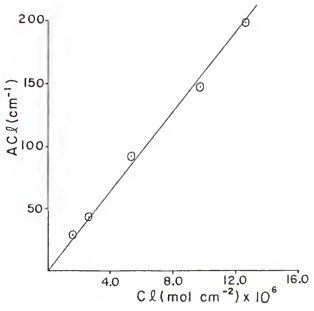
200
150
100
50
A C ℓ (cm⁻¹)
4.0
8.0
12.0
16.0
C ℓ (mol cm⁻²) x 10⁶

(b)

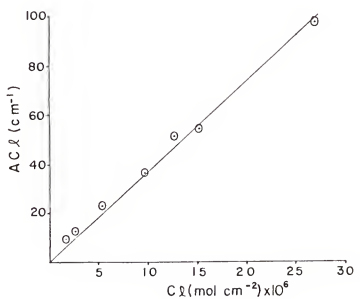
100
80
60
40
20
A C ℓ (c m⁻¹)
5
10
15
20
25
30
C ℓ (mol cm⁻²) x10⁶

(c)

Fig. 2-7. Beer's law plots for the spectral regions of the infrared spectrum of ethanol involving an ambiguity in the choice of baseline.

(a) The O-H bending region, integrated from 1318 cm^{-1} to 1168 cm^{-1}.
(b) The C-O stretching region, integrated from 1168 cm^{-1} to 952 cm^{-1}.
(c) The C-C stretching region, integrated from 952 cm^{-1} to 825 cm^{-1}.

The least squares line fit to the data for each of the regions is indicated. The points encircled (○) and the solid lines indicate data analyzed with respect to a baseline drawn from 1600 cm^{-1} to 700 cm^{-1}. The points enclosed by a triangle (△) and the dashed lines indicate data analyzed with respect to baselines drawn to connect the two minima for each band.

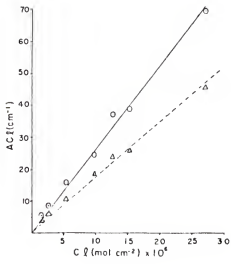
AC ℓ (cm⁻¹)
C ℓ (mol cm⁻²) x 10⁴

(a)

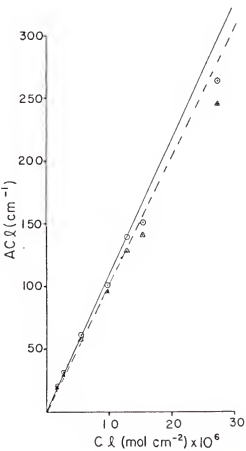
AC ℓ (cm⁻¹)
C ℓ (mol cm⁻²) x 10⁶

(b)

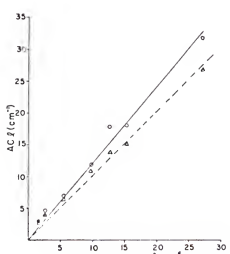
AC ℓ (cm⁻¹)
C ℓ (mol cm⁻²) x 10⁴

(c)

TABLE 2-3
ABSOLUTE INTENSITIES FOR ETHANOL
(units are km mol^{-1})

Mode[a]	This Work	Zemlyanukhina et al.(18)
	Absolute Intensity	
ν(OH) ν_1(3660)	16.4±0.6	17
ν(CH) ν_{14}(2987)	72	78
ν_2 (2971)		
ν_{15}(2930)	87	72
ν_3 (2901)	159±6	150
ν_4 (2890)		
δ(CH) ν_5 (1482)		12
ν_6 (1450)		
ν_{16}(1451)	37±2	48
ν_7 (1393)		36
ν_8 (1393)		
δ(OH) ν_9 (1241)	26.4±1.4[b]	30
δ(CH) ν_{17}(1241)	17.5±1[c]	
δ(CH) ν_{18}(1098)	109±5[b]	113
ν(CO) ν_{10}(1061)		
δ(CH) ν_{11}(1027)	102±4[c]	
ν(CC) ν_{12}(883)	12.1±0.6[b]	16
	10.2±0.6[c]	
δ(CH) ν_{19}(801)	1.1±0.04	1.2
δ(CCO)ν_{13}(422)	-[d]	7.2

---

continued

TABLE 2-3-continued

τ(CH) ν_{20}(224) τ(OH) ν_{21}(224)	-[d]	}58

[a] Assignments and frequencies from reference (18). See footnote (a) in TABLE 2-2 for explanation of symbols.

[b] Integration baseline drawn from 1600 cm^{-1} to 700 cm^{-1}.

[c] Integration baseline drawn between band minima.

[d] Not measured

We have also indicated in Table 2-3 an approximate separation of the two overlapping bands in the C-H stretching region. This separation was made by using the Curve Analysis Program (CAP) supplied by Nicolet Instrument Corp. as part of the FT-IR software package (39). CAP allows the user to fit up to 26 functions to an infrared spectrum; the functions may be Gaussian, Lorentzian, or a fixed percentage of each. The half-width, maximum intensity, and position of each function are continuously variable and under user control. When the best visual fit to the spectral region is obtained, the computer can be instructed to print out the relative areas of each of the fitted functions. The estimated intensity distribution obtained by fitting two Gaussian functions to the C-H stretching region indicates that the higher frequency set of bands (ν_2 and ν_{14}) contribute about 45% to the total intensity of the C-H stretching region of the infrared spectrum of ethanol.

The absolute intensity measurements in the region from 1600 cm^{-1} to 700 cm^{-1} present a problem since the twelve fundamental modes appearing in this region overlap to some extent. Examination of the infrared spectrum (Fig. 2-5) shows that the most intense band in this region is the one near 1060 cm^{-1} due to ν_{18}, ν_{10}, and ν_{11} where ν_{10} (the C-O stretch) is expected to dominate in intensity. We can see that the absorbance on the low frequency side of this band drops to a lower absorbance value than does the high frequency side. In fact, the general trend is that each band in the 1600 cm^{-1} to 700 cm^{-1} region has a higher absorbance value on the high frequency side. This phenomenon causes problems in the choice of a suitable baseline for this region since the extent of overlap of the bands is unknown.

Consequently, we have determined two intensities for bands in this region differing only in baseline choice. In one case, a baseline was drawn from 1600 cm^{-1} to 700 cm^{-1}; band intensities relative to that baseline were then determined between the limits of integration. This procedure would be expected to place an upper limit on the true absolute band intensity. A second choice was to draw a baseline that connected at the limits of integration the two minima of each absorption band region. This procedure should then give a lower bound to the true absolute band intensity. The actual estimation of the absolute band intensity was taken to be the average of the two values. We can see from Fig. 2-7 that either choice of baseline gives a satisfactorily linear plot obeying Beer's law with only minor scatter about the least squares line.

The integrated area of the very weak fundamental mode at 801 cm^{-1} (ν_{19}) was estimated by assuming a triangular band shape centered at 801 cm^{-1}. The absolute intensity was then calculated from the integrated area for each of the three largest Cℓ values and averaged. The result was an absolute intensity estimated to be 1.06 km mol^{-1} with a standard deviation of 0.02 km mol^{-1}.

Our results may be compared with those of Zemlyanukhina, Sverdlov, and Finkel (18). We see in Table 2-3 that with the exceptions of the O-H and C-H stretching regions we have determined absolute intensities that are systematically lower than the absolute intensities reported by Zemlyanukhina et al. (18). Since the regions for which the discrepancies in the absolute intensities occur are in the 1600 - 700 cm^{-1} region, we suspect that part of the disagreement is due to the ambiguity in the choice of a baseline absorbance in this region. We note in

particular that our higher value for the absolute intensity of the C-O stretching region is in excellent agreement with the value reported by Zemlyanukhina et al. (18). Furthermore, our higher value for the absolute intensity of the O-H bending region is in reasonable agreement. On the other hand, our value for the absolute intensity of the CH_3 and CH_2 bending region (1600-1318 cm^{-1}) seems definitely lower than the value reported by Zemlyanukhina et al. (18). This region shows strong water absorption lines which may effect the intensity measurements. As we discussed earlier, we subtracted by computer the water absorption lines in this region from the ethanol absorbance spectra.

As the absolute band intensities of the vibrational bands of ethanol were measured under 0.1 MPa total pressure, the possibility of insufficient pressure broadening exists. This possibility was investigated in two ways; first, a spectrum of one of the samples pressurized to 0.1 MPa was recorded at 0.06 cm^{-1} resolution rather than 0.24 cm^{-1} resolution. A noticeable increase in the absolute intensities for the spectral regions of ethanol would be expected for the spectrum at 0.06 cm^{-1} resolution compared to the spectrum taken at 0.24 cm^{-1} resolution if 0.1 MPa were insufficient total pressure. The apparent intensity for each of the absorption bands would increase because any very narrow, intense absorption lines would be better measured by the scan at 0.06 cm^{-1} resolution. Secondly, five ethanol spectra were recorded at 0.5 cm^{-1} resolution and 1.13 MPa total pressure; again, higher apparent intensities for the spectral regions would be expected for the samples pressurized to 1.13 MPa if 0.1 MPa were insufficient. The results of these two studies for

Fig. 2-8. Beer's law plots for regions of the infrared spectrum of ethanol under different sample conditions.

(a) The C-H stretching region
(b) The C-O stretching region
(c) The C-C stretching region

Here data for the circled points (Ⓞ) were measured at 0.24 cm^{-1} resolution with 0.1 MPa of nitrogen added. Data for the points enclosed in triangles (△) were measured at 0.5 cm^{-1} resolution with 1.13 MPa of nitrogen added. The points enclosed by a square (⊡) were measured at 0.06 cm^{-1} resolution with 0.1 MPa of nitrogen added. The solid lines are the least squares fits to the circled points.

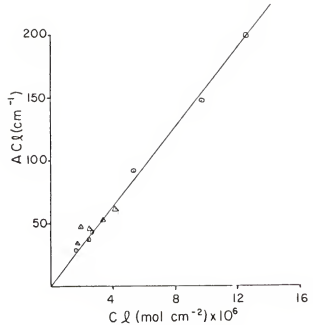
200
150
100
50
A C ℓ (cm⁻¹)
4
8
12
16
C ℓ (mol cm⁻²) x 10⁶

(a)

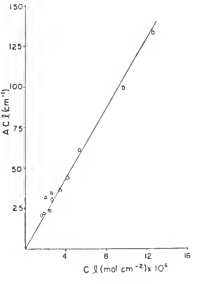
150
125
100
75
50
25
A C ℓ (cm⁻¹)
4
8
12
16
C ℓ (mol cm⁻²) x 10⁶

(b)

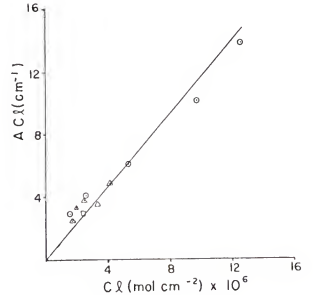
16
12
8
4
A C ℓ (cm⁻¹)
4
8
12
16
C ℓ (mol cm⁻²) x 10⁶

(c)

three of the absorption regions of ethanol are shown in Fig. 2-8. In each of these regions, both the 0.06 cm^{-1} resolution datum and the 1.13 MPa total pressure data satisfactorily fall on the Beer's law plots for those regions. We conclude that the samples pressurized to 0.1 MPa which were scanned at 0.24 cm^{-1} resolution are suitable for the intensity measurements.

We wish to digress briefly to compare the absolute intensities we measured for methanol and ethanol with the values obtained by a completely different method. Absorption cross sections for several liquid-phase alcohols have been calculated from the infrared reflectance spectra of the alcohols (40, 41). From these measurements the absorption index component of the complex index of refraction is obtained. This absorption index, $k(\nu)$ is related to the Lambert absorption coefficient, $\alpha(\nu)$, by (40):

$$k(\nu) = (1/4\pi\nu)\alpha(\nu) \quad , \quad \alpha(\nu) = \log_e(I_o/I) \qquad (2\text{-}4)$$

Absolute intensities may be calculated from these absorption indices, so we may compare our results for the gas phase intensities of methanol and ethanol with the results for the liquid phase intensities (41). Such a comparison is interesting because it indicates the magnitude of the intensity perturbations due to intermolecular interactions in the liquid state. Table 2-4 shows such a comparison. The most obvious feature in Table 2-4 is the tremendous intensity enhancement of the O-H stretching mode of the alcohols in the liquid phase. This is similar to the intensity enhancement found for the O-H stretch of the water dimer compared to the water monomer (42). The absolute intensities for the other vibrational modes listed in Table 2-4, however, show remarkable agreement between the two sets

TABLE 2-4
COMPARISON OF ABSOLUTE INTENSITIES FOR METHANOL AND ETHANOL MEASURED HERE AND MEASURED WITH LIGHT REFRACTION STUDIES
(units are km mol^{-1})

	Methanol	
	Absolute Intensity	
Region	Gas Phase[a]	Liquid[b]
O-H Stretch	22±1	505±76
C-H Stretch	127±10	167±25
C-O Stretch	100±10	105±16

	Ethanol	
	Absolute Intensity	
Region	Gas Phase[c]	Liquid[b]
O-H Stretch	16.4±0.6	417±63
C-H Stretch	159±6	173±26
C-O Stretch	106±4	126±19

[a] Taken from TABLE 2-1

[b] Sethna and Williams (41). Note that $A(km\ mol^{-1}) = (1/100)4\pi\nu_o(cm^{-1})(1/C(mol\ dm^{-3}) \int k(\nu)d\nu(cm^{-1})$

[c] Taken from TABLE 2-3

of absolute intensities. That one set of data is for the gas phase and the other set of data is for the liquid phase makes the level of agreement between the two sets of data even more impressive.

Dimethyl Ether

Survey Spectrum

Figure 2-9 presents a survey spectrum of dimethyl ether measured with the Nicolet Model 7199 FT-IR. The C-H stretching region of dimethyl ether occurs around 3000 cm^{-1}; five normal modes (ν_1, ν_2, ν_8, ν_{16}, and ν_{17}) are present in this region. The C-H bending modes (ν_3, ν_4, ν_9, ν_{18}, and ν_{19}) absorb around 1450 cm^{-1}. A CH_2 rocking mode (ν_{10}) and a CH_3 rocking mode (ν_{20}) occur near 1170 cm^{-1} and strongly overlap another CH_3 rocking mode (ν_5) at 1251 cm^{-1}. The absorption band near 1100 cm^{-1} is the antisymmetric C-O stretching mode (ν_{21}). The P-R structure at 920 cm^{-1} is due to the symmetric C-O stretching mode (ν_6). The COC bending mode (ν_7) at 425 cm^{-1} is not visible above the noise in that region of the spectrum, and the out-of-phase methyl torsional mode (ν_{11}) at 268 cm^{-1} falls outside the range of the potassium bromide cell windows. The vibrational modes of a_2 symmetry are infrared inactive.

Experimental Conditions

As with ethanol, absolute intensities for the vibrational bands of dimethyl ether (Matheson) were measured using the Nicolet Model 7199 FT-IR. Sample pressures were in the range of 1.3 kPa up to 8.0 kPa (vapor pressure at 25°C = 0.6 MPa (28)) and were measured with the MKS baratron. All intensity measurements were made at 1.48 MPa total pressure in the 3.28 cm brass cell. The broadening gas was prepurified nitrogen (Airco). Resolution was set for

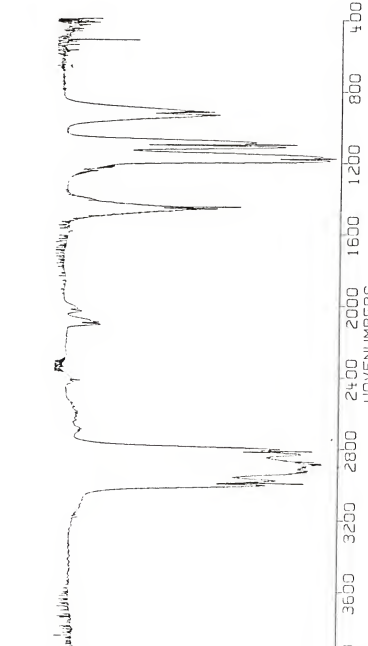

Fig. 2-9. Survey infrared spectrum of dimethyl ether vapor. The sample pressure was 3.45 kPa in a 10 cm cell. The spectrum was measured at 0.5 cm^{-1} resolution with the Nicolet Model 7199 FT-IR.

0.5 cm^{-1} with one level of zero filling. Triangular apodization was used in transforming the 100 scans collected of each I_o and I. Cell handling procedures were the same as with ethanol.

We have determined absolute intensities for four of the infrared absorption regions of dimethyl ether. The C-H stretching region was integrated between 3400 cm^{-1} and 2470 cm^{-1}, the C-H bending region was integrated between 1563 cm^{-1} and 1353 cm^{-1}, and the symmetric C-O stretching region was integrated between 1025 cm^{-1} and 810 cm^{-1}. The C-H rocking region and the antisymmetric C-O stretching region overlap (see Fig. 2-9), so we carried out the integration over both regions; the limits of integration were 1320 cm^{-1} to 1025 cm^{-1}. We shall consider in the next section how the absolute intensities for the C-H rocking band and the antisymmetric C-O stretching band may be obtained from the total absolute intensity for both bands.

Absolute Band Intensities for Dimethyl Ether

Beer's law plots for the intensities of the infrared bands of dimethyl ether are shown in Fig. 2-10. The absolute intensities calculated from the slope of the least squares line (27) fit to these plots are given in Table 2-5. Error limits quoted are the 2σ scatter limits about the least squares lines. The two modes ν_7 (425 cm^{-1}) and ν_{11} (268 cm^{-1}) fall outside the accessible range of the potassium bromide windows.

Approximate separations of the C-H stretching modes (ν_1, ν_2, ν_8, ν_{16}, and ν_{17}) are indicated in Table 2-5. The separation of these modes, as well as the separation of the modes in the 1320 cm^{-1} to 1025 cm^{-1} region (ν_5, ν_{10}, ν_{20}, and ν_{21}), was done by fitting Gaussian curves to the structures of the overlapped bands and calculating

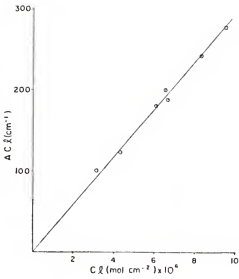

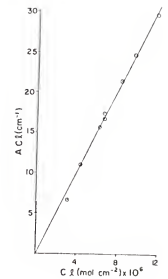

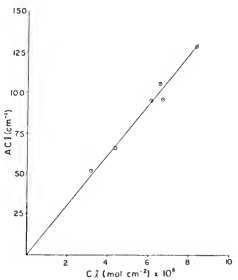

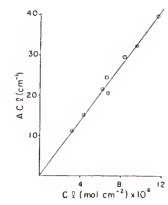

Fig. 2-10. Beer's law plots for the spectral regions of the infrared spectrum of dimethyl ether.

(a) The C-H stretching region, integrated from 3400 cm^{-1} to 2470 cm^{-1}.

(b) The C-H bending region, integrated from 1563 cm^{-1} to 1353 cm^{-1}.

(c) The C-H rocking region and the antisymmetric C-O stretching region, integrated from 1320 cm^{-1} to 1025 cm^{-1}.

(d) The symmetric C-O stretching region, integrated from 1025 cm^{-1} to 810 cm^{-1}.

The least squares line fit to the data for each region is indicated.

TABLE 2-5
ABSOLUTE INTENSITIES FOR DIMETHYL ETHER
(units are km mol^{-1})

Mode (cm^{-1})[a]		This Work	Blom et al.[b]
ν(CH)	ν_1 (2992)	47	253
	ν_{16} (2987)		
	ν_{12} (2934)	164	
	ν_2 (2817)	82	
	ν_{17} (2826)		
		294±6[c]	
δ(CH)	ν_3 (1487)	25.6±0.6	22
	ν_{13} (1464)		
	ν_{18} (1469)		
	ν_{19} (1450)		
	ν_4 (1434)		
δ(CH)	ν_5 (1251)	3	88
	ν_{20} (1166)	104	
	ν_{14} (1179)		
		155±6[c]	
ν_a(CO)	ν_{21} (1095)	48	39
ν_s(CO)	ν_6 (920)	34.3±1.2	26
δ(COC)	ν_7 (425)	-[d]	4
τ(CH_3)	ν_{15} (268)	-[d]	-[d]

[a] Assignments and frequencies from reference (84). See footnote (a) in TABLE 2-2 for explanation of symbols.

[b] Measured by Blom, Oskam, and Altona (43).

[c] Approximate band separations made by fitting Gaussian functions to the bands using the Curve Analysis Program (CAP) (39).

[d] Not measured

the relative intensities from the relative Gaussian areas. The CAP program (39) was used to do this. The intensity of ν_5 was estimated by computing its area under the assumption that the low frequency side of the band was of the same shape as the high frequency side.

Also included in Table 2-5 are the absolute intensities measured by Blom, Oskam, and Altona (43). Our values are seen to be systematically higher than those reported by Blom et al. (43). A possible explanation for this discrepancy could be pressure broadening effects. If the 0.1 MPa (one atmosphere) total pressure employed by Blom et al. (43) were not enough to broaden the rotational structure sufficiently for accurate intensity measurements, then we would expect to see an apparent increase in the total intensities if 1.48 MPa (14.6 atmospheres) total pressure were used. This explanation is perhaps precluded, though, because Blom et al. (43) reported almost no pressure dependence of the intensities over the range of 1 kPa to 0.1 MPa (zero pressurizing gas pressure up to one atmosphere of pressurizing gas).

CHAPTER 3
ATOMIC POLAR TENSORS

Before discussing the analysis of infrared intensity data in terms of atomic polar tensors (APT's), we shall first briefly describe the procedure for determining the normal coordinates for a vibrating molecule; we shall then consider how the APT's may be derived from infrared intensity data.

Normal Coordinate Analysis

The normal coordinate analysis of a polyatomic molecule is a rather involved subject which has been discussed elsewhere (3, 44, 45) in great detail, so here only the general procedure will be discussed. The absolute intensity of a normal vibrational mode of a molecule is proportional to the square of the molecular dipole moment change with respect to the normal coordinate; the form of the normal coordinates for the molecule must thus be known to analyze infrared intensity data. The usefulness of the normal coordinates is that the Schrodinger equation for a set of harmonic oscillators (the fundamental vibrations of the molecule) is separable in terms of these normal coordinates (2).

Displacement Coordinate Spaces

The molecular vibration represented by a particular normal coordinate may be considered as an appropriate linear combination of simple internal coordinates, where these internal coordinates are bond stretches, valence angle bends, or torsional motions about

chemical bonds (46). Other types of internal coordinates may also be defined (3, 45). In practice, one normally makes use of the molecular symmetry by constructing symmetry coordinates (47) from the internal coordinates. This leads to block factorization of the secular equation, as will be discussed later. We now consider the relationships between various displacement coordinate spaces.

There are 3N degrees of freedom for an N-atomic nonlinear molecule. Of these 3N degrees of freedom, three will be translations and three will be rotations of the molecule as a whole. Thus, (3N-6) vibrational degrees of freedom for a nonlinear molecule remain; these vibrations are represented by the (3N-6) normal coordinates Q_j. Each symmetry coordinate (S_i) will be, in general, involved in each of the normal coordinate motions so that S_i is a function of all the Q_j (3, 44):

$$S_i = \sum_j (\partial S_i/\partial Q_j) Q_j,$$

$$i = 1, 2, \text{---- } (3N-6) \qquad (3\text{-}1)$$

Eq. (3-1) may be rewritten in matrix notation to give

$$\underline{S} = \underline{L}\,\underline{Q} \qquad (3\text{-}2)$$

where $\underline{S}$ and $\underline{Q}$ are (3N-6) dimensional column vectors of the symmetry coordinate and normal coordinate displacements, respectively. Here $\underline{L}$ is a (3N-6) x (3N-6) matrix with element L_{ij} defined to be $(\partial S_i/\partial Q_j)$. We shall discuss below how $\underline{L}$ is obtained; for now, we meerly note that the inverse transformation is given by

$$\underline{Q} = \underline{L}^{-1}\,\underline{S} \qquad (3\text{-}3)$$

The coordinates S_i are symmetry adapted linear combinations (47) of the internal coordinates R_k; the transformation between the two coordinate spaces is:

$$\underline{S} = \underline{U}\ \underline{R} \tag{3-4}$$

The $\underline{R}$ matrix in Eq. (3-4) is a (3N-6) column vector of the changes in the internal coordinates R_k. The $\underline{U}$ matrix is the matrix of the coefficients multiplying each internal coordinate to form the symmetry coordinates (see reference 47). The construction of symmetry coordinates for a molecule may actually require the introduction of more internal coordinates than would be necessary to specify the (3N-6) vibrational degrees of freedom. These redundant coordinates have zero vibrational frequency, and the removal of the redundancies in the normal coordinate problem has been discussed by Wilson, Decius, and Cross (3).

The reverse transformation of Eq. (3-4) is then

$$\underline{R} = \underline{U}^{-1}\ \underline{S} = \underline{U}'\ \underline{S} \tag{3-5}$$

Here, we have used the fact that $\underline{U}$ is an orthogonal matrix so that its inverse, $\underline{U}^{-1}$, is equal to its transpose, $\underline{U}'$. To summarize, vibrations may be transformed from internal coordinate space to normal coordinate space by the use of Eq. (3-4) and Eq. (3-3), provided that $\underline{L}$ is known. Conversely, vibrations in normal coordinate space may be transformed back to $\underline{R}$ using Eq. (3-2) and Eq. (3-5).

Normal coordinate analyses are performed by first using the equilibrium molecular geometry to locate each of the atoms in a space-fixed cartesian coordinate system. The molecule may be oriented in any convenient way in this coordinate system, but usually the space-fixed cartesian axes are chosen to coincide with the molecular

principal axes of inertia. The cartesian coordinates of the mth atom are then x_m, y_m, and z_m; we shall denote any one of the 3N space-fixed cartesian coordinates by x_i. The internal coordinate R_k is then related to the cartesian coordinates by

$$R_k = \sum (\partial R_k/\partial x_i) x_i, \quad k = 1,2, \cdots (3N-6) \tag{3-6}$$

where x_i is one of the 3N cartesian coordinates. A column vector of 3N rows having entries x_1, y_1, z_1, x_2, $\cdots$ x_i, $\cdots$ Z_N may be introduced and given the symbol X. The matrix equivalent of Eq. (3-6) is thus

$$\underline{R} = \underline{B}\ \underline{X} \tag{3-7}$$

where $\underline{B}$ is a (3N-6) x (3N) dimensional matrix with a typical element B_{ki} defined as $(\partial R_k/\partial x_i)$. The $\underline{B}$ matrix is a function solely of the molecular geometry, and formulas for determining the elements of $\underline{B}$ have been tabulated (3, 45). A matrix $\underline{A}$ may also be defined which transforms $\underline{R}$ back to $\underline{X}$:

$$\underline{X} = \underline{A}\ \underline{R} \tag{3-8}$$

Here $\underline{A}$ is a (3N) x (3N-6) matrix with a typical element A_{ij} defined as $(\partial x_i/\partial R_j)$.

We must carefully consider Eqs. (3-7) and (3-8) because we specified that we started with an $\underline{X}$ matrix expressed in a space-fixed cartesian axis system. The transformation of $\underline{X}$ into $\underline{R}$ expressed by Eq. (3-7) results in a set of (3N-6) molecule-fixed internal coordinates. Consequently, the transformation of $\underline{R}$ back into $\underline{X}$ expressed by Eq. (3-8) will result in a set of (3N-6) molecule fixed cartesian coordinates rather than the original (3N) space-fixed cartesian coordinates. The form of Eq. (3-8) necessary to transform the

internal coordinates back to the original space-fixed axis system becomes

$$\underline{X} = (\underline{A} \mid \underline{\alpha}) \begin{pmatrix} \underline{R} \\ \hline \underline{\rho} \end{pmatrix} \tag{3-9}$$

Likewise, the form of Eq. (3-7) is now

$$\begin{pmatrix} \underline{R} \\ \hline \underline{\rho} \end{pmatrix} = \begin{pmatrix} \underline{B} \\ \hline \underline{\beta} \end{pmatrix} \underline{X} \tag{3-10}$$

Here the six elements of the column matrix $\underline{\rho}$ (three translations and three rotations) are given by the six Eckart conditions ($\underline{\rho} = \underline{\beta}\ \underline{X}$) expressing conservation of angular and linear momenta (3). The expression for $\underline{\beta}$ may be found in reference 13. The importance of the distinction betewen space-fixed and molecule-fixed axis systems will become clear when the dipole moment derivatives in space-fixed and molecule-fixed coordinate systems are discussed later in this Chapter. For now, it is sufficient to realize that vibrational coordinates ($\underline{R}$ or $\underline{X}$) expressed in molecule-fixed axes will normally also involve both a displacement of the molecular center of mass and a rotation of the principal axes of inertia relative to a set of space-fixed axes. The normal coordinates and hence the dipole moment derivatives with respect to the normal coordinates do not involve a center of mass displacement or rotation of the principal axes.

Evaluation of the Normal Coordinates

We now turn our attention very briefly to the determination of the form of the normal coordinates and hence the form of $\underline{L}$ in Eq. (3-2). Molecular vibrations must satisfy the condition that the total energy of the molecule is constant (2); the total energy of the molecule is at all times equal to the sum of the kinetic

energy and the potential energy. The kinetic energy (T) of the molecule may be expressed as (3, 45)

$$2\,\underline{T} = \underline{P}'\,\underline{G}\,\underline{P} \tag{3-11}$$

where $\underline{P}$ is the conjugate momentum matrix to the internal coordinates ($\underline{R}$) and $\underline{G}$ is the inverse kinetic energy matrix. The $\underline{G}$ matrix is given by (3)

$$\underline{G} = \underline{B}\,\underline{M}^{-1}\,\underline{B}' \tag{3-12}$$

where $\underline{B}$ is the matrix defined by Eq. (3-7), and $\underline{M}^{-1}$ is a diagonal matrix of the reciprocals of the atomic masses. The $\underline{G}$ matrix is of dimension (3N-6) x (3N-6). The $\underline{M}^{-1}$ matrix is not simply the reciprocal masses of the N atoms in the molecule, but rather the i<u>th</u> reciprocal mass entry in $\underline{M}^{-1}$ is for the atom whose motion is described by the i<u>th</u> column of $\underline{B}$ (45).

The potential energy of the molecule may be expressed as (3, 45)

$$2\,\underline{V} = \underline{R}\,\underline{F}\,\underline{R}' \tag{3-13}$$

where $\underline{R}$ is the column vector of the internal coordinates and $\underline{V}$ is the potential energy matrix. The $\underline{F}$ matrix in Eq. (3-13) is a (3N-6) x (3N-6) matrix of the force constants of the molecule. The molecular force constants are the forces between the atoms acting to restore the equilibrium configuration upon vibration. A typical element F_{ij} of $\underline{F}$ is defined as $\partial^2 V/\partial R_i \partial R_j$.

To utilize any symmetry the molecule possesses we may symmetrize $\underline{F}$ and $\underline{G}$ to obtain matrices that are block diagonal in form. Thus, we have (3)

$$\underline{\mathit{F}} = \underline{U}\,\underline{F}\,\underline{U}' \tag{3-14a}$$

and

$$\underline{\mathit{G}} = \underline{U}\,\underline{G}\,\underline{U}' \tag{3-14b}$$

where $\underline{U}$ has been previously defined in Eq. (3-4). The $\underline{F}$ and $\underline{G}$ matrices are now combined to give the secular equation which is to be solved for the normal vibrational frequencies (3, 45):

$$\underline{G}\,\underline{F}\,\underline{L} = \underline{L}\,\underline{\Lambda} \tag{3-15}$$

Here $\underline{L}$ is the matrix defined in Eq. (3-2) and $\underline{\Lambda}$ is a (3N-6) diagonal matrix of the frequency parameters λ_n with

$$\lambda_n = 4\pi^2 \nu_n^2 c^2 \tag{3-16}$$

where ν_n is the wavenumber in cm^{-1} of the nth normal vibration.

Eq. (3-15) may be solved by evaluating the determinant (3, 45):

$$\left|\underline{G}\,\underline{F} - \lambda_n \underline{I}\right| = 0 \tag{3-17}$$

where $\underline{I}$ is a (3N-6) diagonal unit matrix.

The units we have used in the normal coordinate analyses are as follows. If the cartesian coordinates (the $\underline{X}$ matrix) of the atoms of a molecule are expressed in Å (1 Å = 0.1 nm), then the internal coordinate for a bond stretch will have units of Å and the internal coordinate for an angle change will be unitless. Thus, the $\underline{B}$ matrix element for a bond stretch will be dimensionless, while the $\underline{B}$ element for a bending internal coordinate will have units of $Å^{-1}$. We have used atomic mass units (lu = 1.66056 x 10^{-27}kg) throughout, so $\underline{M}^{-1}$ has units of u^{-1}. The $\underline{G}$ matrix elements all have units of u^{-1}; that is, we have used a weighted $\underline{G}$ matrix wherein the bend-bend elements are weighted by 1 $Å^2$, the stretch-bend elements are weighted by 1 Å, and the stretch-stretch elements of $\underline{G}$ are unweighted. All of the elements in the $\underline{F}$ matrix thus have units of mdyn/Å (1 mdyn/Å = 100 Nm^{-1}), and finally the $\underline{L}$ matrix has units of $u^{-1/2}$.

Intensity Analysis

As we pointed out in Chapter 1 (see Eq. (1-5)), the absolute intensity (A_i) of the ith fundamental vibrational mode of a molecule is proportional to the square of the dipole moment change with respect to the ith normal coordinate. We may evaluate the physical constants in Eq. (1-5) using values from reference 48 to obtain

$$A(\text{km mol}^{-1}) = 974.9\, d_i \left|\partial\vec{p}/\partial Q_i\ (\text{e u}^{-1/2})\right|^2 \qquad (3\text{-}18)$$

where d_i is the degeneracy of the ith vibrational mode. If the value of the dipole moment change with respect to the ith normal coordinate is known, the absolute intensity for that mode may be directly calculated from Eq. (3-18). The problem of intensity analysis thus reduces to calculating these dipole moment changes.

Atomic Polar Tensors

The vector dipole moment change ($\partial\vec{p}/\partial Q_i$) may be considered to have dipole moment component changes $\partial p_x/\partial Q_i$, $\partial p_y/\partial Q_i$, and $\partial p_z/\partial Q_i$ along each of the space-fixed cartesian axes (chosen parallel to the principal axes a, b, and c). Column vector components of the dipole moment derivatives may be juxtaposed for the (3N-6) normal modes. The resulting $\underline{P}_Q$ matrix has the form (13)

$$\underline{P}_Q = \begin{pmatrix} \partial p_x/\partial Q_1 & - - - - & \partial p_x/\partial Q_{3N-6} \\ \partial p_y/\partial Q_1 & - - - - & \partial p_y/\partial Q_{3N-6} \\ \partial p_z/\partial Q_1 & - - - - & \partial p_z/\partial Q_{3N-6} \end{pmatrix}. \qquad (3\text{-}19)$$

The dipole derivatives in normal coordinate space are related to dipole derivatives in internal coordinate space by (13)

$$\underline{P}_R = \underline{P}_Q\, \underline{L}^{-1}\, \underline{U} \qquad (3\text{-}20)$$

Here $\underline{P}_R$ is analogous to Eq. (3-19) except that the dipole derivatives are now with respect to the internal coordinates; $\underline{L}^{-1}$ and $\underline{U}$ have been previously defined in Eq. (3-3) and Eq. (3-4), respectively.

The $\underline{P}_R$ matrix may be further transformed into dipole moment derivatives expressed in a space-fixed cartesian coordinate system (13):

$$\underline{P}_X = \underline{P}_Q \underline{L}^{-1} \underline{U} \underline{B} + \underline{P}_\rho \underline{\beta} \tag{3-21}$$

Here $\underline{B}$ was defined in Eq. (3-7) and $\underline{P}_\rho \underline{\beta}$ is a rotation correction matrix (13) which will be dicussed below.

The $\underline{P}_X$ matrix in Eq. (3-21) is a juxtaposition of tensors on each atom of the molecule. Thus we have

$$\underline{P}_X = (P_X^1 \vdots P_X^2 \vdots \text{---} \vdots P_X^\alpha \vdots \cdots P_X^N) \tag{3-22}$$

with

$$P_X^\alpha = \begin{pmatrix} \partial p_x/\partial x_\alpha & \partial p_x \partial y_\alpha & \partial p_x/\partial z_\alpha \\ \partial p_y/\partial x_\alpha & \partial p_y/\partial y_\alpha & \partial p_y/\partial z_\alpha \\ \partial p_z/\partial x_\alpha & \partial p_z/\partial y_\alpha & \partial p_z/\partial z_\alpha \end{pmatrix} \tag{3-23}$$

where x, y, and z refer to the space-fixed cartesian axes, α is the αth atom in the molecule, and P_X^α is the atomic polar tensor (12) for the αth atom.

We shall now consider why the rotation correction matrix $\underline{P}_\rho \underline{\beta}$ occurs in Eq. (3-21) and how this matrix may be calculated. As we pointed out in the discussion of normal coordinate analyses, vibrational displacements expressed in internal coordinate space may be transformed back into cartesian coordinate space (see Eq. (3-8)) through the use of the $\underline{A}$ matrix, but the transformation results in molecule-fixed cartesian displacements. To obtain space-fixed

cartesian displacements from the internal coordinate displacements, we must use the augmented $\underline{R}$, $\underline{B}$, and $\underline{A}$ matrices (see Eqs. (3-9) and (3-10)). Hence, when dipole derivatives are transformed from internal coordinate space to a space-fixed cartesian coordinate system, a rotation correction matrix, $\underline{P}_{\rho}\ \underline{\beta}$ in Eq. (3-21), must be added if $\underline{B}$ is defined as in Eq. (3-7). The rotation correction matrix may be expressed as a tensor for each atom of the molecule, just as the total $\underline{P}_X$ matrix is expressed as a juxtaposition of tensors for each atom of the molecule. The rotation correction tensor for the αth atom of the molecule is given by (12)

$$(\underline{P}_{\rho}\ \underline{\beta})^{\alpha} = m_{\alpha}((p^{o}))\ \underline{I}^{-1}\ ((r_{\alpha}))' \tag{3-24}$$

where the notation $(\underline{P}_{\rho}\ \underline{\beta})^{\alpha}$ has been used instead of Morcillo's $\underline{D}$ matrix notation. Here m_{α} is the mass of atom α, $((p^{o}))$ is the antisymmetric tensor * of the permanent dipole moment components along the principal axes a, b, and c, $\underline{I}^{-1}$ is the inverse diagonal matrix of the moments of intertia about a, b, and c, and $((r_{\alpha}))'$ is the transpose of the antisymmetric tensor of the equilibrium a, b, and c coordinates of the molecule. For molecules with no permanent dipole moment, $((p^{o}))$ will be a null tensor, and consequently the rotation correction matrix will be the null matrix. An alternate way of expressing the rotation correction tensor for each atom is to

---

*The antisymmetric tensor for a vector $\vec{\rho}$ is (12)

$$((\vec{\rho})) = \begin{pmatrix} 0 & \rho_z & -\rho_y \\ -\rho_z & 0 & \rho_x \\ \rho_y & -\rho_x & 0 \end{pmatrix}$$

use the expressions for $\underline{P}_\rho$ and $\underline{\beta}$ for each atom (13). The two methods for calculating the rotation correction matrix are of course equivalent.

The atomic polar tensors (APT's) for each of the atoms in a molecule are not all independent; one APT can always be determined from the APT's for the other atoms through the application of the null constraint (12):

$$\sum_\alpha P_X^\alpha = \underline{0} \tag{3-25}$$

Thus, we have for example

$$\sum_\alpha \partial p_y / \partial z_\alpha = 0 \tag{3-26}$$

An expression similar to Eq. (3-26) exists for all the other APT components. The null constraint arises because the $\underline{P}_\rho$ matrix for translations is the null matrix. This result may be appreciated by realizing that movement of every atom in the same direction by the same amount along one of the space-fixed cartesian axes produces no change in the molecular dipole moment.

Atomic polar tensors are always expressed relative to a particular cartesian coordinate system. An APT expressed in a new rotated coordinate system is calculated from the APT expressed in the old coordinate system by (14)

$$P_X^\alpha \text{ (new)} = \underline{T} \quad P_X^\alpha \text{ (old)} \ \underline{T}' \tag{3-27}$$

Here the transformation matrix $\underline{T}$ is composed of the cosines between the new axes and the old axes. The element T_{ij} is the cosine of the angle between the ith rotated axis and the jth original axis.

Let us now consider the reverse transformation of the dipole moment derivatives, where we transform a set of dipole derivatives with respect to a space-fixed cartesian

coordinate system to dipole derivatives with respect to normal coordinates. This transformation is given by (13)

$$\underline{P}_Q = \underline{P}_x \underline{A} \underline{U}' \underline{L} \tag{3-28}$$

Here $\underline{A}$ is defined in Eq. (3-8), $\underline{U}'$ is the transpose of $\underline{U}$ in Eq. (3-4), and $\underline{L}$ is defined in Eq. (3-2).

We might note here how we may obtain the $\underline{L}^{-1}$ needed in Eq. (3-21) and the $\underline{A}$ needed in Eq. (3-28). These two matrices are normally not reported in the literature or in normal coordinate analysis programs, as they are not directly needed to calculate the normal mode frequencies of a molecule. We obtain $\underline{L}^{-1}$ from the relation given by Crawford and Fletcher (49)

$$\underline{L}^{-1} = \underline{\Lambda}^{-1} \underline{L}' \underline{F} \tag{3-29}$$

where $\underline{\Lambda}^{-1}$ is the inverse of $\underline{\Lambda}$ (see Eq. (3-16)) and $\underline{F}$ is the matrix of the internal force constants of the molecule (see Eq. (3-14a)).

The $\underline{A}$ matrix can not be calculated by a simple inversion of $\underline{B}$ as neither matrix is square. Instead, $\underline{A}$ can be calculated from (49)

$$\underline{A} = \underline{M}^{-1} \underline{B}' \underline{G}^{-1} \tag{3-30}$$

where $\underline{M}^{-1}$ and $\underline{B}'$ have been previously discussed in relation to Eq. (3-12). The inverse of the unsymmetrized $\underline{G}$ may be calculated from (49)

$$\underline{G}^{-1} = \underline{U}' (\underline{L}^{-1})' \underline{L}^{-1} \underline{U} \tag{3-31}$$

The L^{-1} matrix is calculated from Eq. (3-29).

We can avoid some of the confusion caused by the symmetrized $\underline{G}$ and unsymmetrized $\underline{G}$ matrices by introducing symmetrized $\underline{A}$ and $\underline{B}$ matrices which transform symmetry coordinates to cartesian coordinates and cartesian coordinates to symmetry coordinates, respectively:

$$\underline{A} = \underline{A}\ \underline{U}' \tag{3-32a}$$
$$\underline{B} = \underline{U}\ \underline{B} \tag{3-32b}$$

We can now calculate the symmetrized $\underline{A}$ matrix from the symmetrized $\underline{G}^{-1}$ matrix:

$$\underline{A} = \underline{M}^{-1}\ \underline{B}'\ \underline{G}^{-1}$$
$$\underline{G}^{-1} = (\underline{L}^{-1})'\ \underline{L}^{-1} \tag{3-33}$$

The $\underline{P}_Q$ matrix is now given by

$$\underline{P}_Q = \underline{P}_X\ \underline{A}\ \underline{L} \tag{3-34}$$

in terms of the symmetrized $\underline{A}$, and $\underline{P}_X$ is given by

$$\underline{P}_X = \underline{P}_Q\ \underline{L}^{-1}\ \underline{B} + \underline{P}_\rho\ \underline{\beta} \tag{3-35}$$

We shall report symmetrized $\underline{A}$ matrices and unsymmetrized $\underline{B}$ matrices in this dissertation.

Finally, we wish to acknowledge that all the intensity calculations were performed using the program PVDTEN developed by Newton (50). The program allows one to calculate either $\underline{P}_X$ from $\underline{P}_Q$ or $\underline{P}_Q$ from $\underline{P}_X$.

Effective Charges

The atomic polar tensors are dependent upon the definition of the coordinate system; hence, the tensor components will change when the coordinate system is rotated. An APT invariant which is independent of the choice of coordinate system may be obtained by taking the trace of the product of the APT and the transpose of the APT (13):

$$\xi_\alpha^2 = \text{Trace}\ [P_X^\alpha\ (P_X^\alpha)'] \tag{3-36}$$

where P_X^α is the APT for atom α, the prime indicates the transpose, and ξ_α is the effective charge on atom α. The effective charge was first deduced by King, Mast, and Blanchette (52) from a consideration of Crawford's G sum rule (53) expressed in cartesian space. The relationship between the effective charge and the APT was derived

by Person and Newton (13).

Two other invariants of the APT for the αth atom are the mean dipole derivative and the anisotropy (51). The mean dipole derivative $\bar{p}_\alpha$ is given by

$$\bar{p}_\alpha = (1/3)\ \text{Trace}\ \underline{p}^\alpha_X \tag{3-37}$$

The anisotropy β^2_α measures the deviation of the APT from a constant diagonal tensor of value $\bar{p}_\alpha$ and is given by (51):

$$\beta^2_\alpha = (1/2)[(p_{xx}-p_{yy})^2 + (p_{yy}-p_{zz})^2 + (p_{zz}-p_{xx})^2 + 3\ (p^2_{xy} + p^2_{yz} + p^2_{zx} + p^2_{zy} + p^2_{xz} + p^2_{yx})] \tag{3-38}$$

where, for example, p_{xz} stands for $(\partial p_x/\partial z_\alpha)$. The relationship between the effective charge, the mean dipole derivative, and the anisotropy is (51, 54):

$$\chi^2_\alpha = (\bar{p}_\alpha)^2 + (2/9)\ \beta^2_\alpha \tag{3-39}$$

Here we have used the new definition of the effective charge given by King (54):

$$\chi_\alpha = (1/\sqrt{3})\ \xi_\alpha \tag{3-40}$$

We have found the effective charge to be perhaps the most useful of the APT invariants, so we shall report only the effective charges for the APT's. The effective charges we report are in terms of χ rather than ξ, and will have units of electrons (e).

King et al. (52) also derived a useful expression relating the effective charges for the atoms in a molecule to the sum of the absolute intensities for all the vibrational modes of that molecule:

$$\sum_\alpha (\chi^2_\alpha/m_\alpha) = (c^2/N\pi) \sum_i (A_i/d_i) + \Omega \tag{3-41}$$

(here the equation has been converted to be consistent with the definition of χ_α). Most of the terms in Eq. (3-41) have been defined

earlier. The Ω in Eq. (3-41) is the total rotational correction given by (13)

$$\Omega = \frac{(p_z^o)^2 + (p_x^o)^2}{I_y} + \frac{(p_z^o)^2 + (p_y^o)^2}{I_x} + \frac{(p_x^o)^2 + (p_y^o)^2}{I_z} \qquad (3\text{-}42)$$

We may express A_i and Ω in units of km mol^{-1}; if χ_α is then expressed in electrons, we have

$$\sum_\alpha \frac{\chi_\alpha}{m_\alpha} \left(e^2\ u^{-1}\right) = 1.0258 \times 10^{-3} \left[\sum_i (A_i/d_i) + \Omega\right] \text{ (km mol}^{-1}\text{)} \qquad (3\text{-}43)$$

King et al. (52) have suggested that the effective charge for an atom may be a transferable intensity parameter; since subsequent work (54) agrees with this idea, we shall routinely tabulate effective charges along with APT's.

CHAPTER 4
EXPERIMENTAL ATOMIC POLAR TENSORS FOR METHANOL

We now wish to derive experimental atomic polar tensors for methanol from the best estimates given in Table 2-2 for the experimental absolute intensities of the normal modes. The rotational correction tensors and the normal coordinates necessary to calculate the APT's from the experimental intensity data will be described later; first we shall outline the procedure for obtaining the experimental $\underset{\sim}{P}_Q$ matrix from the absolute intensities.

The Experimental $\underset{\sim}{P}_Q$ Matrix for Methanol

The absolute intensities presented in Table 2-2 for the normal modes of methanol may be converted to $|\partial\vec{p}/\partial Q_i|$ absolute values using the relationship (from Eq. (3-18))

$$|\partial\vec{p}/\partial Q_i| \ (\text{e u}^{-1/2}) = 0.03203 \ [A_i(\text{km mol}^{-1})/d_i]^{1/2} \qquad (4\text{-}1)$$

where the components on the space-fixed cartesian axes of the $|\partial\vec{p}/\partial Q_i|$ values comprise the elements of the $\underset{\sim}{P}_Q$ matrix. The degeneracy (d_i) is unity for all the vibrational bands of methanol, so its presence in Eq. (4-1) can be ignored. The experimental intensity measurements provide only the magnitude of the vector dipole moment change for each of the normal modes. To analyze the intensity data, both the direction and the sign of each dipole derivative must also be known. We first consider the determination of the direction of the dipole moment derivatives associated with each of the normal modes.

For the vibrations of a'' symmetry (ν_9 through ν_{12}), the direction of the dipole moment change is determined by the C_s symmetry of the molecule. Only the $|\partial p_x/\partial Q_i|$ component of the dipole moment change is nonzero. (See Fig. 4-2 for the definition of the coordinate system for methanol.) Thus, the conversion of the absolute intensities for ν_9 through ν_{12} to the absolute values of the corresponding $\underline{P}_Q$ matrix elements is straightforward through the use of Eq. (4-1).

The directions of the dipole moment changes for the vibrations of methanol having a' symmetry (ν_1 through ν_8) are more difficult to establish since these vibrational modes have, in general, nonzero changes in both y and z dipole moment components under the C_s point group. We have used local C_{3v} symmetry at the methyl carbon to determine the direction of each of the dipole derivatives for the methyl group vibrations (ν_2, ν_3, ν_4, ν_5, and ν_7). Under C_{3v} symmetry, each of these five normal modes will induce a dipole moment change along either y or z, but not both. The decision as to whether the dipole derivatives for each of the five vibrations are directed along y or along z was made by comparing these vibrations with the corresponding ones in methyl fluoride (50).

The three remaining normal modes having a' symmetry are associated with the COH structural unit of methanol. For the O-H stretching mode (ν_1), the dipole moment change was taken to be directed along the O-H bond, while the COH bending mode (ν_6) was assumed to give a dipole moment change directed perpendicular to the O-H bond. The components of the dipole moment changes along the y and z axes were then calculated using the experimental COH angle of 108° 32' (55). This "bond moment hypothesis" was also applied to the C-O stretching mode (ν_8);

consequently, that dipole moment change is directed along the C-O bond.

Based on the above discussion, the absolute values of the $\underline{P}_Q$ elements are presented in Table 4-1. To see how accurate our estimation of the direction of each of the dipole moment derivatives is, we may compare the results presented in Table 4-1 with the $\underline{P}_Q$ matrix (Table 4-2) which we derived for methanol from an ab initio calculation using a 4-31G basis set (see Chapter 5 for details). A comparison of the distribution between y and z of the $\underline{P}_Q$ elements derived from the ab initio calculation and the distribution derived from the experimental intensities indicates that local C_{3v} symmetry for the methyl group vibrations and the bond moment approximation for the hydroxyl group vibrations lead to good descriptions of the dipole derivatives. Only ν_7 is poorly represented under C_{3v} symmetry, but since ν_7 has an absolute intensity of only 4 km mol^{-1}, the distribution of the dipole derivative between the y and z axes will have but a minimal effect on the APT's.

Atomic Polar Tensors for Methanol

Eq. (3-21) provides the relationship between dipole moment derivatives in normal coordinate space and dipole moment derivatives expressed in a space-fixed cartesian coordinate system. To calculate the APT's for methanol from the experimental intensities, we shall use the experimental geometry reported by Lees and Baker (55) and the normal coordinates calculated from the force field for methanol reported by Mallinson (56). Appendix A presents the $\underline{L}^{-1}$, $\underline{U}$, and $\underline{B}$ matrices based on this geometry and force field as well as a more

TABLE 4-1

EXPERIMENTAL MAGNITUDES FOR THE P_Q MATRIX ELEMENTS FOR METHANOL
(units are $\bar{e}\ u^{-1/2}$)

	Q_1[a]	Q_2[d]	Q_3[c]	Q_4[d]	Q_5[c]	Q_6[a,b]	Q_7[d]	Q_8[a]	Q_9	Q_{10}	Q_{11}	Q_{12}
P_x	0[e]	0	0	0	0	0	0	0	0.2458	0.0405	0.0320	0.2395
P_y	0.0477	0.0[e]	0.1693	0.0	0.0853	0.1214	0.0	0.3135	0	0	0	0
P_z	0.1423	0.1893	0.0	0.0351	0.0	0.0407	0.0640	0.0	0	0	0	0

[a] Bond moment hypothesis assumed to be valid

[b] Dipole moment change directed perpendicular to the O-H bond

[c] Dipole moment change directed along the C-O bond

[d] Assumed local of C_{3v} symmetry for the CH_3 group

[e] An integer zero indicates that the dipole moment derivative component is zero due to symmetry constraints, while a decimal zero indicates the derivative is assumed to be zero

TABLE 4-2
QUANTUM MECHANICAL P_O MATRIX FOR METHANOL
(units of e)

0	0	0	0	0	0	0	0	-0.318	-0.046	0.078	0.456
-0.076	-0.009	-0.204	0.010	0.051	-0.177	-0.115	-0.360	0	0	0	0
-0.130	0.161	0.015	-0.045	0.037	0.026	0.022	0.012	0	0	0	0

Note: See TABLE 5-5 in Chapter 5. Signs are relative to the normal coordinates calculated from the force field for methanol reported by Mallinson (56)

complete description of the normal coordinate analysis. The rotational correction tensors and signs for the elements of the P_Q matrix in Table 4-1 are also needed to calculate the APT's.

The rotational correction tensors (given by Eq. (3-24)) for methanol were calculated with respect to the principal axes of inertia derived from the experimental geometry of methanol (55). The orientation of the principal axes is indicated in Fig. 4-1. Components along the principal axes of the permanent dipole moment were taken from the microwave study of methanol by Ivash and Dennison (57). Principal cartesian coordinates, principal moments of inertia, and the components along the principal axes of the permanent dipole moment from which the rotational correction tensors were calculated are given in Table 4-3. The principal cartesian coordinate system was then rotated to the coordinate system used in the normal coordinate analysis, and the rotational correction tensors expressed in this new coordinate system are presented in Table 4-4. This coordinate system, which is shown in Fig. 4-2, has the y axis directed along the C-O bond with z in the symmetry plane of the molecule and perpendicular to y.

Signs for the dipole derivatives listed in Table 4-1 cannot be deduced from the experimental absolute intensities we measured for methanol; a knowledge of these signs is necessary, however, to analyze the intensity data. In the absence of high resolution intensity data which might provide information about the relative signs of the dipole moment derivatives (58), signs are often chosen on the basis of quantum mechanical calculations of the dipole derivatives, and this is the method we have used.

TABLE 4-3
DATA FOR THE ROTATIONAL CORRECTION TENSOR
CALCULATIONS FOR METHANOL

Dipole Moment[a] (e nm)		Moments of Inertia[b] (u nm^2)	
x	0.0	x	0.211852
y	-0.0184	y	0.039916
z	0.0300	z	0.203746

Principal Cartesian Coordinates[b] (nm)

C_1	(0.0 , -0.073230, 0.001155)
O_2	(0.0 , 0.069170, -0.006363)
H_3	(0.0 , 0.103892, 0.081535)
H_4	(0.0 , -0.110728, -0.101573)
H_5	(0.08883 , -0.109525, 0.053609)
H_6	(-0.08883, -0.109525, 0.053609)

[a] Dipole moment taken from Ivash and Dennison (57)

[b] Calculated from the geometry for methanol reported by Lees and Baker (55).

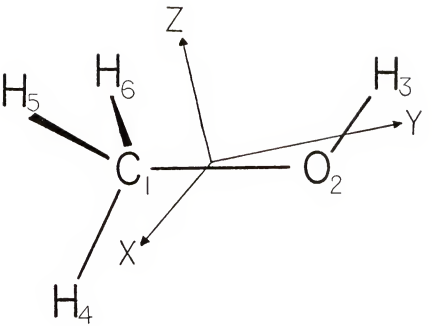

Fig. 4-1. Location of the principal axes of inertia of methanol. The data in Table 4-3 is relative to this axis system. The angle between the C-O bond and the y axis is 3°.

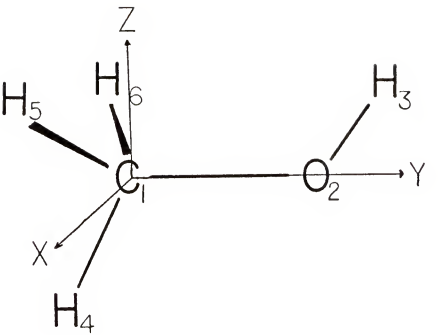

Fig. 4-2. Space-fixed cartesian coordinate system for methanol. The yz plane lies in the symmetry plane of the molecule; the y axis is directed along the C-O bond. The APT's given in Table 4-5 are relative to this coordinate system.

TABLE 4-4
ROTATIONAL CORRECTION TENSORS FOR METHANOL
(units are e)

$$\underline{P}_{\rho}^{\beta}(C_1) = \begin{pmatrix} 0.0899 & 0 & 0 \\ 0 & -0.0045 & 0.1201 \\ 0 & -0.0031 & 0.0829 \end{pmatrix}$$

$$\underline{P}_{\rho}^{\beta}(O_2) = \begin{pmatrix} -0.1765 & 0 & 0 \\ 0 & -0.0059 & -0.1518 \\ 0 & -0.0041 & -0.1047 \end{pmatrix}$$

$$\underline{P}_{\rho}^{\beta}(H_3) = \begin{pmatrix} 0.0523 & 0 & 0 \\ 0 & 0.0120 & -0.0137 \\ 0 & 0.0083 & -0.0095 \end{pmatrix}$$

$$\underline{P}_{\rho}^{\beta}(H_4) = \begin{pmatrix} -0.0668 & 0 & 0 \\ 0 & -0.0148 & 0.0145 \\ 0 & -0.0102 & 0.0100 \end{pmatrix}$$

$$\underline{P}_{\rho}^{\beta}(H_5) \quad \begin{pmatrix} 0.0506 & 0.0116 & -0.0667 \\ 0 & 0.0066 & 0.0155 \\ 0 & 0.0045 & 0.0107 \end{pmatrix}$$

$$\underline{P}_{\rho}^{\beta}(H_6) \quad \begin{pmatrix} 0.0506 & -0.0116 & 0.0667 \\ 0 & 0.0066 & 0.0155 \\ 0 & 0.0045 & 0.0107 \end{pmatrix}$$

Note: The atomic numbering scheme and the coordinate system are defined in Fig. 4-2

Included with the $\underline{P}_Q$ matrix given in Table 4-2 are the signs of the dipole moment derivatives which were obtained from the ab initio calculation described in Chapter 5 for methanol. This theoretical $\underline{P}_Q$ matrix was calculated from the normal coordinates for methanol calculated using the force field reported by Mallinson (56). The signs of the $\underline{P}_Q$ matrix elements depend upon the phase definitions of the normal coordinates and the symmetry coordinates, so we report in Appendix A the $\underline{A}$ and $\underline{L}$ matrices derived from the force field data reported by Mallinson (56). The signs of the $\underline{P}_Q$ elements in Table 4-2 form the basis for assigning signs to the experimental $\underline{P}_Q$ matrix elements presented in Table 4-1. This assignment of course assumes that we shall use the same definitions of phase for the symmetry coordinates as we used to calculate the theoretical $\underline{P}_Q$ matrix from the $\underline{P}_X$ matrix.

The most straightforward choice of signs is to choose the sign of each nonzero experimental $\underline{P}_Q$ element exactly as it is calculated from the ab initio study. The experimental $\underline{P}_Q$ matrix for this set of signs is shown in Table 4-5; the experimental APT's resulting from this sign choice are presented in Table 4-6. The coordinate system for these APT's is shown in Fig. 4-2. Since, however, some of the magnitudes for the $\underline{P}_Q$ elements are rather small, notably the dipole derivatives for ν_4, ν_6, ν_7, and ν_{11}, several other sign choices were investigated. These alternate sign choices were made by simply reversing the sign of the dipole derivative for one of the four low intensity modes and recalculating the experimental APT's. The APT's which result for two such alternate sign choices are presented in Table 4-7. The APT's for methanol which were calculated

TABLE 4-5

THE EXPERIMENTAL $\underline{P}_Q$ MATRIX FOR METHANOL

(units are e $u^{-1/2}$)

$$\begin{pmatrix} 0 & 0 & 0 & 0 & 0 & 0 & 0 & 0 & -0.2458 & -0.0405 & 0.0320 & 0.2395 \\ -0.0477 & 0.0 & -0.1693 & 0.0 & 0.0853 & -0.1214 & 0.0 & -0.3135 & 0 & 0 & 0 & 0 \\ -0.1423 & 0.1893 & 0.0 & -0.0351 & 0.0 & 0.0407 & -0.064 & 0.0 & 0 & 0 & 0 & 0 \end{pmatrix}$$

Note: The signs for the $\underline{P}_Q$ elements are taken directly from the results of the ab initio calculation (TABLE 4-2). See $\underline{P}_Q$ footnotes for TABLE 4-1

TABLE 4-6
ATOMIC POLAR TENSORS FOR METHANOL
(Dipole derivative signs are indicated in TABLE 4-5)

$$P_X(C_1) = \begin{pmatrix} 0.379 & 0 & 0 \\ 0 & 0.826 & 0.032 \\ 0 & -0.061 & 0.359 \end{pmatrix}$$

$\chi = 0.57e$

$$P_X(O_2) = \begin{pmatrix} -0.444 & 0 & 0 \\ 0 & -0.875 & -0.059 \\ 0 & 0.010 & -0.304 \end{pmatrix}$$

$\chi = 0.58e$

$$P_X(H_3) = \begin{pmatrix} 0.260 & 0 & 0 \\ 0 & 0.175 & -0.029 \\ 0 & 0.059 & 0.128 \end{pmatrix}$$

$\chi = 0.20e$

$$P_X(H_4) = \begin{pmatrix} 0.025 & 0 & 0 \\ 0 & -0.024 & -0.043 \\ 0 & 0.001 & -0.164 \end{pmatrix}$$

$\chi = 0.10e$

$$P_X(H_5) = \begin{pmatrix} -0.110 & 0.053 & -0.107 \\ 0.057 & -0.051 & 0.049 \\ -0.048 & -0.005 & -0.009 \end{pmatrix}$$

$\chi = 0.11e$

Note: The atomic numbering scheme and coordinate system are shown in Fig. 4-2. Effective charges (χ) are calculated from Eq. (3-40). Units are electrons (e). The APT for H_6 is obtained from that for H_5 by simply reversing the signs of all off-diagonal tensor elements involving the x axis.

TABLE 4-7
ALTERNATE APT'S FOR METHANOL
BASED ON OTHER SIGN CHOICES
(units are e)

$$P_X(C_1) = \begin{pmatrix} 0.379 & 0 & 0 \\ 0 & 0.826 & 0.032 \\ 0 & -0.079 & 0.255 \end{pmatrix} \quad \chi = 0.55e$$

$$P_X(C_1) = \begin{pmatrix} 0.379 & 0 & 0 \\ 0 & 0.826 & 0.032 \\ 0 & 0.084 & 0.264 \end{pmatrix} \quad \chi = 0.55e$$

$$P_X(O_2) = \begin{pmatrix} -0.444 & 0 & 0 \\ 0 & -0.875 & -0.059 \\ 0 & -0.016 & -0.203 \end{pmatrix} \quad \chi = 0.58e$$

$$P_X(O_2) = \begin{pmatrix} -0.444 & 0 & 0 \\ 0 & -0.875 & -0.059 \\ 0 & -0.087 & -0.283 \end{pmatrix} \quad \chi = 0.58e$$

$$P_X(H_3) = \begin{pmatrix} 0.260 & 0 & 0 \\ 0 & 0.175 & -0.029 \\ 0 & 0.112 & 0.105 \end{pmatrix} \quad \chi = 0.20e$$

$$P_X(H_3) = \begin{pmatrix} 0.260 & 0 & 0 \\ 0 & 0.175 & -0.029 \\ 0 & -0.017 & 0.141 \end{pmatrix} \quad \chi = 0.20e$$

$$P_X(H_4) = \begin{pmatrix} 0.025 & 0 & 0 \\ 0 & -0.024 & -0.043 \\ 0 & -0.033 & -0.162 \end{pmatrix} \quad \chi = 0.10e$$

$$P_X(H_4) = \begin{pmatrix} 0.025 & 0 & 0 \\ 0 & -0.024 & -0.043 \\ 0 & -0.053 & -0.148 \end{pmatrix} \quad \chi = 0.10e$$

---

continued

TABLE 4-7-continued

$$P_X(H_5) = \begin{pmatrix} -0.110 & 0.053 & -0.107 \\ 0.057 & -0.051 & 0.049 \\ -0.053 & 0.008 & 0.003 \end{pmatrix}$$

$\chi = 0.11e$

$$P_X(H_5) = \begin{pmatrix} -0.110 & 0.053 & -0.107 \\ 0.057 & -0.051 & 0.049 \\ -0.053 & 0.036 & 0.013 \end{pmatrix}$$

$\chi = 0.11e$

Note: The atomic numbering scheme and coordinate system are shown in Fig. 4-2. Effective charges (χ) are calculated from Eq. (3-40). The first column of APT's is for a negative sign in the $\partial P_z/\partial Q_5$ element in the $\underline{P}_Q$ matrix in TABLE 4-5, while the second column of APT's is for a positive sign in the $\partial P_z/\partial Q_7$ element in $\underline{P}_Q$. All other signs for the $\underline{P}_Q$ elements are the same as given in TABLE 4-5.

by reversing the sign (from positive to negative) of the $\partial p_z/\partial Q_6$ element are shown in the first column of Table 4-7. The APT's which result from changing the sign of $\partial p_z/\partial Q_7$ from negative to positive are shown in the second column of Table 4-7. The major difference in the APT's calculated from the alternate sign choices compared to the APT's given in Table 4-6 occurs in the dipole moment change along z for displacement of the atom along each of the cartesian coordiante axes. Even the changes in these elements are not all that great. Given the uncertainties in the experimental absolute intensities and the ambiguities in the division of intensity for overlapping regions, we do not feel that the APT's resulting from the alternate sign choices appreciably differ from the APT's given in Table 4-6.

Effect of the Normal Coordinates on the APT's for Methanol

Even after allowing for symmetry constraints, the complete force field for methanol contains 46 force constants. Because of the limited number of independent pieces of experimental data, some of these force constants will be indeterminant if the force field is determined from a fit to the experimentally observed frequencies. Yet the transformation from dipole derivatives with respect to normal coordinates to dipole derivatives expressed in a space-fixed cartesian coordinate system depends explicitly upon the form of the normal coordinates and hence the force field.

We can investigate the effect on the experimental APT's of the form of the normal coordinates by recalculating the APT's using the normal coordinates obtained from another force field for methanol. The alternate force field we have chosen to use is that reported by

Blom, Otto, and Altona (59). (See Appendix A for data.) The force fields for methanol reported by Mallinson (56) and by Blom et al. (59) differ in that the force field reported by Mallinson is an experimental harmonic one, while Blom et al. report an ab initio force field they calculate using a 4-31G basis set. Blom et al. (59) then scaled the theoretical force field to reproduce the observed frequencies for methanol. The two force fields are therefore quite different, mainly because Blom et al. (59) calculated all possible interaction force constants, while Mallinson (56) was forced to assume many of the interaction force constants to be zero.

To calculate the APT's for methanol using the normal coordinates determined from the force field reported by Blom et al. (59), we again need to know the signs of the experimental $\underline{P}_Q$ elements in Table 4-1. The signs given in Table 4-2, however, cannot be used because they were calculated with respect to the normal coordinates derived from the force field reported by Mallinson (56). In other words, the phase definitions will not be the same for the normal coordinate analyses using the two force fields. We therefore recalculated the theoretical $\underline{P}_Q$ matrix from the ab initio APT's given in Chapter 5 for methanol. The $\underline{A}$ and $\underline{L}$ matrices for the force field reported by Blom et al. (59) are given in Appendix A. The signs of the theoretical $\underline{P}_Q$ elements relative to these normal coordinates were then assigned to the experimental $\underline{P}_Q$ matrix exactly as predicted by the ab initio calculation. The rotational correction tensors used in conjunction with the $\underline{L}^{-1}$, $\underline{U}$, and $\underline{B}$ matrices in Appendix A for the force field reported by Blom et al. (59) are different from the ones given in Table 4-4 because the geometry for

methanol assumed by Blom et al. (59) differs slightly from the geometry used by Mallinson (56).

The experimental APT's calculated using the alternate force field (59) for methanol are presented in Table 4-8. The coordinate system for these APT's is again the coordinate system shown in Fig. 4-2. These APT's may be directly compared with the APT's given in Table 4-6 because both sets of APT's are based on the assumption that the ab initio calculation correctly predicts the sign of each $\underline{P}_Q$ element. The APT's in Tables 4-6 and 4-8 are somewhat different with the largest differences occuring in the elements involving the y and z axis components. The effective charges for the methyl hydrogen APT's in the two Tables are the same within $\pm$0.01e. The hydroxyl hydrogen effective charge is also the same when an 0.02e difference is compared to the magnitude of about 0.2e. The largest difference in effective charges occurs for the carbon APT (0.57e for the $\underline{L}^{-1}$ from Mallinson (56) and 0.48e for the $\underline{L}^{-1}$ from Blom et al. (59).

Choice of APT's for Methanol

We must now decide upon the normal coordinates and the sign choices we shall adopt to derive our working set of experimental APT's for methanol. We choose to use the APT's calculated relative to Mallinson's (56) set of normal coordinates; we do so because the scaling procedure used by Blom, Otto, and Altona (59) is somewhat arbitrary (60). More specifically, all the interaction force constants are scaled by a single factor; this casts some doubt upon their true magnitudes. Since more interaction terms result in a larger degree of mixing in the normal coordinates, the APT elements

TABLE 4-8
ATOMIC POLAR TENSORS FOR METHANOL
BASED ON AN ALTERNATE SET OF NORMAL COORDINATES
(units are e)

$$P_X(C_1) = \begin{pmatrix} 0.385 & 0 & 0 \\ 0 & 0.658 & 0.136 \\ 0 & 0.132 & 0.276 \end{pmatrix}$$

$\chi = 0.48e$

$$P_X(O_2) = \begin{pmatrix} -0.452 & 0 & 0 \\ 0 & -0.768 & -0.039 \\ 0 & -0.138 & -0.287 \end{pmatrix}$$

$\chi = 0.55e$

$$P_X(H_3) = \begin{pmatrix} 0.258 & 0 & 0 \\ 0 & 0.222 & -0.051 \\ 0 & -0.006 & 0.141 \end{pmatrix}$$

$\chi = 0.22e$

$$P_X(H_4) = \begin{pmatrix} 0.030 & 0 & 0 \\ 0 & -0.002 & -0.073 \\ 0 & -0.048 & -0.129 \end{pmatrix}$$

$\chi = 0.09e$

$$P_X(H_5) = \begin{pmatrix} -0.110 & 0.048 & -0.106 \\ 0.073 & -0.061 & 0.014 \\ -0.072 & 0.030 & -0.000 \end{pmatrix}$$

$\chi = 0.12e$

Note: The atomic numbering scheme and coordinate system are shown in Fig. 4-2. Effective charges (χ) are calculated from Eq. (3-40). To obtain $P_X(H_6)$, see the note for TABLE 4-6. These APT's are calculated using the normal coordinates obtained from the force field reported by Blom, Otto, and Altona (59).

may be incorrectly distributed within the APT due to the dependence of the APT's on $\underline{L}^{-1}$. For the choice of signs for the experimental $\underline{P}_Q$ matrix elements, we have chosen the set of signs given in Table 4-5. Our justification for this particular choice of signs is that the experimental $\underline{P}_Q$ elements are assigned signs exactly as calculated by the ab initio calculation.

Our final choice for the experimental APT's for the oxygen and hydroxyl hydrogen is given in Table 4-9. The coordinate system is shown in Fig. 4-3. This particular choice of cartesian axes is the bond system; it is with respect to this axis definition that these APT's should be transferred to other molecules containing an O-H group. If the oxygen APT presented in Table 4-9 is transferred to another C-O group, the axes should first be rotated about y such that z is directed along the C-O bond. This distinction for oxygen arises because there exists no unique bond coordinate system for the oxygen APT.

Our final choice for the experimental APT's for the methyl hydrogens and carbon are presented in Table 4-10. The coordinate system is shown in Fig. 4-4. This coordinate system is again the bond coordinate system.

The experimental APT for the hydroxyl hydrogen of methanol may be compared with the hydrogen APT for water (42). Such a comparison is presented in Table 4-11; both APT's are with respect to the same bond system which is that shown in Fig. 4-5. We may first note that displacement of the hydroxyl hydrogen along the O-H bond (the z axis) results in the same dipole moment change ($\partial p_z/\partial z$ = 0.13e) for both water and methanol. This implies that the O-H stretching mode in

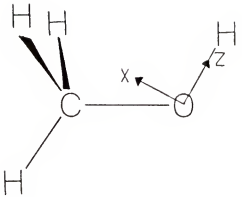

(a) Bond coordinate system for oxygen

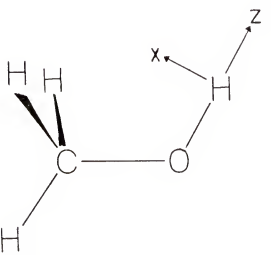

(b) Bond coordinate system for hydrogen

Fig. 4-3. Bond cartesian coordinate systems for the two atoms of the hydroxyl group of methanol. Here the x axis is in the COH plane, and z is directed along the OH bond.

TABLE 4-9
HYDROXYL GROUP APT'S FOR METHANOL
THE APT'S ARE EXPRESSED IN A BOND COORDINATE SYSTEM
(units are e)

$$P_X(O)^a = \begin{pmatrix} -0.803 & 0 & 0.226 \\ 0 & -0.444 & 0 \\ 0.157 & 0 & -0.376 \end{pmatrix}$$

$\chi = 0.59e$

$$P_X(H)^b = \begin{pmatrix} 0.161 & 0 & 0.018 \\ 0 & 0.260 & 0 \\ -0.070 & 0 & 0.141 \end{pmatrix}$$

$\chi = 0.20e$

[a]Coordinate system is shown in Fig. 4-3(a)
[b]Coordinate system is shown in Fig. 4-3(b)

Fig. 4-4. Bond cartesian coordinate systems for the methyl group experimental atomic polar tensors for methanol presented in Table 4-10.

(a) Bond system for carbon
(b) Bond system for the in-plane methyl hydrogen
(c) Bond system for the out-of-plane methyl hydrogen; x is in the H_6CH_5 plane and directed inside the $H_6C_1H_5$ angle.

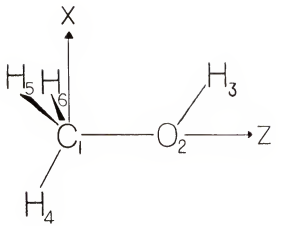

(a)

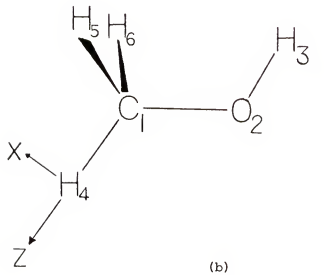

(b)

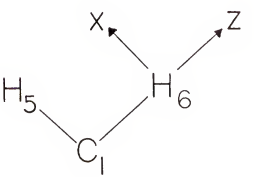

(c)

TABLE 4-10
METHYL GROUP EXPERIMENTAL APT'S FOR METHANOL
(units are e)

$$P_X(C)^a = \begin{pmatrix} 0.359 & & -0.061 \\ 0 & 0.379 & 0 \\ 0.032 & 0 & 0.826 \end{pmatrix}$$

$\chi = 0.57e$

$$P_X(H_4)^b = \begin{pmatrix} -0.025 & 0 & 0 \\ 0 & 0.025 & 0 \\ 0.044 & 0 & -0.164 \end{pmatrix}$$

$\chi = 0.10e$

$$P_X(H_6)^c = \begin{pmatrix} 0.022 & 0.013 & 0.022 \\ 0.034 & -0.014 & 0.044 \\ -0.022 & -0.020 & -0.178 \end{pmatrix}$$

$\chi = 0.11e$

[a] Coordinate system is shown in Fig. 4-4(a)
[b] Coordinate system is shown in Fig. 4-4(b)
[c] Coordinate system is shown in Fig. 4-4(c)

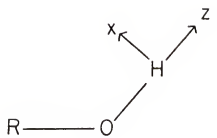

Fig. 4-5. Bond cartesian coordinate system for the hydroxyl hydrogen. The R stands for either H or CH_3.

TABLE 4-11
HYDROXYL HYDROGEN APT'S FOR WATER AND METHANOL
(units are e)

$$P_X(H) = \begin{pmatrix} 0.247 & 0 & -0.049 \\ 0 & 0.330 & 0 \\ -0.064 & 0 & 0.132 \end{pmatrix} \quad H_2O^a$$

$$\chi = 0.25e$$

$$P_X(H) = \begin{pmatrix} 0.161 & 0 & 0.018 \\ 0 & 0.260 & 0 \\ -0.070 & 0 & 0.141 \end{pmatrix} \quad CH_3OH^b$$

$$\chi = 0.20e$$

[a] Taken from Zilles (42) and expressed in the coordinate system shown in Fig. 4-5

[b] Taken from TABLE 4-6 and expressed in the coordinate system shown in Fig. 4-5

methanol has nearly the same dipole moment change associated with it as does water. The O-H bending mode, however, has dipole derivatives that are quite different in the two molecules; if we consider only the diagonal terms in the two APT's corresponding to a bending motion ($\partial p_x/\partial x$), we see that the value for water is one and half times larger than in methanol. It is difficult to compare the $\partial p_y/\partial y$ derivatives for water and methanol because this term contains a large contribution due to molecular rotation; the level of agreement is thus somewhat surprising. The only difference in the two off-diagonal APT terms occurs for $\partial p_x/\partial z$, but the magnitude of the values is not very large. Finally, we note that we may assign an effective charge of 0.23 ± 0.02e to the hydroxyl hydrogen and that this value of the effective charge includes both molecules.

To compare the experimental APT's for the methyl hydrogens of methanol with those for other molecules, we need to consider an average APT for the methyl hydrogens of methanol. The low symmetry (C_s) of the methanol molecule removes the constraint that the APT's for each of the three methyl hydrogens be equivalent when expressed in the same bond coordinate system. An average APT for the methyl hydrogens of methanol was obtained as follows. A bond coordinate system for each of the three hydrogens was chosen so that the z axis was directed along the C-H bond. The x axis was then oriented such that the xz plane bisected the opposite HCH angle and x was directed toward the opposite HCH plane. This coordinate system is perhaps best understood by referring to Fig. 4-6 where it is illustrated. The APT's expressed in this coordinate system for each of the three hydrogens were then averaged to yield an average APT

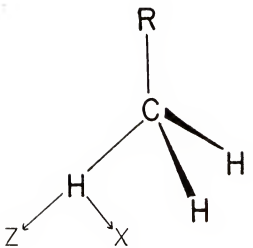

Fig. 4-6. Bond cartesian coordinate system for the methyl hydrogen of various molecules. The x axis lies in the RCH plane. The R group is a general substituent on the methyl group.

TABLE 4-12
METHYL HYDROGEN APT'S FOR VARIOUS MOLECULES.
THE COORDINATE SYSTEM IS SHOWN IN Fig.4-6

$$P_X(H) = \begin{pmatrix} 0.034 & 0 & -0.028 \\ 0 & 0.055 & 0 \\ 0.017 & 0 & -0.169 \end{pmatrix} \quad CH_3CH_3{}^a$$

$$\chi = 0.11e$$

$$P_X(H) = \begin{pmatrix} 0.012 & 0 & -0.021 \\ 0 & 0.073 & 0 \\ 0.007 & 0 & -0.143 \end{pmatrix} \quad CH_3F^b$$

$$\chi = 0.09e$$

$$P_X(H) = \begin{pmatrix} -0.036 & 0 & -0.056 \\ 0 & 0.073 & 0 \\ 0.024 & 0 & -0.061 \end{pmatrix} \quad CH_3Cl^b$$

$$\chi = 0.07e$$

$$P_X(H) = \begin{pmatrix} -0.026 & 0 & -0.024 \\ 0 & 0.030 & 0 \\ 0.011 & 0 & -0.172 \end{pmatrix} \quad CH_3OH^c$$

$$\chi = 0.10e$$

[a] Private communication from J. H. Newton

[b] Newton and Person (51)

[c] Average APT for the methyl hydrogens of methanol; see text

for the methyl hydrogens of methanol. This average APT is presented in Table 4-12 along with experimental APT's calculated for the methyl hydrogens of some other molecules; the coordinate system is illustrated in Fig. 4-6.

One can see from Table 4-12 that the average APT for the methyl hydrogens of methanol is almost the same as the experimental APT for the methyl hydrogen of ethane (61). The only difference in the two APT's occurs for the $\partial p_x/\partial x$ and $\partial p_y/\partial y$ terms and even these two elements are fairly close in magnitude. The effective charges for the methyl hydrogens of methanol and ethane are the same within 0.01e.

A comparison of the experimental APT's for the methyl hydrogens of methanol and the methyl hydrogens of two of the methyl halides (CH_3F and CH_3Cl) (50,51) is also given in Table 4-12. An examination of the APT's for the methyl hydrogens of methanol and methyl fluoride shows that the two APT's are similar. The $\partial p_z/\partial z$ element, especially, shows nearly the same value. This is surprising because Newton and Person (51) have noted that the dipole moment change for displacement of the methyl hydrogen along the C-H bond is linearly related to the electronegativity of the halide atom. The electronegativity of the O-H group (about 3.5 (62)) falls about halfway between the electronegativities for fluorine (4.0) and chlorine (3.2) (63); yet, the $\partial p_z/\partial z$ element of the APT for the methyl hydrogen of methanol does not appear to be midway between the values in the CH_3F and CH_3Cl molecules. The electronegativity of the O-H group is apparently not the only factor governing the perturbation on the APT for the methyl hydrogens of methanol. One could speculate that the

polarizability of the hydroxyl group is different enough from the halides to produce a change in the electrical properties of the methyl group above what would be expected from electronegativity considerations alone.

CHAPTER 5
PREDICTION OF INFRARED INTENSITIES

We now wish to investigate the accuracy to which we may calculate absolute intensities for our series of molecules (methanol, ethanol, dimethyl ether, formaldehyde, and acetone). The absolute intensities for a molecule may be calculated by two methods. One method that can be used is to transfer experimentally derived intensity parameters (the experimental APT's) from one molecule to another. The other method uses quantum mechanical calculations to predict the absolute intensities for a molecule. We shall use both methods of intensity predictions to calculate absolute intensities for the organic molecules studied here. The results of the two methods will be compared, and the use of quantum mechanical calculations as an indication of the transferability of APT's will be discussed. We shall first outline the method by which absolute intensities may be predicted from transferred APT's.

Transferred APT's and Predicted Intensities

As we pointed out in Chapter 1, we might expect, for example, to be able to derive from the absolute intensity of the O-H stretch in methanol some sort of intensity parameter which would be transferable to the hydroxyl group in ethanol. The intensity parameters which we choose to transfer are the atomic polar tensors.

Let us briefly sketch the procedure followed in transferring APT's from one molecule to another. The APT for a particular atom

was always transferred in a bond coordinate system for that atom both in the original molecule and the new molecule. This bond coordinate system was then transformed to a space-fixed cartesian coordinate system for the molecule to which the APT was transferred. The orientation of the space-fixed coordinate system was chosen to coincide with the coordinate system used in the normal coordinate analysis for the new molecule.

The APT for one of the atoms in the new molecule was not transferred; this APT may be determined from the null condition (Eq. 3-25)). The APT calculated from the null condition was chosen to correspond to the atom whose electrical properties would be expected to be most changed when the molecular fragments from the original molecule(s) were combined to form the new molecule. To predict the absolute intensities of methanol using transferred APT's, for example, we could transfer APT's for the methyl hydrogens from methyl fluoride and transfer the APT for the hydroxyl hydrogen from water. We would not, however, necessarily expect to be able to transfer the oxygen APT for methanol from water and successfully predict absolute intensities.

Once the APT's all expressed in the same space-fixed cartesian coordinate system were obtained for the new molecule, the $\underline{P}_X$ matrix was constructed according to Eq. (3-22). The $\underline{P}_Q$ matrix was then calculated using Eq. (3-34) from $\underline{P}_X$ and the normal coordinate analysis matrices $\underline{\Delta}$ and $\underline{L}$ of the molecule. The program used for this calculation was PVDTEN written by Newton (50). The absolute intensity for each normal mode of vibration was calculated using Eq. (3-18).

Ab Initio APT's and Predicted Intensities

Besides testing the transferability of experimental APT's from one molecule to another, we wish also to investigate the accuracy to which ab initio quantum mechanical calculations predict absolute intensities for the series of organic molecules studied here. We may also compare quantum mechanically calculated APT's for a molecule with the APT's transferred to that molecule to determine if the transferred APT's adequately represent the electrical properties of the molecule.

While intensity calculations have been extensively done using semi-empirical quantum mechanical calculations (64) (notably using CNDO/2 (65)), many fewer ab initio calculations of infrared intensities have been done (66) for polyatomic molecules containing several atoms. One reason for this is that the semi-empirical calculations require much less computer time than do the ab initio calculations. The CNDO calculations have also proved to be useful for establishing the sign of the dipole moment derivatives. Ab initio calculations of infrared intensities, though, would presumably yield more exact dipole derivatives than would the semi-empirical claculations as the ab initio calculations would result in more accurate wavefunctions.

Easy-to-use programs for ab initio calculations of one electron properties have become readily available in recent years, and we have used the GAUSSIAN 70 set of programs (67) developed by Pople and coworkers (68). This program calculates self-consistent-field (SCF) molecular wavefunctions, energies, atomic populations, and dipole moments. The program is particularly straightforward to

use as essentially only the molecular geometry and specification of one of the standard basis sets are required as input.

For our ab initio calculations of APT's, we have chosen to use the 4-31G basis set (68) for the description of each molecule studied here (methanol, ethanol, formaldehyde, and acetone). This 4-31G basis set is available as one of the standard basis sets available in GAUSSIAN 70. Other basis set options include STO-3G or 6-31G, but the STO-3G basis set (Slater-type orbitals represented by three gaussian functions) has been found to predict poorer dipole moments (34) and dipole derivatives (69) than do the Gaussian-type orbital representations such as 4-31G or 6-31G. On the other hand, little improvement in calculated vibrational properties has been found to occur when the number of gaussians is increased (such as 6-31G compared to 4-31G). Use of the 6-31G basis set also requires more computational time than does the 4-31G basis set.

A detailed discussion of the 4-31G basis set (and other basis sets) can be found in reference 34. In the 4-31G basis set expansion, the core atomic orbitals on each first and second atom are described by a sum of four gaussian functions, while the valence atomic orbitals are split into an inner part, represented by the sum of three gaussians, and an outer part, represented by one gaussian. The atomic orbital of hydrogen is also split into an inner part (sum of three gaussians) and an outer part (one gaussian). Since the valence orbitals are represented by two independent functions, the 4-31G expansion comprises an extended basis set. Although dipole moments calculated with this basis set are usually larger than experimental dipole moments (34), we shall calculate changes in the

dipole moment and shall be concerned with trends in the calculated dipole derivatives. Furthermore, we shall make comparisons of quantum mechanically calculated APT's using only the 4-31G basis set expansion.

Ab initio calculations of APT's and absolute intensities have not been previously done with a 4-31G basis set for methanol, ethanol, formaldehyde, or acetone. Absolute intensities for dimethyl ether have been calculated using a 4-31G basis set by Blom, Oskam, and Altona (43), but Blom et al. reported electro-optical parameters (10) rather than APT's. We have therefore not repeated the ab initio calculation for dimethyl ether.

We might add that the force fields for methanol (59,70) and dimethyl ether (43) have been calculated using a 4-31G basis set to generate the self-consistent field (SCF) wavefunctions from which the force constants were calculated. Net atomic charges calculated with a 4-31G basis set for methanol have been reported by Momany (71), although he assumed a slightly different geometry (72) than the geometry for methanol we have used (55). The net atomic charges we obtained agree with those found by Momany (71). The relative absolute intensities for methanol have also been quantum mechanically calculated by Serrallach, Meyer, and Günthard (32).

Let us now consider in some detail how the APT's were quantum mechanically calculated. The APT for the αth atom was obtained by first calculating the equilibrium configuration dipole moment and then again calculating the dipole moment after displacement of the αth atom by $\pm$ 0.02 Å along each of the space-fixed cartesian axes in turn. The two-electron integral threshold value was 1×10^{-6}

and convergence on the density matrix was 5×10^{-5}. More rapid convergence for acetone was achieved by using the equilibrium configuration density matrix as the initial guess for the wave-function of the displaced atomic configurations. The equilibrium experimental geometries about which the atoms were displaced were taken from Sasada, Takano, and Saton (73) for ethanol, from Oka, Hirakawa and Shimoda (74) for formaldehyde, and from Nelson and Pierce (75) for acetone. Calculation of the APT's for atomic displacements about the experimental equilibrium geometries rather than the theoretical equilibrium geometries was done because the APT's are not usually overly sensitive to small changes in the equilibrium geometry (64). Furthermore, Schwendeman (76) has suggested that distinct advantages exist for using the experimental geometries rather than theoretical geometries in quantum mechanical calculations.

The requisite APT derivatives were approximated as

$$\partial p_i / \partial j_\alpha \cong \Delta p_i / \Delta j_\alpha \qquad (6\text{-}1)$$

where Δp_i is the dipole moment component change along i = x, y, or z, and Δj_α is the displacement magnitude of the αth atom along the space-fixed cartesian axis j = x, y, or z. Displacement of the αth atom along x, for example, thus gives three APT elements: $\partial p_x / \partial x_\alpha$, $\partial p_y / \partial x_\alpha$, and $\partial p_z / \partial x_\alpha$. The atoms were displaced along the cartesian axes in both positive and negative directions; the APT elements were then calculated as the arithmetic mean of the derivative in Eq. (5-1) for the two displacement directions.

Polar tensors for every atom in the molecules studied here were not quantum mechanically calculated by the method just described.

Symmetry considerations dictate that in formaldehyde, for example, the APT for one of the two hydrogens can be calculated from the APT for the other hydrogen. Also, the APT for one of the atoms in a molecule can be calculated using the null condition (Eq. (3-25)).

Methanol

Absolute intensities for methanol were predicted both by transferring APT's from other molecules and by quantum mechanically calculating the APT's for methanol. We are interested in comparing the APT's and the absolute intensities calculated by the two methods. We wish to compare also the signs for the dipole moment derivatives predicted by the transferred APT's with the signs predicted by the quantum mechanical calculation. The quantum mechanically calculated signs for the dipole derivatives were used to derive experimental APT's for methanol (Chapter 4); if the same signs were also predicted by the transferred APT's, we would be confident that the signs we have chosen are correct for methanol.

APT's and Absolute Intensities for Methanol

We shall first consider the method by which APT's from various molecules were transferred to methanol. The APT for a hydroxyl hydrogen in another molecule might be expected to be transferable to the hydroxyl hydrogen of methanol. The only other molecule containing a hydroxyl group for which experimental APT's have been determined is water (42). We shall transfer this hydroxyl hydrogen APT from water to methanol. The oxygen APT of water could be transferred to the oxygen atom in methanol but the oxygen atom in methanol is bonded to a carbon atom rather than another hydrogen, and the electrical characteristics of the oxygen atom may be different in

methanol. This point will be further discussed later when the quantum mechanically calculated APT's are compared with the transferred APT's.

Experimental APT's have been evaluated for the methyl halide series CH_3X(X = F, Cl, Br, or I) (51), so we can test the transferability of the methyl hydrogen APT's from this series to the methyl hydrogens of methanol. The elements of the APT's for the hydrogens in the CH_3X series correlate linearly with the electronegativity of the X atom (51), so CH_3OH might be expected to fit in the CH_3X series. Consequently, each of the elements of the APT's for the methyl hydrogens in the CH_3X series was plotted against the electronegativity of the substituent atom (F, Cl, Br, or I). The electronegativities were taken from values given by Huheey (62,63). The elements of the APT for the methyl hydrogens of methanol were then read off the plots using the electronegativity of the OH group (3.5) (62).

Absolute intensities for methanol were also calculated by transferring the methyl hydrogen APT's for methanol from methyl fluoride(51). This calculation was motivated in part by the fact that the experimental APT's for the methyl group of methanol are more similar to those for CH_3F than electronegativity considerations would suggest (see Chapter 4). The electronegativity of the OH group (3.5) falls about halfway between the values for CH_3F (4.0) and CH_3Cl (3.2) (62).

Atomic polar tensors for the carbon and oxygen atoms of methanol must also be obtained. The APT for either atom could be calculated from the null condition (Eq. (3-25)); both of these possibilities were investigated. Determination of the oxygen APT by difference meant that the carbon APT was obtained either from electronegativity considerations (as described above for the methyl hydrogen APT's) or

from methyl fluoride. We also transferred the oxygen APT from water and then calculated the carbon APT from the null condition, but this set of APT's gave poorly predicted intensities. The ab initio calculations, to be discussed later, show that the oxygen APT in methanol is more different from the oxygen APT in water than the carbon APT in methanol is different from the carbon APT in methyl fluoride.

The two sets of transferred APT's for methanol are presented in Table 5-1. The set of transferred APT's based on electronegativity considerations in the CH_3X series (S = F, OH, Cl, Br, and I) will be referred to for brevity as APT's transferred from CH_3X. The APT's transferred from CH_3X and H_2O are listed in the first column of Table 5-1. The APT's transferred from CH_3F and H_2O to methanol are shown in the second column of Table 5-1. The APT for only one of the two out-of-plane hydrogens of methanol is presented in Table 5-1 since these two hydrogen APT's are related. The hydrogen atom numbered 6 in Fig. 4-2 is related to H_5 by a reflection through the yz plane. Hence, $P_X(H_6)$ is obtained from $P_X(H_5)$ by reversing the signs in the APT of all the off-diagonal elements involving an x component of either the dipole moment or the atomic displacement direction.

Also presented in Table 5-1 are the quantum mechanically calculated APT's for methanol. These APT's were calculated using the GAUSSIAN 70 program and the 4-31G basis set described earlier. For brevity, these APT's will be referred to as ab initio APT's since they were obtained from an ab initio quantum mechanical calculation. The APT for the carbon atom of methanol was not calculated quantum

TABLE 5-1

TRANSFERRED AND QUANTUM MECHANICAL APT'S FOR METHANOL

THE COORDINATE SYSTEM IS SHOWN IN FIG. 4-2.

(units are electrons (e))

APT's transferred from[a]:

	CH_3X and H_2O[b]			CH_3F and H_2O[c]			ab initio[d]		
$P_X(C_1)$	0.259	0	0	0.331	0	0	0.573	0	0
	0	0.748	0	0	0.955	0	0	0.764	0.095
	0	0	0.259	0	0	0.331	0	0.036	0.295
$\chi(C_1)$		0.40			0.61			0.58	
$P_X(O_2)$	-0.570	0	0	-0.586	0	0	-0.748	0	0
	0	-0.920	0.015	0	-1.201	0.015	0	-0.952	-0.074
	0	0.029	-0.352	0	0.029	-0.368	0	-0.016	-0.344
$\chi(O_2)$		0.66			0.80			0.73	
$P_X(H_3)$	0.330	0	0	0.330	0	0	0.444	0	0
	0	0.267	-0.015	0	0.267	-0.015	0	0.302	-0.043
	0	-0.029	0.112	0	-0.029	0.112	0	0.016	0.115
$\chi(H_3)$		0.25			0.25			0.32	

---

continued

TABLE 5-1-continued

$P_X(H_4)$	0.071	0	0	0.073	0	0	0.079	0	0
	0	-0.032	-0.060	0	-0.007	-0.066	0	0.018	-0.061
	0	-0.006	-0.084	0	-0.039	-0.123	0	-0.053	-0.113
$\chi(H_4)$		0.07			0.09			0.09	
$P_X(H_5)$	-0.045	0.005	-0.067	-0.074	0.034	-0.085	-0.174	0.055	-0.084
	0.052	-0.032	0.030	0.057	-0.007	0.033	0.090	-0.066	0.041
	-0.067	0.003	0.033	-0.085	0.020	0.024	-0.067	0.009	0.023
$\chi(H_5)$		0.07			0.09			0.14	

[a]The APT for the oxygen atom is calcuated from the null condition. The APT for H_6 is obtained by reversing the signs of all the off-diagonal elements in $P_X(H_5)$ involving x.

[b]$P_X(H_3)$ transferred from H_2O (42); all other APT's except for the oxygen APT were transferred from the methyl halides (51) using electronegativity correlations.

[c]$P_X(H_3)$ transferred from H_2O (42); all other APT's except for the oxygen APT were transferred from CH_3F (51).

[d]APT's calculated using GAUSSIAN 70 program (67) and a 4-31G basis set (68)

mechanically, but was calculated from the null condition. The APT for one of the two out-of-plane hydrogens in the methyl group was also not quantum mechanically calculated because the APT for one of the out-of-plane hydrogens can easily be obtained from the APT for the other out-of-plane hydrogen.

The APT's given in Table 5-1 were used in conjunction with the $\underline{A}$ and $\underline{L}$ matrices given in Appendix A for both sets of normal coordinates (from Mallinson (56) and from Blom, Otto, and Altona (59)) to calculate the absolute band intensities for methanol according to Eq. (3-34). Although both sets of normal coordinates were used together with each of the three sets of APT's in Table 5-1 to predict the absolute intensities for methanol, we shall present the results for only some of the calculations. Absolute intensities predicted for methanol using the three sets of APT's in Table 5-1 are compared with experiment in Table 5-2.

The results of three intensity calculations using the transferred APT's for methanol are given in Table 5-2. The APT's transferred from water and from the methyl halides (using electronegativities) were used in calculation I to predict the absolute intensities for methanol. The set of APT's used for calculation I are given in the first column of Table 5-1, and the normal coordinates (the $\underline{L}$ matrix) were calculated from the force field reported by Mallinson (56) for methanol. Calculation II in Table 5-2 made use of the APT's transferred from water and methyl fluoride. These APT's are listed in the second column of Table 5-1. The normal coordinates used in calculation II are again obtained from the force field reported by Mallinson. A comparison of calculations I and II thus shows the

TABLE 5-2
PREDICTED ABSOLUTE INTENSITIES FOR METHANOL
(units are km mol^{-1})

Mode[b]	A(exp)[c]	A(pred.,transferred APT's)[a] I[d]	II[e]	III[f]	A(pred., ab initio APT's)[g]
ν_1(3667)	22	19.7	20.9	28.3	22.2
ν_2(3005)	39	14.1	31.8	33.5	25.3
ν_9(2962)	63	13.6	32.0	32.2	98.7
ν_3(2848)	28	22.8	25.8	22.3	40.8
ν_4(1474)	1.2	6.2	4.3	4.0	2.1
ν_{10}(1466)	1.6	7.7	6.1	4.9	2.1
ν_5(1451)	7.1	3.8	1.6	4.3	3.9
ν_6(1335)	18.4	42.8	41.7	32.2	31.1
ν_{11}(1145)	1.0	1.9	0.9	0.7	5.9
ν_7(1077)	4	2.7	1.7	15.3	13.4
ν_8(1034)	96	105	170	157	127
ν_{12}(272)	56	99	101	101	203

[a] The APT for the oxygen atom is calculated from the null condition.

[b] See Appendix A for normal coordinate data; frequencies are from Mallinson (56).

[c] The best estimates for the experimental absolute intensities for methanol are taken from TABLE 2-2.

[d] Calculated using APT's transferred from water (42) and from the methyl halides (51), using electronegativity correlations for the APT;s of the methyl group atoms. The APT's are listed in the first column of TABLE 5-1. The normal coordinates are calculated from the force field for methanol reported by Mallinson (56).

---

continued

TABLE 5-2-continued

[e]Calculated using APT's transferred from water (42) and from methyl fluoride (51). The APT's are given in the second column of TABLE 5-1. The normal coordinates are again calculated from the force field reported by Mallinson(56).

[f]Same as calculation II, except that the normal coordinates are calculated from the force field reported by Blom, Otto, and Altona (59).

[g]Calculated using the ab initio APT's for methanol. The quantum mechanical APT's are given in the third column of TABLE 5-1. The L matrix is the same as used for calculation I.

effect of transferring APT's for the methyl group atoms from CH_3F rather than CH_3X. Calculation III uses the APT's transferred from methyl fluoride and from water, but the normal coordinates were derived from the force field reported by Blom, Otto, and Altona (59) for methanol. Calculations II and III thus illustrate the dependence on the normal coordinates of the predicted absolute intensities. The $\underline{A}$ and $\underline{L}$ matrices for the two force fields considered for methanol are presented in Appendix A.

The absolute intensities predicted by the quantum mechanically calculated APT's for methanol are presented in the last column of Table 5-2. These intensities were calculated using the ab initio APT's given in Table 5-1 and the normal coordinates derived from the force field reported by Mallinson (56) for methanol.

Discussion of Results for Methanol

Predicted absolute intensities

We shall first consider the absolute intensities predicted for methanol using APT's transferred from water and from the methyl halide series, based on electronegativity considerations. Here we refer to calculation I in Table 5-2. The normal coordinates for this calculation were derived from the force field for methanol reported by Mallinson (56).

Considering first the absolute intensities predicted for the vibrations of the COH group, we see that the intensity predicted (20 km mol^{-1}) for the O-H stretch, ν_1, is almost the same as the experimental value (22 km mol^{-1}). The COH bending mode (ν_6), however, is predicted to be too intense by a factor of two. The absolute intensity predicted for the C-O stretch (ν_8) is within

the 10% uncertainity of the experimental value. Finally, the O-H torsion (ν_{12}) is predicted to have an absolute intensity too large by a factor of almost two. The predicted intensities for the two deformation modes of the COH group thus agree poorly with experiment (though the predicted values are both within a factor of two) while the two stretching modes have intensities that are predicted very well by the transferred APT's. Although the intensities predicted by calculation I, modified to obtain the carbon APT from the null condition, are not reported in Table 5-2, the only significant change in the predicted intensities for the above vibrations was that the intensity predicted for the C-O stretch was too low by a factor of four.

The absolute intensities predicted by calculation I for the methyl group vibrations, however, are in generally poor agreement with experiment. Although the intensity predicted for the symmetric C-H stretch (ν_3) compares favorably with experiment, the total intensity predicted for the other two C-H stretches (ν_2 and ν_9) is too low by a factor of almost four. The experimental values for the absolute intensities of methyl group deformation modes are perhaps less accurate because the intensities are small, but the predicted intensities do not appear to agree well. Certainly the intensity distribution predicted by calculation I for ν_4,ν_{10}, and ν_5 seems to be inverted. The intensity predictions for the methyl group vibrations are also more poorly predicted when the carbon APT rather than the oxygen APT is calculated from the null condition. Based on the discrepancies in the predicted intensities for the methyl group vibrations, we conclude that the APT's for

the methyl hydrogens of methanol are not correctly given by a consideration of the electronegativities of the substituent atom or group in the CH_3X series. The result of transferring the APT's for the atoms in the methyl group from methyl fluoride is therefore next considered.

The absolute intensities predicted for the vibrational modes of methanol were found to be in much better agreement with experiment when the APT's for the methyl group were transferred from methyl fluoride (calculation II in Table 5-2). The prediction of the intensity for the C-O stretching vibration has somewhat worsened (170 km mol^{-1} predicted, 96 km mol^{-1} measured), but this is more than offset by the increased accuracy in prediction of the intensities for the methyl group vibrations. The C-H stretching region has only one mode, the antisymmetric stretch (ν_9), for which the intensity is poorly predicted (a factor of two too low). The predicted intensity of the O-H torsional mode is still too large by a factor of almost two, but most of the remaining vibrational modes have intensities that are predicted quite well.

The absolute intensities calculated from the APT's depend upon the normal coordinates (see Eq. (3-34)), so we wish to examine also the effect of the $\underline{L}$ matrix on the predicted intensities for methanol. As discussed in Chapter 4, we have calculated two sets of normal coordinates for methanol, one set using the experimental force field reported by Mallinson (56) and the other set using the scaled *ab initio* force field reported by Blom, Otto, and Altona (59). We also explained in Chapter 4 why we expect the force field reported by Mallinson to be the better one for methanol.

Calculations II and III in Table 5-2 are identical except that calculation II uses the L matrix from Mallinson (56), while calculation III uses the L matrix from Blom et al. (59). The differences in the intensities predicted using the two different L matrices are for the most part small. The intensity of the O-H stretch is predicted to be more intense by the L matrix from Blom et al.; the intensity predicted for the O-H bending mode (ν_6) compares more favorably with experiment using the L from Blom et al. The intensities calculated with the different L matrices also differ in the predicted intensity ratio between ν_7, a CH_3 deformation mode, and ν_8, the C-O stretch. We shall return to a discussion of the intensity ratio of ν_7 to ν_8 later.

The final set of predicted intensities listed in Table 5-2 were calculated using the quantum mechanically calculated APT's for methanol and the L matrix from Mallinson (56). The quantum mechanical calculation using the 4-31G basis set predicts perfectly the absolute intensity for the O-H stretch (ν_1). The intensity for the C-O stretching vibration (ν_8) is also predicted well, but the intensities for the other two vibrations of the COH group are more poorly reproduced by the quantum mechanical calculation. The intensity for the COH bending mode (ν_6) is calculated to be too large, but the predicted value is within a factor of two; the O-H torsional mode (ν_{12}), however, is predicted to have an absolute intensity four times larger than the experimental value. These results for the intensities of the vibrations involving the oxygen are in accord with the experience that the 4-31G basis set, although suitable for intensities involving motion along the bonds, is

inadequate for calculating intensities which involve large contributions from lone pairs of electrons, such as the O-H torsion (77).

The quantum mechanically calculated intensities for the vibrations of the methyl group are all calculated within a factor of two of the experimental values except the parallel (ν_7) and perpendicular (ν_{11}) twisting modes of the methyl group. The intensity ratio for ν_7 to ν_8 is especially interesting. The quantum mechanical predicts that ν_7 is almost 11% as intense as the C-O stretch (ν_8). Such a large intensity for ν_7 is difficult to accept because the experimental spectrum of the C-O stretching region of methanol does not seem to indicate that ν_7 is nearly that intense. If the intensity of ν_7 (at 1077 cm^{-1}) were 11% of the intensity of ν_8 (at 1034 cm^{-1}), one would expect to see a much more intense R-branch in Fig. 2-3. Based on the experimental evidence, the value of about 4% calculated by Serrallach, Meyer, and Gunthard (32) appears more reasonable. A much lower intensity for ν_7 is also suggested by the predicted intensities using the transferred APT's for methanol (calculations I and II in Table 5-2).

Simulated spectra

The intensities predicted for methanol may be compared visually by plotting "simulated spectra" using the absolute intensities given in Table 5-2. The simulated spectra may then be directly compared with the experimentally observed spectrum. A detailed description of how these and all other simulated spectra we shall present were plotted is explained in Appendix B. The procedure is outlined here.

First, no attempt has been made to reproduce the P, Q, R or P, R structure that is present for many of the absorption bands; rather, Gaussian functions are fitted to the broad contours of the bands. Full widths at half maximum (FWHM) are estimated from the experimental absorption spectra; these values are listed in Appendix B. One final point is that only as many Gaussian functions are used as bands can be discerned in the experimental spectrum. In the C-H stretching region around 3000 cm^{-1} of the gas phase spectrum of methanol (see Fig. 5-1(c)), we observe only two distinct, but partially overlapped bands; therefore we use only two Gaussian functions to describe this region. The Gaussian function for the higher frequency band contains the intensities due to both ν_2 and ν_9. The Gaussian function for the lower frequency band contains only the intensity for ν_3. We have chosen this procedure because we have no easy way of estimating half-widths for gas phase spectral bands that are very much overlapped. The predicted absolute intensities were then used together with the Gaussian parameters to calculate the percent transmittance as a function of wavenumber. The cell pathlength and sample pressure were chosen to be the same as was used to measure the experimental spectrum.

The simulated spectrum using the intensities predicted for methanol using APT's transferred from CH_3F and H_2O (calculation II) is shown in Fig. 5-1(a). Shown in Fig. 5-1(b) is the simulated spectrum for methanol using the quantum mechanically calculated APT's. These two simulated spectra may be compared with the experimentally observed spectrum for methanol, shown in Fig. 5-1(c).

Fig. 5-1. Comparison of simulated and experimental spectra for methanol. All three spectra are plotted for 3.04 kPa of methanol in a 10.2 cm cell.

(a) Simulated spectrum of methanol using absolute intensities predicted by transferring APT's from methyl fluoride and water.
(b) Simulated spectrum using quantum mechanically calculated intensities.
(c) Experimental spectrum of methanol measured with the Nicolet Model 7199 FT-IR.

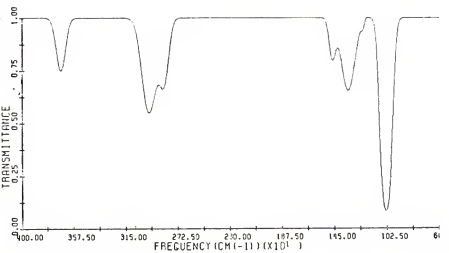
TRANSMITTANCE
1.00
0.75
0.50
0.25
0.00
400.00
357.50
315.00
272.50
230.00
187.50
145.00
102.50
FREQUENCY (CM(-1)) (X10( ))

(a)

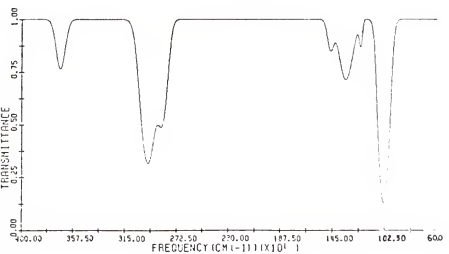
TRANSMITTANCE
1.00
0.75
0.50
0.25
0.00
400.00
357.50
315.00
272.50
230.00
187.50
145.00
102.50
600
FREQUENCY (CM(-1)) (X10( ))

(b)

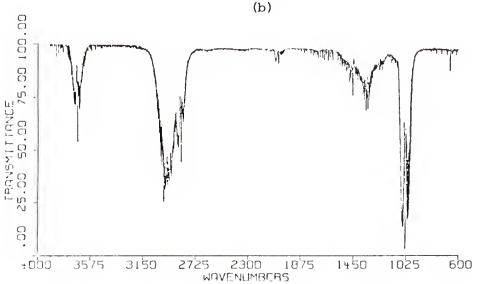
TRANSMITTANCE
.00
25.00
50.00
75.00
100.00
4000
3575
3150
2725
2300
1875
1450
1025
600
WAVENUMBERS

(c)

The experimental spectrum was measured with the Nicolet Model 7199 FT-IR; the pressure of methanol was 3.04 kPa in a 10.2 cm cell. The two simulated spectra in Fig. 5-1 are plotted for the same pathlength and sample pressure.

Comparison of the simulated spectrum based on the transferred APT's (Fig. 5-1(a)) with the experimental spectrum (Fig. 5-1(c)) shows that the most obvious discrepancy between prediction and experiment occurs in the methyl group and hydroxyl group bending region (the bands near 1400 cm^{-1}). The transferred APT's predict a much stronger absorption in this region than is present in the experimental spectrum. The two spectra agree very well over all, with most of the band intensities predicted within a factor of two, and the predicted relative intensities of the bands certainly agree with the experimental spectrum of methanol. We thus conclude that the APT's transferred to methanol from CH_3F and H_2O predict the intensities of the spectrum of methanol within a factor of two.

The experimental spectrum and the simulated spectrum based on the transferred APT's may be compared also with the simulated spectrum (Fig. 5-1(b)) based on the quantum mechanically calculated APT's for methanol. As with the transferred APT's the "ab initio" APT's have overestimated the intensity in the C-H and O-H bend region near 1400 cm^{-1}. The ab initio APT's also overestimate the intensities in the C-H stretching region near 3000 cm^{-1} and in the C-O stretching region near 1000 cm^{-1}, but both predictions are within a factor of two. The intensity for the O-H stretch (3667 cm^{-1}), on the other hand, is perfectly predicted by the quantum mechanical calculation.

Comparison of the simulated spectra based on the transferred APT's and based on the quantum mechanically calculated APT's shows few differences;only the intensity for the C-H stretching region visually differs in the two spectra. While the transferred APT's appear to underestimate the intensity in the C-H stretching region, the ab initio APT's have overestimated this intensity.

We conclude this discussion of the comparison of the simulated spectra with the experimental spectrum of methanol by emphasizing some general observations. The APT's transferred from methyl fluoride and from water predict almost all of the intensities for methanol within a factor of two. Some of the more intense bands are predicted much better than this, and of course the predicted intensities for some of the weak bands are predicted worse than a factor of two. The same factor-of-two agreement was found also for the quantum mechanically predicted intensities. Because of possible uncertanties in the normal coordinates for methanol (see calculations II and III in Table 5-2), this factor-of-two agreement is very good.

Comparison of APT's for methanol

We now examine the APT's transferred from CH_3F and H_2O, the quantum mechanically calculated APT's, and the experimental APT's derived in Chapter 4 to see if we may draw any conclusions about the factor-of-two disagreements in the predicted intensities for methanol. The APT's for the hydroxyl group will be discussed first. (See Table 5-3).

TABLE 5-3
COMPARISON OF APT'S FOR METHANOL.
THE COORDINATE SYSTEM AND NUMBERING SYSTEM IS SHOWN IN FIG. 4-2.
(units are e)

	experimental[a]			transferred[b]			ab initio[c]		
$P_x(C_1)$	0.379	0	0	0.331	0	0	0.573	0	0
	0	0.826	0.032	0	0.955	0	0	0.764	0.095
	0	-0.061	0.359	0	0	0.331	0	0.036	0.295
$\chi(C_1)$		0.57			0.61			0.58	
$P_x(O_2)$	-0.444	0	0	-0.586	0	0	-0.748	0	0
	0	-0.875	-0.059	0	-1.201	0.015	0	-0.952	-0.074
	0	0.010	-0.304	0	0.029	-0.368	0	-0.016	-0.344
$\chi(O_2)$		0.58			0.80			0.73	
$P_x(H_3)$	0.260	0	0	0.330	0	0	0.444	0	0
	0	0.175	-0.029	0	0.267	-0.015	0	0.302	-0.043
	0	0.059	0.128	0	-0.029	0.112	0	0.016	0.115
$\chi(H_3)$		0.20			0.25			0.32	

---

continued

TABLE 5-3-continued

$P_X(H_4)$	0.025	0	0	0.073	0	0	0.079	0	0
	0	-0.024	-0.043	0	-0.007	-0.066	0	0.018	-0.061
	0	0.001	-0.164	0	-0.039	-0.123	0	-0.053	-0.113
$\chi(H_4)$		0.10			0.09			0.09	
$P_X(H_5)$	-0.110	0.053	-0.107	-0.074	0.034	-0.085	-0.174	0.055	-0.084
	0.057	-0.051	0.049	0.057	-0.007	0.033	0.090	-0.066	0.041
	-0.048	-0.005	-0.009	-0.085	0.020	0.024	-0.067	0.009	0.023
$\chi(H_5)$		0.11			0.09			0.14	

[a] From the experimentally derived APT's for methanol (TABLE 4-6). These APT's correspond to the best sign choice for the $\underline{P}_Q$ matrix.

[b] Transferred from CH_3F and H_2O. See TABLE 5-1.

[c] Quantum mechanically calculated APT's for methanol. See TALBE 5-1

The transferred and ab initio APT's for the hydroxyl hydrogen (H_3) obviously predict a much larger dipole moment change in $\partial p_x/\partial x$ than is indicated by the experimental APT. Since x is out-of-plane direction (Fig. 4-2), this is why the intensity predicted for the O-H torsion by both the transferred APT's and the ab initio APT's is much too large. The other differences in the three APT's are somewhat smaller, although the $\partial p_y/\partial y$ value is overestimated by the quantum mechanical calculation. These large dipole derivatives predicted by the ab initio calculation are probably due to the inadequate description by the 4-31G basis set of the lone pairs of electrons on the oxygen atom. Indeed, the ab initio APT for the oxygen also shows a $\partial p_x/\partial x$ value that is larger than experiment. The other elements of the oxygen APT are well predicted by the ab initio calculation. The effective charge of the oxygen atom is predicted perfectly by the ab initio calculation.

If we recall that the oxygen APT for methanol was calculated using the null condition when APT's were transferred to methanol, the agreement between the predicted APT for oxygen and the experimental APT is most impressive. Of course, the predicted value for $\partial p_y/\partial y$ is too large, and this is one of the reasons that the predicted intensity of the C-O stretch was much too large when APT's were transferred to methanol.

If the experimental APT's for the carbon and oxygen atoms are compared with the ab initio APT's and also with the transferred APT's, we see that the carbon APT transferred from CH_3F agrees very well with both the experimental APT for carbon and the ab initio APT for carbon. One discrepancy is that because the carbon in CH_3F is on

a C_3 axis, the APT is diagonal; in methanol, however, this symmetry constraint is removed and the APT for carbon is no longer diagonal. If, however, the APT for oxygen had been transferred from water, and the carbon APT calculated from the null condition, the results would be quite different. The oxygen APT transferred from water to methanol is given in Table 5-4. The carbon APT that would then be calculated from the null condition is also indicated. In this case, the oxygen APT transferred from water to methanol does not agree as well with either the experimental APT or the ab initio APT for the oxygen atom in methanol. The element related to the C-O stretch, $\partial p_y/\partial y$, in the transferred APT for oxygen is only half as large as it should be. If we now examine in Table 5-4 the carbon APT calculated from the null condition, we find poor agreement with the experimental or ab initio APT for the carbon atom, just as the oxygen APT transferred from water did not agree. In fact, the carbon APT calculated from the null condition is especially incorrect for methanol. The effective charge is only half of what if should be, and the $\partial p_y/\partial y$ element is only one fifth the value for the experimental APT. Based on both the experimentally derived APT's for methanol and the ab initio APT's, we thus conclude that the carbon APT should be transferred and the oxygen APT calculated by difference. The carbon APT is transferable from CH_3F to CH_3OH because the very electronegative fluorine atom to which the carbon is bonded is replaced by the OH group which is also quite electronegative (63). The oxygen APT in water, however, is not transferable to methanol because replacing a hydrogen by a methyl group causes a substantial change in the electrical properties of the oxygen atom. (Compare the ab initio

TABLE 5-4

APT'S RESULTING FROM TRANSFERRING THE OXYGEN APT FROM WATER. THE COORDINATE SYSTEM IS THAT SHOWN IN FIG. 4-2 (units are e)

$$P_X(O)^a = \begin{pmatrix} -0.659 & 0 & 0 \\ 0 & -0.410 & -0.075 \\ 0 & -0.075 & -0.348 \end{pmatrix}$$

$\chi(O) = 0.50$

$$P_X(C)^b = \begin{pmatrix} 0.405 & 0 & 0 \\ 0 & 0.164 & 0.089 \\ 0 & 0.104 & 0.311 \end{pmatrix}$$

$\chi(C) = 0.32$

[a] Transferred to methanol from water (42)

[b] Calculated from the null condition using the APT's for the hydrogens given in the second column of TABLE 5-1

APT given in Table 5-3 for the oxygen APT in methanol with the oxygen APT, transferred from water, in Table 5-4.)

Finally, we compare the transferred and ab initio APT's for the methyl hydrogens with the experimental APT's. (Here we are comparing the hydrogens referred to as H_4 and H_5 in Table 5-3). The quantum mechanically predicted effective charges differ dramatically for the methyl hydrogen in the symmetry plane of the molecule and the methyl out-of-plane hydrogen (0.09e vs. 0.14e, respectively). This difference is also apparent, but to a lesser degree, for the experimental APT's. The transferred APT's do not show this effect because the APT's were transferred from CH_3F for which the hydrogens are equivalent. The differences in the three sets of APT's for the methyl hydrogens are much less obvious than for the APT's for some of the other atoms in methanol. The APT for the out-of-plane hdyrogen is especially difficult to compare because all nine elements are nonzero. We can see, though, that the hydrogen APT's transferred from methyl fluoride compare favorably with both the ab initio APT's and the experimental APT's. The small changes that we observe in Table 5-3 for the methyl hydrogen APT's are, however, significant as the simulated spectra using the intensities predicted by the transferred APT's (Fig. 5-1(a)) and using the quantum mechanically calculated intensities (Fig. 5-1(b)) are different in appearance.

$\underline{P}_Q$ matrices for methanol

Experimental APT's were derived in Chapter 4 for methanol. This required that the signs for the dipole derivatives with respect to the normal coordinates be determined. Some assumptions about the directions of the dipole moment changes for the vibrations of a' symmetry had to be also made. These two questions, the signs and directions of the dipole moment changes, will now be considered in more detail.

Both the transferred APT's and the ab initio APT's, when transformed to the $\underline{P}_Q$ matrix, provide information concerning the sign and direction of each dipole derivative. We present in Table 5-5 the magnitudes for the $\underline{P}_Q$ elements calculated from the measured absolute intensities for methanol. (See Chapter 4.) The $\underline{P}_Q$ matrices calculated from the APT's transferred from CH_3F and H_2O and the APT's calculated quantum mechanically are given also in Table 5-5. The comparison between the quantum mechanically calculated $\underline{P}_Q$ matrix and the $\underline{P}_Q$ matrix predicted by the transferred APT's is remarkable: both $\underline{P}_Q$ matrices predict the same signs for the nonzero elements in the experimental $\underline{P}_Q$ matrix. We would have deduced the same set of signs as predicted by the ab initio quantum mechanical calculation if we had simply used the signs predicted by the APT's transferred from CH_3F and H_2O (calculation II in Table 5-2). We should point out that the same set of signs is predicted also by the APT's transferred from the CH_3X series and H_2O (calculation I in Table 5-2). It is interesting to speculate that transferred APT's which predict intensities within a factor of two

TABLE 5-5

P_Q MATRICES FOR METHANOL

(units are e $u^{-1/2}$)

experiment[a]	0	0	0	0	0	0	0	0	0.246	0.041	0.032	0.240
	0.048	0.0	0.169	0.0	0.085	0.121	0.0	0.314	0	0	0	0
	0.142	0.189	0.0	0.035	0.0	0.041	0.064	0.0	0	0	0	0
transferred[b]	0	0	0	0	0	0	0	0	-0.181	-0.079	0.030	0.321
	-0.091	0.024	-0.158	0.014	0.031	-0.197	-0.006	-0.417	0	0	0	0
	-0.115	0.179	0.039	-0.065	0.027	0.062	0.041	0.028	0	0	0	0
ab initio[c]	0	0	0	0	0	0	0	0	-0.318	-0.046	0.078	0.456
	-0.076	-0.009	-0.204	0.010	0.051	-0.177	-0.115	-0.360	0	0	0	0
	-0.130	0.161	0.015	-0.045	0.037	0.026	0.022	0.012	0	0	0	0

[a] Taken from TABLE 4-1. Only magnitudes are shown

[b] APT's transferred from CH_3F (51) and H_2O (42). The APT for oxygen is obtained from the null condition. Force field is that reported by Mallinson. The same set of signs were calculated when APT's from CH_3X and H_2O were transferred

[c] Ab initio calculation using the 4-31G basis set

for organic molecules perhaps also predict reasonably well the signs for the dipole derivatives. In any case, because the signs of the dipole derivatives for methanol are consistently predicted no matter how the APT's are obtained (transferred or calculated quantum mechanically), we can be confident that we have chosen the correct set of signs to derive the experimental APT's for methanol.

The two predicted $\underline{P}_Q$ matrices for methanol also indicate the direction of the dipole derivatives; that is, the distribution of $\partial\vec{p}/\partial Q_i$ among the y and z components in the $\underline{P}_Q$ matrix. The use of C_{3v} symmetry to describe the methyl group vibrations of a' symmetry (ν_2, ν_3, ν_4, ν_5, and ν_7) is well justified by both the $\underline{P}_Q$ matrix calculated from the transferred APT's and the $\underline{P}_Q$ matrix calculated quantum mechanically. A discrepancy occurs for ν_5 where the calculations indicate that a change in $\partial p_z/\partial Q_5$ occurs as well as the change in $\partial p_y/\partial Q_5$ we assumed for the experimental $\underline{P}_Q$ matrix. The other discrepancy occurs for ν_7; however, the intensity for this mode was discussed earlier when it was pointed out that the intensities predicted by either of the two calculations seem to be much to large when compared to the experimental spectrum (Fig. 2-3). The low absolute intensities measured for ν_5 and ν_7 means that these dipole derivatives will not make a large contribution to the APT's, so the exact direction of the dipole derivatives for ν_5 and ν_7 are not so important.

The other three vibrations of a' symmetry involve the COH group of methanol. The dipole derivative for the C-O stretch (ν_8) certainly follows the C-O bond, as we assumed in Chapter 4. This direction is indicated by both the transferred APT's and the <u>ab initio</u>

APT's. Taking the dipole moment change for the O-H stretch (ν_1) to be directed along the O-H bond is also qualitatively confirmed by the calculated $\underset{\sim}{P}_Q$ matrices. The calculations indicate that the dipole derivative direction for the O-H bending mode (ν_6) which we assumed to be perpendicular to the O-H bond is also reasonable. From the comparisons of the signs and directions of the dipole derivatives in the predicted $\underset{\sim}{P}_Q$ matrices, we may be reasonably confident of the APT's derived from the experimental absolute intensities for methanol.

Ethanol

We now consider the prediction of absolute intensities for the twenty-one vibrational modes of ethanol. The intensities for ethanol will be predicted by transferring APT's from other molecules. The APT's for some of the atoms in ethanol were also quantum mechanically calculated; these "ab initio" APT's will be compared with the APT's transferred to ethanol and with the ab initio APT's for methanol.

APT's and Absolute Intensities for Ethanol

The APT's for the hydroxyl hydrogen and oxygen of ethanol were transferred from the experimental APT's derived for these atoms in methanol (Table 4-9). The APT's for the out-of-plane hydrogens of the methyl group in methanol (Table 4-10) were transferred to the methylene hydrogens in ethanol. Intensities calculated for ethanol using an average APT for the methyl hydrogens in methanol (Table 4-12) were in worse agreement with the experimental intensities and shall not be presented. The APT's for the atoms in the methyl group of

ethanol were transferred either from ethane (61) or from methane (78). Either the methyl or the methylene carbon could be calculated from the null condition, and both possibilities were investigated.

The APT's transferred to ethanol from other molecules are presented in Table 5-6; the coordinate system and atomic numbering system is shown in Fig. 5-2. The quantum mechanically calculated APT's for some of the atoms of ethanol are also shown for comparison; we did not do quantum mechanical calculations to obtain every APT for ethanol. Only the independent APT's are listed in Table 5-6; the methyl and methylene out-of-plane hydrogens are related by reflection through the xz plane in Fig. 5-2. Thus, $P_X(H_2)$ may be obtained from $P_X(H_1)$ by reversing the signs of all off-diagonal elements in $P_X(H_1)$ involving y.

Either carbon APT might be expected to be not transferable, and we have calculated intensities for ethanol using the assumption that the methylene carbon APT was transferable and also the assumption that the methyl carbon APT was transferable. For either assumption the APT for the other carbon atom is then determined by the null condition. The various APT's based on these assumptions for the methyl and methylene carbon atoms are shown in Table 5-7.

The absolute intensities we have calculated for ethanol using various combinations of the APT's given in Tables 5-6 and 5-7 are presented in Table 5-8. The predicted absolute intensities are compared with the experimental absolute intensities we measured for ethanol (Table 2-3). The absolute intensities predicted for ethanol using APT's transferred from methanol and ethane are shown in calculation I. The APT for the methyl carbon was calculated by

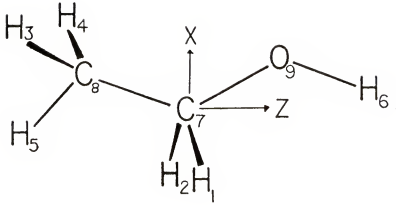

Fig. 5-2. Cartesian coordinate system for ethanol. Here both x and z lie in the $C_8C_7O_9$ plane with x also in the $H_1C_7H_2$ plane. The y axis is directed perpendicular to the symmetry plane of the molecule and determined by the right hand rule

TABLE 5-6
TRANSFERRED AND QUANTUM MECHANICAL APT'S FOR ETHANOL.
THE COORDINATE SYSTEM AND NUMBERING SCHEME ARE SHOWN IN FIG.5-2.
(units are electrons (e))

	APT's transferred from: CH_3OH[a]	ab initio APT's[b]
$P_X(H_1)$[c]	$\begin{pmatrix} -0.042 & 0.071 & -0.001 \\ 0.119 & -0.110 & -0.013 \\ -0.056 & 0.022 & -0.019 \end{pmatrix}$	$\begin{pmatrix} -0.095 & 0.138 & -0.003 \\ 0.117 & -0.149 & -0.021 \\ -0.022 & -0.016 & -0.048 \end{pmatrix}$
$\chi(H_1)$	0.11	0.15
$P_X(H_6)$	$\begin{pmatrix} 0.129 & 0 & -0.028 \\ 0 & 0.260 & 0 \\ 0.060 & 0 & 0.174 \end{pmatrix}$	$\begin{pmatrix} 0.195 & 0 & 0.078 \\ 0 & 0.436 & 0 \\ 0.146 & 0 & 0.221 \end{pmatrix}$
$\chi(H_6)$	0.20	0.32
$P_X(O_9)$	$\begin{pmatrix} -0.454 & 0 & -0.287 \\ 0 & -0.444 & 0 \\ -0.218 & 0 & -0.725 \end{pmatrix}$	$\begin{pmatrix} -0.493 & 0 & -0.275 \\ 0 & -0.722 & 0 \\ -0.292 & 0 & -0.884 \end{pmatrix}$
$\chi(O_9)$	0.59	0.75
	C_2H_6[d]	
$P_X(H_3)$[e]	$\begin{pmatrix} -0.026 & -0.116 & -0.002 \\ -0.093 & -0.094 & -0.019 \\ 0.020 & 0.013 & 0.040 \end{pmatrix}$	not calculated[f]
$\chi(H_3)$	0.11	
$P_X(H_5)$	$\begin{pmatrix} -0.025 & 0 & -0.070 \\ 0 & 0.055 & 0 \\ -0.115 & 0 & -0.111 \end{pmatrix}$	not calculated
$\chi(H_5)$	0.11	

---

continued

TABLE 5-6-continued

	CH_4[g]			
$P_X(H_3)$[e]	0.019	-0.078	0.032	not calculated
	-0.078	-0.070	0.055	
	0.032	0.055	0.041	
$\chi(H_3)$		0.10		
$P_X(H_5)$	0.0	0	-0.093	not calculated
	0	0.064	0	
	-0.093	0	-0.074	
$\chi(H_5)$		0.10		

[a] Taken from TABLES 4-9 and 4-10. Here we transfer the APT's for the out-of-plane hydrogens in methanol to the methylene hydrogens in ethanol.

[b] Quantum mechanically calculated APT's using the GAUSSIAN 70 program with a 4-31G basis set.

[c] $P_X(H_2)$ may be obtained by reversing the signs of all the off-diagonal elements in $P_X(H_1)$ involving y.

[d] Transferred from ethane (61).

[e] $P_X(H_4)$ is obtained by reversing the signs of all the off-diagonal elements in $P_X(H_3)$ involving y.

[f] We have not calculated ab initio APT's for all the atoms in ethanol.

[g] Transferred from methane (78)

TABLE 5-7
APT'S FOR THE METHYL AND METHYLENE CARBONS IN ETHANOL
SEE ALSO TABLE 5-6

	Transferred from: CH_3OH[a]			ab initio APT's[b]		
$P_X(C_7)$	0.513	0	0.267	0.467	0	0.220
	0	0.379	0	0	0.559	0
	0.174	0	0.673	0.155	0	0.727
$\chi(C_7)$		0.57			0.61	

	C_2H_6[c]		
$P_X(C_8)$	0.078	0	0.066
	0	0.127	0
	0.066	0	0.037
$\chi(C_8)$		0.10	

not[d] calculated

APT's from null constraint

$P_X(C_8)$[e]	-0.027	0	0.125	-0.143	0	0.081
	0	0.157	0	0	0.102	0
	0.170	0	-0.053	0.126	0	-0.093
$\chi(C_8)$		0.16			0.14	

$P_X(C_7)$[f]	0.408	0	0.326
	0	0.410	0
	0.277	0	0.583
$\chi(C_7)$		0.53	

[a] Taken from TABLE 4-10.

[b] Quantum mechanically calculated APT using the GAUSSIAN 70 program with a 4-31G basis set.

[c] Transferred from ethane (61).

[d] We did not calculate the quantum mechanically predicted APT for this atom.

---

continued

TABLE 5-7-continued

[e]Calculated from the null condition. The first APT for C_8 in this row was calculated by difference from the APT's transferred from methanol and ethane. The second APT for C_8 was calculated by difference from the APT's transferred from methanol and methane. The APT for C_7 was transferred in both cases from methanol. See also TABLE 5-6.

[f]Calculated by difference from the APT's transferred from methanol and ethane. The APT for C_8 was transferred from ethane. See also TABLE 5-6.

TABLE 5-8
PREDICTED ABSOLUTE INTENSITIES FOR ETHANOL
(units are km mol^{-1})

Mode (cm^{-1})[a]	A(exp)[b]	A(predicted) I[c]	II[d]	III[e]	IV[f]
ν_1 (3660)	16.4	26.2	26.2	27.0	26.6
ν_{14} (2987)	72	25.0	92.2	92.1	73.9
ν_2 (2971)		35.4	40.8	41.3	19.3
ν_{15} (2930)	87	68.2 → 174	3.0 → 173	3.5 → 176	7.2 → 136
ν_3 (2901)		26.2	18.1	17.3	21.4
ν_4 (2890)		19.1	19.1	21.4	14.2
ν_5 (1482)	37	14.6	1.6	1.3	4.0
ν_6 (1450)		5.5	2.0	1.3	2.0
ν_{16} (1451)		3.1 → 33	3.4 → 30	3.6 → 25	0.1 → 31
ν_7 (1393)		1.2	14.1	14.3	15.4
ν_8 (1393)		8.2	8.7	4.2	9.4
ν_9 (1241)	22	39.1 → 40	48.7 → 49	48.7 → 49	53.9 → 54
ν_{17} (1241)		1.0	0.2	0.1	0.5
ν_{18} (1098)	106	1.6	0.5	0.8	3.1
ν_{10} (1061)		41.1 → 68	24.5 → 59	23.5 → 51	30.0 → 65
ν_{11} (1027)		24.9	33.8	26.5	32.1
ν_{12} (883)	11	4.1	7.6	6.3	3.5
ν_{19} (801)	1.1	0.6	0.4	0.4	5.8
ν_{13} (422)	7.2[g]	7.1	7.1	6.4	7.4

---

continued

TABLE 5-8-continued

$\nu_{20}(224)$	} 58[g]	4.2	} 73	3.1	} 73	3.4	} 72	0.1	} 73
$\nu_{21}(224)$		68.6		69.4		68.6		73.1	

[a] Experimental frequencies taken from Zemlyanukhina, Sverdlov, and Finkel (18).

[b] Experimental absolute intensities are the values measured here. See TABLE 2-3. Probable accuracy is ±10%.

[c] Calculated using APT's transferred from methanol and ethane. The APT for the methyl carbon was calculated by difference. See TABLES 5-6 and 5-7 for data. The normal coordinate transformation matrices are generated from the force field reported by Zemlyanukhina and Sverdlov (79).

[d] Same as calculation I, except the normal coordinates are derived using force constants transferred to ethanol from propane (80) and methanol (59).

[e] Calculated using APT's transferred from methanol and ethane. The APT for the methylene carbon was calculated by difference. See TABLES 5-6 and 5-7 for data. The normal coordinates are calculated using the transferred force constants for ethanol.

[f] Calculated using APT's transferred from methanol and methane. The APT for the methyl carbon was calculated by difference. See TABLES 5-6 and 5-7 for data. Normal coordinates are generated from the transferred force constants.

[g] Absolute intensities are from Zemlyanukhina et al. (18).

difference. The normal coordinate transformation matrices for calculation I were generated from the force constants reported by Zemlyanukhina and Sverdlov (79) for ethanol. The absolute intensities predicted in calculation II for ethanol are calculated from the same data as in calculation I, except that the normal coordinate transformation matrices were derived from force constants transferred to ethanol from propane (80) and from methanol (59). Data for both force fields for ethanol are given in Appendix I, and we shall discuss these two force fields for ethanol later. A comparison of the absolute intensities predicted by calculations I and II for ethanol thus shows the effect on the intensities of the normal coordinates. Calculation III is the same as calculation II, except that for calculation III the APT for the methylene carbon was calculated using the null condition. The APT's for calculation III were transferred from methanol and ethane. Calculations II and III thus illustrate the differences in the predicted intensities when the methylene carbon APT is transferred (calculation II) and when the methyl carbon APT is transferred (calculation III). The final calculation (IV) presented in Table 5-8 shows the absolute intensities predicted for ehtanol using APT's transferred from methanol and methane. The APT for the methyl carbon was calculated by difference. The normal coordinates are generated from the transferred force constants for ethanol. A comparison of calculations II and IV shows the differences in the predicted intensities that result when the APT's are transferred from methane (calculation IV) rather than ethane (calculation II).

Discussion of Results for Ethanol

Force fields for ethanol

The calculation of absolute intensities for ethanol requires an accurate set of normal coordinates (the $\underline{L}$ matrix needed in Eq. (3-34). The determination of $\underline{L}$ for ethanol is rather complicated, for ethanol has only C_s symmetry. Of the twenty-one normal modes of vibration, thirteen will be of a' symmetry and eight will have a'' symmetry. The low symmetry of the molecule makes the normal coordinate analysis particularly challenging because the $\underline{L}$ matrix will block factor only into a (13 x 13) matrix and a (8 x 8) matrix. Hence, the symmetry coordinates appreciably mix to give the normal modes of vibration. Although infrared spectra for several isotopic species of ethanol have been published (81, 82), assignment of the gas phase spectra is a difficult task because many of the absorption bands overlap. Since there are 231 internal force constants in the general case for ethanol many of these force constants can not be determined from the experimentally observed frequencies.

The only reasonably complete force field for ethanol is the one reported by Zemlyanukhina and Sverdlov (79). They determined 48 force constants for ethanol by fitting the force constants to the experimentally observed frequencies for ethanol and seven of its deuterium derivatives. We have used the $\underline{L}$ matrix derived from this force field to predict absolute intensities for ethanol. But because of the complexity of the normal coordinate analysis for ethanol, we have derived also a force field by transferring force constants to ethanol from other molecules.

As we pointed out above, many of the interaction force constants for ethanol are not easily determined from the experimental frequencies. Yet some of these interaction force constants may be large and thus significantly change the L matrix. Quantum mechanical calculations provide a way to obtain such force constants, and Blom and Altona (83) have noted that ab initio force constants scaled (80) to fit experimentally observed frequencies seem to be transferable among small organic molecules. We have, therefore, transferred scaled ab initio force constants from methanol (59) and from propane (80) to ethanol. We transferred to ethanol all of the diagonal force constants and the interaction force constants for the $HOCH_2$ group from methanol. All of the force constants for the CH_3CH_2 group were transferred to ethanol from propane. We do, however, have to use five force constants from the force field reported by Zemlyanukhina and Sverdlov (79). These five force constants are: the CCO bending force constant the CCO bend - COH bend interaction, the C-O stretch - CCO bend interaction, the C-C stretch - CCO bend interaction, and the C-C stretch - C-O stretch interaction. These five force constants may not be evaluated from propane or from methanol. The details of the normal coordinate analyses using the two force fields are presented in Appendix A. Frequencies calculated using the transferred force constants for ethanol are also given in Appendix A. We might note here that the maximum calculated error in any frequency for ethanol using the transferred force constants was just over 50 cm^{-1}, and that the average error was only 18 cm^{-1}. The force constants could have been adjusted to give a better least squares fit to the experimentally

observed frequencies, but this would have lessened the predictive aspect of the analysis for ethanol.

Predicted absolute intensities

Calculation I in Table 5-8 shows the intensities which are predicted for ethanol when APT's are transferred from methanol and from ethane. The APT for the methyl carbon was calculated by difference, and the normal coordinates are generated from the force field reported by Zemlyanukhina and Sverdlov (79). We see that calculation I predicts an absolute intensity for the O-H stretch (ν_1) which is quite larger than the experimental value. The predicted value is, however, within a factor of two of the experimental value. The C-H stretching region (near 3000 cm^{-1}) has a predicted total intensity that is only 9% larger than the experimentally measured total intensity for the region. The approximate experimental separation of the intensities for the higher frequency modes (ν_{14} and ν_2) and for the lower frequency modes (ν_{15}, ν_3, and ν_4) indicates, however, that the predicted intensity distribution for these modes is not as good as the predicted total intensity for this region. The total intensity predicted for the C-H bending region (near 1450 cm^{-1}) is also very good (only 11% too high), but the predicted intensity distribution is difficult to compare with experiment. The COH bending mode (ν_9) has an intensity which is predicted in calculation I to be too high by a factor of two. The intensity predicted for the C-O stretching region near 1000 cm^{-1} is predicted too low by less than a factor of two. Finally, we observe that the predicted total intensity for the methyl and hydroxyl torsions (ν_{20} and ν_{21}) compares favorably with experiment.

The predicted absolute intensities depend upon the form of the normal coordinates, and as we discussed above, an alternate $\underline{L}$ matrix was derived for ethanol using transferred force constants from methanol and from propane. One of the motivations for predicting the intensities using an alternate $\underline{L}$ matrix arises from a consideration of the O-H stretching intensity in ethanol and in methanol.

The O-H stretch in methanol has an experimental absolute intensity of 22 km mol^{-1} (See Table 2-2); in ethanol, however, the absolute intensity for the O-H stretch has dropped to 16.4 km mol^{-1} (See Table 2-3). The calculation using APT's for the hydroxyl group atoms transferred from methanol to ethanol, however, has predicted an increase rather than a decrease in the intensity for the O-H stretch in ethanol. We shall see later that the quantum mechanically calculated APT's for the hydroxyl hydrogen and oxygen atoms in methanol and in ethanol are very similar. The possibility thus arises that the decrease in intensity of the O-H stretch in ethanol is due to the normal coordinates. Indeed, if we merely reverse the sign of the $L_{13,1}$ element (from -0.04172 to +0.04172) in the $\underline{L}$ matrix derived from the force field reported by Zemlyanukhina and Sverdlov (See Appendix A for data), the intensity predicted by calculation I for the O-H stretch in ethanol decreases to 20 km mol^{-1}. Symmetry coordinate number thirteen is the change in the CCO angle of ethanol, so the $L_{13,1}$ element represents an interaction of the O-H stretch with the CCO bend. Such an interaction, which is not possible in methanol, represents a plausible explanation for the decreased intensity of the O-H stretch in ethanol. Thus, we

transferred force constants to ethanol in hopes of obtaining a different L matrix, one which would reproduce the experimentally observed absolute intensity of the O-H stretch. Although the new L matrix for ethanol still does not predict the decrease in the intensity of the O-H stretch, the new L does predict significant variations in the intensities predicted for many of the other normal modes.

The effect of the form of the normal coordinates on the predicted intensities for ethanol may be seen in calculations I and II in Table 5-8. The APT's for both of these calculations were transferred from methanol and ethane, but the normal coordinates for calculation I were derived from the force field reported by Zemlyanukhina and Sverdlov (79), while the normal coordinates for calculation II were generated using the force constants we transferred to ethanol. The intensities predicted for modes whose frequency is far from other vibrational modes of the same symmetry show little variation with respect to changing L. The O-H stretching mode (ν_1) has a predicted intensity of 26 km mol^{-1} which is essentially unaffected by differences in the two force fields for ethanol. The same result is true for the methyl and hydroxyl group torsions (ν_{20} and ν_{21}) where the predicted intensity for the two bands remains about 71 km mol^{-1} for either of the two force fields. The predicted intensity for the C-H stretching region (around 3000 cm^{-1}) and for the region between 1500 cm^{-1} and 800 cm^{-1} is, however, extremely complicated and sensitive to the form of the L matrix.

Calculations III and IV in Table 5-8 present the absolute intensities predicted for ethanol using different assumptions about the transferability of the APT's. The normal coordinates for both calculations are generated from the transferred force constants. Instead of discussing these predicted intensities in terms of Table 5-8, we shall compare the simulated infrared spectra (See Appendix B) for the four calculations with the experimental spectrum. The simulated spectra make the data presented in Table 5-8 much easier to compare.

Simulated spectra

The effect of the L matrix on the distribution of intensity among the vibrational modes of ethanol is shown in Fig. 5-3. Here the simulated spectrum based on calculation I is shown in Fig. 5-3(a), the simulated spectrum based on calculation II is shown in Fig. 5-3(b), and the experimentally observed infrared spectrum of ethanol is shown for comparison in Fig. 5-3(c). The L matrix derived from the force field reported by Zemlyanukhina and Sverdlov (79) is used in calculation I, while the L matrix derived from the transferred force constants is used in calculation II.

If we compare the two simulated spectra in Fig. 5-3, we see that the form of the L matrix does indeed change the appearance of the simulated spectrum in the regions of overlapping vibrational modes. The C-H stretching region near 3000 cm^{-1} shows a reversal in the predicted relative intensity for the higher (ν_2 and ν_{14}) vs. the lower (ν_3, ν_4, and ν_{15}) frequency C-H stretches. The intensity distribution among the C-H bending modes near 1450 cm^{-1} is also different for the two sets of normal coordinates. Finally, the

relative intensities for the COH bending region (near 1250 cm^{-1}) and the C-O stretching region (near 1000 cm^{-1}) are reversed in the two calculations.

We may also compare the two simulated spectra in Fig. 5-3 with the experimental spectrum of ethanol (Fig. 5-3(c)). The simulated spectra for both calculations I and II agree well with the experimental spectrum in the O-H stretching region (near 3600 cm^{-1}). Calculation II, however, more closely compares with the experimental spectrum both in the C-H stretching region (near 3000 cm^{-1}) and in the C-H bending region (near 1450 cm^{-1}). Neither simulated spectrum, however, accurately predicts the remaining spectral regions. The intensity of the COH bending mode near 1250 cm^{-1} is predicted too high by both calculations I and II, and the intensity of the C-O stretching mode near 1000 cm^{-1} is predicted too low. The discrepancies are factor-of-two disagreements (See also Table 5-8). We conclude that calculation II agrees better than calculation I with the experimental spectrum, so we shall use the normal coordinates derived from the transferred force constants in subsequent calculations (calculations III and IV).

The simulated spectra based on calculations III and IV are shown in Fig. 5-4(a) and 5-4(b), respectively. Calculation III is based on APT's transferred from methanol and from ethane; the APT for the methylene carbon is calculated by difference. We may thus compare Fig. 5-3(b), the simulated spectrum for calculation II, with Fig. 5-4(a), the simulated spectrum for calculation III, to see the effect of transferring the methyl carbon APT vs. the

Fig. 5-3. Simulated spectra for ethanol showing the effect of $\underline{L}$ on the predicted intensities. The experimental spectrum (2.67 kPa, 10.2 cm cell) is shown also for comparison.

(a) The spectrum simulated using APT's transferred from methanol and ethane with the APT for the methyl carbon determined by difference. The normal coordinates are derived from the force constants reported by Zemlyanukhina and Sverdlov (79). See calculation I in TABLE 5-8 for data.

(b) Same as (a) except that the normal coordinates are generated from the force constants transferred to ethanol. See calculation II in TABLE 5-8 for data.

(c) The experimentally observed infrared spectrum of ethanol, measured with the Nicolet Model 7199 FT-IR.

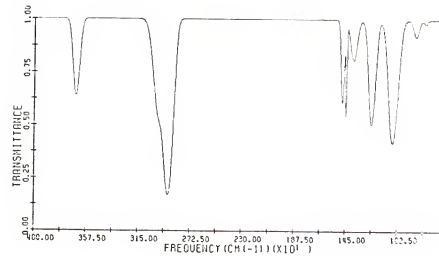

(a) Calculation I

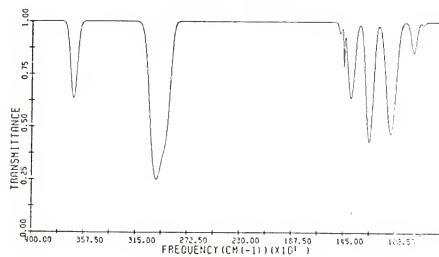

(b) Calculation II

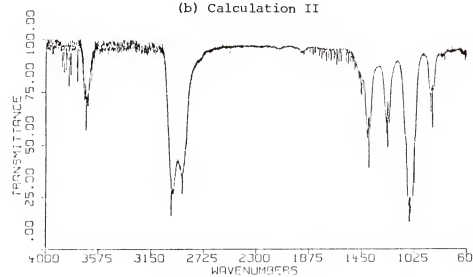

(c) Experimental

Fig. 5-4. Simulated spectra for ethanol showing the effect of APT's transferred from different molecules. The experimental spectrum (2.67 kPa, 10.3 cm cell) is shown also for comparison.

(a) The spectrum simulated using APT's transferred from methanol and ethane with the APT for the methylene carbon determined by difference. Normal coordinates are derived from the transferred force constants for ethanol. See calculation III in TABLE 5-8 for data.

(b) The spectrum simulated using APT's transferred from methanol and methane with the APT for the methyl carbon determined by difference. Normal coordinates are derived from the transferred force constants. See calculation IV in TABLE 5-8 for data.

(c) The experimentally observed infrared spectrum of ethanol, measured with the Nicolet Model 7199 FT-IR.

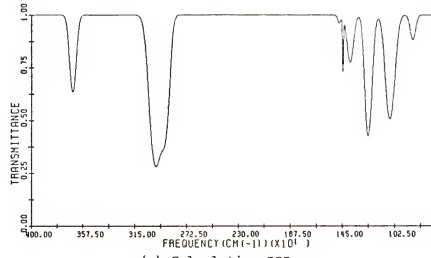

(a) Calculation III

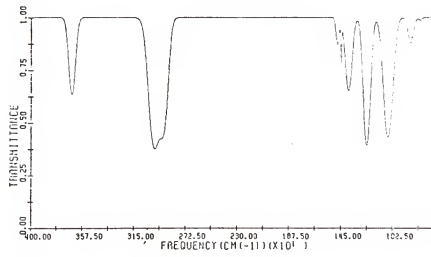

(b) Calculation IV

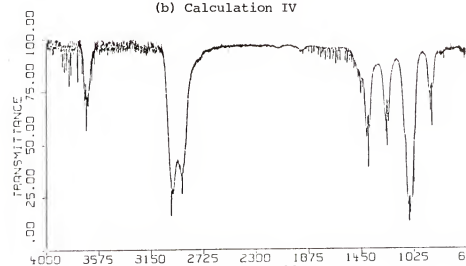

(c) Experimental

effect of transferring the methylene carbon APT. The two simulated spectra appear different in only the C-H bending region near 1450 cm^{-1}. Although the overall differences in the simulated spectra are small, the simulated spectrum based on calculation III seems to agree slightly better with the experimental spectrum (Fig. 5-4(c)) than does calculation II. This implies that the methylene carbon APT is more transferable from methanol than is the methyl carbon APT transferable from ethane. We shall discuss this point further when we compare the quantum mechanically calculated APT's for methanol and for ethanol.

The simulated spectrum based on calculation IV is shown in Fig. 5-4(b). The APT's for the methyl hydrogens were transferred from methane; the methyl carbon APT was calculated by difference. As with the three previous calculations, APT's were transferred from methanol to the remaining atoms. A comparison of the simulated spectra for calculations II and IV shows that using methane (calculation IV) rather than ethane (calculation II) as the source for the APT's for the methyl group atoms of ethanol results in only a small change in the appearance of the simulated spectrum. The intensity for the C-H stretching region shows a small increase in the intensity for the lower frequency modes (near 2900 cm^{-1}) when the APT's are transferred from methane (calculation IV). Calculation IV also results in a slight increase for the intensity of ν_5 (a C-H bend at 1482 cm^{-1}). Otherwise the two spectra are remarkably similar. Calculation IV does not accurately predict the experimentally observed spectrum (Fig. 5-4(c)), but the overall agreement is within a factor of two.

An examination of the simulated spectra for the calculations I through IV shows that none of the calculations yields completely satisfactory agreement with the experimental infrared spectrum of ethanol. Although all of the simulated spectra show factor-of-two agreement and show the same pattern of intensities as in the experimental spectrum, we would like to know if the remaining discrepancies in the predicted intensities for ethanol are due to changes in the APT's for ethanol. As we discussed earlier, the normal coordinate analysis for ethanol is complicated and could be responsible for some of the remaining discrepancies. We therefore now compare the transferred APT's for ethanol with some quantum mechanically calculated APT's for ethanol and for methanol.

Comparison of APT's for ethanol

We have included in Tables 5-6 and 5-7 quantum mechanically calculated APT's for several atoms of ethanol. These ab initio APT's may be compared with the APT's transferred to ethanol. Let us first consider the APT for the hydroxyl hydrogen of ethanol.

The APT transferred to the hydroxyl hydrogen in ethanol from the corresponding atom in methanol agrees reasonably well with the ab initio APT for that atom (See $P_x(H_6)$ in Table 5-6). The large apparent discrepancy in the $\partial p_y/\partial y$ element for out-of-plane displacement of H_6 is actually misleading because the ab initio calculation using the 4-31G basis set overestimates the intensity of the O-H torsion by a factor of almost four (as shown, for example, in Table 5-2). Based on the comparison of the APT transferred from methanol for the hydroxyl hydrogen and the ab initio APT, we would expect the APT to be transferable. This is shown

more clearly in Table 5-9, where the ab initio APT's for the hydroxyl hydrogens of methanol and ethanol are compared in a bond coordinate system (Fig. 5-5(a)). Here we see that the agreement for the two APT's is essentially complete. The only significant difference in these two APT's is possibly the slight decrease in the dipole derivative along the O-H bond as the hydrogen atom is displaced (the $\partial p_z/\partial z$ element). We conclude that the hydroxyl hydrogen APT in methanol should be transferable to ethanol without modification.

The slight decrease in the value of $\partial p_z/\partial z$ for the hydroxyl hydrogen APT in ethanol has some significance with regard to the intensity of the O-H stretch. As we saw in Table 5-8, the absolute intensity for the O-H stretch of ethanol is predicted to be about 26 km mol^{-1} using experimental APT's transferred from methanol. However, the experimental absolute intensity for this mode in ethanol is only 16.4 km mol^{-1}, while the corresponding intensity in methanol is 22 km mol^{-1}. As we noted earlier, the predicted intensity for this mode in ethanol decreases from 26 km mol^{-1} to 20 km mol^{-1} if the sign of the $L_{13,1}$ matrix element is reversed. Combined with the slight decrease predicted for the $\partial p_z/\partial z$ element, the intensity predicted for the O-H stretch in ethanol using the reversed sign for $L_{13,1}$ would approach the experimental absolute intensity. The major cause for the decrease in the intensity for the O-H stretch in ethanol compared to methanol appears, however, to be the L matrix because the APT's for the hydroxyl hydrogens in the two molecules are remarkably similar.

Fig. 5-5. Bond coordinate systems for comparing APT's in methanol and ethanol. See TABLE 5-9.

(a) Coordinate system for the hydroxyl hydrogen atom. Here R is CH_3 for methanol and CH_3CH_2 for ethanol. The x axis lies in the COH plane, and y is determined by the right hand rule.
(b) Coordinate system for the carbon and oxygen atoms. Here R is H for methanol and CH_3 for ethanol.
(c) Coordinate system for the out-of-plane methyl hydrogens.

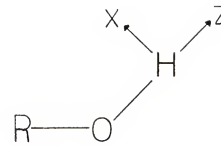

(a)

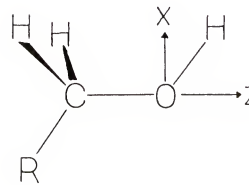

(b)

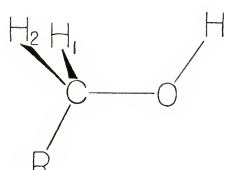

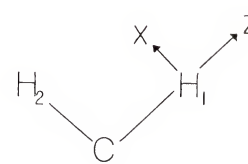

(c)

TABLE 5-9
COMPARISON OF AB INITIO APT'S FOR METHANOL AND ETHANOL
(units are electrons (e))

APT[a]	Methanol			Ethanol		
$P_X(H)$[b]	0.292	0	-0.016	0.309	0	-0.016
	0	0.444	0	0	0.436	0
	-0.075	0.32	0.126	-0.084	0	0.107
$\chi(H)$			0.32			0.32
$P_X(O)$[c]	-0.344	0	-0.016	-0.360	0	-0.110
	0	-0.748	0	0	-0.722	0
	-0.074	0	-0.952	-0.094	0	-1.02
$\chi(O)$		0.73			0.75	
$P_X(C)$[d]	0.295	0	0.036	0.380	0	0.036
	0	0.573	0	0	0.559	0
	0.095	0	0.764	0.101	0	0.815
$\chi(C)$		0.58			0.61	
$P_X(H)$[e]	0.017	0.032	0.029	0.007	0.015	-0.027
	0.036	-0.009	0.063	0.027	-0.048	0.000
	0.037	0.013	-0.225	-0.006	-0.015	-0.251
$\chi(H)$		0.14			0.15	

[a] Quantum mechanically calculated APT's using the GAUSSIAN 70 program with a 4-31G basis set.

[b] The APT for the hydroxyl hydrogen. The coordinate system is shown in Fig. 5-5(a).

[c] The APT for the hydroxyl oxygen. The coordinate system is shown in Fig. 5-5(b).

[d] The APT's for the methyl carbon of methanol and for the methylene carbon of ethanol. The coordinate system is shown in Fig. 5-5(b).

[e] The APT's for the methyl out-of-plane hydrogen of methanol and for the methylene hydrogen of ethanol. The coordinate system is shown in Fig. 5-5(c)

If we now compare the oxygen APT transferred to ethanol from methanol and the quantum mechanically calculated APT for the oxygen in ethanol, we find that the two APT's agree very well as shown in Table 5-6. As with the hydroxyl hydrogen APT's, however, the ab initio APT for the oxygen has an $\partial p_y/\partial y$ element that is too large compared to the value in the transferred APT. This abnormally large value predicted by the quantum mechanical calculation for the change in the dipole moment with respect to the out-of-plane motion of the oxygen atom ($\partial p_y/\partial y$) is probably caused by an inadequate description by the 4-31G basis set of the lone pairs of electrons on the oxygen atom.

If we compare also the quantum mechanically predicted APT's for the oxygen atoms in methanol and in ethanol we observe further confirmation of the similarity of the APT's for the oxygen atoms in the two alcohols. These two ab initio APT's are shown in Table 5-9; the bond coordinate system is shown in Fig. 5-5(b). The quantum mechanically predicted effective charge for the oxygen atom is the same (0.74 ± 0.01e) for either methanol or ethanol. The only substantial change which occurs in the ab initio APT for the oxygen atom upon replacing one of the methyl hydrogens in methanol with a methyl group is in the $\partial p_x/\partial z$ element of the APT. This element actually shows a dramatic increase from nearly zero in methanol to -0.1e in ethanol. The overall differences in the two APT's are only minor, and we should be able to successfully transfer an experimental APT for oxygen in methanol to ethanol.

We may compare also the quantum mechanicallly calculated APT's for the methylene hydrogens in ethanol with the ab initio APT's

for the methyl out-of-plane hydrogens in methanol. These APT's are compared in Table 5-9; the bond coordinate system is shown in Fig. 5-5(c). These APT's have nonzero numbers in all nine elements, and hence it is difficult to compare the APT's. Many of the elements in these APT's do show small, but significant differences. The motion corresponding to a C-H stretch, $\partial p_z/\partial z$, produces essentially the same dipole moment change in both molecules; we thus expect to predict reasonable intensities for the methylene hydrogen C-H stretches of ethanol by transferring APT's from methanol. Finally, we note that the quantum mechanically predicted effective charge for the methylene hydrogen in ethanol is the same within 0.01e as that predicted for the out-of-plane hydrogens in methanol.

We now consider the transferability of APT's from other molecules to the methyl and methylene carbon atoms in ethanol. The APT's obtained by various methods for these two carbon atoms are presented in Table 5-7. The coordinate system is shown in Fig. 5-2. The quantum mechanically calculated APT's for the methylene carbon of ethanol and for the methyl carbon of methanol are compared in Table 5-9; here the coordinate system is shown in Fig. 5-5(b). We shall refer to both Table 5-7 and 5-9, but it should be kept in mind that we may compare only APT's expressed in the same coordinate system. The ab initio APT's in Table 5-9 for the carbon atoms show that the APT for the methylene carbon atom of ethanol is changed significantly in only the $\partial p_x/\partial x$ element. We may conclude that the APT for the methyl carbon of methanol is essentially unchanged by replacement of one of the methyl hydrogens

by a methyl group. If, however, we attempt to transfer the APT for the methyl carbon of ethanol from ethane and then calculate the methylene carbon APT by difference, an APT for the methylene carbon is obtained which agrees poorly with the ab initio APT. This result may be seen in Table 5-7; there, C_8 is the methyl carbon atom of ethanol and C_7 is the methylene carbon. We did not quantum mechanically calculate the APT for the methyl carbon atom of ethanol, but the considerations just mentioned suggest that the methyl carbon APT should be calculated by difference rather than the methylene carbon APT for ethanol.

Even though the quantum mechanically calculated APT's for the same atoms in ethanol and in methanol showed detailed agreement, we were still unable to obtain much better than factor-of-two agreement in the predicted intensities for ethanol using transferred APT's. The normal coordinates for ethanol are very important in determining the predicted intensity distribution among the normal modes, and they are probably more in error than are the APT's transferred to ethanol.

Dimethyl Ether

The best molecule to test transferability of the experimental APT's derived for methanol is perhaps dimethyl ether. Both carbon atoms of dimethyl ether are bonded to the same atoms as in methanol, so the oxygen APT is the only reasonable choice to be considered for the APT to be calculated from the null condition. Hence we avoid the ambiguity in which central atom APT to transfer and which one to calculate from the null condition; this was one of the problems with the calculation of absolute intensities for

ethanol. Thus, we shall transfer the experimental APT's for the methyl carbon and hydrogens from methanol to dimethyl ether and calculate the predicted absolute intensities. This is not to say that APT's transferred from other molecules, such as CH_3F or CH_3CH_3, would not result in successful intensity predictions for dimethyl ether.

To predict the absolute intensities for dimethyl ether, we may transfer the methyl hydrogen APT's calculated for methanol (see Chapter 4) in two different ways. Calculation I makes use of the average APT derived for the three methyl hydrogens of methanol (Table 4-12). The other calculation (II) will be done using the different APT's found for the in-plane and out-of-plane methyl hydrogens of methanol (Table 4-10). The experimental APT's differ for the in-plane and out-of-plane methyl hydrogens because the methyl group in methanol significantly deviates from local C_{3v} symmetry (32).

The normal coordinates for both methanol and dimethyl ether are calculated by fixing the atoms of the molecules in one equilibrium configuration. But nearly free internal rotation occurs about the C-O bonds in methanol and dimethyl ether for the gas phase, room temperature species; such motion would average out the differences in the APT's for the in-plane and out-of-plane hydrogens of the methyl group. We thus wish to examine whether an average APT for the methyl hydrogens of methanol transfers better than APT's which differ for the in-plane and out-of-plane hydrogens.

APT's and Absolute Intensities for Dimethyl Ether

The APT's transferred from methanol to dimethyl ether are presented in Table 5-10. The coordinate system and atomic numbering convention are shown in Fig. 5-6. The APT's for the carbon atoms were both transferred from the methyl carbon of methanol (Table 4-10), and the APT for the oxygen atom was calculated using the null condition. For calculation I, the average APT for the methyl hydrogens of methanol (Table 4-12) was transferred to each of the six hydrogens of dimethyl ether. For calculation II, the APT for the in-plane methyl hydrogen of methanol was of course transferred to the two in-plane methyl hydrogens of dimethyl ether, and the APT for the out-of-plane methyl hydrogen of methanol was transferred to the four out-of-plane methyl hydrogens of dimethyl ether.

The absolute intensities for dimethyl ether were calculated using the $\underline{A}$ and $\underline{L}$ matrices given in Appendix A. The $\underline{L}$ matrix was calculated from the force field reported by Levin, Pearce, and Spiker (84) for dimethyl ether. Absolute intensities for the normal modes of dimethyl ether predicted by the two sets of transferred APT's are listed in Table 5-11; the experimental absolute intensities we measured for dimethyl ether (See Table 2-5) are also lised in Table 5-11. The last column in Table 5-11 lists the quantum mechanically predicted absolute intensities calculated by Blom, Oskam, and Altona (43) for dimethyl ether. Blom et al. (43) used GAUSSIAN 70 with a 4-31G basis set to calculate electro-optical parameters and absolute intensities for dimethyl ether.

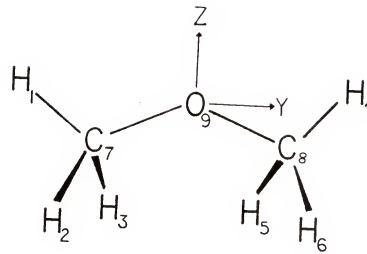

Fig. 5-6. Coordinate system for dimethyl ether. The x axis is determined by the right hand rule. The APT's in TABLE 5-10 are expressed in this coordinate system

TABLE 5-10
TRANSFERRED APT'S FOR DIMETHYL ETHER
COORDINATE SYSTEM IS INDICATED IN FIG. 5-6;
(units are e)

	Calculation I[a]	Calculation II[b]
$P_X(H_1)$[c]	$\begin{pmatrix} 0.030 & 0 & 0 \\ 0 & -0.121 & 0.088 \\ 0 & 0.052 & -0.077 \end{pmatrix}$	$\begin{pmatrix} 0.025 & 0 & 0 \\ 0 & -0.088 & 0.095 \\ 0 & 0.051 & -0.101 \end{pmatrix}$
$\chi(H_1)$	0.10	0.10
$P_X(H_2)$[d]	$\begin{pmatrix} -0.106 & -0.016 & 0.082 \\ 0.010 & -0.015 & -0.034 \\ 0.098 & -0.017 & -0.047 \end{pmatrix}$	$\begin{pmatrix} -0.105 & -0.006 & 0.119 \\ 0.027 & -0.022 & -0.061 \\ 0.071 & -0.005 & -0.043 \end{pmatrix}$
$\chi(H_2)$	0.10	0.11
$P_X(C_7)$[e]	$\begin{pmatrix} 0.379 & 0 & 0 \\ 0 & 0.666 & 0.176 \\ 0 & 0.269 & 0.519 \end{pmatrix}$	$\begin{pmatrix} 0.379 & 0 & 0 \\ 0 & 0.666 & -0.176 \\ 0 & -0.269 & 0.519 \end{pmatrix}$
$\chi(C_7)$	0.57	0.57
$P_X(O_9)$[f]	$\begin{pmatrix} -0.395 & 0 & 0 \\ 0 & -1.029 & 0 \\ 0 & 0 & -0.698 \end{pmatrix}$	$\begin{pmatrix} -0.388 & 0 & 0 \\ 0 & -1.068 & 0 \\ 0 & 0 & -0.664 \end{pmatrix}$
$\chi(O_9)$	0.75	0.76

[a] Calculation I uses an average APT calculated for the methyl hydrogen in methanol (from TABLE 4-12).

[b] Calculation II uses the different APT's for the in-plane and out-of-plane methyl hydrogens in methanol (from TABLE 4-10).

[c] $P_X(H_4)$ is obtained by reversing the signs of the off-diagonal components of $P_X(H_1)$ involving y.

[d] $P_X(H_6)$ is obtained by reversing the signs of the off-diagonal components of $P_X(H_2)$ involving y. $P_X(H_3)$ is obtained by reversing the signs of the off-diagonal components of $P_X(H_2)$ involving x. $P_X(H_5)$ is obtained by reversing the signs of the off-diagonal components of $P_X(H_2)$ involving z.

continued

TABLE 5-10-continued

[e]Transferred from the methyl carbon of methanol (from TABLE 4-10).
[f]Calculated from the null condition

TABLE 5-11
PREDICTED ABSOLUTE INTENSITIES FOR DIMETHYL ETHER
(units are km mol^{-1})

Mode(cm^{-1})[a]	A(exp)[b]	A(pred., transferred APT's)[c] I[d]		II[e]		A(pred., ab initio)[f]	
ν_1 (2992)	47	68.0		63.0		27.5	
ν_{16}(2987)		16.5		5.5		49.7	
ν_{12}(2934)	164	83.5	244	109	256	302	472
ν_2 (2817)	82	17.8		6.9		55.8	
ν_{17}(2826)		58.5		72.0		36.9	
ν_3 (1487)		6.2		3.6		0.9	
ν_{13}(1464)		6.7		6.4		33.9	
ν_{18}(1469)	25.6 ± 0.6	2.1	18	6.1	21	12.7	49
ν_{19}(1450)		0.0		0.4		1.8	
ν_4 (1434)		3.0		4.6		0.2	
ν_5 (1251)	3	13.7		21.2		3.4	
ν_{20}(1160)	104	43.9	131	55.2	133	108	183
ν_{14}(1179)		5.4		0.7		0.8	
ν_{21}(1095)	48	68.0		56.1		71.1	
ν_6 (920)	34.3±1.2	38.3		34.1		34.0	
ν_7 (425)	4	2.2		0.5		6.3	
ν_{15}(268)	-	3.4		1.3		0.8	

[a] Frequencies and assignments are from Levin, Pearce, and Spiker(84).

[b] Experimental absolute intensities we measured for dimethyl ether. See TABLE 2-5

---

continued

TABLE 5-11-continued

[c]Predicted absolute intensities based on APT's transferred from methanol. The oxygen APT is calculated by difference.

[d]Calculation I based on an average APT for the methyl hydrogen atoms. See TABLE 5-10 and text.

[e]Calculation II based on the different APT's for the in-plane and out-of-plane methyl hydrogens. See TABLE 5-10 and text.

[f]Taken from Blom, Oskam, and Altona (43). Blom et al. calculated electro-optical parameters for dimethyl ether using GAUSSIAN 70 with a 4-31G basis set

Discussion of Results for Dimethyl Ether

Predicted absolute intensities

Let us first consider the intensities predicted for the methyl C-H stretching region (near 3000 cm^{-1}). The experimental intensities listed in Table 5-11 indicate approximate intensities for each of the three bands distinguishable in the experimental spectrum. Use of an average APT to represent each of the methyl hydrogens (calculation I) results in a total intensity for the region only 17% too low; the intensity distribution, though, shows some factor-of-two disagreement with the experimental separation of intensity. Using different APT's for the in-plane and out-of-plane methyl hydrogens (calculation II) results in an improvement of the calculated intensity distribution in the methyl C-H stretching region. An improvement in the calculated total intensity also occurs (now only 13% too low).

Intensities for the other regions of the dimethyl ether spectrum also show small, but significant, variations depending upon which methyl group hydrogen APT's are transferred. The calculated total intensity for the methyl group bending region near 1450 cm^{-1} agrees better with experiment when different APT's for the in-plane and out-of-plane hydrogens are used.

The intensities of two other vibrational modes deserve mention: the antisymmetric (ν_{21}) and the symmetric (ν_6) C-O stretches. The intensities for these two modes show a definite improvement compared to experiment when different APT's are used for the in-plane and out-of-plane methyl hydrogens. Because the oxygen APT is calculated by difference from the APT's transferred to all the other atoms of

dimethyl ether, a different set of transferred APT's (for example, sets I and II in Table 5-10) will result also in a different APT for the oxygen atom. An examination of the two oxygen APT's in Table 5-10 shows that the APT's differ only sightly; yet the small differences seen there are sufficient to cause the intensity predicted (34.1 km mol^{-1}) for the symmetric C-O stretch (ν_6) to agree with the experimental value (34.3±1.2 km mol^{-1}).

Simulated spectra

Simulated spectra for dimethyl ether were plotted using the absolute intensities predicted by calculations I and II in Table 5-11. Band parameters used in the simulated spectra may be found in Appendix B. The spectrum simulated for dimethyl ether using the intensities predicted by calculation I is shown in Fig. 5-7(a). Fig. 5-7(b) shows the simulated spectrum using the absolute intensities predicted by calculation II. The experimentally observed infrared spectrum of dimethyl ether is presented in Fig. 5-7(c).

Figure 5-7 graphically illustrates the improvement in the predicted absolute intensities which results from using different APT's for the in-plane and out-of-plane methyl hydrogens rather than an average APT for both the in-plane and out-of-plane methyl hydrogens. In particular, the intensity distribution for the C-H stretching region near 3000 cm^{-1} is much better predicted in Fig. 5-7(b) than it is in Fig. 5-7(a), if these two simulated spectra are compared with the experimental spectrum in Fig. 5-7(c). The C-H rocking modes (near 1200 cm^{-1}) and the antisymmetric C-O stretching mode (near 1100 cm^{-1}) also have a much better predicted intensity distribution when different APT's are used for the in-plane and

Fig. 5-7. Comparison of simulated and experimental spectra for dimethyl ether. All three spectra are plotted for 3.45 kPa of dimethyl ether in a 10 cm cell.

(a) Simulated spectrum of dimethyl ether using absolute intensities predicted by transferring APT's from methanol. An average APT for the methyl hydrogens is used (calculation I).

(b) Simulated spectrum of dimethyl ether using absolute intensities predicted by transferring APT's from methanol. The APT's for the in-plane and out-of-plane methyl hydrogens are different (calculation II).

(c) Experimental infrared spectrum of dimethyl ether measured with the Nicolet Model 7199 FT-IR

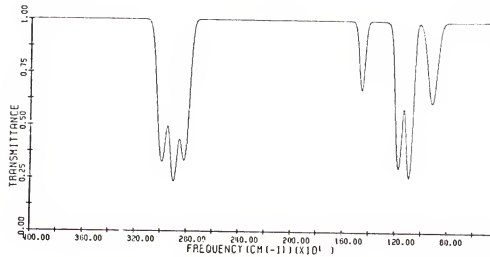

(a) Calculation I

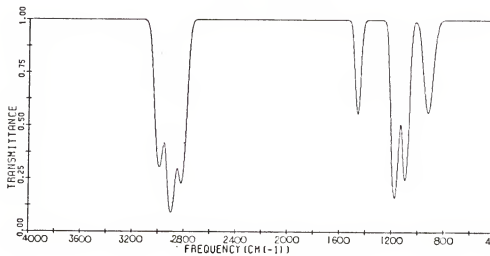

(b) Calculation II

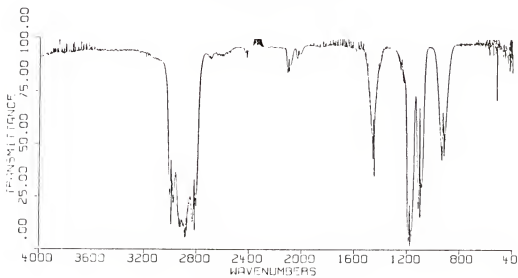

(c) Experimental

out-of-plane methyl hydrogens; that is, the simulated spectrum in Fig. 5-7(b) agrees better in the 1200 cm^{-1} to 1000 cm^{-1} region with the experimental spectrum shown in Fig. 5-7(c).

The fact that calculation II produces a simulated spectrum that compares more favorably with the experimental spectrum than does calculation I is somewhat surprising if we examine the two sets of APT's in Table 5-10. The differences in the two sets of APT's appear to be only minor and could be easily overlooked; however, these small differences become important if we try to predict intensities accurate to ten or twenty percent. For factor-of-two predictions, the differences seen in the APT's listed in Table 5-10 are much less important. We might add also that the simulated spectrum obtained from calculation I has been discussed by Person (85), but that the simulated spectrum based on calculation II represents a further refinement in the absolute intensities predicted for dimethyl ether.

Comparison of absolute intensities predicted by transferred APT's and by quantum mechanical calculations

We conclude our discussion of the absolute intensities of dimethyl ether by noting that the APT's transferred from methanol have predicted very well the intensities for dimethyl ether. The intensities predicted by either set of transferred APT's given in Table 5-10 are certainly in much better agreement with experiment than are the intensities calculated for dimethyl ether quantum mechanically (43). These quantum mechanically calculated intensities, reported by Blom, Oskam, and Altona (43), are presented in the last column of Table 5-11; these intensities were calculated using a 4-31G basis set; and we see the same factor-of-two level of agreement with experiment that

we found for the quantum mechanically calculated absolute intensities for methanol (See Table 5-2). The quantum mechanically calculated intensities both for the C-H stretching region and for the C-H bending region of dimethyl ether are too large by a factor of two. We do, however, observe in Table 5-11 that the absolute intensity predicted quantum mechanically for the symmetric C-O stretch agrees with the experimental value to within the experimental uncertainty (34.3±1.2 km mol^{-1} experimental, 34.0 km mol^{-1} calculated).

Formaldehyde

Absolute intensities for formaldehyde were measured some years ago by Hisatsune and Eggers (86); Person and Newton (13) later used these absolute intensities to derive experimental APT's for formaldehyde. We shall transfer some of these APT's to acetone in order to predict intensities for acetone. We have calculated quantum mechanically the APT's for both for acetone and for formaldehyde in an attempt to understand the changes that occur in the intensities for corresponding modes in acetone and formaldehyde. For example, the intensity for the C=O stretch is three times more intense in acetone than in formaldehyde. We wish now to discuss the quantum mechanically calculated APT's and the predicted absolute intensities for formaldehyde.

APT's and Absolute Intensities for Formaldehyde

The quantum mechanically calculated APT's we derived for formaldehyde using a 4-31G basis set are compared in Table 5-12 with the experimentally derived APT's (13). The definition of the cartesian

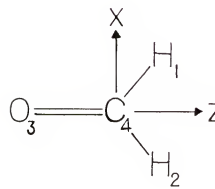

Fig. 5-8. Coordinate system for formaldehyde. The y axis is directed perpendicular to the plane of the molecule and determined by the right hand rule. The APT's given in TABLE 5-12 are expressed in this coordinate system

TABLE 5-12
EXPERIMENTAL AND QUANTUM MECHANICAL APT'S FOR FORMALDEHYDE
(units are e)

APT[a]	Experimental[b]	ab initio[c]
$P_x(H_1)$[d]	$\begin{pmatrix} -0.127 & 0 & -0.064 \\ 0 & 0.081 & 0 \\ -0.098 & 0 & -0.081 \end{pmatrix}$	$\begin{pmatrix} -0.185 & 0 & -0.083 \\ 0 & 0.103 & 0 \\ -0.074 & 0 & -0.022 \end{pmatrix}$
$\chi(H_1)$	0.12	0.14
$P_x(O_3)$	$\begin{pmatrix} -0.412 & 0 & 0 \\ 0 & -0.327 & 0 \\ 0 & 0 & -0.741 \end{pmatrix}$	$\begin{pmatrix} -0.569 & 0 & 0 \\ 0 & -0.416 & 0 \\ 0 & 0 & -0.956 \end{pmatrix}$
$\chi(O_3)$	0.52	0.69
$P_x(C_4)$	$\begin{pmatrix} 0.664 & 0 & 0 \\ 0 & 0.162 & 0 \\ 0 & 0 & 0.904 \end{pmatrix}$	$\begin{pmatrix} 0.939 & 0 & 0 \\ 0 & 0.211 & 0 \\ 0 & 0 & 0.999 \end{pmatrix}$
$\chi(C_4)$	0.65	0.80

[a] The coordinate system and atomic numbering scheme is shown in Fig. 5-8.

[b] Taken from Person and Newton (13).

[c] Quantum mechanically calculated using GAUSSIAN 70 with a 4-31G basis set.

[d] The APT for H_2 is obtained by reversing the signs of all the off-diagonal elements in $P_x(H_1)$ involving x. The experimental APT given here for H_1 corrects a typographical error in reference (13) where the experimental APT actually given in Table V of reference (13) is for H_2

coordinate axes and the atomic numbering system are shown in Fig. 5-8. Absolute intensities for formaldehyde were calculated from the quantum mechanically calculated APT's given in Table 5-12 and the normal coordinates (87) given in Appendix A. The quantum mechanically predicted absolute intensities for formaldehyde are compared with the experimental values (86) in Table 5-13. The approximate separations of intensities assumed in reference (13) for ν_1 and ν_4 and for ν_5 and ν_6 are also indicated.

Discussion of Results for Formaldehyde

Predicted absolute intensities

If we examine the predicted absolute intensities in Table 5-13 for formaldehyde, we see that the quantum mechanically predicted intensity for the C=O stretch (ν_2) is predicted only 35% too high; if we consider the uncertainty (20%) in the experimental value, the agreement between calculation and experiment is impressive indeed. The quantum mechanically predicted intensity for the CH_2 bending mode (ν_3), however, is a factor of three too large.

The ν_3 mode might be considered in somewhat more detail. The infrared spectrum of gaseous formaldehyde shows a definite P, Q, R structure for ν_3 (88). Accurate measurement of the absolute intensity of such a band with a lot of rotational structure would thus require high broadening gas pressures. Hisatsune and Eggers (86) used 2.8 MPa (27 atm) of nitrogen; the spectral slit width, however, was only 4 cm^{-1}. It is thus possible that, as suggested by the quantum mechanical calculation, the absolute intensity for ν_3 is somewhat larger than 9.3 ± 2.8 km mol^{-1}. Indeed, if we examine infrared spectra of matrix-isolated formaldehyde (89, 90), the relative intensity of

TABLE 5-13
QUANTUM MECHANICALLY PREDICTED ABSOLUTE INTENSITIES FOR FORMALDEHYDE
(units are km mol^{-1})

Mode(cm^{-1})[a]		A(exp)[b]	A(pred., ab initio APT's)[c]
$\nu_{a.sym}$ (C-H)	ν_4(2874)	64[d] } 128	129 } 166
ν_{sym} (C-H)	ν_1(2780)	64[d] } ±26	37 }
ν(C=O)	ν_2(1744)	59±12	80
δ(C-H)	ν_3(1503)	9.3±2.8	31
δ(OCH)	ν_5(1280)	6[e] } 10	15 } 21
ρ(C=O)	ν_6(1167)	4[e] } ±5	6 }

[a] Assignments and experimental frequencies from Hisatsune and Eggers (86). ν ≡ stretch, δ ≡ bend, ρ ≡ rock.

[b] Experimental absolute intensities and uncertainties taken from Hisatsune and Eggers (86).

[c] Quantum mechanically calculated intensities using the ab initio APT's given in TABLE 5-12.

[d] Assumed separation to be 50% for each ν_4 and ν_1 (13).

[e] Assumed separation to be 60%: 40% for the ratio of ν_5 to ν_6 (13)

ν_3 to the intensity of the C=O stretch, for example, appears to be more intense than is suggested by the measured intensity ratio of 1:6.3 (See Table 5-13).

The infrared spectrum of formaldehyde has two regions of overlapping bands, the ν_1 and ν_4 region and the ν_5 and ν_6 region. We shall first consider the intensities predicted for the antisymmetric C-H stretch (ν_4) and the symmetric C-H stretch (ν_1). The total intensity calculated for the C-H stretching region (ν_1 and ν_4) is seen in Table 5-13 to be in reasonable agreement with the experimental total intensity (predicted only 30% too high). If, however, we examine the assumed separation of intensities for ν_1 and for ν_4 (13) and the separation predicted by the quantum mechanical calculation, serious discrepancies are seen. The experimental separation of the total intensity as 50% each for ν_1 and ν_4 is not at all indicated by the quantum mechanical calculation, which suggests that ν_4 is 3.5 times more intense than is ν_1. The situation becomes even more complex when the infrared spectrum of matrix-isolated formaldehyde (89, 90) is examined: the intensity for ν_1 appears to be much more intense than is ν_4. We thus cannot estimate at this time the true intensity ratio of ν_4 to ν_1. A careful measurement of the relative intensities in a matrix-isolated sample of formaldehyde might be helpful in answering this question.

Finally, we consider the predicted absolute intensities for the CH_2 rocking mode (ν_5) and for the CH_2 wagging mode (ν_6). The total intensity for the region (ν_5 and ν_6) is seen in Table 5-13 to be predicted a factor of two too high by the quantum mechanical calculation, but the uncertainty in the experimental value is 50% so the

discrepancy is perhaps less than a factor of two. The experimental separation of intensities (13) for ν_5 and for ν_6 is confirmed by the quantum mechanical calculation.

Comparison of APT's for formaldehyde

The quantum mechanically calculated APT's for the oxygen and carbon atoms of formaldehyde are seen in Table 5-12 to agree reasonably well with the experimental APT's derived for those atoms (13). The general trend observed in the quantum mechanically calculated APT's for the oxygen and carbon atoms is that each element in the calculated APT's is slightly larger than the corresponding value in the experimental APT's. Larger differences, however, are expected in the calculated and experimental APT's for the hydrogen atoms of formaldehyde because the modes for which the predicted intensities most disagreed with experiment were the ones involving displacement of the hydrogen atoms.

We have chosen to compare the APT's for the hydrogen atom in the bond cartesian coordinate system illustrated in Fig. 5-9. The experimental APT and the quantum mechanically calculated APT for the hydrogen atom expressed in this coordinate system are compared in Table 5-14. We have included also in Table 5-14 the APT calculated for the hydrogen atom by the CNDO method (13). The APT quantum mechanically calculated with a 4-31G basis set shall be denoted the "ab initio APT" and the APT calculated by the CNDO method shall be called the "CNDO APT" in the discussion which follows. The $\partial p_z/\partial z$ element is the same (-0.20±0.01e) in each of the three APT's presented in Table 5-14, so we may be reasonably confident of the value.

Fig. 5-9. Bond coordinate system for hydrogen. The APT's given in TABLE 5-14 for the hydrogens of formaldehyde are expressed in this coordinate system. The y axis is directed out of the plane of the molecule and determined by the right hand rule.

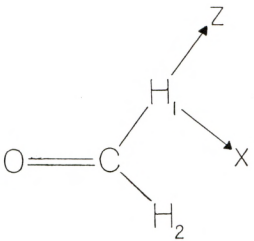
Z
H1
O
C
X
H2

TABLE 5-14
COMPARISON OF EXPERIMENTAL AND QUANTUM MECHANICAL APT'S FOR HYDROGEN IN FORMALDEHYDE
(units are e)

$$P_X(H_1)^a = \begin{pmatrix} -0.021 & 0 & -0.032 \\ 0 & 0.081 & 0 \\ 0.002 & 0 & -0.187 \end{pmatrix}$$ experimental

$\chi(H_1)$ 0.12

$$P_X(H_1)^b = \begin{pmatrix} 0.003 & 0 & 0.044 \\ 0 & 0.103 & 0 \\ 0.035 & 0 & -0.210 \end{pmatrix}$$ ab initio

$\chi(H_1)$ 0.14

$$P_X(H_1)^c = \begin{pmatrix} -0.050 & 0 & 0.019 \\ 0 & 0.050 & 0 \\ 0.060 & 0 & -0.19 \end{pmatrix}$$ CNDO

$\chi(H_1)$ 0.12

[a] Experimental APT for H_1 taken from Person and Newton (13).

[b] Quantum mechanically calculated APT for H_1 using GAUSSIAN 70 with a 4-31G basis set.

[c] Calculated by the CNDO method; taken from reference (13). The bond coordinate system is shown in Fig. 5-9

This derivative corresponds to the C-H stretching motion(See Fig. 5-9). The experimental derivative for displacement of the hydrogen out of the plane of the molecule ($\partial p_y/\partial y$) is well predicted by the ab initio APT and almost equally as well by the CNDO APT. When we examine the dipole moment changes that occur when the hydrogen atom is displaced along x (a CH_2 bending motion), we find that neither the ab initio APT nor the CNDO APT agrees with the experimental APT. In particular, the ab initio APT predicts essentially no change in the dipole moment along x as the hydrogen atom is displaced in that direction (the $\partial p_x/\partial x$ term); rather the z component of the dipole moment changes most when the hydrogen atom is displaced along x (the $\partial p_z/\partial x$ term). The situation is reversed in the experimental APT where the $\partial p_z/\partial x$ term is essentially zero. The CNDO APT predicts a nonzero dipole moment change for $\partial p_x/\partial x$, but also a nonzero dipole moment change for $\partial p_z/\partial x$. Thus, a nonzero value for the $\partial p_z/\partial x$ term is probably correct. Such a nonzero value for this term might be found for the experimental APT if different assumptions were made for the experimental intensity ratios of ν_4 to ν_1 and ν_5 to ν_6.

Acetone

We have transferred APT's to both alcohols and ethers and have thus been able to predict the absolute intensities within at least a factor of two. We now wish to consider the possibility of predicting absolute intensities for ketones through the use of transferred APT's. The ketone chosen for this study was acetone. We shall transfer APT's from ethane to the atoms in the two methyl groups of acetone and transfer the carbonyl oxygen APT from formaldehyde to acetone.

Quantum mechanical APT's for acetone were calculated also, and these APT's will be compared with those calculated for methanol.

APT's and Absolute Intensities for Acetone

Absolute intensities for acetone were predicted by transferring experimental APT's to acetone from ethane (61) (see also Table 4-12) and from formaldehyde (13). The APT's for the methyl hydrogen atoms and the methyl carbon atoms were transferred from ethane, while the carbonyl oxygen APT was transferred from formaldehyde. This left the carbonyl carbon APT to be determined by the null condition. The resulting set of APT's transferred to acetone is shown in Table 5-15; the orientation of the cartesian coordinate axes and the atomic numbering system are shown in Fig. 5-10. The APT's for all of the atoms of acetone are not listed in Table 5-15 since several atoms of acetone are related by reflections through the symmetry planes of the molecule.

We calculated also the quantum mechanical APT's for acetone using the GAUSSIAN 70 program with a 4-31G basis set. These quantum mechanical APT's are presented in Table 5-15.

Absolute intensities were calculated for acetone using both sets of APT's given in Table 5-15. The normal coordinates were calculated from the Urey-Bradley force field for acetone reported by Mann and Dixon (91). The experimental geometry was taken from the microwave study of acetone by Nelson and Pierce (75). The details of the normal coordinate analysis and the $\underline{\Lambda}$ and $\underline{L}$ matrices may be found in Appendix A. The absolute intensities predicted for acetone are presented in Table 5-16. Included also in Table 5-16 are the experimental absolute intensities measured for acetone by Vakhlueva,

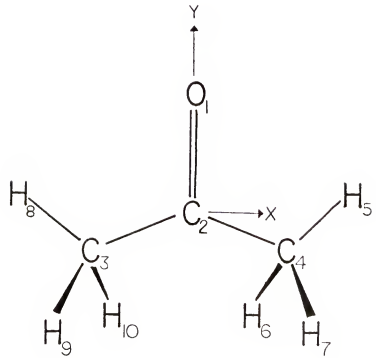

Fig. 5-10. Coordinate system for acetone. The y axis is determined by the right hand rule. The APT's given in TABLE 5-15 are expressed in this coordinate system

TABLE 5-15
TRANSFERRED AND QUANTUM MECHANICAL APT'S FOR ACETONE
THE COORDINATE SYSTEM IS SHOWN IN FIG. 5-10.
(units are electrons (e))

	APT's transferred from:[a] CH_3CH_3 and H_2CO			ab initio[b]		
$P_X(O_1)$	-0.412	0	0	-0.724	0	0
	0	-0.741	0	0	-1.13	0
	0	0	-0.327	0	0	-0.390
$\chi(O_1)$		0.53			0.81	
$P_X(C_2)$	0.412	0	0	1.04	0	0
	0	0.619	0	0	1.17	0
	0	0	0.449	0	0	0.223
$\chi(C_2)$		0.50			0.92	
$P_X(C_3)$	0.026	-0.061	0	-0.274	-0.076	0
	-0.061	0.089	0	-0.114	-0.069	0
	0	0	0.127	0	0	0.039
$\chi(C_3)$		0.10			0.18	
$P_X(H_5)$[d]	-0.092	-0.122	0	-0.050	-0.099	0
	-0.077	-0.044	0	-0.056	0.023	0
	0	0	0.055	0	0	0.101
$\chi(H_5)$		0.11			0.09	
$P_X(H_6)$[e]	0.033	0.031	0.046	0.082	0.013	0.008
	0.016	0.008	-0.096	0.001	0.012	-0.120
	0.009	-0.074	-0.121	-0.041	-0.085	-0.028
$\chi(H_6)$		0.11			0.10	

---

continued

TABLE 5-15-continued

[a]The APT for the carbonyl oxygen atom was transferred from formaldehyde (13), the APT for the carbonyl carbon atom was calculated by difference, and the APT's for the remaining atoms were transferred from ethane (61).

[b]APT's calculated using GAUSSIAN 70 with a 4-31G basis set.

[c]The APT for C_4 is obtained by reversing the signs of all the off-diagonal elements in $P_X(C_3)$ involving x.

[d]The APT for H_8 is obtained by reversing the signs of all the off-diagonal elements in $P_X(H_5)$ involving x.

[e]The APT for H_{10} is obtained by reversing the signs of all the off-diagonal elements in $P_X(H_6)$ involving x. The APT for H_7 is obtained by reversing the signs of all the off-diagonal elements in $P_X(H_6)$ involving z. The APT for H_9 is obtained by reversing the signs of all the off-diagonal elements in $P_X(H_6)$ involving y

TABLE 5-16
PREDICTED ABSOLUTE INTENSITIES FOR ACETONE
(units are km mol^{-1})

Mode (cm^{-1})[a]		A(exp)[b]		A(pred., transferred APT's)[c]		A(pred., ab initio)[d]	
ν(C-H)	ν_1 (3020)	14	44	27	169	7.7	62
	ν_{13} (3020)			27		14	
	ν_{20} (2973)	30		79		17	
	ν_2 (2926)			10		21	
	ν_{14} (2926)			26		2.5	
ν(C=O	ν_3 (1738)	150		53		170	
δ(C-H)	ν_{15} (1456)	35	104	0.4	25	6.4	101
	ν_4 (1438)			23		43	
	ν_{21} (1438)			1.2		25	
	ν_{16} (1363)	69		6.0		17	
	ν_5 (1360)			0.1		10	
ν_a(C-C)	ν_{17} (1218)	68		13		112	
δ(CCH)	ν_{22} (1093)	5		8.2	8	15	15
	ν_6 (1067)			0		0.1	
δ(CCH)	ν_{18} (896)	7.8		0.9		3.3	
ν_s(C-C)	ν_7 (779)	2.3		3.0		2.1	
δ(CCO)	ν_{19} (528)	17		10	13	25	29
ρ(C=O)	ν_8 (483)			3.0		3.9	
δ(CCC)	ν_{23} (384)	0.7		18		3.4	

---

continued

TABLE 5-16-continued

$\tau(CH_3)$	$\nu_{24}(105)$	-[e]	3.5	0.01

[a]Assignments and observed frequencies from Mann and Dixon (91). $\nu \equiv$ stretch, $\delta \equiv$ bend, $\rho \equiv$ rock, $\tau \equiv$ torsion.

[b]Measured by Vakhlueva, Finkel, Sverdlov, and Zaitseva (92). We have confirmed within $\pm$10% the values reported by Vakhlueva et al. (92). Uncertainties are thus about 10%.

[c]Calculated using the APT's transferred from ethane and from formaldehyde. See TABLE 5-15.

[d]Calculated using the quantum mechanically calculated APT's given in TABLE 5-15.

[e]Not measured by Vakhlueva et al. (92)

Finkel, Sverdlov, and Zaitseva (92). The absolute intensities measured by Vakhlueva et al. (92) have been confirmed in our laboratory to within ± 10%.

Discussion of Results for Acetone

Predicted absolute intensities

The absolute intensities predicted using the transferred APT's for acetone will be discussed first. A comparison with experiment of the total intensity predicted for the C-H stretching region near 3000 cm^{-1} shows that the predicted intensity is too large almost by a factor of four. The total intensity predicted for the C-H bending region (near 1400 cm^{-1}) is over a factor of four too small. The absolute intensity predicted for the C=O stretch (ν_3) is a factor of three too low. We observe also that the predicted intensity of the antisymmetric C-C stretch (ν_{17}) is a factor of over five too small. The experimental absolute intensities for most of the remaining vibrational modes are small, and we certainly do not expect to predict accurately intensities for these modes since the predicted intensities for the more intense modes are in error by multiples of the experimental values. Thus, the agreement with experiment of the predicted intensity (3.0 km mol^{-1} predicted, 2.3 km mol^{-1} experimental) for the symmetric C-C stretch (ν_7) is probably fortuitous.

The intensities predicted for acetone by transferring APT's from ethane and from formaldehyde are thus seen to be in much worse agreement with experiment than were the intensities predicted for the alcohols and ethers. We were able to predict absolute intensities for methanol, ethanol, and dimethyl ether to within a factor of two,

and some vibrational intensities were predicted very well indeed, as seen for example in Fig. 5-7. The intensities predicted for acetone, on the other hand, are in error by several multiples of the experimental value.

We could transfer APT's from other molecules such as methanol in an attempt to improve the prediction for the C-H stretching and bending regions, but the predicted intensities would still be in error. We can see why this is so if we examine the experimental APT's for the methyl hydrogens in ethane and in methanol (Table 4-12). Both these APT's have the same value for the $\partial p_z/\partial z$ term. (Here we are considering a bond coordinate system with the z axis directed along the C-H bond, as in Fig. 4-6). To predict the drastic decrease in the intensity for the C-H stretching region of acetone, however, the $\partial p_z/\partial z$ term in the hydrogen APT must change dramatically from that in ethane.

We noted above that the intensity predicted for the carbonyl stretching mode in acetone is a factor of three too small using the oxygen APT transferred from formaldehyde. The absolute intensity for the carbonyl stretching mode is 59 km mol^{-1} in formaldehyde (86) and 150 km mol^{-1} in acetone.* This increase in intensity could be due either to differences in the normal coordinates or to changes in the APT's. Differences in the normal coordinates may be investigated as follows. The carbonyl carbon APT was calculated by difference and thus is not the same as in formaldehyde. We therefore repeated the calculation of the absolute intensities for acetone using APT's both for the carbonyl carbon and for

*Interestingly, the absolute intensity for the carbonyl stretch in acetaldehyde is 146 km mol^{-1} (93) and thus not midway between the values for formaldehyde and for acetone.

the carbonyl oxygen atoms transferred from formaldehyde. The methyl carbon APT's were calculated by difference. This procedure does not give the correct form of the APT's for the methyl carbon atoms because the off-diagonal APT elements $\partial p_y/\partial x$ and $\partial p_x/\partial y$ are then indeterminant because of the symmetry of the molecule, but the calculation does indicate whether the intensity for the carbonyl stretching vibration can be predicted accurately. This new calculation predicted an intensity of 96 km mol^{-1} for the C=O stretch in acetone. Since the two same APT's (carbonyl carbon and oxygen) in formaldehyde give an intensity of 59 km mol^{-1} for the carbonyl stretching mode, the $\underline{L}$ matrix in acetone must be responsible for the increase in intensity of 37 km mol^{-1}. A mixing of the pure carbonyl stretch with other vibrations of acetone (through the $\underline{L}$ matrix) is thus responsible for about half the total increase in intensity of the carbonyl stretching mode in acetone compared to formaldehyde. How the remaining increase of 50 km mol^{-1} in intensity comes about will be discussed when the quantum mechanically calculated APT's for formaldehyde and for acetone are compared.

Let us now consider the absolute intensities predicted using the quantum mechanically calculated APT's for acetone. We see in Table 5-16 that the total intensity for the C-H stretching region is well reproduced by the ab initio calculation, but that the distribution of intensity among the five vibrational modes is calculated rather poorly compared to the experimental distribution. A similar situation occurs in the C-H bending region from about 1480 cm^{-1} to 1350 cm^{-1} where, although the total intensity is calculated amazingly close to the experimental value (101 km mol^{-1}

calculated, 104 km mol^{-1} measured), the distribution of intensity is again inaccurately calculated.

As with formaldehyde (see Table 5-13), the intensity for the carbonyl stretching mode (ν_3) in acetone is quite accurately predicted using the APT's calculated with the 4-31G basis set; the intensity predicted by the 4-31G calculation is only 13% too large. Since the intensity for the carbonyl stretching vibration is in good agreement with experiment for both formaldehyde and acetone, we suggest that the 4-31G basis set provides a good representation for the dipole moment function for a carbonyl group.

The ab initio calculation overestimates the intensity of the antisymmetric C-C stretching mode (ν_{17}), but the predicted intensity is still well within a factor of two. The symmetric C-C stretching mode (ν_7) has an experimental intensity of 2.3 km mol^{-1}; this value is almost exactly reproduced by the quantum mechanical calculation (2.1 km mol^{-1}), but the experimental intensity is so small and therefore uncertain that the agreement is probably fortuitous.

We have seen that the quantum mechanically predicted absolute intensities for acetone are in much better agreement with experiment than are the intensities predicted by transferred APT's. The absolute intensities predicted for acetone by the two methods can be compared easily by plotting simulated spectra.

Simulated spectra

The simulated spectrum (See Appendix B) for acetone using the absolute intensities predicted by the transferred APT's is shown in Fig. 5-11(a). The simulated spectrum based on the quantum mechanically calculated intensities is shown in Fig. 5-11(b).

Fig. 5-11. Comparison of simulated and experimental spectra for acetone. All three spectra are plotted for 1.29 kPa in a 10 cm cell.

(a) Simulated spectrum of acetone using absolute intensities predicted by transferring APT's from ethane and formaldehyde.
(b) Simulated spectrum using quantum mechanically calculated intensities.
(c) Experimental spectrum of acetone measured with the Nicolet Model 7199 FT-IR

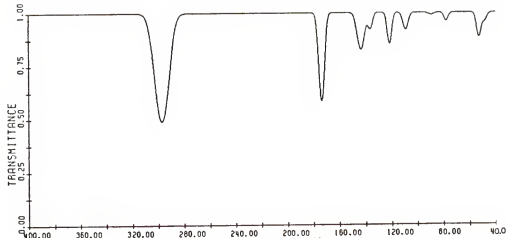
TRANSMITTANCE
1.00
0.75
0.50
0.25
0.00
400.00
360.00
320.00
280.00
240.00
200.00
160.00
120.00
80.00
40.0
FREQUENCY (CM(-1))(X10¹)

(a)

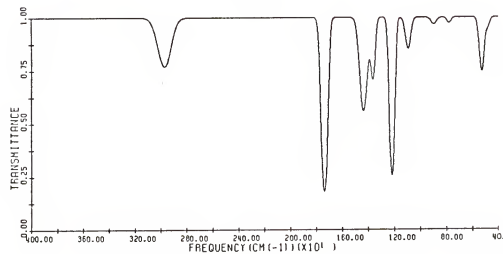
TRANSMITTANCE
1.00
0.75
0.50
0.25
0.00
400.00
360.00
320.00
280.00
240.00
200.00
160.00
120.00
80.00
40.0
FREQUENCY (CM(-1))(X10¹)

(b)

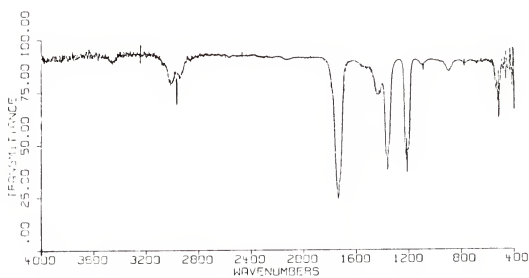
TRANSMITTANCE
.00
25.00
50.00
75.00
100.00
4000
3600
3200
2800
2400
2000
1600
1200
800
400
WAVENUMBERS

(c)

Both simulated spectra are compared with the experimental spectrum (Fig. 5-11(c)) of acetone.

The simulated spectrum based on the transferred APT's does not look at all like the experimental spectrum of acetone. Indeed, one would have difficulty in identifying Fig. 5-11(a) on the basis of the intensity pattern as a spectrum of acetone. The simulated spectrum based on the quantum mechanically calculated intensities, however, shows much better agreement with the experimental spectrum. Although the relative intensities for the two moderately intense bands in the C-H bending region are reversed compared with the experimental spectrum, the overall intensity pattern in the simulated spectrum compares favorably with the experimentally observed spectrum of acetone. We see, in general, factor-of-two agreement with experiment for the quantum mechanically calculated intensities and much worse agreement for the intensities based on the transferred APT's.

Significant differences are also seen between the two simulated spectra for acetone. In particular, the quantum mechanical calculation predicts the C-H stretching region to be less intense than the C-H bending region; the transferred APT's predict exactly the reverse situation. The APT's for the methyl hydrogen atoms of acetone were transferred from ethane; the C-H stretching region for ethane is more intense than is the C-H bending region, so a similar prediction for acetone is expected. The intensity for the carbonyl stretching mode is seen to be predicted much too low by the APT's transferred from formaldehyde; yet the intensity predicted quantum mechanically is in good agreement with experiment. We turn now to a comparison

of the various sets of APT's for acetone to see what changes take place in the APT's on going from formaldehyde and ethane to acetone.

Comparison of APT's for acetone with the APT's for other molecules

A comparison of the quantum mechanically calculated APT's and the APT's transferred to acetone from formaldehyde and from ethane shows why the transferred APT's so inaccurately predict the absolute intensities for acetone. The two sets of APT's given in Table 5-15 are seen to be not at all similar.

We first consider the APT's for the carbonyl carbon and oxygen atoms. Neither the carbonyl oxygen APT transferred from formaldehyde nor the carbonyl carbon APT calculated by difference agrees with the APT's calculated quantum mechanically for those two atoms. The overall disagreement is indicated by the effective charges: the effective charge of the oxygen atom is 35% lower in formaldehyde than in acetone, while the effective charge of the carbonyl carbon atom is almost 50% lower in formaldehyde. A comparison of the APT's given in Table 5-15 for the carbonyl oxygen atom in the two molecules shows the major differences to be associated with displacing the oxygen atom along the C=O bond and with the in-plane bending motion of the carbonyl group.

The APT quantum mechanically calculated for the carbonyl carbon atom of acetone indicates that the APT calculated by difference for this atom is in serious error also. The APT elements show factor-of-two errors. These large differences have profound implications for the intensities predicted for acetone using the transferred APT's because the intensities depend upon the squares of the dipole moment derivatives.

The comparison of the experimental APT's transferred to acetone and the APT's calculated quantum mechanically may be somewhat misleading because the quantum mechanical calculation has intrinsic errors such as the use of a finite basis set and the neglect of electron correlation. The changes, however, that occur in the APT's for similar molecules should be reasonably well predicted by the quantum mechanical calculations we have made because many of the same errors will affect the results for both molecules.

We therefore compare the APT's quantum mechanically calculated for formaldehyde and for acetone. By this comparison, we hope to account for the much larger experimental absolute intensity for the carbonyl stretch in acetone compared to formaldehyde (150 km mol^{-1} for acetone, 59 km mol^{-1} for formaldehyde). As seen earlier, about half the increase in intensity can be accounted for by mixing through the $\underline{L}$ matrix of the pure carbonyl stretch with other vibrational modes of acetone. The remaining increase in intensity must be due to changes in the APT's.

The quantum mechanically calculated APT's for the carbonyl carbon and oxygen atoms of formaldehyde and acetone are compared in Table 5-17. The bond cartesian coordinate system for the comparison is shown in Fig. 5-12. As indicated by the greater intensity of the carbonyl stretch in acetone, displacement of the carbonyl oxygen atom along the C=O bond in acetone is seen to result in a larger dipole moment change ($\partial p_z/\partial z$ = -1.13e) than occurs in formaldehyde ($\partial p_z/\partial z$ = -0.956e). The same result is seen for displacement of the

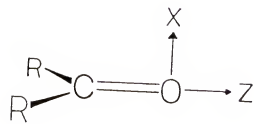

Fig. 5-12. Bond cartesian coordinate system for comparison of the APT's for the carbonyl carbon and oxygen atoms of formaldehyde (R=H) and acetone ($R=CH_3$). The x axis is directed perpendicular to the plane of symmetry determined by the carbonyl group and the two R groups. The y axis is determined by the right hand rule. The APT's given in TABLE 5-17 are relative to this coordinate system

TABLE 5-17
COMPARISON OF AB INITIO APT'S FOR
FORMALDEHYDE AND ACETONE
(units are e)

APT[a]	Formaldehyde			Acetone		
$P_X(O)$[b]	-0.416	0	0	-0.390	0	0
	0	-0.569	0	0	-0.724	0
	0	0	-0.956	0	0	-1.13
$\chi(O)$		0.69			0.81	
$P_X(C)$[c]	0.211	0	0	0.223	0	0
	0	0.939	0	0	1.04	0
	0	0	0.999	0	0	1.17
$\chi(C)$		0.80			0.91	

[a] Quantum mechanically calculated APT's using the GAUSSIAN 70 program with a 4-31G basis set. The coordinate system is shown in Fig. 5-12.

[b] Carbonyl oxygen APT.

[c] Carbonyl carbon APT.

carbonyl carbon atom along the C=O bond; here the $\partial p_z/\partial z$ term for acetone is 1.17e compared to 0.999e for formaldehyde.

The increase observed in the dipole derivative (and the absolute intensity) for the carbonyl stretch in acetone compared to formaldehyde has been explained as resulting from a decrease in the effective electronegativity of the carbonyl carbon atom in acetone and a corresponding shift of the π electrons toward the more electronegative carbonyl oxygen atom (94). Such an effect can be seen here by considering the results of the ab initio quantum mechanical calculations for formaldehyde and for acetone. Part of the output of the GAUSSIAN 70 program is a Mulliken population analysis (95) of the distribution of the electrons among the atoms in the molecule. The oxygen atom in formaldehyde has a Mulliken gross atomic population of 8.483e ("8.483 electrons" on the oxygen atom), while in acetone the value is 8.563e. The Mulliken gross atomic population on the carbonyl carbon is 5.825e in formaldehyde and 5.518e in acetone. A shift of the π electrons in acetone toward the oxygen atom is thus predicted by the quantum mechanical calculations, in accordance with reference (94).

The Mulliken gross atomic populations indicate also that the methyl groups in acetone are donating electrons toward the carbonyl group upon stretching the C=O bond. For this discussion, the methyl hydrogen atoms lying out of the plane formed by the carbonyl group and the methyl carbon atoms will be denoted as "out-of-plane" hydrogens. The remaining two hydrogen atoms in acetone will be denoted as "in-plane" hydrogens. The Mulliken gross atomic populations on the

methyl hydrogens in acetone show that when the carbonyl oxygen atom is stretched 0.02 Å along the C=O bond, each out-of-plane hydrogen atom loses 0.0011e and each in-plane hydrogen atom loses 0.0016e. The methyl carbon atoms also donate electrons toward the carbonyl group, but to a much smaller extent. Another contribution to the larger dipole derivative for the carbonyl stretch in acetone compared to formaldehyde is therefore the inductive effect of the two methyl groups.

Two effects are thus responsible for the factor-of-three increase in intensity of the carbonyl stretching mode in acetone compared to formaldehyde. One effect is mixing in the normal coordinates through the L matrix, and the other effect is due to the inductive properties of the two methyl groups.

Let us now consider the APT's transferred to the atoms in the methyl groups of acetone. As seen in Table 5-15, the APT's transferred from ethane do not agree well with the APT's calculated quantum mechanically for acetone. The methyl carbon APT transferred from ethane to acetone is very different from the quantum mechanically calculated APT. Even the diagonal APT elements are very different; the $\partial p_x/\partial x$ term in the transferred APT, for example, is only 0.026e, while the same term in the quantum mechanically calculated APT is -0.274e. Furthermore, the quantum mechanically predicted effective charge for the methyl carbon atoms is almost twice as large as the effective charge transferred from ethane.

If we examine the effective charges transferred from ethane to the methyl hydrogen atoms in acetone, we find essentially the same effective charges as calculated quantum mechanically. This agreement is deceptive, however, because the distribution of the dipole derivatives within the hydrogen APT's is much different from the distribution in the quantum mechanically calculated APT's. This inaccurate distribution in the transferred APT's is reflected in the absolute intensities predicted for the vibrational modes of acetone involving displacement of the hydrogen atoms.

We recall that the total intensity predicted for the C-H stretching region was much larger than the total intensity predicted for the C-H bending region (See Table 5-16); the experimental absolute intensities, however, show the opposite to be the case with the C-H bending region being twice as intense as the C-H stretching region. We saw also that the experimental APT's for the methyl hydrogen atoms in ethane and in methanol were nearly identical (See Table 4-12), so let us compare the APT's calculated quantum mechanically for the in-plane and out-of-plane hydrogen atoms in acetone and in methanol. (Atomic polar tensors calculated for ethane using a 4-31G basis set are not available in the literature.)

The APT's quantum mechanically calculated for the methyl hydrogens of methanol and acetone are compared in Table 5-18. The coordinate system for the in-plane hydrogen atom is shown in Fig. 5-13(a), while the coordinate system for the out-of-plane hydrogen atom is shown in Fig. 5-13(b). Comparing first the APT's

Fig. 5-13. Coordinate system for comparison of APT's in methanol and in acetone. See TABLE 5-18.

(a) Coordinate system for the in-plane hydrogen, the hydrogen lying in the COH (CCO) plane of methanol (acetone). The y axis is determined by the right hand rule.

(b) Coordinate system for the out-of-plane hydrogen. The x axis lies in the H_2CH_1 plane, and y is determined by the right hand rule.

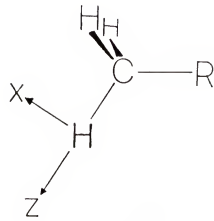

(a)

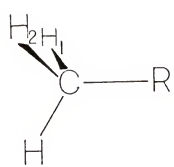

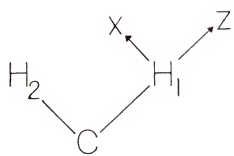

(b)

TABLE 5-18
COMPARISON OF QUANTUM MECHANICAL APT'S FOR METHANOL AND ACETONE
(units are e)

APT[a]	Methanol			Acetone		
$P_X(H)$[b] in pl.	0.04	0	-0.01	0.07	0	-0.04
	0	0.08	0	0	0.10	0
	-0.01	0	-0.13	-0.0	0	-0.10
$\chi(H)$		0.09			0.09	
$P_X(H_1)$[c] out pl.	0.02	0.03	0.03	0.10	0.02	-0.03
	0.04	-0.01	0.06	0.01	0.08	0.0
	0.04	0.01	-0.22	0.0	-0.05	-0.11
$\chi(H)$		0.14			0.10	

[a] Quantum mechanically calculated APT's using the GAUSSIAN 70 program with a 4-31G basis set.

[b] APT for the in-plane methyl hydrogen atom. See Fig. 5-13(a).

[c] APT for the out-of-plane methyl hydrogen atom. See Fig. 5-13(b)

for the in-plane hydrogen atoms in methanol and in acetone, we see that the differences are not extremely large in magnitude. These differences are important, though, for a hydrogen APT becuase the transformation from the $\underset{\sim}{P}_X$ matrix to the $\underset{\sim}{P}_Q$ matrix introduces an inverse dependence on the atomic masses. Consequently, the magnitudes of the differences observed in the APT's for the in-plane hydrogen atom are much more important for the predicted intensities than would be the same differences in an APT for a heavier atom such as carbon.

Now we examine in Table 5-18 the APT's for the out-of-plane methyl hydrogens in methanol and in acetone. The $\partial p_z/\partial z$ term (the dipole moment change induced along the C-H bond when the hydrogen atom is stretched along the C-H bond) is twice as big in methanol as it is in acetone. In contrast, the $\partial p_x/\partial x$ term corresponding to the dipole moment change when the HCH angle is bent (See Fig. 5-13(b)) is much larger in acetone (0.10e) than in methanol (0.02e). This then is why the intensity of the C-H stretching region in acetone is smaller, but the intensity of the C-H bending region is larger when these two regions are compared with the spectrum observed for methanol.

The reason for the differences in the methyl out-of-plane hydrogen APT's in methanol and in acetone can be understood by considering the effect of the two nonbonding pairs of electrons on the oxygen atom in methanol. Lone pairs of electrons on atoms to which a methyl group is attached are known to affect the equilibrium geometry of the methyl group (96). The C-H bonds trans to a lone pair are longer and weaker than normal (96), and thus have force

constants smaller than normal (70). One explanation of these observations is that the lone pairs of electrons are being partially donated to the σ^* antibonding C-H orbitals of the out-of-plane C-H bonds (97). Such interactions do not occur in methanol for the in-plane C-H bond, but they do occur for the two out-of-plane C-H bonds which are trans to the two lone pairs of electrons on the oxygen atom. Thus, the out-of-plane C-H bonds in methanol are 0.006 Å longer than the in-plane C-H bond (98), and the out-of-plane C-H bonds have a stretching force constant which is 0.11 mdyn/Å lower than that for the in-plane C-H bond (70).* The lower stretching force constants for the out-of-plane C-H bonds lower the frequencies for these stretches and hence, along with Fermi resonance (99), contribute to the Bohlmann bands observed near 2780 cm^{-1} for methanol (70).

The APT's we have calculated quantum mechanically for the out-of-plane methyl hydrogens of methanol enables us to see another effect on the methyl group of the lone pairs of electrons on the oxygen atom. We see in Table 5-18 that the $\partial p_z/\partial z$ term is almost twice as large as for the out-of-plane hydrogens as it is for the in-plane hydrogen. The density of electrons in the region of space "occupied" by the lone pair of electrons trans to the out-of-plane C-H bond

---

*The methyl group in methanol is also tilted 3.3° away from the O-H bond (55), but this has been attributed to repulsions between the O-H bond and the out-of-plane C-H bonds rather than interactions due to the lone pairs of electrons on the oxygen atom (96).

apparently decreases when the out-of-plane C-H bond is stretched, with an electron flow from the oxygen toward to methyl group. Such an enhanced dipole moment change when the in-plane C-H bond is stretched is not possible, and the $\partial p_z/\partial z$ term is thus much smaller for the in-plane C-H stretch.

Summary

We have seen in this Chapter that atomic polar tensors transferred from other molecules to methanol, to ethanol, and to dimethyl ether result in predicted absolute intensities which show factor-of-two agreement with experiment. The ab initio quantum mechanical calculations using a 4-31G basis set (and using much more computer time) also predict within a factor-of-two the experimental absolute intensities for these molecules. The absolute intensities calculated for acetone using transferred APT's, however, were seen to give predicted intensities showing factor-of-five (or six) disagreement with the experimental intensities. The ab initio quantum mechanical calculations for acetone predicted absolute intensities having factor-of-two agreement with experiment. A comparison of APT's calculated quantum mechanically for acetone and the APT's transferred to acetone indicated that the transferred APT's inaccurately described the electrical properties of the atoms in acetone.

We should certainly be able to use the APT's presented in this dissertation to predict infrared intensities accurate to a factor-of-two for other alcohols and ethers. If the experimentally measured absolute intensities for the absorption regions of acetone could be accurately divided into intensities for each of the normal modes of vibration, experimental APT's could

be obtained also for acetone. We see no reason why such a set of experimental APT's for acetone could not be used to predict accurate intensities for other ketones.

APPENDIX A
NORMAL COORDINATE ANALYSIS

Normal coordinates for methanol, ethanol, dimethyl ether, and acetone were calculated using the normal coordinate analysis programs WMAT and CHARLY developed at the University of Minnesota and modified by Sanchez (100) for use on the IBM 370/175 computer at the University of Florida. Dr. J. Newton provided us with a consistent set of $\underline{f}$ and $\underline{L}$ matrices for formaldehyde, so the calculation of the normal coordinates was unnecessary.

Methanol

The force field for methanol (C_s symmetry) has been investigated several times (56, 59, 70, 101); the normal coordinate analysis has been complicated because the alcohol has many overlapping normal modes so that accurate frequencies and assignments have proved difficult. We have chosen to use the force field for methanol reported by Mallinson (56) because it appears to be the most complete experimentally derived force field for methanol. The analysis by Mallinson (56) is based on matrix data for ten isotopic species of methanol. We have also used an ab initio force field scaled to reproduce the experimental frequencies of methanol; this force field was reported by Blom, Otto, and Altona (59). The molecular geometry for methanol was taken from the microwave study of methanol by Lees and Baker (55); this geometry was used for the normal coordinate analysis using the force field reported by Mallinson (56).

For the normal coordinate analysis using the force field reported by Blom et al. (59), we used the geometry, atomic numbering system, coordinate system, and symmetry coordinates given by Blom et al. (59). The two geometries for methanol are shown in Fig. A-1. The internal displacement coordinates and symmetry coordinates for methanol are presented in Tables A-1 and A-2. The $\underline{A}$, $\underline{L}$, $\underline{B}$, and $\underline{L}^{-1}$ matrices derived from the two force fields for methanol are shown in Tables A-3 through A-10. (Throughout the tables in this Appendix, only nonzero elements are indicated. The order is row, column and matrix element.)

Ethanol

The force field for ethanol was discussed in Chapter 5. The only force field available in the literature is the force field reported by Zemlyanukhina and Sverdlov (79). We have calculated the normal coordinates from this force field and also from a force field we derived for ethanol using force constants transferred from methanol (59) and from propane (80). The geometry for ethanol is taken from the microwave study of ethanol by Sasada, Takano, and Saton (73). This geometry is shown in Fig. A-2. The internal displacement coordinates and symmetry coordinates are shown in Tables A-11 and A-12. The symmetrized $\underline{F}$ matrix from the transferred force constants is shown in Table A-13, and the frequencies calculated from these force constants are compared with the experimentally observed frequencies in Table A-14. The $\underline{A}$ and $\underline{L}$ matrices derived from both force fields for ethanol are presented in Tables A-15 through A-18.

We note here also the conversion from the force constants in units of cm^{-2} reported by Zemlyanukhina and Sverdlov (79) to force constants in units of dyn/cm. Let us denote any particular force constant given in reference (79) by f'; then we derive that

$$f(dyn/cm)=gf'(cm^{-2})(4\ ^2c^2/N)$$

or, evaluating the constants,

$$f(dyn/cm)=gf'(cm^{-2})(0.058919\ cm^2sec^{-2}u^{-1}g)$$

Here g is a weighting factor which arises because Soviet workers use a dimensionless G matrix (6) and is given by the following:

$g = m_H$, for stretching force constants

$g = m_H r_{CH}$, for stretch-bend interactions

$g = m_H r_{CH}^2$, for bending force constants.

See Sverdlov et al. (6) for a discussion of the values of m_H and r_{CH}.

Dimethyl Ether

The force field for dimethyl ether has been studied a number of times (43, 84, 102), and we have again selectively chosen one of these published force fields. We chose for dimethyl ether the force field derived by Levin, Pearce, and Spiker (84); this force field is based on an adjustment of eighteen internal force constants to reproduce the experimentally observed frequencies. The geometry for dimethyl ether was taken from Blukis, Kasai, and Myers (103). The geometry for dimethyl ether is indicated in Fig. A-3. Internal displacement coordinates and symmetry coordinates (84) for dimethyl ether are shown in Tables A-19 and A-20. The $\underline{A}$ and $\underline{L}$ matrices are shown in Tables A-21 and A-22.

Formaldehyde

The normal coordinates for formaldehyde were kindly provided to us by Dr. J. Newton; this normal coordinate treatment is essentially the same as described in reference (13). We reproduce here the data. The geometry (86) for this normal coordinate analysis is indicated in Fig. A-4. (For the ab initio calculation of the APT's, we used the geometry reported by Oka, Hirakawa, and Shimoda (74). The internal displacement coordinates and the symmetry coordinates are listed in Tables A-23 and A-24. The $\underline{A}$ and $\underline{L}$ matrices are presented in Tables A-25 and A-26.

Acetone

Several force fields have been proposed for acetone (91, 104); we have chosen the Urey-Bradley force field for acetone reported by Mann and Dixon (91). Acetone has C_{2v} symmetry and twenty-four (3N-6) normal modes of vibration. Of these modes, eight have a_1 symmetry, four have a_2 symmetry, seven are b_1, and five are of b_2 symmetry. The vibrations of a_2 symmetry are infrared inactive. The geometry for acetone (See Fig. A-5) was taken from Nelson and Pierce (75). Symmetry coordinates for acetone taken from Cossee and Schachtschneider (105) are shown in Table A-28. The internal displacement coordinates are shown in Table A-27. The $\underline{A}$ and $\underline{L}$ matrices are presented in Tables A-29 and A-30.

Fig. A-1. Geometry for methanol. The atoms are numbered as used in the normal coordinate analysis.

(a) Geometry used with the force field reported by Mallinson (56):

$\alpha(2,1,4) = 107°2'$ $r(1,4) = 1.0936_{o}$ Å

$\alpha(2,1,5) = 110°54'$ $r(1,2) = 1.426$ A_{o}

$\alpha(5,1,6) = 108°38'$ $r(2,3) = 0.9451$ Å

$\alpha(1,2,3) = 108°32'$

(b) Geometry used by Blom et al. (59):

$\alpha(2,1,3) = 106.2°$ $r(1,3) = 1.087$ Å

$\alpha(2,1,5) = 111.7°$ $r(1,5) = 1.093_{o}$ Å

$\alpha(5,1,4) = 109.3°$ $r(1,2) = 1.43$ A_{o}

$\alpha(5,1,3) = 109.0°$ $r(2,6) = 0.961$ Å

$\alpha(1,2,6) = 108.5°$

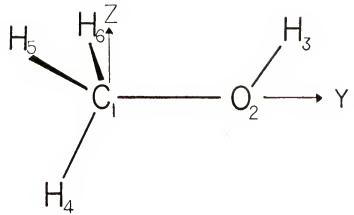

(a)

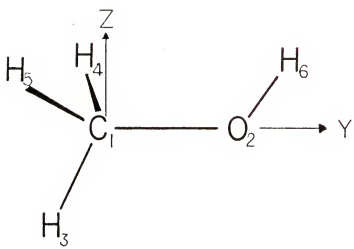

(b)

TABLE A-1
INTERNAL DISPLACEMENT COORDINATES FOR METHANOL

$r_1 = R(2,3)$[a]
$r_2 = R(1,4)$
$r_3 = R(1,5)$
$r_4 = R(1,6)$
$r_5 = \alpha(5,1,6)$[b]
$r_6 = \alpha(4,1,6)$
$r_7 = \alpha(4,1,5)$
$r_8 = \alpha(1,2,3)$
$r_9 = \alpha(2,1,4)$
$r_{10} = \alpha(2,1,6)$
$r_{11} = \alpha(2,1,5)$
$r_{12} = R(1,2)$
$r_{13} = \tau(4,1,2,3)$[c]

[a] R(i,j) indicates a bond stretching internal coordinate between atoms i and j.

[b] α(i,j,k,l) is an angle bending coordinate for atoms i, j, and k. Atom j is the apex atom.

[c] τ(i, j, k, l) is a torsional internal coordinate with τ being the change in the dihedral angle between the vectors $\vec{ji}$ and $\vec{kl}$

TABLE A-2
UNNORMALIZED SYMMETRY COORDINATES FOR METHANOL

$$S_1 = r_1$$

$$S_2 = 2r_2 - r_3 - r_4$$

$$S_3 = r_2 + r_3 + r_4$$

$$S_4 = 2r_5 - r_6 - r_7$$

$$S_5 = r_5 + r_6 + r_7$$

$$S_6 = r_8$$

$$S_7 = 2r_9 - r_{11} - r_{10}$$

$$S_8 = r_{12}$$

$$S_9 = r_3 - r_4$$

$$S_{10} = r_7 - r_6$$

$$S_{11} = r_{11} - r_{10}$$

$$S_{12} = r_{13}$$

Note: Symmetry coordinates are taken from reference 56. S_{10} here is the negative of S_{10} in reference (56); also, the K factor in S_5 in reference (56) was accounted for by adjusting the symmetry force constants involving S_5.

TABLE A-3

THE $\underline{A}$ MATRIX FOR METHANOL

BASED ON MALLINSON'S FORCE FIELD

1	9	-0.066588	1	10	0.064243	1	11	0.111277	1	12	0.003302
2	1	-0.010860	2	2	-0.002732	2	3	0.018283	2	4	-0.002407
2	5	-0.055754	2	6	-0.026813	2	7	0.003906	2	8	-0.530334
3	1	-0.006624	3	2	0.065971	3	3	0.000540	3	4	0.063699
3	5	-0.002804	3	6	-0.029063	3	7	-0.108776	3	8	-0.015304
4	9	-0.007217	4	10	-0.032153	4	11	-0.063476	4	12	-0.048122
5	1	-0.010860	5	2	-0.002732	5	3	0.018287	5	4	-0.002406
5	5	-0.055793	5	6	-0.026812	5	7	0.003904	5	8	0.469663
6	1	-0.051352	6	2	0.008406	6	3	0.000659	6	4	-0.005082
6	5	-0.001919	6	6	0.045034	6	7	0.047843	6	8	0.014514
7	9	0.004245	7	10	0.360317	7	11	0.108243	7	12	0.667975
8	1	0.335407	8	2	0.033444	8	3	0.013215	8	4	0.040813
8	5	-0.056351	8	6	0.823367	8	7	-0.094505	8	8	0.450939
9	1	0.886771	9	2	-0.003722	9	3	0.000684	9	4	-0.019570
9	5	-0.001737	9	6	-0.239976	9	7	0.030838	9	8	0.020796
10	9	-0.578589	10	10	-0.395745	10	11	-0.092801	10	12	0.212269
11	1	-0.044030	11	2	-0.291114	11	3	-0.150751	11	4	-0.040992
11	5	0.543200	11	6	0.026780	11	7	-0.738413	11	8	-0.538457
12	1	0.003338	12	2	-0.701781	12	3	-0.551516	12	4	0.075518
12	5	-0.186929	12	6	-0.044483	12	7	0.118651	12	8	-0.022002
13	2	-0.331596	13	3	0.468952	13	4	0.260433	13	5	0.184152
13	8	0.000006	13	9	0.490917	13	10	-0.109609	13	11	-0.166499
13	12	-0.077918	14	1	0.035148	14	2	0.163290	14	3	-0.187719
14	4	0.333513	14	5	0.530431	14	6	-0.052682	14	7	0.362231
14	8	-0.540390	14	9	-0.289234	14	10	0.060050	14	11	0.613572
14	12	0.032037	15	1	0.005750	15	2	-0.106701	15	3	0.266973
15	4	-0.366873	15	5	0.126255	15	6	-0.048057	15	7	0.168191
15	8	-0.023462	15	9	0.327402	15	10	0.352386	15	11	0.014610
15	12	0.167719	16	2	0.331596	16	3	-0.468952	16	4	-0.260433
16	5	-0.184152	16	8	-0.000006	16	9	0.490917	16	10	-0.109609
16	11	-0.166499	16	12	-0.077918	17	1	0.005148	17	2	0.163290
17	3	-0.187719	17	4	0.333513	17	5	0.530481	17	6	-0.052682
17	7	0.362231	17	8	-0.540890	17	9	0.289234	17	10	-0.060050
17	11	0.613572	17	12	-0.032037	18	1	0.005750	18	2	-0.106701
18	3	0.266973	18	4	-0.366873	18	5	0.126255	18	6	-0.048057
18	7	0.168191	18	8	-0.023462	18	9	-0.327402	18	10	-0.352386
18	11	-0.014610	18	12	-0.167719						

TABLE A-4

THE L MATRIX FOR METHANOL

BASED ON MALLINSON'S FORCE FIELD

1	1	-1.026953	1	2	0.001021	1	3	-0.000625	1	4	0.002419
1	5	0.000460	1	6	-0.009498	1	7	-0.000998	1	8	0.004513
2	1	0.000863	2	2	1.031046	2	3	0.197820	2	4	0.034325
2	5	-0.011013	2	6	0.007490	2	7	-0.021097	2	8	-0.010976
3	1	0.000657	3	2	0.191264	3	3	-0.983751	3	4	-0.367292
3	5	0.034217	3	6	0.004298	3	7	-0.020645	3	8	0.006285
4	1	0.000875	4	2	0.099482	4	3	-0.087569	4	4	1.409339
4	5	-0.418136	4	6	0.247241	4	7	-0.125509	4	8	-0.055774
5	1	-0.000694	5	2	-0.011043	5	3	0.058773	5	4	-0.234295
5	5	-0.692349	5	6	0.010793	5	7	-0.027984	5	8	0.119468
6	1	0.347596	6	2	-0.373133	6	3	-0.012114	6	4	0.023116
6	5	-0.356056	6	6	-0.911842	6	7	-0.523358	6	8	-0.406503
7	1	0.000332	7	2	-0.394161	7	3	-0.059	7	4	0.356077
7	5	-0.000977	7	6	-0.600201	7	7	0.641337	7	8	0.270453
8	1	0.000545	8	2	-0.005316	8	3	0.051590	8	4	-0.015706
8	5	-0.000366	8	6	0.003981	8	7	-0.143148	8	8	0.341019
9	9	1.043316	9	10	-0.043754	9	11	-0.036408	9	12	-0.001647
10	9	-0.000196	10	10	1.473272	10	11	0.271744	10	12	0.032732
11	9	-0.000664	11	10	-0.335992	11	11	0.941721	11	12	0.006264
12	9	0.044537	12	10	-0.765309	12	11	-0.316528	12	12	1.268486

TABLE A-5

THE B MATRIX FOR METHANOL

BASED ON MALLINSON'S FORCE FIELD

1	5	-0.317846	1	6	-0.948142	1	8	0.317846	1	9	0.948142
2	2	0.292928	2	3	0.956135	2	11	-0.292928	2	12	-0.956135
3	1	-0.812240	3	2	0.356733	3	3	-0.461528	3	13	0.812240
3	14	-0.356733	3	15	0.461528	4	1	0.812240	4	2	0.356733
4	3	-0.461528	4	16	-0.812240	4	17	-0.356733	4	18	0.461528
5	2	-0.903411	5	3	1.175270	5	13	0.533389	5	14	0.454206
5	15	-0.587635	5	16	-0.533389	5	17	0.454206	5	18	-0.587635
6	1	-1.054457	6	2	-0.943392	6	3	-0.642093	6	10	0.788803
6	11	0.442247	6	12	-0.135490	6	16	0.265653	6	17	0.401145
6	18	0.777582	7	1	1.054457	7	2	-0.943392	7	3	-0.642093
7	10	-0.788803	7	11	0.442247	7	12	-0.135490	7	13	-0.265653
7	14	0.401145	7	15	0.777582	8	3	-0.701263	8	5	-1.003207
8	6	1.337568	8	8	1.003207	8	9	-0.336305	9	2	0.874301
9	3	-0.369120	9	6	0.701263	9	11	-0.874301	9	12	0.267857
10	1	-0.893317	10	2	0.854235	10	3	0.507597	10	4	0.609708
10	6	-0.346446	10	16	0.283608	10	17	-0.854235	10	18	-0.161151
11	1	0.893317	11	2	0.854235	11	3	0.507597	11	4	-0.609708
11	6	-0.346446	11	13	-0.283608	11	14	-0.854235	11	15	-0.161151
12	2	-1.000000	12	5	1.000000	13	1	-0.936123	13	4	-1.136188
13	7	1.115947	13	10	0.956364						

TABLE A-6

THE L^{-1} MATRIX FOR METHANOL

BASED ON MALLINSON'S FORCE FIELD

1	1	-0.972814	1	2	0.001837	1	3	0.001213	1	4	-0.000398
1	5	-0.002492	1	6	0.005771	1	7	0.006552	1	8	0.015418
2	1	0.001439	2	2	0.938078	2	3	0.187894	2	4	-0.018796
2	5	0.003119	2	6	-0.011204	2	7	0.022307	2	8	-0.008504
3	1	-0.000973	3	2	0.181930	3	3	-0.968078	3	4	-0.047213
3	5	-0.010759	3	6	0.000688	3	7	-0.025159	3	8	0.042632
4	1	0.014733	4	2	-0.026921	4	3	-0.080671	4	4	0.604351
4	5	-0.295391	4	6	0.048147	4	7	0.170174	4	8	0.125179
5	1	0.002902	5	2	0.006874	5	3	-0.021759	5	4	-0.184427
5	5	-0.577535	5	6	-0.034209	5	7	-0.039680	5	8	0.303560
6	1	-0.069533	6	2	-0.116385	6	3	-0.008832	6	4	0.169402
6	5	0.052726	6	6	-0.666757	6	7	-0.535416	6	8	-0.324091
7	1	-0.011419	7	2	0.056265	7	3	-0.074661	7	4	-0.178762
7	5	0.132838	7	6	-0.560018	7	7	0.770932	7	8	-1.351429
8	1	0.056977	8	2	0.012241	8	3	0.109545	8	4	-0.083054
8	5	-0.171728	8	6	-0.233266	8	7	0.333263	8	8	2.434203
9	9	0.959574	9	10	0.334760	9	11	0.327132	9	12	0.000214
10	9	0.022637	10	10	0.629123	10	11	-0.185303	10	12	-0.015287
11	9	0.106430	11	10	0.225138	11	11	0.997474	11	12	-0.010597
12	9	0.006572	12	10	0.434532	12	11	0.135945	12	12	0.776473

TABLE A-7

THE $\underline{A}$ MATRIX FOR METHANOL

BASED ON BLOM, OTTO, AND ALTONA'S FORCE FIELD

1	9	0.066787	1	10	0.062823	1	11	-0.111211	1	12	0.003156
2	1	-0.010825	2	2	-0.303383	2	3	0.018470	2	4	-0.002274
2	5	0.039184	2	6	-0.027283	2	7	0.004143	2	8	-0.530320
3	1	-0.006639	3	2	0.065437	3	3	0.001712	3	4	0.065398
3	5	0.003783	3	6	-0.028982	3	7	-0.109478	3	8	-0.016089
4	9	0.007274	4	10	-0.032009	4	11	0.063114	4	12	-0.048790
5	1	-0.010324	5	2	-0.303380	5	3	0.018471	5	4	-0.002275
5	5	0.039185	5	6	-0.027285	5	7	0.004145	5	8	0.466682
6	1	-0.051257	6	2	0.308327	6	3	0.000833	6	4	-0.005571
6	5	0.001479	6	6	0.041197	6	7	0.047331	6	8	0.015262
7	9	0.077761	7	10	-0.391614	7	11	0.085166	7	12	0.217919
8	1	-0.043834	8	2	-0.272861	8	3	-0.143272	8	4	-0.043757
8	5	-0.385246	8	6	0.027587	8	7	-0.739516	8	8	-0.507446
9	1	0.002952	9	2	-0.706542	9	3	-0.552529	9	4	0.077448
9	5	0.127094	9	6	-0.044927	9	7	0.106579	9	8	-0.022735
10	2	0.332878	10	3	-0.473763	10	4	-0.255529	10	5	0.133163
10	6	0.000004	10	7	-0.011783	10	9	-0.492186	10	10	-0.105249
10	11	0.170391	10	12	-0.077385	11	1	0.004637	11	2	0.166864
11	3	-0.194419	11	4	0.031997	11	5	-0.371930	11	6	-0.052933
11	7	0.360112	11	8	-0.541014	11	9	-0.298255	11	10	-0.059169
11	11	-0.610390	11	12	-0.032402	12	1	0.006141	12	2	-0.100459
12	3	0.259401	12	4	-0.373506	12	5	-0.398304	12	6	-0.050224
12	7	0.182081	12	8	-0.024437	12	9	0.316693	12	10	-0.356397
12	11	0.039461	12	12	-0.159226	13	2	-0.332878	13	3	0.473763
13	4	0.255529	13	5	-0.133163	13	6	-0.000004	13	7	0.011783
13	9	-0.492186	13	10	-0.105249	13	11	0.170391	13	12	-0.077385
14	1	0.004637	14	2	0.166864	14	3	-0.194419	14	4	0.031997
14	5	-0.371930	14	6	-0.052933	14	7	0.360112	14	8	-0.541014
14	9	0.298255	14	10	0.059169	14	11	0.610390	14	12	0.032402
15	1	0.006141	15	2	-0.100458	15	3	0.259401	15	4	-0.373506
15	5	-0.398304	15	6	-0.050226	15	7	0.182081	15	8	-0.024437
15	9	-0.316693	15	10	0.356397	15	11	-0.039461	15	12	0.159226
16	9	-0.004046	16	10	0.362101	16	11	-0.133450	16	12	0.673604
17	1	0.335297	17	2	0.033022	17	3	0.019049	17	4	0.042950
17	5	0.040652	17	6	0.836161	17	7	-0.095813	17	8	0.449700
18	1	0.886932	18	2	-0.003853	18	3	0.000609	18	4	-0.020703
18	5	0.000988	18	6	-0.242713	18	7	0.080830	18	8	0.021957

TABLE A-8

THE L MATRIX FOR METHANOL

BASED ON BLOM, OTTO, AND ALTONA'S FORCE FIELD

1	1	1.026528	1	2	-0.020002	1	3	-0.003691	1	4	-0.001816
1	5	0.000573	1	6	0.018431	1	7	0.002286	1	8	0.015160
2	1	-0.020198	2	2	-1.048649	2	3	0.032378	2	4	0.036371
2	5	-0.006959	2	6	-0.001555	2	7	-0.005871	2	8	-0.001235
3	1	-0.004112	3	2	-0.031687	3	3	-1.009557	3	4	-0.016549
3	5	-0.023389	3	6	-0.002355	3	7	0.003332	3	8	-0.007441
4	1	-0.003756	4	2	-0.084622	4	3	-0.008307	4	4	1.352637
4	5	-0.513653	4	6	0.341777	4	7	-0.123726	4	8	-0.090824
5	1	-0.000155	5	2	-0.007439	5	3	-0.062567	5	4	-0.541704
5	5	-1.324939	5	6	0.009343	5	7	0.058934	5	8	-0.086613
6	1	-0.014536	6	2	0.071389	6	3	0.004090	6	4	0.083525
6	5	-0.019558	6	6	-0.850446	6	7	-0.357838	6	8	-0.554806
7	1	-0.041372	7	2	0.121446	7	3	-0.003624	7	4	0.399383
7	5	-0.174773	7	6	-0.565501	7	7	0.541753	7	8	0.422111
8	1	-0.023119	8	2	-0.002316	8	3	0.043188	8	4	0.038674
8	5	0.086734	8	6	-0.009351	8	7	-0.234839	8	8	0.281413
9	9	1.045525	9	10	0.039177	9	11	-0.001294	9	12	-0.002441
10	9	0.080348	10	10	1.477464	10	11	-0.266016	10	12	-0.021523
11	9	-0.128735	11	10	0.323715	11	11	0.944323	11	12	-0.016875
12	9	-0.054548	12	10	-0.723037	12	11	0.303738	12	12	1.280051

TABLE A-9

THE B MATRIX FOR METHANOL

BASED ON BLOM, OTTO, AND ALTONA'S FORCE FIELD

1	2	-1.000000	1	5	1.000000	2	5	-0.317305	2	6	-0.943324
2	17	0.317305	2	18	0.943324	3	2	0.278991	3	3	0.960294
3	8	-0.278991	3	9	-0.960294	4	1	0.815373	4	2	0.369271
4	3	-0.445877	4	10	-0.815373	4	11	-0.369271	4	12	0.445877
5	1	-0.815373	5	2	0.369271	5	3	-0.445877	5	13	0.815373
5	14	-0.369271	5	15	0.445877	6	3	-0.699301	6	5	-0.986809
6	6	1.229482	6	17	0.986809	6	18	-0.330132	7	2	0.883436
7	3	-0.555963	7	6	0.699302	7	8	-0.383436	7	9	0.256662
8	1	-0.909601	8	2	0.849156	8	3	0.497404	8	4	0.613556
8	6	-0.335516	8	10	0.296044	8	11	-0.849156	8	12	-0.161888
9	1	0.909601	9	2	0.849156	9	3	0.497404	9	4	-0.613556
9	6	-0.335516	9	13	-0.296044	9	14	-0.849156	9	15	-0.161888
10	2	-0.950434	10	3	1.147603	10	10	-0.528996	10	11	0.475217
10	12	-0.573802	10	13	0.528996	10	14	0.475217	10	15	-0.573802
11	1	1.049382	11	2	-0.833072	11	3	-0.657786	11	7	-0.793215
11	8	0.447485	11	9	-0.130006	11	13	-0.256168	11	14	0.385587
11	15	0.787792	12	1	-1.049382	12	2	-0.833072	12	3	-0.657786
12	7	0.793215	12	8	0.447485	12	9	-0.130006	12	10	0.256168
12	11	0.385587	12	12	0.787792	13	1	-0.927136	13	4	-1.129104
13	7	0.958004	13	16	1.097286		0				

TABLE A-10

THE L^{-1} MATRIX FOR METHANOL

BASED ON BOLM, OTTO, AND ALTONA'S FORCE FIELD

1	1	0.973716	1	2	-0.016770	1	3	-0.004833	1	4	-0.000250
1	5	-0.001291	1	6	0.018566	1	7	0.002736	1	8	-0.020635
2	1	-0.018334	2	2	-0.953173	2	3	-0.330062	2	4	0.022053
2	5	-0.333023	2	6	0.007052	2	7	0.004161	2	8	0.009855
3	1	-0.003768	3	2	0.030254	3	3	-0.991280	3	4	-0.004770
3	5	0.018408	3	6	0.002119	3	7	-0.001747	3	8	-0.014952
4	1	0.010790	4	2	-0.015198	4	3	0.008878	4	4	0.573325
4	5	-0.252384	4	6	0.087934	4	7	0.204674	4	8	-0.026701
5	1	-0.005565	5	2	0.009322	5	3	0.034893	5	4	-0.231127
5	5	-0.666589	5	6	-0.034721	5	7	-0.093084	5	8	-0.207106
6	1	-0.043809	6	2	-0.126928	6	3	-0.022310	6	4	0.217463
6	5	-0.324750	6	6	-0.673683	6	7	-0.570790	6	8	-0.408218
7	1	-0.024297	7	2	0.066222	7	3	-0.076937	7	4	-0.167047
7	5	-0.144392	7	6	-0.461654	7	7	0.655873	7	8	-1.992735
8	1	0.060156	8	2	0.036240	8	3	0.074569	8	4	-0.138839
8	5	0.115861	8	6	-0.407761	8	7	0.529454	8	8	1.945189
9	9	0.953978	9	10	-0.323383	9	11	-0.005714	9	12	0.001350
10	9	-0.026936	10	10	0.645094	10	11	0.177461	10	12	0.013135
11	9	0.139151	11	10	-0.216913	11	11	0.994915	11	12	0.009734
12	9	-0.007636	12	10	0.414866	12	11	-0.136094	12	12	0.786394

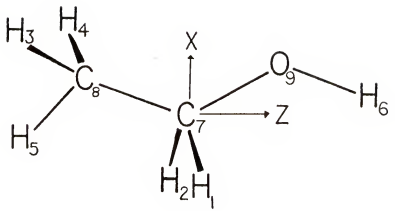

Fig. A-2. Geometry for ethanol. The atoms are numbered as used in the normal coordinate analysis. From reference (73):

$\alpha(3,8,4) = 108°38'$	$r(8,3) = 1.0936$ Å
$\alpha(2,7,1) = 109°5'$	$r(7,8) = 1.5297$ Å
$\alpha(8,7,1) = 110°18'$	$r(7,9) = 1.4247$ Å
$\alpha(8,7,9) = 107°20'$	$r(6,9) = 0.9451$ Å
$\alpha(7,9,6) = 108°32'$	$r(1,7) = 1.0936$ Å

TABLE A-11
INTERNAL DISPLACEMENT COORDINATES FOR ETHANOL

$r_1 = R(7,1)$
$r_2 = R(7,2)$
$r_3 = R(7,9)$
$r_4 = R(7,8)$
$r_5 = R(9,6)$
$r_6 = R(8,3)$
$r_7 = R(8,4)$
$r_8 = R(8,5)$
$r_9 = \alpha(8,7,9)$
$r_{10} = \alpha(7,9,6)$
$r_{11} = \alpha(1,7,2)$
$r_{12} = \alpha(3,8,4)$
$r_{13} = \alpha(3,8,5)$
$r_{14} = \alpha(4,8,5)$
$r_{15} = \alpha(9,7,1)$
$r_{16} = \alpha(9,7,2)$
$r_{17} = \alpha(8,7,1)$
$r_{18} = \alpha(8,7,2)$
$r_{19} = \alpha(7,8,3)$
$r_{20} = \alpha(7,8,4)$
$r_{21} = \alpha(7,8,5)$
$r_{22} = \tau(5,8,7,9)$
$r_{23} = \tau(8,7,9,6)$

Note: See footnotes for TABLE A-1

TABLE A-12
UNNORMALIZED SYMMETRY COORDINATES FOR ETHANOL

$$S_1 = r_5$$
$$S_2 = 2r_8 - r_6 - r_7$$
$$S_3 = r_8 + r_6 + r_7$$
$$S_4 = r_1 + r_2$$
$$S_5 = r_{11}$$
$$S_6 = 2r_{12} - r_{13} - r_{14}$$
$$S_7 = r_{12} + r_{13} + r_{14} - r_{19} - r_{20} - r_{21}$$
$$S_8 = r_{17} + r_{18} - r_{15} - r_{16}$$
$$S_9 = r_{10}$$
$$S_{10} = r_3$$
$$S_{11} = 2r_{21} - r_{19} - r_{20}$$
$$S_{12} = r_4$$
$$S_{13} = r_9$$
$$S_{14} = r_6 - r_7$$
$$S_{15} = r_1 - r_2$$
$$S_{16} = r_{13} - r_{14}$$
$$S_{17} = r_{17} - r_{15} - r_{18} + r_{16}$$
$$S_{18} = r_{19} - r_{20}$$
$$S_{19} = r_{17} + r_{15} - r_{18} - r_{16}$$
$$S_{20} = r_{22}$$
$$S_{21} = r_{23}$$

TABLE A-13

UPPER TRIANGLE OF THE SYMMETRIZED $_{o}F$ MATRIX FOR ETHANOL

UNITS ARE MDYN/A

BASED ON TRANSFERRED FORCE CONSTANTS

1	1	7.572000	1	4	0.009999	1	5	-0.006000	1	8	0.024000
1	9	0.169000	1	10	-0.034000	2	2	4.773993	2	3	0.060811
2	4	0.315588	2	6	-0.157667	2	7	-0.004333	2	11	0.120000
2	12	-0.025715	3	3	4.504995	3	4	0.012247	3	6	0.002357
3	7	0.132700	3	11	-0.002828	3	12	0.113738	4	4	4.924000
4	5	0.127279	4	8	-0.003536	4	10	0.241830	4	12	0.104652
5	5	0.656000	5	8	-0.003000	5	10	-0.214000	5	12	-0.135000
6	6	0.569333	6	7	0.006000	6	11	-0.321667	7	7	0.555499
7	8	-0.004682	7	11	0.003000	7	12	-0.311493	7	13	-0.049929
8	8	0.696000	8	9	0.029000	8	10	-0.197000	8	11	-0.053072
8	12	0.292000	9	9	0.749000	9	10	0.417000	9	13	0.084700
10	10	5.270000	10	12	0.318000	10	13	0.347000	11	11	0.642333
11	12	-0.011431	11	13	0.099858	12	12	4.297993	12	13	0.347000
13	13	1.212998	14	14	4.745998	14	15	0.029000	14	16	0.161000
14	18	0.124000	15	15	4.700000	15	17	0.094045	15	19	0.094045
16	16	0.564000	16	18	0.025000	17	17	0.687000	17	18	-0.097581
17	19	-0.061000	18	18	0.651000	18	19	-0.097581	19	19	0.847000
20	20	0.097770	21	21	0.017500						

TABLE A-14
CALCULATED FREQUENCIES
USING TRANSFERRED FORCE CONSTANTS FOR ETHANOL

Symmetry	Frequency (cm^{-1}) Observed[a]	Calculated
	3660.0	3682.08
	2971	2983.96
	2901	2952.51
	2890	2903.68
	1482	1485.13
	1450	1447.18
a'	1416	1422.79
	1394	1350.99
	1241	1233.09
	1070	1072.41
	1027	988.31
	883	900.70
	422	417.58
	2987	2979.55
	2946	2957.08
	1451	1507.49
a''	1241	1266.28
	1098	1154.50
	808	818.82
	243	241.30
	201	201.04

[a]Experimental frequencies taken from reference (79)

TABLE A-15

THE $\underline{A}$ MATRIX FOR ETHANOL

BASED ON TRANSFERRED FORCE CONSTANTS

1	1	0.312321	1	2	0.020795	1	3	-0.007571	1	4	-0.392235
1	5	0.425884	1	6	0.016184	1	7	0.016570	1	8	0.000491
1	9	-0.016407	1	10	-0.216112	1	11	-0.016589	1	12	-0.195599
1	13	0.431767	1	14	0.019415	1	15	-0.451688	1	16	-0.120712
1	17	-0.002940	1	18	-0.118429	1	19	-0.678373	1	20	-0.163650
1	21	0.011165	2	2	0.000003	2	3	0.000002	2	4	0.575970
2	5	0.317203	2	6	0.000002	2	7	-0.000002	2	10	0.000222
2	11	-0.000005	2	12	0.000026	2	13	0.000045	2	14	0.000720
2	15	0.494071	2	16	-0.145350	2	17	-0.004434	2	18	-0.141618
2	19	-0.332944	2	20	-0.224394	2	21	0.034329	3	1	-0.000826
3	2	-0.012432	3	3	0.015658	3	4	-0.000316	3	5	0.000343
3	6	-0.016048	3	7	-0.034260	3	8	0.578857	3	9	-0.043987
3	10	-0.467746	3	11	0.041787	3	12	0.404401	3	13	-0.041618
3	14	-0.023301	3	15	-0.002115	3	16	-0.000244	3	17	0.618343
3	18	0.326463	3	19	0.008291	3	20	-0.038395	3	21	-0.027957
4	1	0.312321	4	2	0.020795	4	3	-0.007571	4	4	-0.392235
4	5	0.425884	4	6	0.016184	4	7	0.016570	4	8	0.000491
4	9	-0.016407	4	10	-0.216112	4	11	-0.016589	4	12	-0.195599
4	13	0.431767	4	14	-0.019415	4	15	0.451688	4	16	0.120712
4	17	0.002940	4	18	0.118429	4	19	0.678373	4	20	0.163650
4	21	-0.011165	5	2	-0.000003	5	3	-0.000002	5	4	-0.575970
5	5	-0.317203	5	6	-0.000002	5	7	0.000002	5	10	0.000222
5	11	0.000005	5	12	-0.000026	5	13	-0.000045	5	14	0.000720
5	15	0.494071	5	16	-0.145350	5	17	-0.004434	5	18	-0.141618
5	19	-0.332944	5	20	-0.224394	5	21	0.034329	6	1	-0.000826
6	2	-0.012432	6	3	0.015658	6	4	-0.000316	6	5	0.000343
6	6	-0.016048	6	7	-0.034260	6	8	0.578857	6	9	-0.043987
6	10	-0.467746	6	11	0.041787	6	12	0.404401	6	13	-0.041618
6	14	0.023301	6	15	-0.002115	6	16	0.000244	6	17	-0.618343
6	18	-0.326463	6	19	-0.008291	6	20	0.038395	6	21	0.027957
7	1	-0.004810	7	2	-0.187324	7	3	0.720144	7	4	0.132277
7	5	-0.019345	7	6	-0.315735	7	7	-0.160860	7	8	0.031248
7	9	0.015783	7	10	-0.045256	7	11	-0.079776	7	12	0.254865
7	13	-0.131618	7	14	0.427531	7	15	-0.041609	7	16	0.501389
7	17	-0.002943	7	18	0.520839	7	19	0.188758	7	20	0.555272
7	21	0.011193	8	2	-0.333371	8	3	0.471455	8	6	0.257711
8	7	0.128847	8	8	0.000001	8	10	-0.000005	8	11	0.000016
8	13	-0.000013	8	14	0.458893	8	15	0.016362	8	16	-0.297663
8	17	-0.023390	8	18	-0.262919	8	19	-0.163429	8	20	-0.393366
8	21	-0.031336	9	1	-0.031312	9	2	0.032096	9	3	0.012102

continued

TABLE A-15-continued

9	4	0.000240	9	5	-0.000267	9	6	-0.231236	9	7	0.370381
9	8	-0.003821	9	9	0.013294	9	10	-0.163746	9	11	0.461896
9	12	-0.653884	9	13	-0.726998	9	14	-0.015756	9	15	-0.002133
9	16	0.457911	9	17	-0.019122	9	18	-0.408139	9	19	0.003309
9	20	0.490608	9	21	-0.028040	10	1	-0.004810	10	2	-0.187324
10	3	0.320144	10	4	0.018277	10	5	-0.019845	10	6	-0.315785
10	7	-0.160960	10	8	0.031248	10	9	0.015783	10	10	-0.045266
10	11	-0.079776	10	12	0.254865	10	13	-0.131618	10	14	-0.427531
10	15	0.041609	10	16	-0.501889	10	17	0.032943	10	18	-0.520839
10	19	-0.188753	10	20	-0.555272	10	21	-0.011193	11	2	0.333371
11	3	-0.471455	11	6	-0.257711	11	7	-0.128847	11	8	-0.000001
11	10	0.000305	11	11	-0.000016	11	13	0.000013	11	14	0.498898
11	15	0.016362	11	16	-0.297663	11	17	-0.023390	11	18	-0.262919
11	19	-0.163429	11	20	-0.393366	11	21	-0.031336	12	1	-0.031312
12	2	0.032096	12	3	0.012402	12	4	0.000240	12	5	-0.000267
12	6	-0.231236	12	7	0.370381	12	8	-0.003821	12	9	0.013294
12	10	-0.163746	12	11	0.461896	12	12	-0.653884	12	13	-0.726998
12	14	0.015756	12	15	0.002133	12	16	-0.457911	12	17	0.019122
12	18	0.408139	12	19	-0.003309	12	20	-0.490608	12	21	0.028040
13	1	-0.017671	13	2	-0.390015	13	3	-0.341716	13	4	0.018509
13	5	-0.020103	13	6	0.064712	13	7	-0.331659	13	8	0.054343
13	9	0.035945	13	10	0.012975	13	11	0.628236	13	12	0.148254
13	13	-0.554569	14	14	-0.075391	14	15	-0.343873	14	16	-0.170398
14	17	-0.047124	14	18	0.044977	14	19	0.108452	14	20	0.884802
14	21	-0.044406	15	1	-0.013827	15	2	-0.656378	15	3	-0.466030
15	4	-0.000377	15	5	0.000080	15	6	0.004989	15	7	0.225837
15	8	-0.035220	15	9	-0.019562	15	10	-0.338110	15	11	-0.500740
15	12	-0.509923	15	13	-0.151915	16	1	-0.536205	16	2	-0.022473
16	3	0.001079	16	4	0.017464	16	5	-0.018964	16	6	-0.027436
16	7	-0.002367	16	8	-0.047917	16	9	0.725860	16	10	0.107576
16	11	0.067656	16	12	0.027905	16	13	-0.622139	17	14	0.033666
17	15	-0.033909	17	16	-0.018106	17	17	0.039772	17	18	-0.074394
17	19	0.063889	17	20	0.030186	17	21	-0.813341	18	1	0.803884
18	2	0.008629	18	3	0.011449	18	4	-0.000070	18	5	0.000077
18	6	0.005181	18	7	-0.025046	18	8	-0.035036	18	9	0.524554
18	10	0.468662	18	11	0.000784	18	12	0.295636	18	13	0.144346
19	1	0.012326	19	2	0.020794	19	3	-0.007571	19	4	0.017966
19	5	-0.019504	19	6	0.016197	19	7	0.016567	19	8	0.000489
19	9	-0.016407	19	10	-0.216088	19	11	-0.016592	19	12	-0.195574
19	13	0.431812	20	14	-0.013104	20	15	-0.052362	20	16	-0.059339

continued

TABLE A-15-continued

20	17	-0.002335	20	18	-0.057260	20	19	0.150219	20	20	-0.107773
20	21	0.026313	21	1	-0.009733	21	2	0.021864	21	3	0.012801
21	4	-0.000151	21	5	0.000164	21	6	-0.001637	21	7	-0.028007
21	8	-0.042571	21	9	-0.027254	21	10	-0.378947	21	11	0.013952
21	12	0.330581	21	13	-0.017277	22	1	-0.004974	22	2	0.048561
22	3	-0.013121	22	4	0.018281	22	5	-0.019849	22	6	0.044177
22	7	0.023719	22	8	0.031544	22	9	0.016033	22	10	-0.043610
22	11	-0.070654	22	12	0.253501	22	13	-0.137055	23	14	-0.065092
23	15	-0.013076	23	16	0.063165	23	17	-0.025726	23	18	0.099844
23	19	-0.029892	23	20	0.005660	23	21	-0.023744	24	1	-0.022455
24	2	0.022284	24	3	0.008721	24	4	0.000080	24	5	-0.000091
24	6	0.018949	24	7	-0.019076	24	8	-0.019731	24	9	-0.003349
24	10	-0.252080	24	11	-0.025809	24	12	-0.580455	24	13	-0.435653
25	1	0.028437	25	2	-0.005060	25	3	-0.002402	25	4	0.017665
25	5	-0.019182	25	6	-0.009980	25	7	0.005255	25	8	-0.028437
25	9	-0.046678	25	10	0.215767	25	11	0.033753	25	12	-0.062027
25	13	-0.186076	25	14	-0.001477	26	15	-0.010328	26	16	0.055383
26	17	0.025023	26	18	0.020894	26	19	-0.038396	26	20	0.396806
26	21	0.051741	27	1	-0.021582	27	2	0.020881	27	3	0.008998
27	4	0.000072	27	5	-0.000074	27	6	0.017534	27	7	-0.019685
27	8	-0.021298	27	9	-0.004992	27	10	0.544774	27	11	-0.023076
27	12	0.232344	27	13	0.437142						

TABLE A-16

THE SYMMETRIZED $\underline{A}$ MATRIX FOR ETHANOL

BASED ON THE FORCE FIELD AND GEOMETRY REPORTED BY ZEMLYANUKHINA AND SVERDLOV

1	1	0.012333	1	2	0.020575	1	3	-0.007261	1	4	-0.392246
1	5	0.425884	1	6	0.016519	1	7	0.016393	1	8	0.000477
1	9	-0.016422	1	10	-0.216145	1	11	-0.016523	1	12	-0.195537
1	13	0.432030	1	14	0.019695	1	15	-0.451698	1	16	-0.119483
1	17	-0.002926	1	18	-0.117600	1	19	-0.678237	1	20	-0.162887
1	21	0.011216	2	3	0.000002	2	4	0.575573	2	5	0.317201
2	6	-0.000002	2	7	0.000003	2	8	-0.000001	2	9	0.000002
2	11	0.000006	2	12	-0.000002	2	13	-0.000234	2	14	0.000846
2	15	0.494076	2	16	-0.144250	2	17	-0.004394	2	18	-0.140796
2	19	-0.332838	2	20	-0.223840	2	21	0.034293	3	1	-0.000820
3	2	-0.012288	3	3	0.015465	3	4	-0.000308	3	5	0.000333
3	6	-0.016467	3	7	-0.034330	3	8	0.578884	3	9	-0.043573
3	10	-0.467598	3	11	0.042025	3	12	0.404786	3	13	-0.041538
3	14	-0.023465	3	15	-0.002687	3	16	-0.000698	3	17	0.618371
3	18	0.026377	3	19	0.008234	3	20	-0.039080	3	21	-0.027926
4	1	0.012333	4	2	0.020575	4	3	-0.007261	4	4	-0.392246
4	5	0.425884	4	6	0.016519	4	7	0.016393	4	8	0.000477
4	9	-0.016422	4	10	-0.216145	4	11	-0.016923	4	12	-0.195537
4	13	0.432030	4	14	-0.019695	4	15	0.451698	4	16	0.119483
4	17	0.002926	4	18	0.117600	4	19	0.678237	4	20	0.162887
4	21	-0.011216	5	3	-0.000002	5	4	-0.575573	5	5	-0.317201
5	6	0.000002	5	7	-0.000003	5	8	0.000001	5	9	-0.000002
5	11	-0.000006	5	12	0.000006	5	13	0.000234	5	14	0.000846
5	15	0.494076	5	16	-0.144250	5	17	-0.004394	5	18	-0.140796
5	19	-0.332838	5	20	-0.223840	5	21	0.034293	6	1	-0.000820
6	2	-0.012288	6	3	0.015465	6	4	-0.000308	6	5	0.000333
6	6	-0.016467	6	7	-0.034330	6	8	0.578884	6	9	-0.043573
6	10	-0.467598	6	11	0.042025	6	12	0.404786	6	13	-0.041538
6	14	0.023465	6	15	0.002687	6	16	0.000698	6	17	-0.618371
6	18	-0.026377	6	19	-0.008234	6	20	0.039080	6	21	0.027926
7	1	-0.004952	7	2	-0.182803	7	3	0.314010	7	4	0.018274
7	5	-0.019840	7	6	-0.321338	7	7	-0.157122	7	8	0.031463
7	9	0.016023	7	10	-0.044063	7	11	-0.074884	7	12	0.253375
7	13	-0.136135	7	14	0.419704	7	15	-0.042014	7	16	0.505125
7	17	-0.002953	7	18	0.520496	7	19	0.196844	7	20	0.561793
7	21	0.011315	8	2	-0.336747	8	3	0.476233	8	5	0.030002
8	6	0.251732	8	7	0.126218	8	8	-0.000001	8	10	0.000003
8	11	0.001329	8	13	0.000015	8	14	0.503934	8	15	0.015786
8	16	-0.286225	8	17	-0.023603	8	18	-0.256627	8	19	-0.160982
8	20	-0.382496	8	21	-0.031448	9	1	-0.031155	9	2	0.034981

continued

TABLE A-16-continued

9	3	0.007681	9	4	0.000245	9	5	-0.000258	9	6	-0.233173
9	7	0.372836	9	8	-0.004147	9	9	0.012568	9	10	-0.165532
9	11	0.461221	9	12	-0.652810	9	13	-0.721556	9	14	-0.022301
9	15	-0.002115	9	16	0.459581	9	17	-0.019283	9	18	-0.407938
9	19	0.008332	9	20	0.494912	9	21	-0.028273	10	1	-0.004952
10	2	-0.182803	10	3	0.314010	10	4	0.018274	10	5	-0.019840
10	6	-0.321338	10	7	-0.157122	10	8	0.031463	10	9	0.016023
10	10	0.044063	10	11	-0.074586	10	12	0.253375	10	13	-0.136135
10	14	-0.419704	10	15	0.042014	10	16	-0.505125	10	17	0.002953
10	18	-0.520496	10	19	-0.190844	10	20	-0.561793	10	21	-0.011315
11	2	0.336747	11	3	-0.476233	11	5	-0.000002	11	6	-0.251732
11	7	-0.126218	11	8	0.000001	11	10	-0.000003	11	11	-0.001329
11	13	-0.000015	11	14	0.503934	11	15	0.015786	11	16	-0.286225
11	17	-0.023603	11	18	-0.256627	11	19	-0.160582	11	20	-0.382496
11	21	-0.031446	12	1	-0.031155	12	2	0.034981	12	3	0.007681
12	4	0.000245	12	5	-0.000258	12	6	-0.233173	12	7	0.372836
12	8	-0.004147	12	9	0.012968	12	10	-0.165532	12	11	0.461221
12	12	-0.652810	12	13	-0.721556	12	14	0.022301	12	15	0.002115
12	16	-0.459581	12	17	0.019283	12	18	0.407938	12	19	-0.008332
12	20	-0.494912	12	21	0.028273	13	1	-0.017697	13	2	-0.390736
13	3	-0.340697	13	4	0.018509	13	5	-0.020095	13	6	0.063955
13	7	-0.331840	13	8	0.054308	13	9	0.039542	13	10	0.082800
13	11	0.631492	13	12	0.147231	13	13	-0.555034	14	14	-0.075991
14	15	-0.043765	14	16	-0.022179	14	17	-0.047030	14	18	0.044729
14	19	0.108233	14	20	0.882856	14	21	-0.044330	15	1	-0.013832
15	2	-0.666952	15	3	-0.465911	15	4	-0.000074	15	5	0.000078
15	6	0.006274	15	7	0.225687	15	8	-0.035205	15	9	-0.019547
15	10	-0.338055	15	11	-0.503245	15	12	-0.568930	15	13	-0.152155
16	1	-0.536174	16	2	-0.022254	16	3	0.000736	16	4	0.017483
16	5	-0.018979	16	6	-0.028850	16	7	-0.002471	16	8	-0.047906
16	9	0.705850	16	10	0.107640	16	11	0.067587	16	12	0.028630
16	13	-0.601507	17	14	0.030937	17	15	-0.033816	17	16	-0.016957
17	17	0.039725	17	18	-0.074271	17	19	0.068939	17	20	0.031328
17	21	-0.813348	18	1	0.803880	18	2	0.006552	18	3	0.011572
18	4	-0.000069	18	5	0.000077	18	6	0.005145	18	7	-0.025152
18	8	-0.034588	18	9	0.524573	18	10	0.468774	18	11	0.000898
18	12	0.295681	18	13	0.144150	19	1	0.012332	19	2	-0.020574
19	3	-0.067262	19	4	0.017960	19	5	-0.019503	19	6	0.016518
19	7	0.016392	19	8	0.000479	19	9	-0.016418	19	10	-0.216155
19	11	-0.016917	19	12	-0.195537	19	13	0.432005	20	14	-0.013183

continued

TABLE A-16-continued

20	15	-0.052341	20	16	-0.059165	20	17	-0.002312	20	18	-0.057047
20	19	0.150169	20	20	-0.107852	20	21	0.026338	21	1	-0.009734
21	2	0.001856	21	3	0.012822	21	4	-0.000147	21	5	0.000160
21	6	-0.001799	21	7	-0.028098	21	8	-0.042550	21	9	-0.027241
21	10	-0.378844	21	11	0.014113	21	12	0.330727	21	13	-0.017381
22	1	-0.004983	22	2	0.048049	22	3	-0.012401	22	4	0.018275
22	5	-0.019842	22	6	0.045009	22	7	0.028494	22	8	0.031520
22	9	0.016062	22	10	-0.043734	22	11	-0.071134	22	12	0.253112
22	13	-0.137198	23	14	-0.065727	23	15	-0.013013	23	16	0.061152
23	17	-0.025682	23	18	0.099081	23	19	-0.030164	23	20	0.003804
23	21	-0.023691	24	1	-0.022467	24	2	0.022063	24	3	0.009043
24	4	0.000083	24	5	-0.000089	24	6	0.019156	24	7	-0.019198
24	8	-0.019721	24	9	-0.003335	24	10	-0.252034	24	11	-0.025763
24	12	-0.580663	24	13	-0.436025	25	1	0.028455	25	2	-0.005018
25	3	-0.002484	25	4	0.017674	25	5	-0.019189	25	6	-0.010019
25	7	0.005124	25	8	-0.028435	25	9	-0.046689	25	10	0.215770
25	11	0.033580	25	12	-0.061584	25	13	-0.185592	26	14	-0.001571
26	15	-0.010333	26	16	0.055223	26	17	0.024990	26	18	0.020409
26	19	-0.038581	26	20	0.096868	26	21	0.051698	27	1	-0.021592
27	2	0.020680	27	3	0.009307	27	4	0.000065	27	5	-0.000072
27	6	0.017718	27	7	-0.019810	27	8	-0.021286	27	9	-0.004975
27	10	0.544859	27	11	-0.023025	27	12	0.232204	27	13	0.436833

TABLE A-17

THE L MATRIX FOR ETHANOL

BASED ON TRANSFERRED FORCE CONSTANTS

1	1	-1.026715	1	2	0.002334	1	3	-0.004777	1	4	-0.000138
1	5	0.000947	1	6	0.013794	1	7	0.003175	1	8	0.004697
1	9	-0.017698	1	10	0.004234	1	11	-0.003873	1	12	-0.003373
1	13	0.003354	2	1	-0.001611	2	2	-1.005615	2	3	-0.159284
2	4	0.256177	2	5	0.029125	2	6	-0.002427	2	7	0.003220
2	8	-0.000691	2	9	0.000727	2	10	0.008623	2	11	0.006627
2	12	0.005513	2	13	0.006550	3	1	-0.000405	3	2	-0.248524
3	3	-0.005210	3	4	-0.978328	3	5	-0.002876	3	6	0.003957
3	7	-0.001511	3	8	-0.013950	3	9	-0.007219	3	10	-0.002774
3	11	0.002546	3	12	-0.005015	3	13	0.000353	4	1	-0.000536
4	2	-0.151725	4	3	1.011586	4	4	0.033270	4	5	0.000553
4	6	-0.006183	4	7	-0.022711	4	8	-0.000249	4	9	-0.012019
4	10	-0.000133	4	11	0.011043	4	12	0.003968	4	13	-0.003398
5	1	0.003110	5	2	0.008384	5	3	-0.064753	5	4	-0.003797
5	5	-0.090087	5	6	0.542165	5	7	1.214582	5	8	0.031749
5	9	0.221321	5	10	-0.042981	5	11	-0.095980	5	12	-0.033463
5	13	0.024344	6	1	-0.000757	6	2	-0.090148	6	3	-0.013172
6	4	0.320971	6	5	1.447248	6	6	-0.236253	6	7	0.242513
6	8	-0.105631	6	9	-0.081261	6	10	0.102655	6	11	0.095517
6	12	0.062356	6	13	0.028970	7	1	0.000083	7	2	0.015145
7	3	0.003123	7	4	0.052911	7	5	0.362804	7	6	-0.256976
7	7	0.041024	7	8	1.377293	7	9	0.229269	7	10	0.023058
7	11	-0.038572	7	12	0.029381	7	13	0.011971	8	1	0.017570
8	2	-0.034880	8	3	-0.003410	8	4	0.012535	8	5	-0.185489
8	6	-0.516428	8	7	0.450110	8	8	-0.094180	8	9	-0.457764
8	10	-0.483706	8	11	-0.152593	8	12	-0.035494	8	13	-0.012393
9	1	0.015437	9	2	-0.004864	9	3	0.042421	9	4	0.003754
9	5	-0.387450	9	6	-0.550318	9	7	0.053630	9	8	-0.239184
9	9	0.895223	9	10	0.033344	9	11	0.320190	9	12	-0.027017
9	13	-0.058527	10	1	0.020063	10	2	0.005082	10	3	-0.036383
10	4	-0.000945	10	5	-0.047294	10	6	-0.113975	10	7	0.120693
10	8	-0.003256	10	9	-0.118663	10	10	0.239529	10	11	-0.132446
10	12	-0.158466	10	13	0.007595	11	1	-0.000320	11	2	0.094789
11	3	0.065275	11	4	-0.024141	11	5	0.353425	11	6	0.123032
11	7	-0.217404	11	8	-0.027363	11	9	0.322293	11	10	-0.442796
11	11	-0.245604	11	12	-0.429286	11	13	-0.118681	12	1	0.001131
12	2	0.017379	12	3	-0.032756	12	4	0.042383	12	5	0.029853
12	6	0.136879	12	7	0.009654	12	8	0.171524	12	9	-0.019453
12	10	-0.362276	12	11	0.245703	12	12	-0.221725	12	13	0.008998
13	1	0.038305	13	2	0.045932	13	3	0.081641	13	4	-0.012200

continued

TABLE A-17-continued

13	5	-0.025905	13	6	-0.049414	13	7	-0.128975	13	8	-0.034799
13	9	0.138731	13	10	-0.126911	13	11	-0.116748	13	12	0.077681
13	13	0.281970	14	14	0.778945	14	15	-0.703859	14	16	-0.030274
14	17	0.005381	14	18	0.004898	14	19	-0.014739	14	20	0.002550
14	21	0.000188	15	14	0.703603	15	15	0.778882	15	16	0.006674
15	17	0.015737	15	18	0.026625	15	19	-0.009474	15	20	0.000966
15	21	-0.000272	16	14	-0.073763	16	15	0.056730	16	16	1.492545
16	17	0.075706	16	18	-0.106359	16	19	0.059602	16	20	-0.057615
16	21	0.000706	17	14	0.063474	17	15	-0.016788	17	16	-0.038894
17	17	-0.973774	17	18	-0.476764	17	19	0.281766	17	20	-0.003982
17	21	0.001437	18	14	-0.021342	18	15	0.136240	18	16	-0.275258
18	17	0.499595	18	18	-0.551106	18	19	0.590947	18	20	-0.024650
18	21	-0.001851	19	14	-0.369336	19	15	-0.161647	19	16	-0.009938
19	17	-0.174283	19	18	0.652798	19	19	0.497116	19	20	-0.018602
19	21	0.002412	20	14	0.094960	20	15	0.006715	20	16	-0.799447
20	17	-0.150713	20	18	0.049554	20	19	-0.305617	20	20	-0.569618
20	21	0.022701	21	14	0.004615	21	15	-0.087273	21	16	-0.042663
21	17	-0.119046	21	18	0.088339	21	19	-0.011703	21	20	-0.063311
21	21	-1.164725									

TABLE A-18

THE L MATRIX FOR ETHANOL

DERIVED FROM THE FORCE FIELD REPORTED BY ZEMLYANUKHINA AND SVERDLOV

1	1	1.026950	1	2	0.000870	1	3	0.002263	1	4	0.000930
1	5	-0.007942	1	6	0.002288	1	7	-0.000209	1	8	0.000324
1	9	0.000866	1	10	0.004370	1	11	0.000845	1	12	0.002489
1	13	0.002019	2	1	-0.001268	2	2	1.030785	2	3	0.107728
2	4	0.156880	2	5	-0.014693	2	6	-0.012452	2	7	0.020281
2	8	-0.028873	2	9	-0.014753	2	10	0.014699	2	11	-0.015381
2	12	-0.002770	2	13	-0.004967	3	1	-0.001878	3	2	-0.180217
3	3	0.704851	3	4	0.019339	3	5	0.013042	3	6	-0.002955
3	7	0.029501	3	8	-0.018360	3	9	-0.016476	3	10	0.011851
3	11	-0.030590	3	12	0.003629	3	13	-0.004201	4	1	-0.000784
4	2	0.033992	4	3	0.723414	4	4	-0.722682	4	5	0.026900
4	6	-0.018555	4	7	0.000408	4	8	-0.005421	4	9	-0.007298
4	10	0.016066	4	11	-0.005566	4	12	0.010779	4	13	-0.002345
5	1	0.002989	5	2	-0.008185	5	3	-0.101366	5	4	0.084984
5	5	0.391244	5	6	-1.972405	5	7	0.361457	5	8	0.439739
5	9	-0.210711	5	10	0.312965	5	11	0.237122	5	12	-0.017247
5	13	0.026393	6	1	0.000034	6	2	0.100721	6	3	-0.027399
6	4	-0.025950	6	5	-0.131795	6	6	0.246186	6	7	1.373837
6	8	-0.424108	6	9	-0.152568	6	10	0.085570	6	11	-0.233371
6	12	-0.075397	6	13	0.032569	7	1	0.002279	7	2	0.055287
7	3	-0.072993	7	4	-0.062148	7	5	0.814542	7	6	0.629930
7	7	0.218292	7	8	0.847723	7	9	0.321581	7	10	0.103917
7	11	-0.264238	7	12	-0.084199	7	13	0.022986	8	1	-0.014133
8	2	0.030786	8	3	0.010355	8	4	-0.002193	8	5	-0.311667
8	6	0.299648	8	7	0.021947	8	8	0.517712	8	9	-1.022856
8	10	-0.081774	8	11	0.088254	8	12	0.205811	8	13	-0.017690
9	1	-0.049040	9	2	-0.001029	9	3	0.049521	9	4	-0.033514
9	5	-0.815215	9	6	-0.082713	9	7	0.082565	9	8	0.556310
9	9	0.376206	9	10	0.173686	9	11	-0.340225	9	12	-0.002832
9	13	-0.032544	10	1	-0.004232	10	2	-0.004232	10	3	-0.004220
10	4	0.029590	10	5	0.023774	10	6	0.066609	10	7	-0.028240
10	8	-0.018513	10	9	-0.124943	10	10	0.322290	10	11	0.093897
10	12	0.093878	10	13	0.008536	11	1	-0.001458	11	2	-0.091449
11	3	0.043442	11	4	-0.043482	11	5	-0.119921	11	6	0.150579
11	7	0.381631	11	8	0.058854	11	9	0.371468	11	10	-0.316256
11	11	0.655518	11	12	0.326063	11	13	-0.095534	12	1	0.001409
12	2	0.009541	12	3	-0.072161	12	4	-0.004229	12	5	0.184687
12	6	-0.067075	12	7	0.029900	12	8	0.004700	12	9	0.100746
12	10	-0.067618	12	11	-0.183467	12	12	0.270911	12	13	0.006349
13	1	-0.041774	13	2	-0.050100	13	3	0.060793	13	4	-0.058526

---

continued

TABLE A-18-continued

13	5	-0.117514	13	6	0.069221	13	7	-0.031011	13	8	0.074306
13	9	0.087209	13	10	-0.137450	13	11	0.110896	13	12	-0.087769
13	13	0.287936	14	14	1.045583	14	15	0.107444	14	16	0.010842
14	17	0.006794	14	18	-0.026062	14	19	0.000059	14	20	0.000052
14	21	0.000177	15	14	-0.107060	15	15	1.044297	15	16	0.013456
15	17	0.010265	15	18	0.018381	15	19	-0.012673	15	20	-0.000512
15	21	-0.000217	16	14	-0.163678	16	15	-0.024941	16	16	1.372603
16	17	-0.076201	16	18	-0.578161	16	19	-0.118229	16	20	0.073051
16	21	0.001807	17	14	0.061342	17	15	0.016569	17	16	-0.086336
17	17	-1.085667	17	18	0.096444	17	19	-0.267685	17	20	0.002184
17	21	0.002357	18	14	-0.132546	18	15	0.678134	18	16	-0.551931
18	17	0.074082	18	18	-0.783336	18	19	-0.231117	18	20	0.023203
18	21	-0.001739	19	14	0.077446	19	15	-0.168413	19	16	0.062692
19	17	0.208685	19	18	0.376731	19	19	-0.714741	19	20	0.019730
19	21	0.004295	20	14	0.103105	20	15	0.080582	20	16	-0.676616
20	17	-0.040850	20	18	0.459484	20	19	0.293559	20	20	0.560156
20	21	0.033351	21	14	0.073525	21	15	-0.056633	21	16	-0.003463
21	17	-0.043514	21	18	0.141365	21	19	-0.040938	21	20	0.096048
21	21	-1.163011									

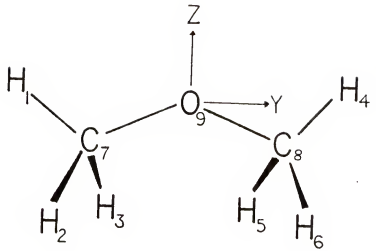

Fig. A-3. Geometry for dimethyl ether. The atoms are numbered as used in the normal coordinate analysis. From reference (103):

$\alpha(2,7,3) = 108°44'$	$\alpha(7,9,8) = 111°43'$
$\alpha(1,7,2) = 109°33'$	$r(1,7) = 1.091$ Å
$\alpha(9,7,1) = 107°14'$	$r(2,7) = 1.100$ Å
$\alpha(9,7,2) = 110°50'$	$r(7,9) = 1.410$ Å

TABLE A-19
INTERNAL DISPLACEMENT COORDINATES FOR DIMETHYL ETHER

r_1 = R(7,1)
r_2 = R(7,2)
r_3 = R(7,3)
r_4 = R(8,4)
r_5 = R(8,5)
r_6 = R(8,6)
r_7 = α(2,7,3)
r_8 = α(1,7,3)
r_9 = α(1,7,2)
r_{10} = α(5,8,6)
r_{11} = α(4,8,6)
r_{12} = α(4,8,5)
r_{13} = α(9,7,1)
r_{14} = α(9,7,2)
r_{15} = α(9,7,3)
r_{16} = α(9,8,4)
r_{17} = α(9,8,5)
r_{18} = α(9,8,6)
r_{19} = R(7,9)
r_{20} = R(8,9)
r_{21} = α(7,9,8)
r_{22} = τ(1,7,9,8)
r_{23} = τ(4,8,9,7)

Note: See footnotes for TABLE A-1

TABLE A-20
UNNORMALIZED SYMMETRY COORDINATES FOR DIMETHYL ETHER

$S_1 = 2r_1 - r_2 - r_3 + 2r_4 - r_5 - r_6$
$S_2 = r_1 + r_2 + r_3 + r_4 + r_5 + r_6$
$S_3 = 2(r_7 + r_{10}) - (r_8 + r_9 + r_{11} + r_{12})$
$S_4 = r_7 + r_{10} + r_8 + r_9 + r_{11} + r_{12} - (r_{13} + r_{16}) - (r_{14} + r_{15} + r_{17} + r_{18})$
$S_5 = 2(r_{13} + r_{16}) - (r_{14} + r_{15} + r_{17} + r_{18})$
$S_6 = r_{19} + r_{20}$
$S_7 = r_{21}$
$S_8 = r_2 - r_3 - r_5 + r_6$
$S_9 = r_8 - r_9 - r_{11} + r_{12}$
$S_{10} = r_{14} - r_{15} - r_{17} + r_{18}$
$S_{11} = r_{22} + r_{23}$
$S_{12} = r_2 - r_3 + r_5 - r_6$
$S_{13} = r_8 - r_9 + r_{11} - r_{12}$
$S_{14} = r_{14} - r_{15} + r_{17} - r_{18}$
$S_{15} = r_{22} - r_{23}$
$S_{16} = 2r_1 - r_2 - r_3 - 2r_4 + r_5 + r_6$
$S_{17} = r_1 + r_2 + r_3 - r_4 - r_5 - r_6$
$S_{18} = 2(r_7 - r_{10}) - (r_8 + r_9 - r_{11} - r_{12})$
$S_{19} = (r_7 - r_{10}) + r_8 + r_9 - r_{11} - r_{12} - (r_{13} - r_{16}) - (r_{14} + r_{15} - r_{17} - r_{18})$
$S_{20} = 2(r_{13} - r_{16}) - (r_{14} + r_{15} - r_{17} - r_{18})$
$S_{21} = r_{19} - r_{20}$

Note: Taken from Levin, Pearce, and Spiker (84)

TABLE A-21

THE $\underline{A}$ MATRIX FOR DIMETHYL ETHER

1	8	-0.022028	1	9	0.063687	1	10	-0.060499	1	11	-0.608946
1	12	-0.077246	1	13	-0.016028	1	14	0.110838	1	15	-0.634387
2	1	-0.451057	2	3	-0.318946	2	3	0.000046	2	4	0.194316
2	5	-0.354945	2	6	-0.585247	2	7	-0.055191	2	16	-0.446384
2	17	-0.301094	2	18	0.001000	2	19	0.155754	2	20	-0.381116
2	21	-0.130027	3	1	0.339741	3	2	0.264445	3	3	-0.023260
3	4	0.222401	3	5	-0.470673	3	6	-0.137863	3	7	0.608503
3	16	0.294208	3	17	0.267047	3	18	-0.069311	3	19	0.217486
3	20	-0.358754	3	21	-0.054522	4	1	-0.234751	4	2	0.331986
4	3	0.182292	4	4	0.095146	4	5	0.000051	4	7	-0.000004
4	8	0.343096	4	9	0.094402	4	10	-0.106621	4	11	0.098375
4	12	0.360431	4	13	0.297823	4	14	-0.248923	4	15	0.419501
4	16	-0.234749	4	17	0.331990	4	18	0.182288	4	19	0.095145
4	20	0.000046	4	21	0.000006	5	1	0.010332	5	2	-0.014617
5	3	-0.180503	5	4	0.280358	5	5	0.370798	5	6	-0.585230
5	7	-0.715138	5	8	-0.017910	5	9	-0.304566	5	10	-0.335955
5	11	-0.355008	5	12	-0.052115	5	13	-0.311659	5	14	-0.286863
5	15	-0.309509	5	16	0.058277	5	17	-0.004740	5	18	-0.134217
5	19	0.258608	5	20	0.296041	5	21	-0.353810	6	1	0.137230
6	2	-0.227539	6	3	0.242990	6	4	0.095121	6	5	0.000848
6	6	-0.137871	6	7	0.222213	6	8	-0.318556	6	9	0.261599
6	10	-0.238162	6	11	0.260656	6	12	-0.290457	6	13	0.449139
6	14	-0.420474	6	15	0.523523	6	16	0.128149	6	17	-0.229860
6	18	0.224874	6	19	0.100558	6	20	0.358194	6	21	-0.192343
7	1	0.234751	7	2	-0.331986	7	3	-0.182292	7	4	-0.095146
7	5	-0.000051	7	7	0.000004	7	8	0.343096	7	9	0.094402
7	10	-0.106621	7	11	0.098375	7	12	0.360431	7	13	0.297823
7	14	-0.248923	7	15	0.419501	7	16	0.234749	7	17	-0.331990
7	18	-0.182288	7	19	-0.095145	7	20	-0.000046	7	21	-0.000006
8	1	0.010332	8	2	-0.014617	8	3	-0.180503	8	4	0.280358
8	5	0.370798	8	6	-0.585230	8	7	-0.715138	8	8	0.017910
8	9	0.304566	8	10	0.335955	8	11	0.355008	8	12	0.052115
8	13	0.311659	8	14	0.286863	8	15	0.309509	8	16	0.058277
8	17	-0.004740	8	18	-0.134217	8	19	0.258608	8	20	0.296041
8	21	-0.353810	9	1	0.137230	9	2	-0.227539	9	3	0.242998

---

continued

TABLE A-21-continued

9	4	0.095121	9	5	0.000848	9	6	-0.137871	9	7	0.202013
9	8	0.313556	9	9	-0.261599	9	10	0.238162	9	11	-0.260656
9	12	0.290457	9	13	-0.449139	9	14	0.420474	9	15	-0.523523
9	16	0.128149	9	17	-0.229860	9	18	0.224874	9	19	0.100558
9	20	0.058194	9	21	-0.182343	10	8	-0.322028	10	9	0.063687
10	10	-0.660499	10	11	-0.608946	10	12	0.377246	10	13	0.016028
10	14	-0.110933	10	15	0.634387	11	1	0.451057	11	2	0.318946
11	3	-0.000046	11	4	-0.194315	11	5	0.194945	11	6	0.585247
11	7	0.055191	11	16	-0.446384	11	17	-0.311094	11	18	0.231300
11	19	0.155754	11	20	-0.381116	11	21	-0.130027	12	1	0.329941
12	2	0.264445	12	3	-0.023260	12	4	0.222401	12	5	-0.476573
12	6	-0.137863	12	7	0.608503	12	16	-0.294208	12	17	-0.267047
12	18	0.069311	12	19	-0.217486	12	20	0.358754	12	21	0.354522
13	1	0.234751	13	2	-0.331986	13	3	-0.182292	13	4	-0.095146
13	5	-0.000051	13	7	0.000304	13	8	0.343096	13	9	0.094402
13	10	-0.106621	13	11	0.098375	13	12	-0.360431	13	13	-0.297823
13	14	0.248923	13	15	-0.419501	13	16	-0.234749	13	17	0.331990
13	18	0.182288	13	19	0.095145	13	20	0.000046	13	21	0.000006
14	1	-0.010332	14	2	0.014617	14	3	0.180503	14	4	-0.280358
14	5	-0.370798	14	6	0.585230	14	7	0.715138	14	8	-0.017910
14	9	-0.304596	14	10	-0.335955	14	11	-0.355008	14	12	0.352115
14	13	0.311659	14	14	0.286863	14	15	0.309609	14	16	0.058277
14	17	-0.004740	14	18	-0.134217	14	19	0.259638	14	20	0.000041
14	21	-0.353810	15	1	0.137230	15	2	-0.227539	15	3	0.242998
15	4	0.095121	15	5	0.000848	15	6	-0.137871	15	7	0.202013
15	8	0.313556	15	9	-0.261599	15	10	0.238162	15	11	-0.260656
15	12	0.290457	15	13	0.449139	15	14	-0.420474	15	15	0.523523
15	16	-0.128149	15	17	0.229860	15	18	-0.224874	15	19	-0.100558
15	20	-0.058194	15	21	0.182343	16	1	-0.234751	16	2	0.331986
16	3	0.182292	16	4	0.095146	16	5	0.000051	16	7	-0.000304
16	8	0.343096	16	9	0.094402	16	10	-0.106621	16	11	0.098375
16	12	-0.360431	16	13	-0.297823	16	14	0.248923	16	15	-0.419501
16	16	0.234749	16	17	-0.331990	16	18	-0.182288	16	19	-0.095145
16	20	-0.000046	16	21	-0.000006	17	1	-0.010332	17	2	0.014617
17	3	0.180503	17	4	-0.280358	17	5	-0.370798	17	6	0.585230

continued

TABLE A-21-continued

17	7	0.715138	17	8	0.017910	17	9	0.304566	17	10	0.335955
17	11	0.355003	17	12	-0.052115	17	13	-0.311659	17	14	-0.286863
17	15	-0.309609	17	16	0.053277	17	17	-0.304745	17	18	-0.134217
17	19	0.258608	17	20	0.296041	17	21	-0.353810	18	1	0.137230
18	2	-0.227539	18	3	0.242998	13	4	0.095121	18	5	0.000848
18	6	-0.137871	18	7	0.202013	18	8	-0.318556	18	9	0.261599
18	10	-0.239162	18	11	0.260656	18	12	0.290457	18	13	-0.449139
18	14	0.420474	18	15	-0.523523	18	16	-0.128149	18	17	0.229860
18	18	-0.224874	18	19	-0.100558	18	20	-0.358194	18	21	0.192343
19	8	-0.043422	19	9	-0.079076	19	10	0.078298	19	11	-0.072227
19	12	-0.044649	19	13	-0.009258	19	14	0.064049	19	15	0.059214
20	3	0.000001	20	4	-0.000001	20	5	0.000002	20	6	-0.585235
20	7	-0.395664	20	16	0.026996	20	17	0.013739	20	18	0.024349
20	19	-0.029887	20	20	-0.031877	20	21	-0.245493	21	1	-0.030460
21	2	0.009608	21	3	-0.023322	21	4	-0.020796	21	5	0.023638
21	6	-0.137871	21	7	0.182315	21	16	-0.038248	21	17	0.007054
21	18	-0.040387	21	19	-0.014857	21	20	0.078337	21	21	-0.199021
22	8	-0.043422	22	9	-0.079076	22	10	0.078298	22	11	-0.072227
22	12	0.044649	22	13	0.009258	22	14	-0.064049	22	15	-0.059214
23	3	-0.000001	23	4	0.000001	23	5	0.000002	23	6	0.585235
23	7	0.395664	23	16	0.026996	23	17	0.013739	23	18	0.024349
23	19	-0.029887	23	20	-0.031877	23	21	-0.245493	24	1	-0.030460
24	2	0.009608	24	3	-0.023322	24	4	-0.020796	24	5	0.023638
24	6	-0.137871	24	7	0.182315	24	16	0.038248	24	17	-0.007054
24	18	0.040387	24	19	0.014857	24	20	-0.078337	24	21	0.199021
25	8	-0.018543	25	9	0.086833	25	10	-0.082988	25	11	0.160319
26	16	0.001058	26	17	0.018522	26	18	-0.002834	26	19	-0.039961
26	20	0.021245	26	21	0.473911	27	1	-0.030461	27	2	0.009607
27	3	-0.023319	27	4	-0.020797	27	5	0.023632	27	6	0.258994
27	7	-0.401156									

TABLE A-22

THE L MATRIX FOR DIMETHYL ETHER

1	1	1.045510	1	2	0.023120	1	3	-0.051628	1	4	-0.057771
1	5	0.364389	1	6	0.011156	1	7	0.333595	2	1	-0.017124
2	2	1.002368	2	3	0.075512	2	4	0.380291	2	5	0.042927
2	6	0.244069	2	7	-0.003639	3	1	0.204651	3	2	-0.023885
3	3	1.276958	3	4	-0.508879	3	5	-0.540768	3	6	-0.073196
3	7	0.346741	4	1	0.113119	4	2	-0.241816	4	3	0.460569
4	4	1.293150	4	5	-0.151553	4	6	0.213871	4	7	-0.021838
5	1	-0.140394	5	2	-0.076503	5	3	0.535676	5	4	-0.155155
5	5	0.773689	5	6	0.271247	5	7	-0.265013	6	1	0.016383
5	2	-0.058790	6	3	-0.022163	6	4	0.263645	6	5	-0.146689
6	6	0.303367	6	7	0.003164	7	1	-0.104366	7	2	-0.015267
7	3	0.327936	7	4	0.045979	7	5	0.248432	7	6	-0.078163
7	7	0.296901	8	8	1.045506	9	9	-0.385301	8	10	-0.046208
9	11	-0.001290	9	8	0.236626	9	9	1.431706	9	10	-0.371202
9	11	0.354569	10	8	-0.041667	10	9	0.410083	10	10	0.938011
10	11	-0.302773	11	8	-0.059156	11	9	-0.711547	11	10	0.229430
11	11	0.661947	12	12	1.045635	12	13	-0.384056	12	14	-0.043005
12	15	0.001155	13	12	0.241703	13	13	1.453032	13	14	-0.269010
13	15	0.366687	14	12	-0.049968	14	13	0.336438	14	14	0.915596
14	15	-0.323400	15	12	-0.164599	15	13	-0.777503	15	14	0.480393
15	15	0.820062	16	16	1.033426	16	17	0.388310	16	18	-0.017792
16	19	-0.103899	16	20	0.032420	16	21	-0.358348	17	16	-0.076562
17	17	0.989033	17	18	0.026459	17	19	0.399740	17	20	0.074277
17	21	0.320506	18	16	0.190893	18	17	-0.300553	18	18	1.437754
18	19	0.358650	18	20	-0.413154	18	21	0.199796	19	16	0.159108
19	17	-0.257032	19	18	0.024129	19	19	1.282989	19	20	0.437053
19	21	0.317053	20	16	-0.159621	20	17	-0.355302	20	18	0.533083
20	19	-0.133040	20	20	0.703298	20	21	-0.436515	21	16	0.016554
21	17	-0.363358	21	18	0.025640	21	19	-0.340943	21	20	0.240740
21	21	0.322104									

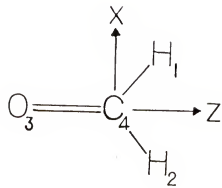

Fig. A-4. Geometry for formaldehyde. The atoms are numbered as used in the normal coordinate analysis. From (86):

$\alpha(1,4,2) = 120°$
$r(1,4) = 1.09$ Å
$r(3,4) = 1.213$ Å

TABLE A-23
INTERNAL DISPLACEMENT COORDINATES FOR FORMALDEHYDE

$r_1 = R(4,1)$[a]

$r_2 = R(4,2)$

$r_3 = R(3,4)$

$r_4 = \alpha(3,4,1)$

$r_5 = \alpha(3,4,2)$

$r_6 = \alpha(1,4,2)$

$r_7 = \beta(3,4)$[b]

[a]See footnotes for TABLE A-1

[b]Carbonyl out of plane wag

TABLE A-24
UNNORMALIZED SYMMETRY COORDINATES FOR FORMALDEHYDE

$S_1 = r_1 + r_2$

$S_2 = r_3$

$S_3 = r_4 + r_5 - 2r_6$

$S_4 = r_1 - r_2$

$S_5 = r_4 - r_5$

$S_6 = r_7$

Note: Taken from Hitsatsune and Eggers (86)

TABLE A-25
THE SYMMETRIZED $\underline{A}$ MATRIX FOR FORMALDEHYDE

1	1	0.612382	1	2	0.000008	1	3	-0.222495	1	4	0.512357
1	5	-0.189994	2	6	0.395431	3	1	0.329812	3	2	0.532971
3	3	0.359489	3	4	0.401678	3	5	0.528953	4	1	-0.612382
4	2	-0.000008	4	3	0.222495	4	4	0.512357	4	5	-0.189994
5	6	0.395431	6	1	0.329812	6	2	0.532971	6	3	0.359489
6	4	-0.401678	6	5	-0.528953	7	4	-0.010382	7	5	-0.062631
8	6	0.022389	9	1	-0.023747	9	2	-0.467025	9	3	-0.025883
10	4	-0.072222	10	5	0.115395	11	6	-0.096264	12	1	-0.023747
12	2	0.532978	12	3	-0.025884						

TABLE A-26
THE $\underline{L}$ MATRIX FOR FORMALDEHYDE

1	1	1.010868	1	2	0.108337	1	3	0.017483	2	1	-0.096462
2	2	0.329005	2	3	0.168237	3	1	0.207347	3	2	-1.080913
3	3	1.268735	4	4	1.056150	4	5	0.042197	5	4	-0.218144
5	5	1.070951	6	6	1.517262						

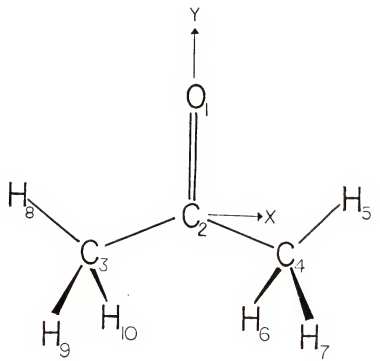

Fig. A-5. Geometry for acetone. The atoms are numbered as used in the normal coordinate analysis. From (75):

$\alpha(6,4,7) = 108°46'$ $r(1,2) = 1.222$ Å
$\alpha(3,2,4) = 117°12'$ $r(4,5) = 1.085$ Å
$r(2,3) = 1.507$ A
The methyl tilt towards oxygen is 1°21'

TABLE A-27
INTERNAL DISPLACEMENT COORDINATES FOR ACETONE

r_1 = R(4,5)[a]
r_2 = R(4,6)
r_3 = R(4,7)
r_4 = R(3,8)
r_5 = R(3,9)
r_6 = R(3,10)
r_7 = R(1,2)
r_8 = α(6,4,7)
r_9 = α(5,4,7)
r_{10} = α(5,4,6)
r_{11} = α(9,3,10)
r_{12} = α(8,3,10)
r_{13} = α(8,3,9)
r_{14} = α(2,4,5)
r_{15} = α(2,4,6)
r_{16} = α(2,4,7)
r_{17} = α(2,3,8)
r_{18} = α(2,3,9)
r_{19} = α(2,3,10)
r_{20} = R(2,3)
r_{21} = R(2,4)
r_{22} = α(3,2,4)
r_{23} = α(1,2,3)
r_{24} = α(1,2,4)
r_{25} = τ(8,3,2,1)
r_{26} = τ(5,4,2,1)
r_{27} = β(1,2)[b]

[a] See footnotes for TABLE A-1

[b] Out-of-plane carbonyl wag

TABLE A-28
UNNORMALIZED SYMMETRY COORDINATES FOR ACETONE

$S_1 = 2r_1 - r_2 - r_3 + 2r_4 - r_5 - r_6$

$S_2 = r_1 + r_2 + r_3 + r_4 + r_5 + r_6$

$S_3 = r_7$

$S_4 = 2r_8 - r_9 - r_{10} + 2r_{11} - r_{12} - r_{13}$

$S_5 = r_8 + r_9 + r_{10} - r_{14} - r_{15} - r_{16} + r_{11} + r_{12} + r_{13} - r_{17} - r_{18} - r_{19}$

$S_6 = 2r_{14} - r_{15} - r_{16} + 2r_{17} - r_{18} - r_{19}$

$S_7 = r_{20} + r_{21}$

$S_8 = 2r_{22} - r_{23} - r_{24}$

$S_9 = r_{22} + r_{23} + r_{24}$ (redundant)

$S_{10} = r_8 + r_9 + r_{10} + r_{14} + r_{15} + r_{16} + r_{11} + r_{12} + r_{13} + r_{17} + r_{18} + r_{19}$ (redundant)

$S_{11} = r_2 - r_3 + r_5 - r_6$

$S_{12} = r_9 - r_{10} + r_{12} - r_{13}$

$S_{13} = r_{15} - r_{16} + r_{18} - r_{19}$

$S_{14} = r_{25} - r_{26}$

$S_{15} = r_2 - r_3 - r_5 + r_6$

$S_{16} = r_9 - r_{10} - r_{12} + r_{13}$

$S_{17} = r_{15} - r_{16} - r_{18} + r_{19}$

$S_{18} = r_{27}$

$S_{19} = r_{25} + r_{26}$

$S_{20} = 2r_1 - r_2 - r_3 - 2r_4 + r_5 + r_6$

---

continued

TABLE A-28-continued

$S_{21} = r_1 + r_2 + r_3 - r_4 - r_5 - r_6$

$S_{22} = 2r_8 - r_9 - r_{10} - 2r_{11} + r_{12} + r_{13}$

$S_{23} = r_8 + r_9 + r_{10} - r_{14} - r_{15} - r_{16} - r_{11} - r_{12} - r_{13} + r_{17} + r_{18} + r_{19}$

$S_{24} = 2r_{14} - r_{15} - r_{16} - 2r_{17} + r_{18} + r_{19}$

$S_{25} = r_{20} - r_{21}$

$S_{26} = r_{23} - r_{24}$

$S_{27} = r_8 + r_9 + r_{10} + r_{14} + r_{15} + r_{16} - r_{11} - r_{12} - r_{17} - r_{18} - r_{19} - r_{13}$ (redundant)

Note: Taken from Mann and Dixon (91)

TABLE A-29

THE $\underline{A}$ MATRIX FOR ACETONE

1	18	0.016529	1	19	-0.013132	1	20	0.019066	1	21	0.027123
1	22	-0.042649	1	23	0.333640	1	24	0.394018	2	1	-0.024444
2	2	0.007334	2	3	0.724432	2	4	-0.019031	2	5	-0.015143
2	6	0.019488	2	7	0.193716	2	8	-0.285645	3	13	-0.002025
3	14	-0.065877	3	15	0.061860	3	16	0.038106	3	17	0.100928
4	18	-0.012042	4	19	-0.012717	4	20	-0.009235	4	21	0.026263
4	22	0.007737	4	23	0.313886	4	24	-0.253682	5	1	-0.024443
5	2	0.007334	5	3	-0.275581	5	4	-0.019030	5	5	-0.015144
5	6	0.019483	5	7	0.190731	5	8	-0.285635	6	13	0.026176
6	14	0.015429	6	15	-0.016471	6	16	-0.395419	6	17	0.007477
7	2	0.000003	7	3	0.000014	7	4	-0.000002	7	6	0.000004
7	7	-0.603537	7	8	-0.320613	7	18	-0.030406	7	19	-0.012447
7	20	-0.027424	7	21	0.025709	7	22	0.040122	7	23	-0.302356
7	24	-0.115011	8	1	-0.024444	8	2	0.007733	8	3	-0.275576
8	4	-0.019029	8	5	-0.015144	8	6	0.019482	8	7	-0.177699
8	8	0.239545	8	18	0.030082	8	19	-0.030441	8	20	0.029797
8	21	0.000906	8	22	-0.053049	8	23	-0.347623	8	24	-0.227492
9	9	-0.045712	9	10	-0.014677	9	11	0.064324	9	12	0.050426
9	13	0.044295	9	14	0.067672	9	15	-0.066812	9	16	0.111230
9	17	-0.052556	10	2	-0.000003	10	3	-0.000014	10	4	0.000002
10	6	-0.000004	10	7	0.603537	10	8	0.320613	10	18	-0.030406
10	19	-0.012447	10	20	-0.027424	10	21	0.025709	10	22	0.040122
10	23	-0.302356	10	24	-0.115011	11	1	-0.024444	11	2	0.007733
11	3	-0.275576	11	4	-0.019029	11	5	-0.015144	11	6	0.019482
11	7	-0.177699	11	8	0.239545	11	18	-0.030082	11	19	0.030441
11	20	-0.029797	11	21	-0.000906	11	22	0.053049	11	23	0.347623
11	24	0.227492	12	9	0.045712	12	10	0.014677	12	11	-0.064324
12	12	-0.050426	12	13	-0.044295	12	14	-0.067672	12	15	0.066812
12	16	0.111230	12	17	-0.052556	13	1	0.443459	13	2	0.313568
13	3	0.000013	13	4	-0.001757	13	5	-0.198096	13	6	0.402061
13	7	0.603508	13	8	0.036918	13	18	0.429304	13	19	0.300885
13	20	-0.013081	13	21	-0.171901	13	22	0.413522	13	23	-0.291112
13	24	-0.237874	14	1	0.345263	14	2	0.268751	14	3	-0.275587
14	4	-0.016924	14	5	0.222470	14	6	-0.462775	14	7	-0.177695
14	8	0.579781	14	18	0.320142	14	19	0.262152	14	20	-0.046597
14	21	0.236123	14	22	-0.354841	14	23	0.334138	14	24	0.374876
15	9	0.075473	15	10	0.024128	15	11	-0.105584	15	12	0.643218
15	13	0.028253	15	14	0.021468	15	15	-0.022273	15	16	0.866561
15	17	-0.725881	16	1	-0.018279	16	2	0.025846	16	3	-0.000027
16	4	0.163621	16	5	-0.278165	16	6	-0.365463	16	7	0.603539

continued

TABLE A-29-continued

16	8	0.577000	16	9	0.063069	16	10	0.292684	16	11	0.298834
16	12	0.290361	16	13	0.031656	16	14	0.282662	16	15	0.342937
16	16	0.538501	16	17	-0.325013	16	18	-0.063367	16	19	0.013619
16	20	0.121648	16	21	-0.252900	16	22	-0.295435	16	23	-0.312522
16	24	-0.003958	17	1	0.142645	17	2	-0.228563	17	3	-0.275581
17	4	0.253908	17	5	0.084085	17	6	-0.019915	17	7	-0.177688
17	8	0.267604	17	9	-0.289295	17	10	0.462890	17	11	-0.411277
17	12	0.532170	17	13	-0.309765	17	14	0.404337	17	15	-0.354756
17	16	0.312995	17	17	-0.464945	17	18	0.135401	17	19	-0.235829
17	20	0.241551	17	21	0.058274	17	22	0.016490	17	23	0.346505
17	24	0.239635	18	1	0.234695	18	2	-0.331904	18	3	0.000007
18	4	-0.181569	18	5	-0.092309	18	6	-0.000416	18	7	0.000009
18	8	0.000008	18	9	-0.358433	18	10	-0.292342	18	11	0.251902
18	12	-0.407119	18	13	-0.347716	18	14	-0.198166	18	15	0.212488
18	16	-0.069627	18	17	0.253122	18	18	0.234654	18	19	-0.331906
18	20	-0.181573	18	21	-0.092311	18	22	-0.000415	18	23	-0.000004
18	24	-0.000008	19	1	-0.018279	19	2	0.025646	19	3	-0.000027
19	4	0.163621	19	5	-0.278165	19	6	-0.265463	19	7	0.035539
19	8	0.577000	19	9	-0.063069	19	10	-0.292684	19	11	-0.298834
19	12	-0.290361	19	13	-0.031656	19	14	-0.282662	19	15	-0.342937
19	16	-0.538501	19	17	0.325013	19	18	-0.063367	19	19	0.013619
19	20	0.121648	19	21	-0.252900	19	22	-0.295435	19	23	-0.312522
19	24	-0.003958	20	1	0.142645	20	2	-0.228563	20	3	-0.275581
20	4	0.253908	20	5	0.084085	20	6	-0.019915	20	7	-0.177688
20	8	0.267604	20	9	0.289295	20	10	-0.462890	20	11	0.411277
20	12	-0.532170	20	13	0.309765	20	14	-0.404337	20	15	0.354756
20	16	-0.312995	20	17	0.464945	20	18	0.135401	20	19	-0.235829
20	20	0.241551	20	21	0.058274	20	22	0.016490	20	23	0.346505
20	24	0.239635	21	1	-0.234695	21	2	0.331904	21	3	0.000007
21	4	0.181569	21	5	0.092309	21	6	0.000416	21	7	-0.000009
21	8	-0.000008	21	9	-0.358433	21	10	-0.292342	21	11	0.251902
21	12	-0.407119	21	13	-0.347716	21	14	-0.198166	21	15	0.212488
21	16	-0.069627	21	17	0.253122	21	18	-0.234654	21	19	0.331906
21	20	0.181573	21	21	0.092311	21	22	0.000415	21	23	0.000004
21	24	0.000008	22	1	-0.443459	22	2	-0.313568	22	3	-0.000013
22	4	0.001757	22	5	0.198096	22	6	-0.402061	22	7	-0.603508
22	8	-0.036918	22	18	0.429304	22	19	0.300885	22	20	-0.013081
22	21	-0.171901	22	22	0.413522	22	23	-0.291112	22	24	-0.237874
23	1	0.345263	23	2	0.268751	23	3	-0.275587	23	4	-0.016924
23	5	0.222470	23	6	-0.462775	23	7	-0.177695	23	8	0.579781

continued

TABLE A-29-continued

23	18	-0.320142	23	19	-0.262152	23	20	0.046997	23	21	-0.236123
23	22	0.354841	23	23	-0.334138	23	24	-0.374876	24	9	-0.075473
24	10	-0.024128	24	11	0.105984	24	12	-0.643218	24	13	0.028253
24	14	0.021468	24	15	-0.022273	24	16	0.866561	24	17	-0.725881
25	1	0.018279	25	2	-0.032846	25	3	0.000027	25	4	-0.163621
25	5	0.278165	25	6	0.365463	25	7	-0.603539	25	8	-0.577000
25	9	-0.063069	25	10	-0.292684	25	11	0.298834	25	12	-0.290361
25	13	0.031656	25	14	0.282662	25	15	0.342937	25	16	0.538501
25	17	-0.325013	25	18	-0.063367	25	19	0.013619	25	20	0.121648
25	21	-0.252900	25	22	-0.299435	25	23	-0.312522	25	24	-0.003958
26	1	0.142645	26	2	-0.228963	26	3	-0.275581	26	4	0.253908
26	5	0.084085	26	6	-0.019915	26	7	-0.177688	26	8	0.267604
26	9	-0.289295	26	10	0.462850	26	11	-0.411277	26	12	0.532170
26	13	0.309765	26	14	-0.404337	26	15	0.354796	26	16	-0.312995
26	17	0.464945	26	18	-0.135401	26	19	0.235629	26	20	-0.241551
26	21	-0.098274	26	22	-0.016490	26	23	-0.346505	26	24	-0.239635
27	1	-0.234695	27	2	0.331904	27	3	0.000007	27	4	0.181569
27	5	0.092309	27	6	0.000416	27	7	-0.000009	27	8	-0.000008
27	9	0.358433	27	10	0.292342	27	11	-0.251902	27	12	0.407119
27	13	-0.347716	27	14	-0.198166	27	15	0.212468	27	16	-0.066627
27	17	0.253122	27	18	0.234694	27	19	-0.331906	27	20	0.181573
27	21	-0.092311	27	22	-0.000415	27	23	-0.000004	27	24	-0.000008
28	1	0.018279	28	2	-0.025846	28	3	0.000027	28	4	-0.163621
28	5	0.278165	28	6	0.365463	28	7	-0.603539	28	8	-0.577000
28	9	0.063069	28	10	0.292684	28	11	0.298834	28	12	0.290361
28	13	-0.031656	28	14	-0.282662	28	15	-0.342937	28	16	-0.538501
28	17	0.325013	28	18	-0.063367	28	19	0.013619	28	20	0.121648
28	21	-0.252900	28	22	-0.299435	28	23	-0.312522	28	24	-0.003958
29	1	0.142645	29	2	-0.228963	29	3	-0.275581	29	4	0.253908
29	5	0.084085	29	6	-0.019915	29	7	-0.177688	29	8	0.267604
29	9	0.289295	29	10	-0.462850	29	11	0.411277	29	12	-0.532170
29	13	-0.309765	29	14	0.404337	29	15	-0.354796	29	16	0.312995
29	17	-0.464945	29	18	-0.135401	29	19	0.235629	29	20	-0.241551
29	21	-0.098274	29	22	-0.016490	29	23	-0.346505	29	24	-0.239635
30	1	0.234695	30	2	-0.331904	30	3	-0.000007	30	4	-0.181569
30	5	-0.092309	30	6	-0.000416	30	7	0.000009	30	8	0.000008
30	9	0.358433	30	10	0.292342	30	11	-0.251902	30	12	0.407119
30	13	-0.347716	30	14	-0.198166	30	15	0.212468	30	16	-0.066627
30	17	0.253122	30	18	-0.234694	30	19	0.331906	30	20	0.181573
30	21	0.092311	30	22	0.000415	30	23	0.000004	30	24	0.000008

TABLE A-30

THE L MATRIX FOR ACETONE

1	1	1.007784	1	2	-0.289694	1	3	0.001071	1	4	0.035581
1	5	-0.023583	1	6	-0.021399	1	7	-0.020625	1	8	0.011957
2	1	0.277049	2	2	0.970458	2	3	0.019515	2	4	0.000708
2	5	-0.046835	2	6	-0.013847	2	7	-0.024285	2	8	-0.001734
3	1	-0.005101	3	2	-0.006211	3	3	0.367774	3	4	0.063516
3	5	0.000399	3	6	-0.072240	3	7	0.032506	3	8	-0.014880
4	1	0.168743	4	2	-0.042629	4	3	0.137250	4	4	-1.330376
4	5	0.360212	4	6	-0.545067	4	7	-0.098867	4	8	0.113366
5	1	-0.065540	5	2	-0.161241	5	3	0.071524	5	4	-0.379873
5	5	-1.387161	5	6	0.006771	5	7	-0.081660	5	8	0.031632
6	1	-0.063519	6	2	0.029516	6	3	0.430081	6	4	-0.480533
6	5	0.145445	6	6	0.740349	6	7	0.135548	6	8	-0.174750
7	1	-0.007310	7	2	-0.045413	7	3	-0.182472	7	4	-0.061033
7	5	-0.130844	7	6	-0.023038	7	7	0.261664	7	8	0.057667
8	1	-0.105869	8	2	0.023176	8	3	0.360641	8	4	0.074568
8	5	-0.005166	8	6	0.211544	8	7	-0.050657	8	8	0.264484
9	9	1.049679	9	10	-0.022341	9	11	-0.008345	9	12	0.000310
10	9	0.159892	10	10	1.382092	10	11	-0.576532	10	12	0.014777
11	9	-0.093280	11	10	0.542670	11	11	0.814596	11	12	-0.006067
12	9	-0.155556	12	10	-0.653849	12	11	0.622069	12	12	0.562135
13	13	1.049671	13	14	-0.023160	13	15	-0.006149	13	16	-0.003263
13	17	-0.000102	14	13	0.160351	14	14	1.334914	14	15	-0.676510
14	16	-0.053051	14	17	-0.012517	15	13	-0.092442	15	14	0.627659
15	15	0.818623	15	16	0.071568	20	21	0.003926	16	13	0.080322
16	14	-0.076495	16	15	-0.341053	16	16	0.585645	16	17	-0.047021
17	13	0.154350	17	14	0.514631	17	15	-0.892402	17	16	0.562373
17	17	0.537572	18	18	1.002570	18	19	-0.305979	18	20	-0.046460
18	21	0.024211	18	22	-0.022575	18	23	-0.014122	18	24	0.013120
19	18	0.291615	19	19	0.965383	19	20	-0.019015	19	21	0.055923
19	22	-0.036003	19	23	0.008454	19	24	0.006705	20	18	0.165707
20	19	-0.043739	20	20	1.245568	20	21	-0.108492	20	22	-0.725112
20	23	-0.371227	20	24	0.080565	21	18	-0.067183	21	19	-0.155773
21	20	0.237847	21	21	1.406110	21	22	0.197722	21	23	-0.044108
21	24	0.080140	22	18	-0.048088	22	19	0.042510	22	20	0.646566
22	21	-0.127311	22	22	0.357005	22	23	0.631804	22	24	-0.155296
23	18	-0.001487	23	19	0.036529	23	20	-0.137667	23	21	-0.046843
23	22	-0.344693	23	23	0.244575	23	24	0.059867	24	18	-0.039583
24	19	0.034655	24	20	0.136329	24	21	-0.103570	24	22	0.435361
24	23	-0.095207	24	24	0.339970						

APPENDIX B
SIMULATED INFRARED SPECTRA

We study in this dissertation molecules large enough to have many vibrational modes and consequently, for the gas phase spectra with which we are concerned, many vibrational mode frequencies for which the vibrational-rotational manifolds overlap. The number of normal modes ranges from twelve for methanol up to twenty-four for acetone. The quality of the predicted absolute intensities for so many vibrational modes is difficult to absorb; we have chosen, therefore, to plot simulated spectra for many of the data tabulated throughout this dissertation. For this, we have used the SPECTRUM program developed by Newton (106) for use in conjunction with a Gould electrostatic plotter (107). We shall now outline the procedure we follow for plotting intensities as a function of wavenumber.

Infrared spectra were simulated by assuming the absorption band shapes were Gaussian. This assumption is not completely correct for spectra of gas phase molecules because the absorption bands have vibrational-rotational structure (e.g. P, Q, R or P, R structure) and hence cannot be fit by simple gaussians. To fit the simulated spectra to actual band shapes would be much more difficult, especially since hot bands due to low frequency torsional modes further complicate the spectra (108).

Bandshapes are thus assumed to be Gaussian functions given by (109, 110)

$$\alpha(\nu) = \alpha_{max} \exp\left\{ \frac{-4 \ln 2 \ (\nu-\nu_o)^2}{(\Delta\nu_{1/2})^2} \right\} \qquad \text{(B-1)}$$

where $\alpha(\nu)$ is the abosrbance at waveneumber ν, ν_o is the frequency (in cm^{-1}) of the band origin, $\Delta\nu_{1/2}$ is the full-width of the absorption band at one half the maximum absorbance value (FWHM), and α_{max} is given by

$$AC\ell = \sqrt{\pi}\,(4 \ln 2)^{-1/2}\, \alpha_{max}\, \Delta\nu_{1/2} \qquad \text{(B-2)}$$

Here A, C, and ℓ are as defined throughout this dissertation. We may substitute Eq. (B-2) into Eq. (B-1) and convert to consistent units to obtain

$$\alpha(\nu) = \frac{93.94\ AC\ell}{\Delta\nu_{1/2}} \exp\left\{ \frac{-2.7726(\nu-\nu_o)^2}{(\Delta\nu_{1/2})^2} \right\} \qquad \text{(B-3)}$$

Here A has units of km mol^{-1}, C is in mol dm^{-3}, ℓ is in cm, and all frequencies ν are expressed in cm^{-1}.

The quantity $\alpha(\nu)$ is unitless, but we have defined it relative to the base e; thus, when the absorbance is computed from an experimental transmittance spectrum, Eq. (B-4) should be used:

$$\alpha(\nu) = \log_e (I_o/I) \qquad \text{(B-4)}$$

Such a definition of absorbance is not the one recommended by the ASTM Committee on Molecular Spectroscopy (111). They recommend the absorbance be defined as

$$\alpha(\nu) = \log_{10} (I_o/I) \qquad \text{(B-5)}$$

The interconversion between Eq. (B-5) and Eq. (B-4) is of course trivial: an $\alpha(\nu)$ value defined by Eq. (B-5) must be multiplied by 2.303 to obtain an $\alpha(\nu)$ consistent with Eq. (B-4) and hence with Eq. (B-3). The simulated spectra actually are plotted in units of transmittance (T):

$$T - (I/I_o) = e^{-\alpha} \tag{B-6}$$

Values for absorption band half-widths (FWHM) were estimated from the experimental absorption spectra. This procedure presents a problem for regions with overlapping modes such as the C-H stretching region at 3000 cm^{-1} for dimethyl ether. Although there are five infrared-active C-H stretching vibrations in this region, only three partially resolved bands are seen in the gas phase spectrum. To best simulate the experimentally observed spectrum, we would therefore add the five intensities calculated for this region to get intensities for three gaussians. Thus, we would add together the intensities for ν_1(2992 cm^{-1}) and ν_{16}(2987 cm^{-1}), to get an intensity for one gaussian; absolute intensities for ν_2 (2817 cm^{-1}) and ν_{17}(2826 cm^{-1}) would also be added to yield an intensity for the second gaussian; finally, the intensity for ν_8 (2934 cm^{-1}) is used as the intensity for the third gaussian. This same procedure is followed for other overlapping bands in our series of molecules; thus, we only fit to as many absorption lines as we can easily estimate from the experimental spectru. The calculated intensities of modes which are not discernable in the experimental spectrum are added to the calculated intensities for modes in that region which are visible. Such a procedure partially accounts for any inadequacies in the normal coordinates ($\underline{L}$) since intensities

for normal modes of the same symmetry with similar frequencies will depend very strongly upon the exact form of L.

Simulated spectra are plotted in transmittance units rather than absorbance units. It is the absorbance which is directly proportional to the number density of absorbers in the light path, but spectrometers commonly in use record spectra in transmittance units. Since one of the goals of infrared intensity calculations is to obtain data to compare with experiment, we have chosen transmittance units. One should keep in mind, though, that plots linear in transmittance visually minimize disagreements with the experiment by virtue of Eq. (B-6).

Finally, only absorption bands of frequencies falling within the regions spanned by the experimental spectra are plotted in the simulated spectra. Intensities for some low frequency absorption modes (such as torsions below 400 cm^{-1}) are consequently not shown in the simulated spectra because the potassium bromide gas cell windows are not transparent to infrared radiation below 400 cm^{-1} (112). Also, the instrumental design of the Nicolet Model 7199 FT-IR with which many of the experimental spectra were measured, precludes simultaneous scanning from 4000 cm^{-1} to beyond 400 cm^{-1}, one reason being the potassium bromide beam splitter.

The data used to plot simulated spectra shown in this dissertation are presented in Tables B-1 through B-4. Again, we emphasize that only distinguishable bands in the experimental spectra are fit by the simulated spectra, and that the half-widths are estimated from the experimental data.

TABLE B-1
PARAMETERS FOR SIMULATED SPECTRA OF METHANOL

Band Maximum (cm^{-1})[a]	Half-width (cm^{-1})[b]
3680.0	85.0
2960.0	125.0
2840.0	85.0
1470.0	60.0
1343.0	120.0
1223.0	30.0
1033.0	80.0

[a] Experimentally observed frequencies

[b] Full width at half maximum, estimated from experimental spectrum

TABLE B-2
PARAMETERS FOR SIMULATED SPECTRA OF ETHANOL

Band Maximum(cm^{-1})[a]	Half-width(cm^{-1})[b]
3660.0	60.0
2980.0	100.0
2900.0	70.0
1480.0	30.0
1450.0	10.0
1390.0	60.0
1240.0	60.0
1065.0	80.0
880.0	50.0
801.0	30.0

[a] Experimentally observed frequencies

[b] Full width at half maximum, estimated from experimental spectrum

TABLE B-3
PARAMETERS FOR SIMULATED SPECTRA OF DIMETHYL ETHER

Band Maximum(cm^{-1})[a]	Half-width(cm^{-1})[b]
2990.0	75.0
2900.0	60.0
2820.0	70.0
1460.0	47.0
1175.0	55.0
1095.0	52.0
920.0	77.0
425.0	25.0

[a] Experimentally observed frequencies

[b] Full width at half maximum, estimated from experimental spectrum

TABLE B-4
PARAMETERS FOR SIMULATED SPECTRA OF ACETONE

Band Maximum(cm^{-1})[a]	Half-width(cm^{-1})[b]
2973.0	115.0
1738.0	48.0
1437.0	62.0
1365.0	39.0
1218.0	40.0
1093.0	47.0
896.0	49.0
779.0	38.0
528.0	41.0
483.0	40.0

[a]Experimentally observed frequencies

[b]Full width at half maximum, estimated from experimental spectrum

REFERENCES

1. W. B. Person and D. Steele, in "Molecular Spectroscopy," D. A. Long, Ed., Specialist Periodical Report of the Chemical Society, No. 29, Vol. 2, 1974, p. 357.

2. G. Herzberg, "Infrared and Raman Spectra of Polyatomic Molecules" (Van Nostrand Reinhold Company, New York, 1945).

3. E. B. Wilson, Jr., J. C. Decius, and P. C. Cross, "Molecular Vibrations" (McGraw-Hill, New York, 1955).

4. J. Overend in "Infrared Spectroscopy and Molecular Structure," M. Davies, Ed. (Elsevier, Amsterdam, 1963), Chap. 10.

5. J. H. Newton and W. B. Person, Appl. Spectrosc. 32, 290 (1978).

6. L. M. Sverdlov, M. A. Kovner, and E. P. Krainov, "Vibrational Spectra of Polyatomic Molecules" (John Wiley & Sons, New York, 1974).

7. B. Crawford, Jr., J. Chem. Phys. 20, 977 (1952).

8. D. F. Hornig and D. C. McKean, J. Phys. Chem. 59, 1133 (1955). This article contains a critical review of intensity data from the bond moment hypothesis.

9. M. Gussoni and S. Abbate, J. Chem. Phys. 65, 3439 (1976).

10. L. A. Gribov, "Intensity Theory for Infrared Spectra of Polyatomic Molecules " (English translation)(Consultants Bureau, New York, 1964).

11. G. B. Mast and J. C. Decius, J. Mol. Spectrosc. 79, 158 (1980).

12. J. F. Biarge, J. Herranz, and J. Morcillo, An. R. Soc. Esp. Fis. Quim. A57, 81 (1961).

13. W. B. Person and J. H. Newton, J. Chem. Phys. 61, 1040 (1974).

14. W. B. Person and J. H. Newton, J. Mol. Struct. 46, 105 (1978).

15. J. H. Newton, R. A. Levine, and W. B. Person, J. Chem. Phys. 67, 3282 (1977).

16. J. H. Newton and W. B. Person, J. Chem. Phys. 68, 2799 (1978).

17. B. J. Krohn, W. B. Person, and J. Overend, J. Chem. Phys. 65, 969 (1976).

18. I. Ya. Zemlyanukhina, L. M. Sverdlov, and A. G. Finkel, Teor. i Esp. Khim. 10, 193 (1974).

19. I. P. Stalmakhova and L. M. Sverdlov, Opt. Spectrosk. 24, 393 (1968).

20. A. Komornicki and J. W. McIver, Jr., J. Chem. Phys. 70, 2014 (1979).

21. A. P. Thorne, "Spectrophysics" (Chapman and Hall & Science Paperbacks, London, 1974).

22. E. B. Wilson, Jr. and A. J. Wells, J. Chem. Phys. 14, 578 (1946).

23. S. S. Penner and D. Weber, J. Chem. Phys. 19, 807 (1951).

24. G. Herzberg, "Spectra of Diatomic Molecules" (Van Nostrand Reinhold Company, New York, 1950).

25. R. A. Levine, M. S. Thesis, University of Florida (1975).

26. Instruction Manual for Model 7199 FT-IR spectrometer (Nicolet Instrument Corp., Madison, 1978).

27. H. D. Young, "Statistical Treatment of Experimental Data" (McGraw-Hill, New York, 1962).

28. "Handbook of Chemistry and Physics," 52nd Edition (Chemical Rubber Company, Cleveland, 1971).

29. E. V. Broun, Opt. Spectrosk. 23, 559 (1967).

30. R. G. Inskeep, J. M. Kelliher, P. E. McMahon, and B. S. Somers, J. Chem. Phys. 28, 1033 (1958).

31. M. Margottin-Maclou and L. Henry, J. de Physique 26, 537 (1965).

32. A. Serrallach, R. Meyer, and Hs. H. Gunthard, J. Mol. Spectrosc. 52, 94 (1974).

33. T. Ha, R. Meyer, and Hs. H. Gunthard, Chem. Phys. Lett. 22, 68 (1973).

34. E. Steiner, "The Determination and Interpretation of Molecular Wave Functions" (Cambridge University Press, London, 1976).

35. P. R. Griffiths, "Chemical Infrared Fourier Transform Spectroscopy" (Wiley, New York, 1975).

36. J. Chamberlain, "Principles of Interferometric Spectroscopy" (Wiley, New York, 1979).

37. K. Scanlon, L. Laux, and J. Overend, Appl. Spectrosc. 33, 346 (1979).

38. R. J. Anderson and P. R. Griffiths, Anal. Chem. 50, 1804 (1978).

39. Instruction Manual for Curve Analysis Program (Nicolet Instrument Corp., Madison, 1978).

40. P. P. Sethna, H. D. Downing, L. W. Pinkley, and D. Williams, J. Opt. Soc. Am. 68, 429 (1978).

41. P. P. Sethna and D. Williams, J. Phys. Chem. 83, 405 (1979).

42. B. Zilles, Ph.D. Dissertation, University of Florida (1980).

43. C. E. Blom, A. Oskam, and C. Altona, Mol. Phys. 34, 557 (1977).

44. I. M. Mills in "Infrared Spectroscopy and Molecular Structure," M. Davies, Ed. (Elsevier, Amsterdam, 1963), Chap. 5.

45. D. Steele, "Theory of Vibrational Spectroscopy" (W. B. Saunders, Philadelphia, 1971).

46. J. C. Decius, J. Chem. Phys. 17, 1315 (1949).

47. F. A. Cotton, "Chemical Applications of Group Theory " (Wiley, New York, 1971).

48. E. R. Cohen and B. N. Taylor, J. Phys. Chem. Ref. Data. 2, 663 (1973).

49. B. L. Crawford, Jr. and W. H. Fletcher, J. Chem. Phys. 19, 141 (1951).

50. J. H. Newton, Ph.D. Dissertation, University of Florida (1974).

51. J. H. Newton and W. B. Person, J. Chem. Phys. 64, 3036 (1976).

52. W. T. King, G. B. Mast, and P. P. Blanchette, J. Chem. Phys. 56, 4440 (1972).

53. B. Crawford, Jr., J. Chem. Phys. 20, 977 (1952).

54. W. T. King in "Vibrational Intensities," W. B. Person and G. Zerbi, Eds. (Elsevier, Amsterdam, to be published, 1980), Chap. 6.

55. R. M. Lees and J. G. Baker, J. Chem. Phys. 48, 5299 (1968).

56. P. D. Mallinson, J. Mol. Spectrosc. 58, 194 (1975). See also P. D. Mallinson and D. C. McKean, Spectrochim. Acta 30A, 1133 (1974).

57. E. V. Ivash and D. M. Dennison, J. Chem. Phys. 21, 1804 (1953).

58. S. Kondo and W. B. Person, J. Mol. Spectrosc. 52, 287 (1974).

59. C. E. Blom, L. P. Otto, and C. Altona, Mol. Phys. 32, 1137 (1976).

60. P. Pulay, G. Fogarasi, F. Pang, and J. E. Boggs, J. Am. Chem. Soc. 101, 2550 (1979).

61. J. H. Newton, unpublished results, at the University of Florida.

62. J. E. Huheey, J. Phys. Chem. 69, 3284 (1965).

63. J. E. Huheey, "Inorganic Chemistry" (Harper & Row, New York, 1972).

64. R. E. Bruns in "Vibrational Intensities," W. B. Person and G. Zerbi, Eds. (Elsevier, Amsterdam, to be published, 1980), Chap. 7.

65. J. A. Pople and D. L. Beveridge, "Approximate Molecular Orbital Theory" (McGraw-Hill, New York, 1966).

66. D. Steele, in "Molecular Spectroscopy," D. A. Long, Ed., Specialist Periodical Report of the Chemical Society, Vol. 5, 1978.

67. W. J. Hehre, W. A. Latham, R. Ditchfield, M. D. Newton, and J. A. Pople, "GAUSSIAN 70," program 236, Quantum Chemistry Program Exchange, Indiana University (1971).

68. R. Ditchfield, W. J. Hehre, and J. A. Pople, J. Chem. Phys. 54, 724 (1971); W. J. Hehre, R. Ditchfield, and J. A. Pople, J. Chem. Phys. 56, 2257 (1972); J. B. Collins, P. von R. Schleyer, J. S. Binkley, and J. A. Pople, J. Chem. Phys. 64, 5142 (1976).

69. D. Steele, Mol. Phys. 38, 145 (1979).

70. H. B. Schlegel, S. Wolfe, and F. Bernardi, J. Chem. Phys. 67, 4181 (1977).

71. F. A. Momany, J. Phys. Chem. 82, 592 (1978).

72. P. Venkalateswarlu and W. Gordy, J. Chem. Phys. 23, 1200 (1955).

73. Y. Sasada, M. Takano, and T. Saton, J. Mol. Spectrosc. 38, 33 (1971).

74. T. Oka, H. Hirakawa, and K. Shimoda, J. Phys. Soc. Japan 15, 2265 (1960).

75. R. Nelson and L. Pierce, J. Mol. Spectrosc. 18, 344 (1965).

76. R. H. Schwendeman, J. Chem. Phys. 44, 2115 (1966).

77. J. J. Wendoloski, Paper WF12, Symposium on Molecular Spectroscopy, Columbus, Ohio, June, 1980.

78. J. H. Newton and W. B. Person, J. Phys. Chem. 82, 226 (1978).

79. I. Y. Zemlyanukhina and L. M. Sverdlov, Opt. Spectrosc. 36, 391 (1974).

80. C. E. Blom and C. Altona, Mol. Phys. 31, 1377 (1976).

81. J. P. Perchard and M. L. Josien, J. Chim. Phys. 65, 1834 (1968).

82. J. P. Perchard and M. L. Josien, J. Chim. Phys. 65, 1856 (1968).

83. C. E. Blom and C. Altona, Mol. Phys. 33, 875 (1977).

84. I. W. Levin, R. A. R. Pearce, and R. C. Spiker, Jr., J. Chem. Phys. 68, 3471 (1978).

85. W. B. Person, in "Proceedings of the NASA Workshop on Vibrational-Rotational Spectroscopy for Planetary Atmospheres," K. Fox, Ed., to be published, 1980.

86. I. C. Hisatsune and D. F. Eggers, J. Chem. Phys. 23, 487 (1955).

87. J. Newton, private communication. The normal coordinate analysis is the same as discussed in reference (13).

88. H. H. Blau and H. H. Nielson, J. Mol. Spectrosc. 1, 124 (1957).

89. H. Khoshkhoo and E. R. Nixon, Spectrochim. Acta 29A, 603 (1973).

90. K. B. Harvey and J. F. Ogilvie, Can. J. Chem. 40, 85 (1962).

91. R. H. Mann and W. B. Dixon, J. Chem. Phys. 57, 792 (1972).

92. V. I. Vakhlueva, A. G. Finkel, L. M. Sverdlov, and L. A. Zaitseva, Opt. Spectrosc. 25, 160 (1968).

93. V. I. Vakhlueva, A. G. Finkel, L. M. Sverdlov, and A. I. Andreeva, Opt. Spectrosc. 25, 234 (1968).

94. S. Besnainou, R. Prat, and S. Bratoz, J. Chim. Phys. 59, 896 (1962).

95. R. S. Mulliken, J. Chem. Phys. 23, 1833 (1955).

96. E. Flood, P. Pulay, and J. E. Boggs, J. Am. Chem. Soc. 99, 5570 (1977).

97. P. J. Krueger, J. Jan, and H. Wieser, J. Mol. Struct. 5, 375 (1970).

98. D. C. McKean, J. L. Duncan, and L. Batt, Spectrochim. Acta 29A, 1037 (1973).

99. The contribution of Fermi resonance to the Bohlmann bands has been suggested by E. E. Ernstbrunner and J. Hudec, J. Mol. Struct. 17, 249 (1973).

100. G. Sanchez, Ph.D. Dissertation, University of Florida, 1971.

101. See, for example, P. Botschwina, W. Meyer, and A. M. Semkow, Chem. Phys. 15, 25 (1976); also, G. Zerbi, J. Overend, and B. Crawford, Jr., J. Chem. Phys. 38, 122 (1963).

102. P. Labarbe, M. T. Forel, and G. Bessis, Spectrochim. Acta 24A, 2165 (1968); R. G. Snyder and G. Zerbi, Spectrochim. Acta 23A, 391 (1967); P. Labarbe and M. T. Forel, J. Chim. Phys. 70, 180 (1973).

103. U. Blukis, P. H. Kasai, and R. J. Meyrs, J. Chem. Phys. 38, 2753 (1963).

104. G. Dellepiane and J. Overend, Spectrochim. Acta 22A, 593 (1966).

105. P. Cossee and J. H. Schachtschneider, J. Chem. Phys. 44, 97 (1966).

106. J. Newton, unpublished work at the University of Florida.

107. Gould 4800/5000 Series, IBM System /360/370, Plot Package Programming Manual, Gould Inc.,Instrument Systems Division, 1974.

108. V. Stern, C. Belorgeot, J. Kachmarsky and K. D. Möller, J. Mol. Spectrosc. 67, 244 (1977).

109. E. D. Hinkley, in "Laser Spectroscopy of Atoms and Molecules," H. Walther, Ed. (Springer-Verlag, New York, 1976).

110. A. P. Thorne, "Spectrophysics" (Chapman and Hall, London, 1974).

111. "Manual on Practices in Molecular Spectroscopy," American Society for Testing and Materials, Philadelphia, 1979.

112. E. D. Olsen, "Modern Optical Methods of Analysis" (McGraw-Hill, New York, 1975).

BIOGRAPHICAL SKETCH

Jerry Dale Rogers was born March 27, 1954, in Nebo, West Virginia. He attended the public school system in Clay County, West Virginia. He then received a B.S. degree in chemistry from West Virginia University in 1976. Since that time he has been at the University of Florida. He is receiving the Ph.D. degree in chemistry from the University of Florida.

I certify that I have read this study and that in my opinion it conforms to acceptable standards of scholarly presentation and is fully adequate, in scope and quality, as a dissertation for the degree of Doctor of Philosophy.

Willis B. Person, Chairman
Professor of Chemistry

I certify that I have read this study and that in my opinion it conforms to acceptable standards of scholarly presentation and is fully adequate, in scope and quality, as a dissertation for the degree of Doctor of Philosophy.

William Weltner, Jr.
Professor of Chemistry

I certify that I have read this study and that in my opinion it conforms to acceptable standards of scholarly presentation and is fully adequate, in scope and quality, as a dissertation for the degree of Doctor of Philosophy.

John Eyler
Professor of Chemistry

I certify that I have read this study and that in my opinion it conforms to acceptable standards of scholarly presentation and is fully adequate, in scope and quality, as a dissertation for the degree of Doctor of Philosophy.

Merle Battiste
Professor of Chemistry

I certify that I have read this study and that in my opinion it conforms to acceptable standards of scholarly presentation and is fully adequate, in scope and quality, as a dissertation for the degree of Doctor of Philosophy.

Charles Burnap

Charles Burnap
Professor of Mathematics

This dissertation was submitted to the Graduate Faculty of the Department of Chemistry in the College of Liberal Arts and Sciences and to the Graduate Council, and was accepted as partial fulfillment of the requirements for the degree of Doctor of Philosophy.

August, 1980

_____

Dean, Graduate School